The Cause of Inorganic Compounds from Auto-flocculated Algal Solids and Their Effect on the Solid and Biocrude Products of Conventional Hydrothermal Liquefaction

By

Robert D. Hable

Submitted to the graduate degree program in Chemical and Petroleum Engineering and the Graduate Faculty of the University of Kansas in partial fulfillment of the requirements for the degree of Doctor of Philosophy.

Co-Chair: Susan M. Stagg-Williams

Co-Chair: Belinda S.M. Sturm

Laurence R. Weatherley

Kevin C. Leonard

External: Edward F. Peltier

Date Defended: 30th August 2018

The dissertation committee for Robert D. Hable certifies that this is the approved version of the following dissertation:

The Cause of Inorganic Compounds from Auto-flocculated Algal Solids and Their Effect on the Solid and Biocrude Products of Conventional Hydrothermal Liquefaction

Co-Chair: Susan M. Stagg-Williams

Co-Chair: Belinda S.M. Sturm

Date Approved: 4th December 2018

Abstract

The recent increase in demand for more sustainable and renewable alternatives to both energy and other commercial products has given rise to a modern bioeconomy. With advances in the life sciences, various biomass resources and conversion techniques have been explored to create such products. Hydrothermal liquefaction (HTL) of algal biomass has been proven to be an effective wet, thermochemical technique for the conversion of biomass to a high quality biocrude oil product. Furthermore, the subcritical water conditions of HTL provide an outstanding environment for the inorganic, solid synthesis of high-valued biomaterials and catalysts. The Feedstock to Tailpipe Initiative at the University of Kansas was one of the first to trial HTL on algal solids that were cultivated in wastewater effluent. In addition to an enhanced biocrude product, HTL of wastewater-cultivated algal solids produced a high amount of solid products. Further analysis of these HTL solids indicated they were a calcium phosphate material known as hydroxyapatite (HAp), $Ca_5(PO_4)_3OH$. With a proven proof of concept that HTL of wastewater-cultivated algal solids yields an abundance of HTL solids and an upgraded biocrude product, the major research thrust of this dissertation was to understand the chemical and biological characteristics that created these unique results.

Lab- and bench-scale light rack tanks and raceway ponds, respectively, were utilized to grow *Chlorella kessleri* in BG-11 media with augmented calcium concentrations. Light rack experiments aided in discovering the cause for high ash or inorganic capture within the algal solids. By harvesting algae at a pH of 11, solids precipitate from the algal growth media causing the algal cells to auto-flocculate, and the resulting algal solids to have a high inorganic, ash content. X-ray diffraction (XRD) revealed the primary, crystalline structure of auto-flocculated and wastewater-cultivated algal solids was calcite or $CaCO_3$. Algal solids cultivated in the light racks with various

Ca:P molar ratios also showed that an increased calcium content causes a nearly 100% recovery of phosphorus in the HTL solid product. Thus, auto-flocculation and subsequent HTL of algal solids provides excellent means for sustainable, renewable P-recovery.

Unlike HTL solids from wastewater-cultivated algal solids, a uniform HAp or alternative calcium phosphate structure, such as tricalcium phosphate (TCP) $Ca_3(PO_4)_2$, was not observed in the HTL solids produced from auto-flocculated algal solids that were cultivated in the light racks. Inorganic synthesis of calcium phosphates via identical HTL conditions (350°C for 60 min.) with calcite and trisodium phosphate, Na_3PO_4, also remained primarily $CaCO_3$ in structure rather than the desired calcium phosphate one. The final, discovered cause for uniform calcium phosphate structure in the HTL solids was the algal growth media and stage at which the algal solids were harvested. Algal solids cultivated at all growth stages of N-limited media and the early stages of P-limited media formed HAp or TCP in the HTL solids when the algal solid Ca:P molar ratio was 2.5 or less. The cause for the observance of HAp and TCP in the HTL solids was that amorphous calcium phosphate was precipitating from the growth media solution which was supported by water chemistry theory. The observance of HAp and TCP structures in the algal solid ash also confirmed this hypothesis.

To distinguish and quantify the amount of amorphous calcium phosphate versus calcite in the algal or HTL solids thermal gravimetric analysis (TGA) was utilized. Calcium carbonate degraded and released CO_2 between 600-800°C while calcium phosphates such as HAp or TCP did not thermally degrade substantially. Independently, the mass of $CaCO_3$ could be measured within 1% error of the theoretical amount. However, the additional organic, biomass of the algal solids, however, delayed the thermal degradation of $CaCO_3$ within the algal solids causing greater error. Correlated trends from both TGA-measured carbonate and the theoretical carbonate of algal

solids, as determined by water chemistry modeling, justified the use of the TGA for estimating carbonate in the algal solids. The balance of calcium not stoichiometrically correlated to the mass of carbonate was then further assumed to be associated with amorphous calcium phosphate. Correlating trends then also existed between the estimated percent of calcium as calcium phosphate, the theoretical solid-P to have precipitated from the growth media, and the observed calcium phosphate structure in the algal solids' ash.

Finally, the algal growth media and growth stage had large impacts on the biocrude composition. The unique biocrude compositional characteristics that were observed from wastewater-cultivated algal solids, low amide content and > CO_{20} hydrocarbons, were also observed in N-limited algal solids harvested from at the later stationary growth stage. Because these are similar growth conditions and harvesting stage as the wastewater-cultivated algal solids, it led to the conclusion that nutrient limitation and growth stage have a larger role on the biocrude's composition than the HTL solids of wastewater-cultivated algal solids. However, substantial variances in biocrude properties still occurred from algal solids cultivated in the same growth media and harvested at the same growth stage with only the inorganic composition varying. Biocrude with the highest H/C molar ratio was achieved when complimented with HTL solids with a primarily calcite structure. Thus, it is suggested that future work focus on the impact and role of $CaCO_3$ during the HTL of algal solids.

Table of Contents

List of Figures

List of Tables

1 Introduction

1.1 Bioeconomy

A bioeconomy refers to the management of biological resources to manufacture commodity fuels, chemicals, and products. The term was first introduced in the genomics field during the economic biotech boom of the late 1980's and 1990's.[1] This economic boom came from the scientific discovery to synthetically create significant biological molecules through gene and DNA manipulation. This led large business mergers between agriculture, pharmaceutical, and chemical companies. Figure 1 depicts several of these well-known mergers such as Monsanto, Dupont, BASF, and Bayer.[1] The merger of primarily agriculture and chemical companies is where the current and modern connotation for a bioeconomy is derived. With agricultural products being the primary raw material of a bioeconomy, and chemicals and fuels becoming the primary products, a great significance has been put on the integration of food, energy, and water systems.

Innovations in food, energy, and water systems (INFEWS) is a recent, federal-level research campaign that shares many objectives with a bioeconomy and the work of this dissertation. Aimed towards more efficiently balancing these global resources for a more sustainable future, INFEWS hope to overcome concerns with land use change, uneven resource distribution, and climate variability.[2] To overcome these challenges the National Science Foundation (NSF) in corporation with the National Institute for Food and Agriculture (NIFA) have sponsored the INFEWS program that initiated in 2015.[3] To date over $100 million in grant funding has become available to aid in this field.[4-6]

The underlying goal of INFEWS is to integrate social, ecological, and physical environments in order to meet the growing demand for food, energy, and water in the short term

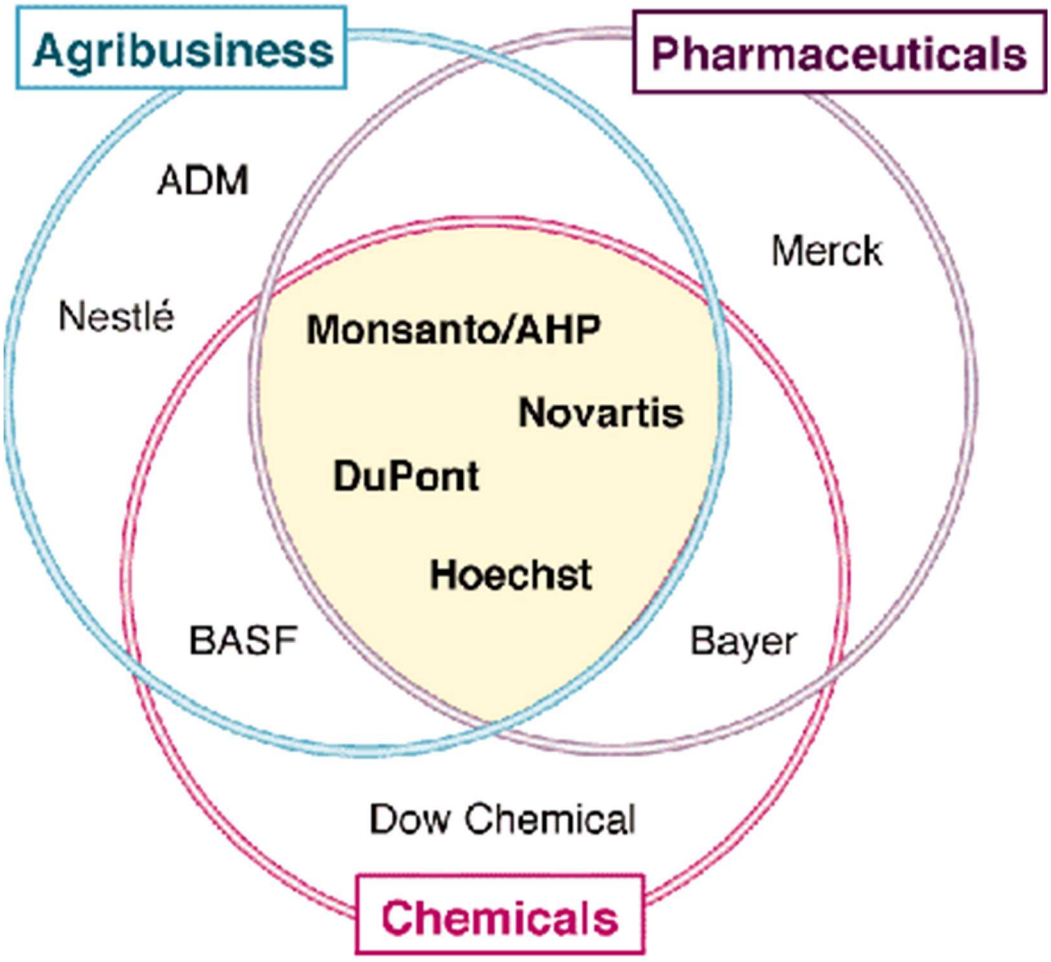

Figure 1: Corporate and industry mergers between agriculture, pharmaceutical, and chemical businesses.

while maintaining existing ecosystems for the future.[2] INFEWS aims to support research towards innovative engineering of natural systems using both physical and biological processes. Outcomes of INFEWS are described as "means of extending resources via methods such as recycling, recovery, and reuse."[2] Working within INFEWS is also expected to be highly collaborative and provide solutions for new and existing infrastructure and agroecosystems.

The bioeconomy is currently in its infancy, and thus, the infrastructure and technological advancements have not yet been achieved to make these bio-based alternatives cost competitive with current petroleum-based products. The current manufacturing practices of petroleum-based

fuels and chemicals have detrimental environmental impacts on local, regional, and global scale. Waste from drilling sites can create local environmental problems while the combustion of petroleum-based fuels can create smog, small particulate matter, and acid rain from sulfur dioxide emissions that have regional environmental concerns. Lastly, nitrous oxides and carbon dioxide create a greenhouse effect that can raise global temperatures and cause global climate change. Bio-based alternatives are not a cure-all to these problems; however, it is widely expected that they would lessen the negative environmental impacts from petroleum-based products. Thus, a bioeconomy is often affiliated with terms such as: sustainability, renewable, environmentally- or eco-friendly, and "green."

1.2 Nutrient Recovery

Often overlooked in a bioeconomy or food, energy, and water system are the nutrients necessary to grow biomass. Nitrogen (N) and phosphorus (P) are critical nutrients for biomass production. In regard to nitrogen supply, the Haber-Bosch process from the early 1900's synthesizes ammonia (NH_3) through N_2 and H_2 gases. Nearly all (99%) of the industrial, fixated nitrogen comes from the Haber-Bosch process.[7] The energy required and CO_2 output for the Haber-Bosch process, however, is extremely high. It has been estimated that one year of ammonia production requires the equivalent energy of 90 million cars and the CO_2 output of 80 million people.[8] Alternatively, P-fertilizer resources are often mined and, similar to crude oil production, is not currently sustainable.[9-10] It has been estimated that these phosphorus resources will be depleted in the next 60-130 years.[11] Thus, innovative, renewable, and sustainable means to manufacture these nutrients is critical.

Unfortunately, when applied for agriculture purposes very little of the N and P is retained in the crops. Nitrogen retention within corn grain is only 39% and 13% for the first and second application of fertilizer respectively.[12] Similarly, 80% of the mined P is applied as fertilizer; however only 16% of that originally mined P results in human consumption.[13] Thus, a majority of the N and P fertilizers remain in the soil or are carried through various waste streams.

Figure 2 depicts the flow of nutrients, N and P, from their organic and fertilizer sources to various water bodies through erosion, tile, and/or subsurface flows.[14] S.R. Carpenter et al. noted that the EPA has identified eutrophication to be the most common impairment to United States surface waters.[14] Eutrophication is caused by the accumulation and excess of N and P nutrients in various water bodies and has several negative impacts. The largest and most notable adverse effect is the increase of algal blooms and aquatic biomass in said water body. Besides many of the marine algal strains being toxic to livestock, humans, and other organisms, the subsequent death and decomposition of this biomass causes large oxygen depletion in the water and ultimately kills large populations of fish.[14] Thus, several environmentalists are urging for greater nutrient management and remediation.[15]

Wastewater treatment facilities (WWTF) are excellent sites to manage and remediate such nutrients to possible profit streams. Li et al. estimated that a WWTF that treats 100,000 m^3 day^{-1} for a population of a half a million people could produce enough electrical energy (17,000 kWh), N and P renewable fertilizers (1 and 5 tonnes respectively), and 1,000 m^3 of potable water to conservatively profit $1.8 million annually. This is compared to the current activated-sludge industry standard that costs $4.6 million per year.[16] The optimum and most economical means to recovering these nutrients varies by location and the properties of the wastewater. Struvite ($MgNH_4PO_4$) or hydroxyapatite ($Ca_5(PO_4)_3OH$) precipitation are often seen as the most popular

method for N and/or P removal and recovery.[9-10, 13, 17] Another favorable method for nutrient recovery from wastewater is microalgae.[18] In addition to proper and effective N and P removal, the algae biomass possess biofuel and bioproduct potential thus providing additional revenue streams for a WWTF.[19-21]

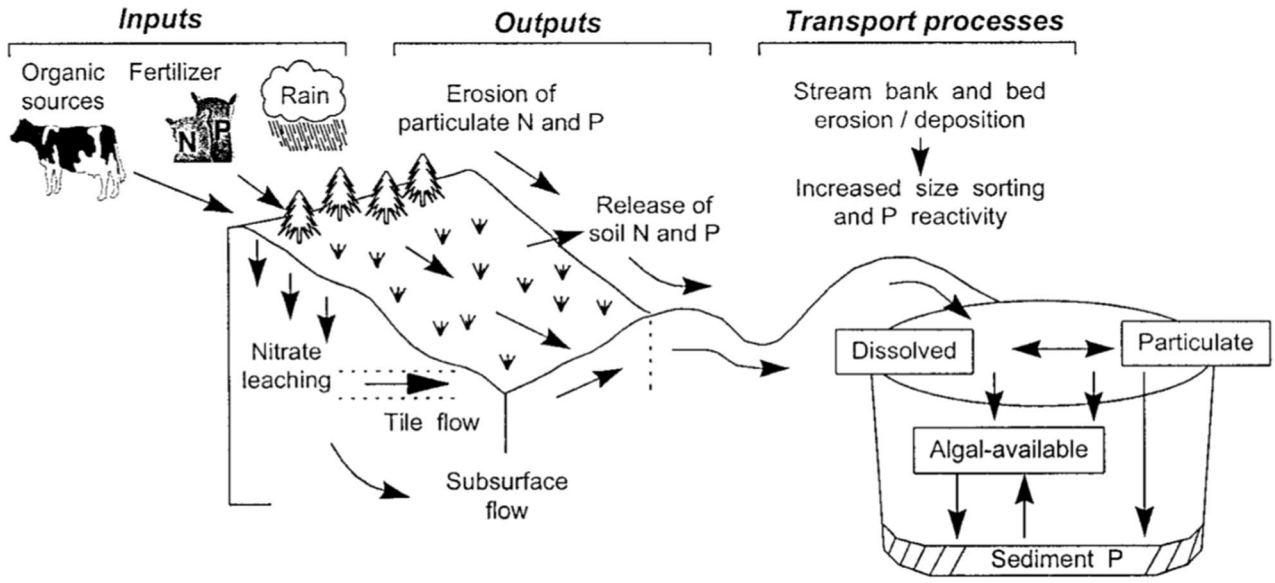

Figure 2: N and P nutrient flows from source to various water bodies through erosion or subsurface and tile paths.

1.3 Biomass

The other well-known and distinct research thrusts for a bioeconomy are 1) the production and securing of biomass feedstocks and 2) the effective conversion of the biomass to alternative products. Over the past decade, new generations of biomass resources have been discovered and studied. Table 1 summarizes several of these common biomass feedstocks and their productivity both as a biomass and the energy derived from fuel per acre per year.[22-23] The first generation of biomass were traditional agricultural crops: corn and soybeans. The recent advances in genomics and biotechnology and an existing, thriving infrastructure had made these strong, viable biomass resources. However as previously mentioned, first generation biomass feedstocks were seen as

direct competitors to the food market and received a great deal of social and political discourse over “food versus fuel” debate

The food vs. fuel controversy led to the develop of second-generation biomass, and that includes nonfood agriculture crops and residue: switchgrass and corn stover. Second generation biomass, however, still required arable land, and there was great and well-founded suspicion that it would not meet the high demand of biomass necessary to produce economical amount of alternative fuels and chemicals. That is where algae, a prolific and highly abundant biomass that can grow on non-arable land and in waste streams became the third and most modern generation of biomass. These advantages as a biomass resources are why algae are the principal biomass feedstock for this dissertation.

Table 1: Popular feedstocks and their biomass and energy derived from fuel yields per acre per year.

Feedstock	Biomass Yield	Fuel Energy
	ton acre^{-1} year^{-1}	*GJ acre^{-1} year^{-1}*
Algae	19 – 106	391 – 5,214
Corn	2.2 – 2.7	24
Soybean	0.4 – 0.9	8
Wheat	1.8 – 2.2	20
Sugar Cane	2.2 – 8.9	73
Palm Oil	4.5 – 6.7	65
Grasses	4.5 – 8.9	69
Perennials	1.3 – 4.5	12

Algae still face challenges as a biomass resource. Similar to other generations of biomass, algae require similar inputs, water and nutrients, for growth and production. However, the amount and application of these inputs differ greatly than century-old and practiced, terrestrial biomass. The absence of an optimized cultivation technique and a lack of existing infrastructure are some of the largest challenges of algal biomass.[24]

1.4 Conversion Techniques

The second area of a bioeconomy is the conversion technique to convert the biomass to the alternative fuels, chemicals, or other products. Conversion methods are often divided into two different categories: biological and thermochemical. Thermochemical conversions have been further split into wet and dry methods. Table 2 summarizes some of the most common, practiced, and studied conversion techniques. Biological conversion relies on microorganisms to convert the biomass feedstock to a desired product. Fermentation is a well-practiced and commercialized biological method that uses yeast to convert carbohydrates from first and second-generation biomass to ethanol. Anaerobic digestion is another biological method that uses a variety of microorganisms to convert primarily second-generation feedstocks to a natural gas alternative, referred to as biogas. Because the biological conversion relies on the livelihood of the microorganism and the microbial conversion may be exothermic, proper temperature control is critical. Thus, fermentation and anaerobic digestion both occur at ambient to mild temperatures.

Table 2: Summary of conversion techniques, their reaction parameters, products, and typical biomass feedstocks.

Conversion Technique		Temperature	Pressure	Products	Feedstock
Biological	Fermentation [25-26]	20 – 35°C	Ambient	Ethanol	Corn Cornstover Switchgrass
	Anaerobic Digestion [27]	30 – 40°C	Ambient	Biogas	Wastewater Solid Waste Manure
Dry Thermochemical	Torrefaction [28-29]	200 – 320°C	0.1 – 2.1	Biocoal	Wood Cornstover Switchgrass
	Fast Pyrolysis [30-31]	480 – 520°C	0.1 – 0.6 MPa	Biocrude Biogas	
Wet Thermochemical (HTT)	HTC [32]	150 – 250°C	0.1 – 5 MPa	Biocoal	Manure
	HTL [33]	250 – 450°C	5 – 25 MPa	Biocrude	Algae Wood
	HTG [34]	500 – 750°C	> 25 MPa	Biogas	Cornstover Food Waste

Thermochemical conversions occur at moderate to high temperatures. A difference in temperature, along with gaseous environment and pressure, are the primary parameters that dictate the phase and quality of the final products. Dry thermochemical conversions require feedstocks to be dry (< 10 wt% moisture) and often operate in the absence of oxygen for optimum product quality.[28-31] Torrefaction is a dry thermochemical conversion process that converts biomass into energy-dense, solid coal alternatives, or biocoal. Fast pyrolysis operates at higher temperatures (310–540°C) than torrefaction (200–320°C). At these higher temperatures and often short reaction times, the biomass is immediately volatized into a biogas. Besides serving as a bio-alternative to

syngas (CO, CO_2, and H_2), this gas can be condensed to a liquid petroleum-crude oil alternative, or biocrude. Because the finest products from fast pyrolysis and torrefaction occur with extremely dry feedstocks, they are often used with second- and some first-generation biomass.

Hydrothermal treatment (HTT) is the more common name for wet thermochemical conversion of biomass. As the name implies, HTT is reaction environment that incorporates water at elevated temperatures. Because it utilizes water as a reaction media, extensive drying of conventional feedstocks is not necessary. Thus, HTT is an ideal conversion technique for algal biomass. Similar to dry thermochemical methods, the temperature of the reaction dictates the phase of the final product. Figure 3 displays the phase diagram for water. Several HTT techniques and products are dependent on the properties of water at these temperatures and pressures.[35]

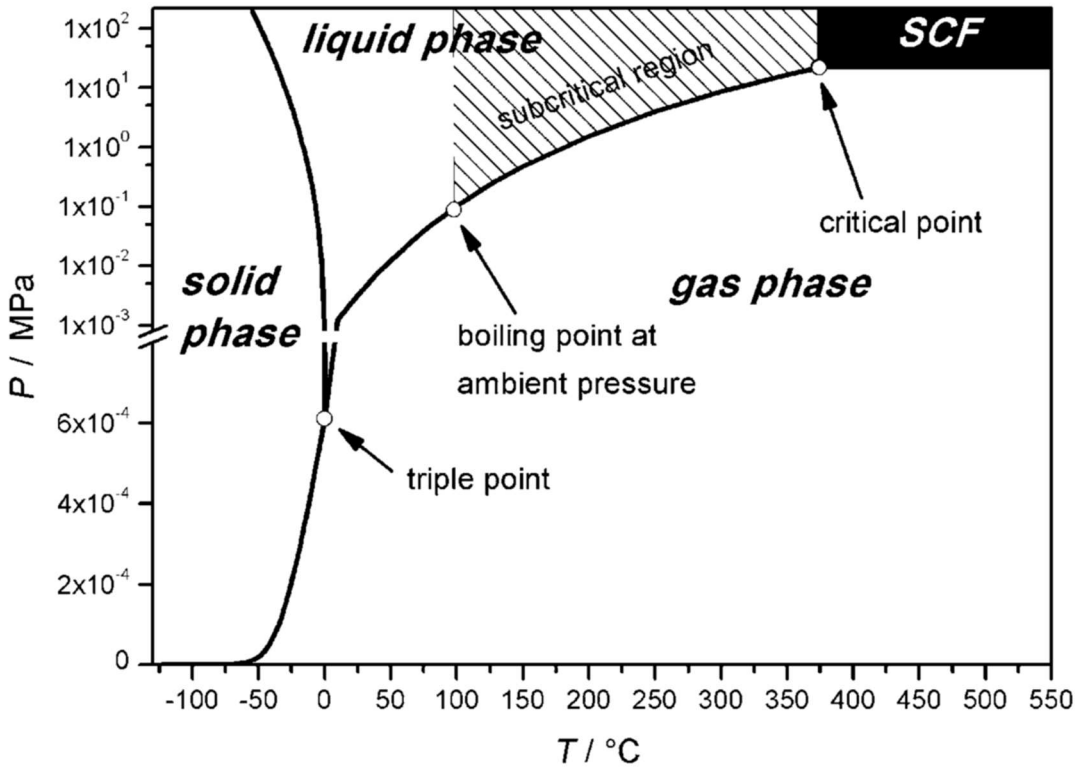

Figure 3: A phase diagram indicating the temperature (T) and pressure (P) of various phases of matter of water and the subcritical and supercritical (SCF) region for HTL and HTG conversion, respectively.

Hydrothermal carbonization (HTC) operates at the lowest temperatures (100–200°C). The primary feedstock for HTC is animal manure that is converted to a biocoal product. Hydrothermal gasification (HTG) occurs above the critical point (374°C; 22.1 MPa) of water and creates a biogas product. Hydrothermal liquefaction (HTL) utilizes subcritical water, as the operating temperature and pressure occur just below the critical point of water (200–350°C and 5–28 MPa) and is the principal conversion technique of this dissertation. The primary product of HTL is a biocrude oil; however, the subcritical environment of HTL also provides a favorable environment for inorganic, solid synthesis that this dissertation will also explore.

Subcritical water has many physical properties that make it beneficial for biomass conversion. Table 3 compares these different properties across the different temperature and pressure ranges of HTT biomass conversion.[36] A few noteworthy properties of subcritical water are the lower viscosity and dielectric constant and higher ionic product. A lower viscosity enhances the fluidity and ensuring an ease of flow of a biomass slurry and product stream. A lower viscosity fluid minimizes energy and operation costs associated with pumping a higher viscosity fluid such as algal slurries and crude oil at ambient temperatures. Second, the dielectric constant is associated with the number of hydrogen-bonds between water molecules. Thus, the lowering of this physical property increases the solubility of typically hydrophobic, molecules, such as lipids, and decreases the solubility of some inorganic salts.[35-37] Finally, the ionic product (K_w) is the ratio of H^+ and OH^- ions in the water. A higher K_w at subcritical conditions indicates a higher presence of these ions and thus promote a variety of acid/base catalysis. Collectively these properties make subcritical water an optimum, homogeneous reactive environment for biomass conversion and inorganic solid co-product synthesis.

Table 3: A comparison of the physical properties of water at ambient, subcrtical, and supercritical phases.

Properties	Ambient	Sub-critical		Super-critical	
Temperature °C	25	250	350	400	400
Pressure MPa	0.1	5	25	25	50
Density g cm^{-3}	1	0.8	0.6	0.17	0.58
Dielectric Constant F m^{-1}	78.5	27.1	14.1	5.9	10.5
Ion Product pK_w	14.0	11.2	12.0	19.4	11.9
Heat Capacity kJ kg^{-1} K^{-1}	4.22	4.86	10.1	13.0	6.8
Dynamic Viscosity mPa s	0.89	0.11	0.064	0.03	0.07

1.5 Collaboration

The nature of this research relied heavily upon the collaboration with environmental engineers. The main thrust of their work was the cultivation and water chemistry management of the algal media and biomass for optimum, aqueous nutrient recovery and HTL product formation. The primary thrust of this dissertation will then be focused on the organic, biocrude and solid, inorganic product from HTL treatment of these algal solids. To better comprehend the cause and creation of these HTL products a strong understanding and characterization of these algal solids is also required. Characterization of these algal solids were often divided between the collaboration. Thus, a clear distinction between the data that was collected and analyzed, or the conclusions drawn between the collaborator and the primary author of this dissertation will be clearly identified within the work of this dissertation.

1.6 Research Outline & Objectives

This dissertation will be framed in the following matter:

1. Focused motivation, background, and literature review
2. Algal solid and HTL product characterization methodology
3. Inorganic capture and yield for HTL solids
4. Inorganic and algal interactions at HTL conditions through model compounds
5. Inorganic speciation and characterization for HTL solids
6. Conclusions and future work

Given the abundant amount of prior research in HTL of algal biomass, the initial chapters will be an extensive literature review. Furthermore, this dissertation is a continuation of prior work; thus, the final observations, conclusions, and major research thrusts from the previous research and work on this topic will also be articulated in Chapter 2: *Literature Review*. The third chapter (Chapter 3: *Methods*) will describe the general methodology for algal cultivation and harvesting, HTL reactions and extraction procedures, and sample characterization. With a substantial and unique emphasis of this dissertation being the inorganics present both in the biomass and HTL products, an in-depth, descriptive methodology for these characterizations will be provided. Further sample characterization methods adopted from previous work will identified and cited for reference.

The following three chapters will be cumulative chapters that exhibit, explain, and discuss data collected for the primary research thrusts of this dissertation. The first research thrust, Chapter 4: *Inorganic Capture*, centers on the solid inorganic yield and capture from HTL of algal biomass. The second research thrust, Chapter 5: *Model Compounds*, is a model compound study that concentrates on the inorganic compounds identified in Chapter 4: *Inorganic Capture*. In addition

to inorganic, hydrothermal synthesis, the potential for catalysis and biocrude enhancement involved with said inorganics is also explored in Chapter 4. The third research thrust, Chapter 6: *Raceway*, goes more in-depth to the inorganic solid produced from HTL. Included in this chapter are the algal cultivation and harvesting techniques and their perceived influence during HTL and the resulting products. Although the research thrusts are centered upon the inorganic molecules, the organic biocrude product is often the underlined product of algal HTL conversion. Thus, the biocrude properties will also be compared in each research thrust. The final chapter (Chapter 7: *Conclusions and Future Work*) will then highlight key conclusions from these three research thrusts and the potential for future work.

1.7 References

1. Enriquez, J., Genomics and the World's Economy. *Science* **1998,** *281* (5379), 925.
2. Innovations at the Nexus of Food, Energy and Water Systems (INFEWS). NSF, Ed. 2018.
3. Innovations at the Nexus of Food, Energy and Water Systems (INFEWS). NSF, Ed. 2015.
4. Dybas, C.; Bates, S., NSF awards $36.6 million in new food-energywater system grants. 2017.
5. Dybas, C., New grants foster research on food, energy and water- a linked system. 2015.
6. Bates, S.; Dybas, C., NSF invests $72 million in innovations at nexus of food, energy and water systems. 2016.
7. Kummer, K. F.; Dawson, C. J. *Understanding Nitrogen and Its Use in Agriculture*; European Fertilizer Manufacturers' Association (EFMA): Brussels, Belgium, 2004.
8. Razon, L. F., Life cycle analysis of an alternative to the haber-bosch process: Non-renewable energy usage and global warming potential of liquid ammonia from cyanobacteria. *Environmental Progress & Sustainable Energy* **2014,** *33* (2), 618-624.
9. Mayer, B. K.; Baker, L. A.; Boyer, T. H.; Drechsel, P.; Gifford, M.; Hanjra, M. A.; Parameswaran, P.; Stoltzfus, J.; Westerhoff, P.; Rittmann, B. E., Total Value of Phosphorus Recovery. *Environ Sci Technol* **2016,** *50* (13), 6606-20.
10. Cordell, D.; Drangert, J.-O.; White, S., The story of phosphorus: Global food security and food for thought. *Global Environmental Change* **2009,** *19* (2), 292-305.
11. Steen, I., Phosphorus availability in the 21st century: Management of a non-renewable resource. *Phosphorus and potassium* (217).
12. Socolow, R. H., Nitrogen management and the future of food: Lessons from the management of energy and carbon. *Proceedings of the National Academy of Sciences* **1999,** *96* (11), 6001.

13. Rittmann, B. E.; Mayer, B.; Westerhoff, P.; Edwards, M., Capturing the lost phosphorus. *Chemosphere* **2011,** *84* (6), 846-53.
14. Carpenter, S. R.; Caraco, N. F.; Correll, D. L.; Howarth, R. W.; Sharpley, A. N.; Smith, V. H., NONPOINT POLLUTION OF SURFACE WATERS WITH PHOSPHORUS AND NITROGEN. *Ecological Applications* **1998,** *8* (3), 559-568.
15. Bellier, N.; Chazarenc, F.; Comeau, Y., Phosphorus removal from wastewater by mineral apatite. *Water Res* **2006,** *40* (15), 2965-71.
16. Li, W.-W.; Wen-Wei, L., Chemistry: Reuse water pollutants. *Nature (London) 528* (7580), 29-31.
17. Cordell, D.; Rosemarin, A.; Schroder, J. J.; Smit, A. L., Towards global phosphorus security: a systems framework for phosphorus recovery and reuse options. *Chemosphere* **2011,** *84* (6), 747-58.
18. Abdel-Raouf, N.; Al-Homaidan, A. A.; Ibraheem, I. B., Microalgae and wastewater treatment. *Saudi J Biol Sci* **2012,** *19* (3), 257-75.
19. Sturm, B. S. M.; Lamer, S. L., An energy evaluation of coupling nutrient removal from wastewater with algal biomass production. *Applied Energy* **2011,** *88* (10), 3499-3506.
20. Shurtz, B. K.; Wood, B.; Quinn, J. C., Nutrient resource requirements for large-scale microalgae biofuel production: Multi-pathway evaluation. *Sustainable Energy Technologies and Assessments* **2017,** *19*, 51-58.
21. Christenson, L.; Sims, R., Production and harvesting of microalgae for wastewater treatment, biofuels, and bioproducts. *Biotechnol Adv* **2011,** *29* (6), 686-702.
22. Bassam, N. E., Handbook of bioenergy crops. *London, Earthscan* **2010**.
23. Weyer, K. M.; Bush, D. R.; Darzins, A.; Willson, B. D., Theoretical Maximum Algal Oil Production. *BioEnergy Research* **2009,** *3* (2), 204-213.
24. DOE, U. S., National Algal Biofuels Technology Review. *Bioenergy Technologies Office* **2016**.
25. Mohd Azhar, S. H.; Abdulla, R.; Jambo, S. A.; Marbawi, H.; Gansau, J. A.; Mohd Faik, A. A.; Rodrigues, K. F., Yeasts in sustainable bioethanol production: A review. *Biochem Biophys Rep* **2017,** *10*, 52-61.
26. Kádár, Z.; Szengyel, Z.; Réczey, K., Simultaneous saccharification and fermentation (SSF) of industrial wastes for the production of ethanol. *Industrial Crops and Products* **2004,** *20* (1), 103-110.
27. Kim, M.-S.; Kim, D.-H.; Yun, Y.-M., Effect of operation temperature on anaerobic digestion of food waste: Performance and microbial analysis. *Fuel* **2017,** *209*, 598-605.
28. Zheng, A.; Zhao, Z.; Chang, S.; Huang, Z.; He, F.; Li, H., Effect of Torrefaction Temperature on Product Distribution from Two-Staged Pyrolysis of Biomass. *Energy & Fuels* **2012,** *26* (5), 2968-2974.
29. Agar, D.; DeMartini, N.; Hupa, M., Influence of Elevated Pressure on the Torrefaction of Wood. *Energy & Fuels* **2016,** *30* (3), 2127-2136.
30. Bridgwater, A. V., Review of fast pyrolysis of biomass and product upgrading. *Biomass and Bioenergy* **2012,** *38*, 68-94.
31. Noumi, E. S.; Blin, J.; Valette, J.; Rousset, P., Combined Effect of Pyrolysis Pressure and Temperature on the Yield and CO2 Gasification Reactivity of Acacia Wood in macro-TG. *Energy & Fuels* **2015,** *29* (11), 7301-7308.

32. Wang, T.; Zhai, Y.; Zhu, Y.; Li, C.; Zeng, G., A review of the hydrothermal carbonization of biomass waste for hydrochar formation: Process conditions, fundamentals, and physicochemical properties. *Renewable and Sustainable Energy Reviews* **2018,** *90*, 223-247.
33. Gollakota, A. R. K.; Kishore, N.; Gu, S., A review on hydrothermal liquefaction of biomass. *Renewable and Sustainable Energy Reviews* **2018,** *81*, 1378-1392.
34. He, C.; Chen, C.-L.; Giannis, A.; Yang, Y.; Wang, J.-Y., Hydrothermal gasification of sewage sludge and model compounds for renewable hydrogen production: A review. *Renewable and Sustainable Energy Reviews* **2014,** *39*, 1127-1142.
35. Moller, M.; Nilges, P.; Harnisch, F.; Schroder, U., Subcritical water as reaction environment: fundamentals of hydrothermal biomass transformation. *ChemSusChem* **2011,** *4* (5), 566-79.
36. Toor, S. S.; Rosendahl, L.; Rudolf, A., Hydrothermal liquefaction of biomass: A review of subcritical water technologies. *Energy* **2011,** *36* (5), 2328-2342.
37. Hodes, M.; Marrone, P. A.; Hong, G. T.; Smith, K. A.; Tester, J. W., Salt precipitation and scale control in supercritical water oxidation—Part A: fundamentals and research. *The Journal of Supercritical Fluids* **2004,** *29* (3), 265-288.

2 Literature Review

2.1 Previous Collaboration

The foundation of this dissertation comes from the initial work by the Feedstock to Tailpipe (FSTP) Initiative. As shown in Figure 4, FSTP was a highly collaborative effort that crossed a multitude of disciplines at the University of Kansas (KU). First environmental, wastewater engineers and ecology and evolutionary biologists evaluated microalgae's potential for nutrient remediation in wastewater, the speciation of algae present in wastewater, and finally the microalgae's physiological and biochemical composition.[1] Chemical engineers then collaborated with the prior groups to evaluate pre-processing techniques that would improve or enhance the

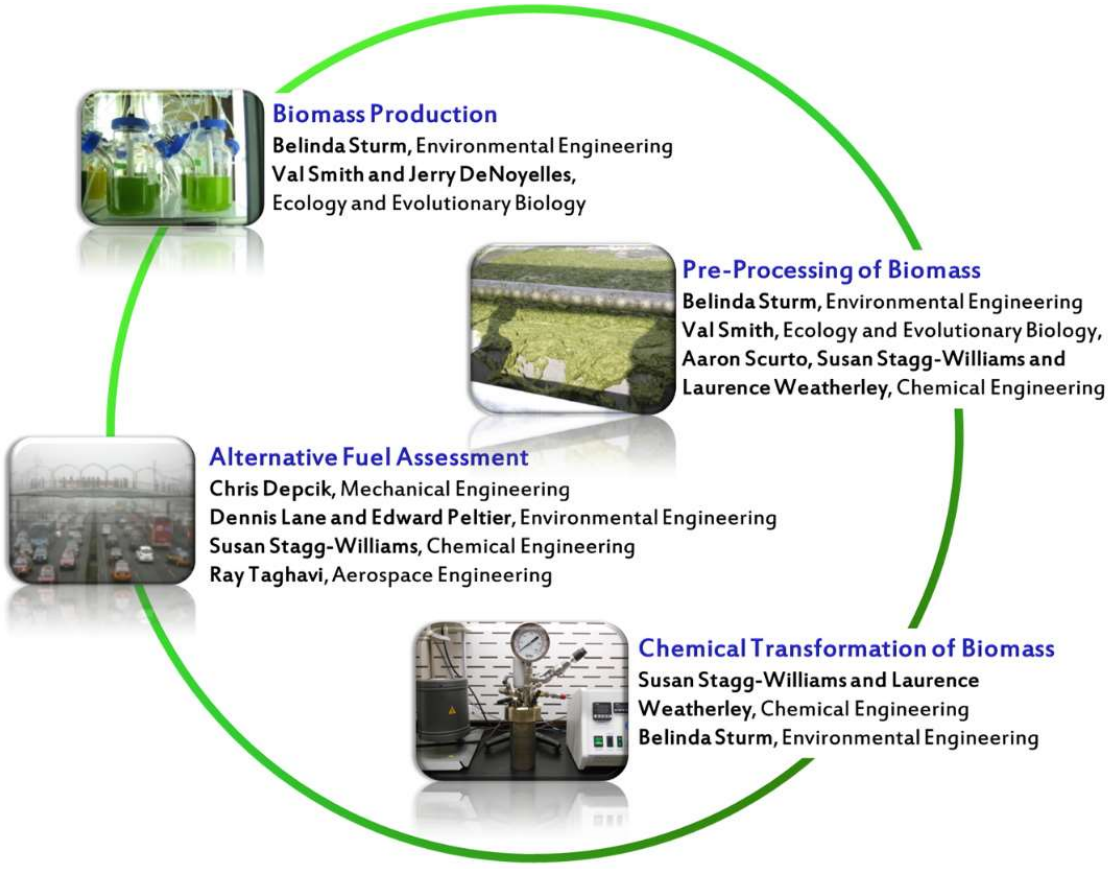

Figure 4: An illustration of the highly collaborative and cyclical-nature of the research thrusts from the Feedstock to Tailpipe (FSTP) Initiative at KU.

ensuing biomass to biofuel conversion process. Mechanical and aerospace engineers then tested the car and potential jet engine performance from the biofuels produced. Finally, air and emissions from these engines were monitored by environmental engineers.

This dissertation focuses and expands on the biomass production, pre-processing, and chemical transformation of wastewater-cultivated algal solids. The idea of utilizing wastewater as a nutrient source for algal biomass production stemmed from the observed negative environmental, energy, and economical impact the addition of external fertilizers has on algal production.[2] Thus, KU and the FSTP were one of the first groups to observe and record microalgae cultivation and biomass production potential in wastewater at a pilot-scale.[3] Additionally, because of the inter-disciplinary collaboration within FSTP, a "cradle-to-tailpipe" life cycle and energy evaluation could be performed.

2.2 Wastewater Algal Cultivation, and Biomass Production

For the pilot-scale study, 4 open-pond, 2,600-gallon bioreactors with a depth of 4 feet were installed following the secondary clarifier at the Lawrence Municipal WWTF. With a population of approximately 90,000 people the Lawrence WWTF treats an average of 12 million gallons of wastewater per day.[3] During the 6-month, April to October, study, the average nitrogen (N) and phosphorus (P) concentrations of the wastewater effluent was 19.5 ± 4.5 mg-N/L and 3.2 ± 0.9 mg-P/L for an average N:P molar ratio of 13.5. Atmospheric CO_2 provided carbon to the system. No additional CO_2 was added to the tank to limit operational, energy and additional materials costs.[3] Another important note on the supply of nutrients within the wastewater effluent is the N-speciation entering the algal, open pond, bioreactors. The Lawrence WWTF utilizes biological nitrification to oxidize the presence of ammonia (NH_3) to nitrate (NO_3^-) prior to the algal

bioreactors.[4] It was well-documented that for algal cultivation NO_3^- is a preferred N-compound over NH_3.[5-6]

Nutrient concentrations of the wastewater effluent are significant as they, along with carbon by means of CO_2 gas, often dictate the algal biomass productivity and biochemical content.[7-8] The Redfield ratio (N:P = 16) refers to the N:P molar ratio of both in algal growth media and solid biomass to determine N- or P-limitations. The widely accepted Redfield ratio, discovered by Alfred Redfield in 1958, is based on his empirical formula for microalgae ($C_{106}H_{263}O_{110}N_{16}P_1$).[7] Growth media and microalgae expressing a N:P ratio less than 16 are considered N-limited while media and biomass with a N:P ratio greater than 16 are considered P-limited. Finally, N-limited growth media, along with other growth factors such as light and temperature, often leads to high lipid content algal biomass that is ideal for potential biofuel production.[6, 8-11]

To initiate growth, the open pond bioreactors were seeded with five gallons of concentrated, mixed-species, algal inoculum that were collected from fertilizer-enriched ponds at the KU Field Station. After a 30-day accumulation period, a continuous flow was initiated with 10-day hydraulic residence time.[12] Biomass production from these wastewater effluent, algal growth ponds ranged from 0.78 – 15.9 g m^{-2} d^{-1} by dry weight. The total dissolved N and P removed during the 6-month experiment period was 19.0 ± 4.3% and 43.8 ± 8.6% respectively.[12] While the wastewater effluent and algal solid N:P ratio indicates a N-limited environment and biomass, the average lipid content was only 10 wt%.[3] This lipid content is much lower compared to the 30-50 wt% observed by other N-limited microalgae stated in the literature.[13-15] The cause for the lower lipid content in the wastewater-cultivated algal solids is the lack of CO_2 supplied to the wastewater bioreactors.[3] Because CO_2 was only supplied to via the atmosphere, the wastewater

bioreactors were exposed to substantially less carbon for lipid production compared to the CO_2-enriched tanks in aforementioned studies. [13-15]

The final, significant step for wastewater-cultivated algal solids is efficient harvesting techniques. Preparing microalgae from ponds to a convertible biomass resource is often a two-step process: thickening followed by dewatering. Chemical coagulation and flocculation are a favorable method for algal thickening technique that enables efficient, gravity separation or dissolved air flotation. From an energy requirement the gravity separation is advantageous over dissolved air flotation following chemical coagulation and flocculation of the algal biomass.[3] For optimum algal biomass conversion, further dewatering is required from 1-2% solids after dewatering. Belt filter press, centrifugation, and evaporation dewatering techniques have all been amenable. The most energetically-viable combination of thickening and dewatering of microalgae biomass was identified to be chemical flocculation and gravity sedimentation and finally belt filter press.[3] The wastewater-cultivated algal solids that were harvested from the Lawrence WWTF for this dissertation were collected by gravity sedimentation at the treatment facility and then dewatered through centrifugation in the laboratory at KU. Finally, to precisely control the solids to water weight loading for future biomass conversions, the centrifuged algal solids were freeze-dried and ground to a fine powder.[16]

2.3 Hydrothermal Liquefaction (HTL)

HTL conversion of biomass dates back to the early 1930's while the first observed commercial-scale practice of using HTL to convert cellulose to heavy oil was by the Pittsburgh Energy Research Centre in 1970.[17] By 1985, Beckman and Elliot at Pacific Northwest National Laboratory (PNNL) had evaluated the influence of key reaction parameters: time, pressure,

temperature, and the presence of catalysts on a biocrude yields and properties from a variety of biomass feedstocks.[18] A decade later, Minowa et al. discovered that the energy density of HTL biocrude produced from microalgae was similar in energy density and viscosity to petroleum crude, 36 kJ g^{-1} and 150-330 mPas.[19] Additionally, this same group recognized that the net energy from microalgae HTL biocrude is positive and renewable given the inputs from fertilization, cultivation, harvesting, and reaction.[20]

With these initial, positive results for a biomass feedstock and conversion combination between microalgae and HTL, further, in depth research was explored. In 2011, Biller and Ross published the first comprehensive study on the impact of algal biomolecules have on the HTL biocrude yield and properties from both model compounds and a variety of algal species.[21] They concluded what others in the literature had suspected, and that is microalgae with high lipid content had greater biocrude yields.[22-23] Furthermore, proteins and carbohydrates were the second and third biomolecules directly related to biocrude yield, respectively.[21] With this knowledge others have begun to model and predict the biocrude yield and properties from these algal biomolecules.[24-25] In addition to yield, biocrude properties such as energy density; carbon (C), hydrogen (H), nitrogen (N), and oxygen (O) content; and the specific organic compounds found in the biocrude are also important and are dictated by these algal biomolecules. Biller and Ross observed that lipids also produced the most ideal and optimum biocrude properties. These properties include a high H/C and low O/C molar ratio, which results in a higher energy density. In addition, the biocrude from HTL of lipid biomolecules is composed primarily of long chain hydrocarbons. The absence of N-containing compounds in the HTL biocrude is also ideal as nitrogen can create coking and catalyst deactivation during the oil refining process. Proteins, the second largest contributor to HTL biocrude yield in microalgae, produce these N-containing

compounds and phenols. Lastly, carbohydrates produce primarily O-containing compounds as a variety of ketones and furans. Exclusively, HTL of carbohydrates also produced a greater amount of solid and gaseous products than biocrude. Table 4 categorizes and summarizes the frequently observed organic compounds found in HTL biocrude produced from microalgae. In addition, the witnessed or perceived biomolecule, or combination of biomolecules, that correlates to the observed biocrude compounds is also included in Table 4.

The mechanistic pathway for how the algal biomolecules – carbohydrates, proteins, and lipids – decompose and rearrange to the final, observed biocrude compounds through hydrothermal treatment (HTT) was recently reviewed by Changi et al.[26] However, one of the largest challenges to grow and develop this technology into the bioeconomy is determining ways to enhance and upgrade the HTL biocrude from microalgae so that it could be used as an alternative to petroleum-crude in existing refineries. There has been extensive work with the addition of several different heterogeneous and homogeneous catalyst and additional thermochemical treatment to improve the oil properties. This includes not just increasing biocrude yields but minimizing O- and N-containing compounds and maximizing the C/H molar ratios.

2.4 HTL Biocrude Upgrading

In Biller and Ross' initial, 2011 HTL study of algal biomolecules, they also observed the impact of various external heterogeneous (sodium carbonate; Na_2CO_3) and homogeneous (formic acid; HCOOH) catalysts on the final biocrude product.[21] They later expanded on this work with the use of alkali metal, potassium hydroxide (KOH) catalyst and another organic acid – acetic acid (CH_3COOH).[23] Key conclusions from these studies were that the organic acids behaved more as

Table 4: Prevalent organic compounds observed in HTL biocrude produced from algal model compounds.

HTL BIOCRUDE	ALGAL BIOMOLECULE				Source
Organic Compounds	Lipid (L)	Protein (P)	Carbohydrate (C)	Other	
Mono-aromatics					
Phenol		**X**			[21, 27]
Benzene/Toluene/Styrene			**X**	L + P	[21]
Cholesterol/Cholestorene	**X**			Cholesterol	[26]
Vitamin E	**X**				[28]
Fatty Acids					
Octanoic (C_8)	**X**			P + C	[21]
Myristic Acid (C_{14})	**X**				[22]
Palmitic Acid (C_{16})	**X**				[21, 26, 27]
Stearic/Oleic Acid (C_{18})	**X**				[21, 26, 27]
Archidic Acid (C_{20})	**X**				[29]
Eicosapentaeonic Acid (C_{20})	**X**				[22]
Alkane/Alkene					
Hexadecane (-ene) (C_{16})	**X**			L + C	[21]
Heptadecane (-ene) (C_{17})	**X**				[21, 27]
Pentadecane (-ene) (C_{15})	**X**				[21]
Phytane (-ene) (C_{20})				Chlorophyll	[26, 28]
Docosane (C_{22})	**X**				[30]
Cholestane				Cholesterol	[30]
> C_{20}	**X**				[29]
Polyaromatic Ring					
Naphthalene				Whole cell	[31, 32]
Quinoline				Whole cell	[32]
Nitrogen Compounds					
Piperidines		**X**			[21, 26, 27]
Pyrroles/Pyrrolidines		**X**			[21, 26, 27]
Indoles		**X**			[21, 26, 27]
Pyrazines		**X**			[27]
Pyrrolidinones		**X**			[21, 26, 27]
Hexadecanamide		**X**			[26, 27]
Amines		**X**			[32]
Nitriles		**X**			[32]
Oxygen Compounds					
Aldehydes		**X**			[26]
Ketones			**X**	P + C	[21, 26, 27]
Furans			**X**		[27]

reagents than catalysts by combining with the biocrude phase thus, artificially increasing the biocrude yield.[23] In addition, higher gas yields were observed with the use of organic acids compared to the control and heterogeneous catalyst.[21]

Sodium carbonate, however, showed great promise. It increased biocrude yields with carbohydrate model compounds: glucose and cellulose. In addition, less nitrogen was recovered in biocrude when Na_2CO_3 was added than when it was absent. The cause for the improved biocrude yields and properties from Na_2CO_3 is hypothesized to be from a water-gas shift reaction. More details on the mechanism and how a water-gas shift reaction benefits biocrude yield and properties is discussed later in the chapter. Similarly, with sunflower oil, a lipid algal model compound, long-chain alkanes and alkenes were observed in the presence of Na_2CO_3 rather than their O-containing, fatty acid counterpart.[21] The secondary study verified these positive results for both Na_2CO_3 and KOH with a microalgal species, *Chlorella vulgaris*, and a cyanobacteria species, *Spirulina,* for which both have a low lipid and high carbohydrate and protein biomolecular content. Furthermore, this study reported the highest energy density, 33 – 40 MJ kg^{-1}, in the biocrude from the use of these catalysts on microalgae of this biomolecular content.[23]

Duan and Savage similarly experimented with noble metal catalysts.[29] Although no substantial changes in biocrude yield were observed from the addition of the catalysts, platinum (Pt), nickel (Ni), and cobalt molybdenum (CoMo) were able to reduce the O/C ratios of the HTL biocrude from *Nannochloropsis sp.* microalgae.[29] In the case where a Pt-catalyst was utilized, it was especially noted that a greater amount of fatty acid, lipid molecules were converted to long chain alkanes, which agrees with previous studies.[33] Ruthenium (Ru) and Ni catalysts also displayed a decreased the N wt% in comparison to the control.[29] Lastly, Duan and Savage were

one of the first to propose the potential for a water-gas shift (WGS) reaction, Equation (1), to occur during the hydrothermal treatment of microalgae.

$$CO + H_2O \rightarrow CO_2 + H_2 \quad (1)$$

The greater presence of carbon dioxide (CO_2) and hydrogen (H_2) produced from a WGS reaction *in-situ* can play a vital role in the synthesis of a high-valued solid product and upgrading the biocrude.

With the primary aim to reduce O- and N-content of the HTL biocrude oil from microalgae, Na_2CO_3 had greater interest due to its success in decreasing the O-content of biocrude produced from the fast pyrolysis of lignocellulosic biomass.[34-36] Shakya et al. further confirmed that Na_2CO_3 reduces the O-content of HTL biocrude by transforming the fatty acid compounds from lipids to alkanes and alkenes.[37] Furthermore, they also confirmed that Na_2CO_3 increased the biocrude yield for microalgae with high carbohydrate content.[37] Jena et al. observed a similar phenomenon with biocrude yield from Na_2CO_3; however, they observed the opposite results regarding O- and long-chain hydrocarbon content from the presence of Na_2CO_3.[32] Biocrude produced in the presence of Na_2CO_3 had over double the amount of carboxylic acids than without a catalyst, and thus a higher O-content as well.[32]

The success of Na_2CO_3 as a catalyst for *in-situ* HTL biocrude upgrading continued to be attributed to the WGS reaction. As shown in Equation (1), the primary products of a WGS are CO_2 and H_2 gas. Thus, Lee et al. studied the impact of initially pressurizing the HTL reactions with CO_2 and observed a reduction in several N-containing compounds and a few O-containing compounds in the biocrude as well.[38] In addition, a greater amount of alkanes and alkenes were also observed from the additional CO_2 pressure.[38] Duan and Savage also experimented with the presence of H_2 in their reactions with or without heterogeneous catalysts. While they observed an

increase in H/C molar ratio and a greater number of H-containing compounds in their HTL biocrude from the presence of H_2 gas and absence of a heterogeneous catalyst, the increase was minimal in comparison to that observed by Lee et al. with CO_2.[29, 38] Overall, these results of improved HTL biocrude properties from the presence of CO_2 and H_2 indicate that an *in-situ* WGS reaction can benefit the biocrude quality.

Another potential biocrude upgrading technique is a secondary thermal treatment of the HTL biocrude product. The primary objective of this techniques is to break apart and reduce the number of large molecular weight compounds in the biocrude. Lower molecular weight compounds are more ideal for traditional, existing oil refineries, as the biocrude oil is more volatile and less viscous. In addition, thermal treatment can also remove the unnecessary heteroatoms, N and O, from the biocrude as previously discussed.

Roussis et al. at Sapphire Energy, one of the first to commercialize the algal HTL technique, pioneered this upgrading technique where they thermally treated algal HTL biocrude at 350, 400, and 450°C for 60 minutes.[39] With each increase in temperature, they observed a decrease in the vacuum gasoline (340-540°C) distillation fraction and increases in the heavy naphtha (< 190°C), kerosene (190-270°C), and gasoline (270-343°C) fractions. Furthermore, the O-content of the initial algal HTL biocrude decreased dramatically, 5.7 to 0.2 wt%, while the C-content increased, 78 to 84 wt%.[39] Meanwhile the H- and N-content remained relatively the same: 11.7 and 4.2 wt%, respectively. However, gas chromatography mass spectrometry (GC-MS) of the biocrude identified that the number of amides and fatty acids compounds decreased while saturated hydrocarbons increased with thermal treatment.[39] Zhao et al. observed similar results when upgrading their algal HTL biocrude; however, they added an initial 4 MPa of hydrogen (H_2) to their thermal upgrading reactor. This addition of H_2 resulted a decrease in N wt% and increase in

H wt% of the final, upgraded biocrude that was not seen by Roussis et al. Finally, Roussis et al. also proposed a general mechanism for the upgrading of the abundance of fatty acids and amides present in initial, algal HTL biocrude shown in Figure 5.[39]

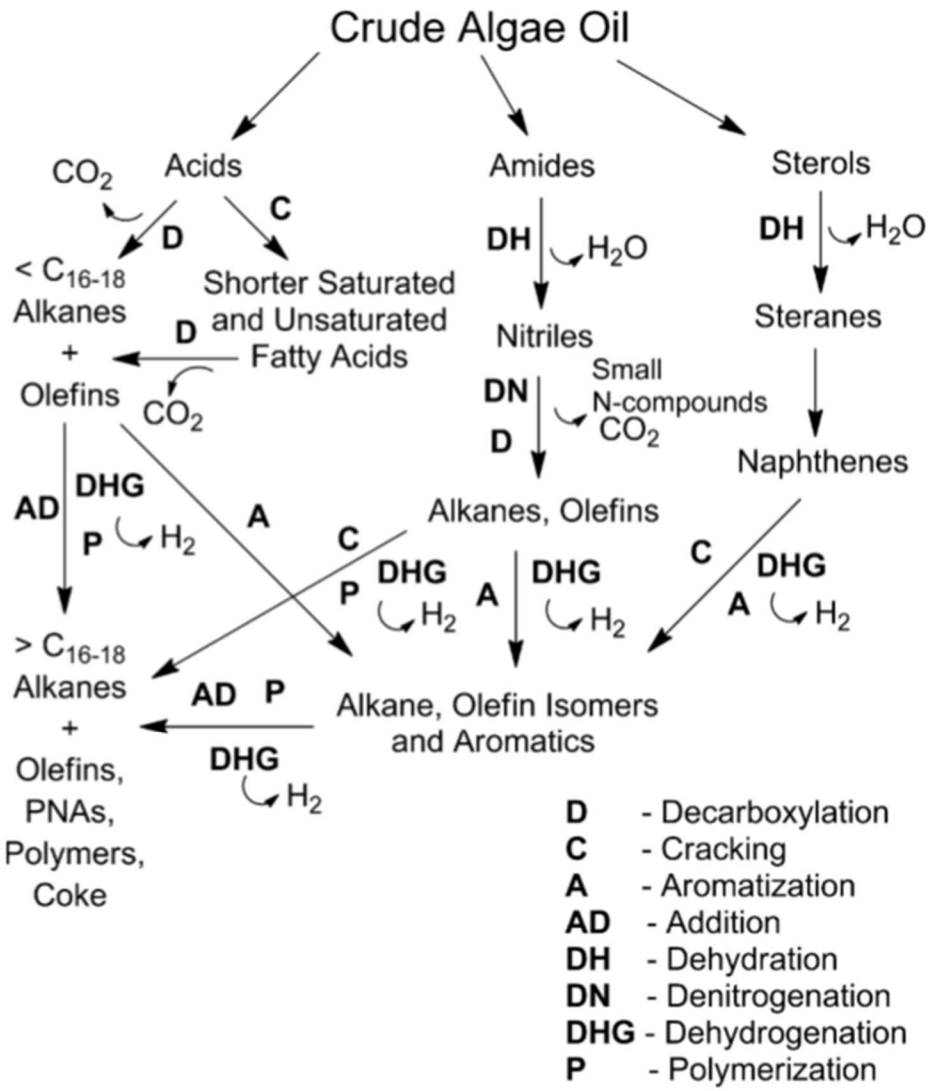

Figure 5: General mechanism proposed by Sapphire Energy for algal HTL biocrude upgrading through various decomposition reaction of fatty acids, amides, and sterols proposed.

2.5 Conventional, Fast-Batch, and Continuous HTL

In addition to achieving a biocrude product that is similar and a valid alternative to petroleum-crude oil, a secondary challenge is optimizing the algal HTL conversion technique. It had been identified by several groups that the ideal reaction time and temperature for algal HTL conversion was between 300-350°C for one hour.[21-23, 40] This slow, batch reaction is unideal for the efficiency needed for commercialization and is often referred to as "conventional HTL." Thus, continuous and fast-batch HTL has been further explored. Faeth et al. proposed the idea of fast-batch HTL when they realized the HTL reactor contents reached reaction temperature within a few minutes of being inserted into a preheated sand bath.[41] They observed biocrude yields of 38, 50, and 45 on an ash-free, dry weight (afdw%) basis after only a 3 minute reaction time at preheated sand bath of 300, 400, and 500°C respectively. Furthermore, biocrude yields of 55 and 66 afdw% were achieved within one minute for preheated sand bath temperatures of 500 and 600°C respectively.[41] Faeth et al. also reported the energy density of the fast-batch HTL, 1 to 5 minute reaction times, to be between 33–37 MJ/kg, and that was agreeable with the 34–38 MJ/kg observed with conventional HTL.[41]

Fast-batch HTL is an excellent simulation for the short residence times observed for continuous HTL; however, differences in yield and biocrude properties can still be observed. Jazrawi et al. observed biocrude maximum yields of 42 afdw% at their most extreme, continuous reaction conditions of 350°C, 3-minute residence time, and 10 wt% solids loading.[42] Biller et al. also observed biocrude yields near 40 afdw% at 350°C, 1- to 6-minute residence time, and 10 wt% solids loading from continuous HTL of microalgae.[43] Finally, Elliot et al. observed biocrude yields near 64 afdw% from 350°C, 15-minute residence time, and 17-35 wt% solids loading.[44] Thus, in a recent review of continuous HTL of biomass, it was concluded that higher algal biomass loading

and severe reaction conditions led to higher biocrude yields for continuous HTL of microalgae, which disagrees with the results observed from fast-batch HTL.[45] The biocrude properties from continuous HTL, however, were similar to fast-batch. Jazrawi et al. and Biller et al. both reported initial biocrude energy densities in the low- to mid-30 MJ/kg while Elliot et al. were closer to 40 MJ/kg.[42-44]. The improved biocrude quality observed by Elliot et al. was attributed to the higher residence time and a gravitational-extraction method of the biocrude as opposed to the traditional solvent-extraction.[45] Lastly, in two out of the three previously mentioned studies a secondary hydrogen treatment was performed at 350-405°C in the absence and presence of various heterogeneous catalysts.[43-44] This resulted in reduction of N- and O-content to below 1 and 2 wt% respectively in the final, hydrotreated biocrude and over 90 wt% of the biocrude boiling and distilling off below 350°C.[43-44]

In addition to HTL reaction system, how the biocrude is separated and extracted from the other HTL products has also shown to play a substantial role for both biocrude yield and properties. As previously mentioned, Elliot et al. observed higher yields and higher quality biocrude from their gravitational and solvent-free extraction.[44] Xu and Savage explored this further by comparing biocrude yields and properties from conventional HTL of microalgae that were extracted with a solvent, dichloromethane (DCM). They extracted the biocrude by adding DCM in the presence and absence of the secondary aqueous coproduct (ACP) and referred to the products as water-soluble and water-insoluble biocrude, respectively.[30, 46] A slight increase in biocrude yields were observed when DCM was added with the aqueous coproduct, as the DCM is able to extract organic, biocrude compounds from the aqueous coproduct. However, the biocrude compounds from the ACP were reported to have an abundance of N- and O-heteroatoms and lower energy density.

Thus, it was concluded that a small sacrifice for biocrude yield from water-insoluble biocrude was advantageous for the benefit of improved biocrude properties.[30, 46]

2.6 Wastewater-Cultivated Algal Solids and HTL Products

Researchers in the FSTP collaboration at KU were some of the first to explore and characterize wastewater-cultivated algal solids and the resulting products from HTL. Seventeen different algal species were identified from microscopic analysis of the wastewater-cultivated algal solids harvested from the Lawrence Municipal WWTF (Table 5).[16] This mixed-culture of algal species is unique compared to the several, aforementioned, monoculture (i.e. single-species) algal and HTL studies. Another unique characteristic of wastewater-cultivated algal solids compared to those in the literature was a considerably higher inorganic, noncombustible ash content.

Table 5: The 17 microalgae species identified from wastewater-cultivated algal solids harvest at the Lawrence WWTF.

Wastewater-Cultivated Microalgae Species	
Scenedesmus quadricauda	*Cyclotella* sp.
Scenedesmus bijuga	*Cladophora* sp.
Micractinium pusillum	*Selenastrum* sp.
Pediastrum boryanum	*Cosmarium* sp.
Golenkinia radiata	*Microcystis* sp.
Oscillatoria sp.	*Oedogonium* sp.
Merismopedia sp.	*Spirogyra* sp.
Chlorella sp.	[D] *Navicula* sp.
Cryptomonas sp.	

Wastewater-cultivated algal solids were 29 dw% ash where previous algal biomass were 5 dw% or less.[16] Higher ash content of 25-30 dw% is observed in marine macroalgae due to the high concentration of sodium and other water-soluble cations.[47]

The high ash content observed in wastewater-cultivated algal solids studied at KU was due to the abundance of calcium and silica.[16] The copious amounts of calcium in the wastewater-cultivated algal solids can be attributed to the addition of lime, $Ca(OH)_2$, that is added during wastewater treatment to increase the buffering capacity, or alkalinity, of the wastewater. Maintaining a stable pH is critical for the microorganisms that provide the biological nutrient removal at a WWTF. The Lawrence WWTF adds approximately 2,000 pounds of lime per day to maintain an average alkalinity of 120 mg/L $CaCO_3$.[48] While over a third of the inorganic material of wastewater-cultivated algal solids was observed to be calcium[16], the speciation or complementing anion with the calcium cation and the mechanism for how it appeared or was captured in the wastewater-cultivated algal solids was not reported. Another third of the wastewater-cultivated algal solids inorganic wt% was silica, and this is attributed to the presence of diatoms in the mixed-culture wastewater-cultivated algal solids. Diatoms are a class of microalgae that utilize silica to construct their cell walls. The remaining and noteworthy metals of the wastewater-cultivated algal solids inorganic content were phosphorus (16 wt%), sulfur (5 wt%), potassium (3 wt%), and magnesium (2 wt%).[16]

Given the unique low lipid and high carbohydrate, protein, and inorganic content of the wastewater-cultivated algal solids, the HTL products were also distinctive. The biocrude yield ranged from 30-40 afdw%, which is similar to other reported biocrude yields of low-ash, single-species, and high-lipid microalgae.[21-22] The HTL solids yield also averaged near 14 afdw% which is expected given the initial high inorganic, ash content in the wastewater-cultivated algal solids.[48]

It has been further estimated that 6-9 barrels of biocrude oil and greater than 1,500 kg of HTL solid products could be produced daily from a algal solid biomass cultivated from a municipal WWTF similar in size to that of Lawrence (90,000 people; 12 million gallons day^{-1} treated).[16]

The most notable differences were observed in the biocrude properties and HTL solid characterization. First, the O/C and H/C ratio was more optimum for biocrude produced by the wastewater-cultivated algal solids than other HTL and pyrolysis biocrude resulting in a better HHV as well.[16] Furthermore, the GC-MS and simulated distillation spectra showed great promise to *in-situ* biocrude upgrading. A noticeable reduction of fatty acid amides (e.g. hexadecanamide) and augmentation of methyl amines were observed in the GC-MS spectra of the wastewater-cultivated algal solids.[48] Moreover, the simulated distillation spectra of the raw HTL biocrude from wastewater-cultivated algal solids showed greater resemblance the thermally treated and upgraded HTL biocrude by Roussis et al. with Sapphire Energy (Figure 6).[39, 48] Denoted RN-Biocrude, the HTL biocrude produced from wastewater-cultivated algal solids had a reduced mass % at the higher and less desirable distillate fractions (630-1,020 and > 1,020°F) and a higher mass % at the lower, more desirable distillate fractions (104-260, 260-400, and 400-490°F).[39, 48] It was further hypothesized that the high quantity of inorganic solids could be acting as a catalysis and upgrading the HTL biocrude *in-situ* from the high-ash, wastewater-cultivated algal solids.[48]

With the hypothesis that the inorganic HTL solids could be acting as an *in-situ* catalysis, further investigation and characterization of these HTL products was necessary. X-ray diffraction (XRD), scanning electron microscopy (SEM), SEM with electron dispersive spectroscopy (SEM-EDS), and transmission electron microscopy (TEM) provided such insight. Figure 7a depicts the XRD pattern for the HTL solids produced by wastewater-cultivated algal solids. The XRD pattern clearly indicates the primary crystalline structure to be hydroxyapatite (HAp), $Ca_5(PO_4)_3OH$. SEM

and TEM images further verify the occurrence of HAp within HTL solids by displaying the flower- or petal-like morphology at the micron-scale (Figure 7b) and the rod-like morphology at the nano-scale (Figure 7c), respectively. Finally, Figure 7d shows the high degree of elemental-substitution prevalent in the HAp, HTL solid structure via SEM-EDS.[48]

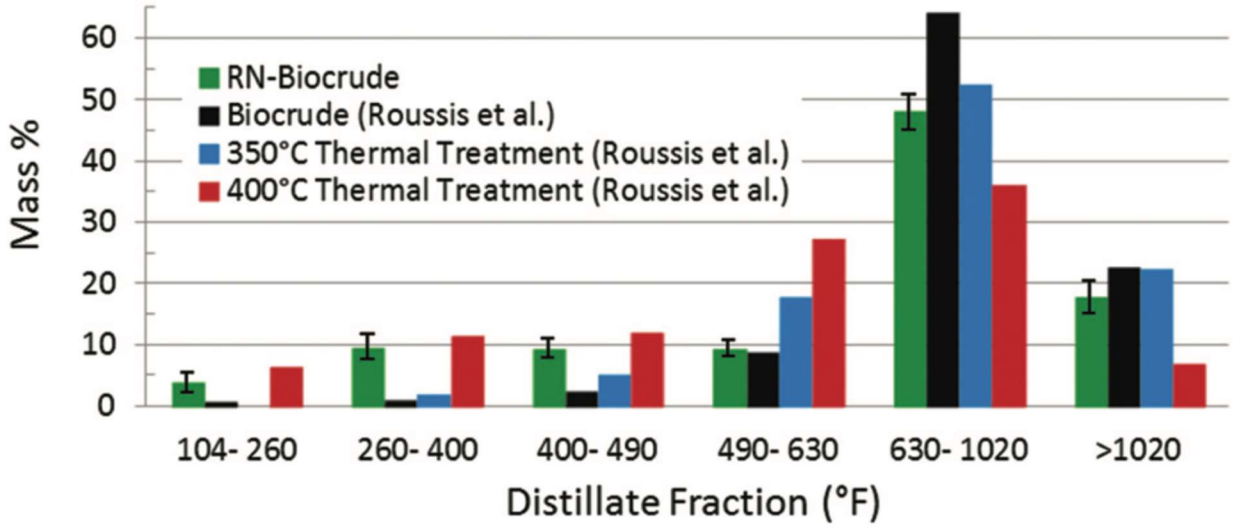

Figure 6: Simulated distillation spectra of wastewater-cultivated algal solids reviuproduced HTL biocrude (RN-biocrude) compared to the raw and thermally-treated and upgraded HTL biocrude by Roussis et al.

Primarily used for bone or dental tissue regeneration, HAp is also a viable catalyst or soil amendment and fertilizer. Preliminary studies indicated the ability for cell regeneration to occur on the HAp HTL solids.[48] Additional literature also reports the ability of HAp and tricalcium phosphate (TCP), $Ca_3(PO_4)_2$ to act as a catalysts. The amenable acid/base properties of HAp due to its high affinity for ion substitution make it an ideal, green catalyst for biocrude upgrading,[32] dehydration of carboxylic acids,[49] alcohol coupling,[50] and WGS reactions.[51] Finally, HAp and TCP are highly insoluble; thus, they are a preferred phosphorus fertilizers with minimal probability of end up in various water bodies due to agricultural runoff.[52] Due to the high amount of inorganics both in the wastewater-cultivated algal solids and HTL solids and the great potential for a variety

of applications through the solid, calcium phosphate products, further investigation how the inorganics were captured and transformed through HTL is critical.

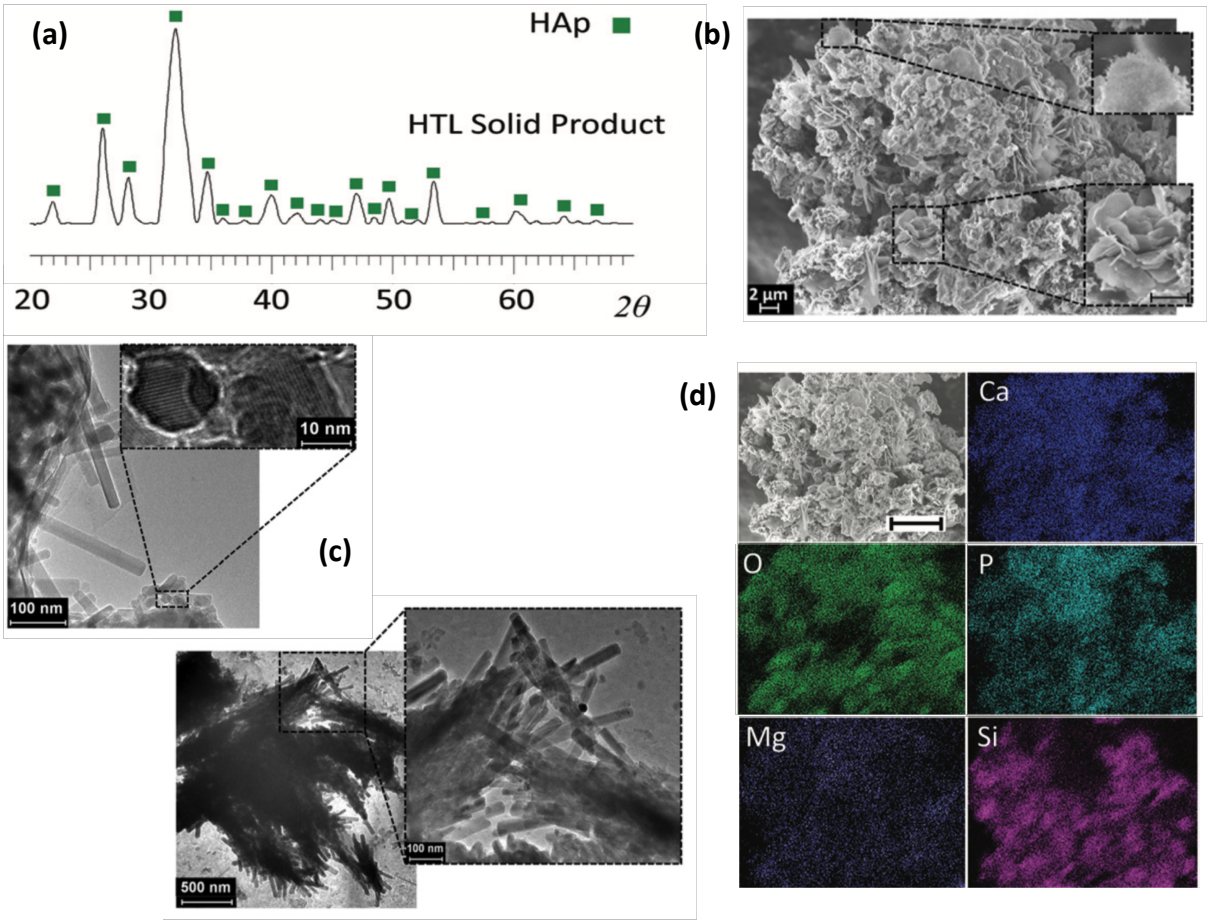

Figure 7: (a) XRD pattern indicating the hydroxyapatite (HAp) to be the prevalent crystalline structure and identity of the HTL solids. (b) SEM images of the HTL solids show flower or petal morphology at the micron-scale. (c) TEM images indicate a rod- like morphology at the nano-scale. (d) SEM-EDS displays the high degree of elemental substitution within the HAp crystal structure.

2.7 Hydrothermal Synthesis of HAp

With the observation of hydroxyapatite in the HTL solids, a greater understanding of inorganic transformation and synthesis in subcritical water is desired. While simple chemical precipitation has been the primary method for HAp synthesis, hydrothermal synthesis has grown

in popularity. Sadat-Shojai et al. reported that 14% of the publications between 1999-2011 regarding HAp synthesis utilized a hydrothermal method. This was the third most common method following chemical precipitation (25%) and a combination of precipitation and hydrothermal synthesis methods (16%).[53] Hydrothermal synthesis is advantageous over traditional precipitation as one can more easily control the morphology and other properties of the HAp product.[53] Typically involving a combination of calcium (Ca^{2+}) and phosphate (PO_4^{3-}) ions, reaction parameters such as pH, temperature, and time all play a critical role in the final HAp morphology. Sadat-Shojai et al. best summarized the resulting morphologies from various reaction parameter shown in Figure 8.[53-54] In addition to rod-, plate-, and leaf-life structures Sadat-Shojai also recounted a variety of spherical morphologies including uniqe dandelion and flower stuctures from hydrothermal synethesis of HAp shown on the right.[53]

Unsurprisingly, there is discrepancy regarding the optimum reaction conditions given the large number of dependent variables and subsequent morphologies. For this work, reaction time and temperature are held constant; therefore, the initial calcium and phosphate reactants and pH are the primary focus. It is well-accepted that the initial step for HAp synthesis is the presence of free Ca^{2+} and PO_4^{3-} ions; therefore, a majority of the literature on hydrothermal HAp synthesis includes highly soluble forms of calcium and phosphate. Calcium nitrate ($Ca(NO_3)_2$) and calcium chloride ($CaCl_2$) are two of the most common Ca-reagents while sodium and ammonia phosphate and phosphoric acid are common PO_4-reagents.[53] Calcium carbonate ($CaCO_3$) is an additional, popular Ca-reagent, for carbonate-substituted HAp has been shown to be more beneficial for biomaterial applications.[55-56] Furthermore the high insolubility of $CaCO_3$ in water, especially at elevated temperatures,[57] allows for greater control or fine tuning of the final HAp morphology as opposed to the sometimes unpredictable, more soluble reagents.[58-61]

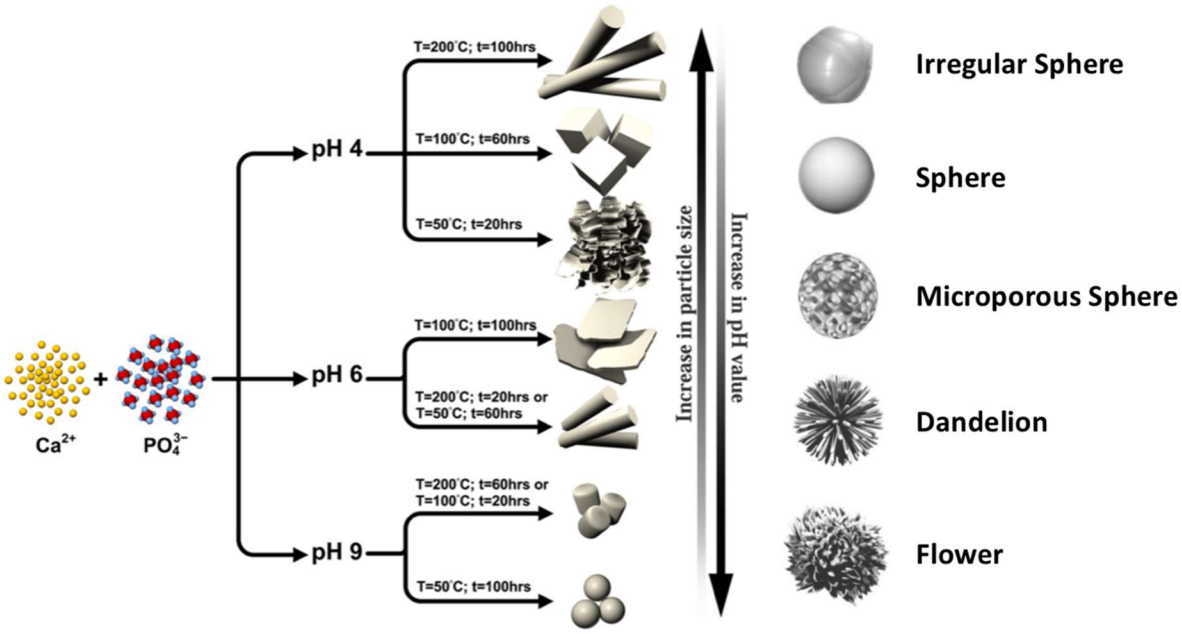

Figure 8: Common morphologies observed from the hydrothermal synthesis of HAp from aqueous Ca and PO_4 precursors.

With the solubility of the initial reagents being key to the hydrothermal synthesis of HAp and calcium phosphates, pH can also substantially dictate the morphology and structure of the final product. For example, Yoshimura et al. observed leaf-like morphology when using phosphoric acid (H_3PO_4) to hydrothermally synthesize HAp from $CaCO_3$.[58] Meanwhile, Kim et al. observed more rod- and dandelion-like morphologies when using diammonia hydrogen phosphate, $(NH_4)_2HPO_4$.[61] Figure 9 shows SEM images depicting these unique morphologies while the XRD pattern of each remained a uniform, HAp structure in both studies.[58, 61]

Besides H^+ and OH^-, which are measured by pH, the presence of other ions can also govern the solubility of the initial materials and ultimately the final morphology and structure of the final products. This is especially true for HAp and the great potential for ionic substitution within its structure. Furthermore, it has been previously shown that a vast number of inorganics are captured

by wastewater-cultivated algal solids and retained in the final HTL solid product. The literature confirms this capture and substitution phenomena for magnesium[62] and silica[63-64] via hydrothermal synthesis of HAp. The ensuing chapters of this dissertation further explore this unique, simultaneous combination of calcium phosphate synthesis and biocrude production through hydrothermal conversion of wastewater-cultivated and high-ash algal solids.

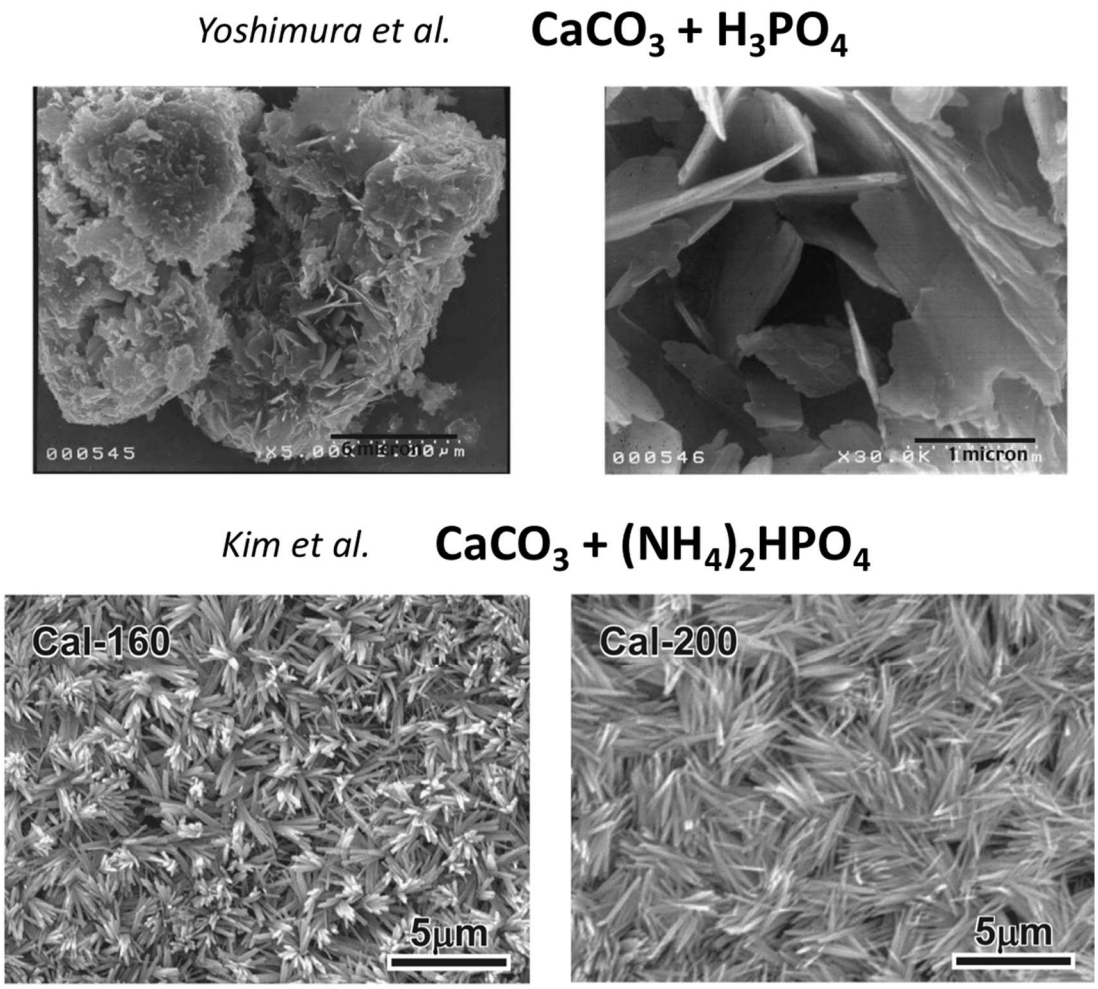

Figure 9: SEM images collected by Yoshimura et al. and Kim et al. depicting the unique HAp morphologies from utilizing acidic (H_3PO_4) and basic ($(NH_4)_2HPO_4$) phosphate reagents.

2.8 References

1. Smith, V. H.; Sturm, B. S.; Denoyelles, F. J.; Billings, S. A., The ecology of algal biodiesel production. *Trends Ecol Evol* **2010,** *25* (5), 301-9.
2. Clarens, A. F.; Resurreccion, E. P.; White, M. A.; Colosi, L. M., Environmental Life Cycle Comparison of Algae to Other Bioenergy Feedstocks. *Environmental Science & Technology* **2010,** *44* (5), 1813-1819.
3. Sturm, B. S. M.; Lamer, S. L., An energy evaluation of coupling nutrient removal from wastewater with algal biomass production. *Applied Energy* **2011,** *88* (10), 3499-3506.
4. Zhu, X.; Burger, M.; Doane, T. A.; Horwath, W. R., Ammonia oxidation pathways and nitrifier denitrification are significant sources of N₂O and NO under low oxygen availability. *Proceedings of the National Academy of Sciences* **2013,** *110* (16), 6328.
5. Abeliovich, A.; Azov, Y., Toxicity of ammonia to algae in sewage oxidation ponds. *Applied and Environmental Microbiology* **1976,** *31* (6), 801-806.
6. Chen, M.; Tang, H.; Ma, H.; Holland, T. C.; Ng, K. Y.; Salley, S. O., Effect of nutrients on growth and lipid accumulation in the green algae Dunaliella tertiolecta. *Bioresource technology* **2011,** *102* (2), 1649-55.
7. Redfield, A. C., THE BIOLOGICAL CONTROL OF CHEMICAL FACTORS IN THE ENVIRONMENT. *American Scientist* **1958,** *46* (3), 230A-221.
8. Rhee, G. Y., Effects of N:P atomic ratios and nitrate limitation on algal growth, cell composition, and nitrate uptake 1. *Limnology and Oceanography* **1978,** *23* (1), 10-25.
9. Tedesco, M. A.; Duerr, E. O., Light, temperature and nitrogen starvation effects on the total lipid and fatty acid content and composition ofSpirulina platensis UTEX 1928. *Journal of Applied Phycology* **1989,** *1* (3), 201-209.
10. Gordillo, F. J. L.; Goutx, M.; Figueroa, F. L.; Niell, F. X., Effects of light intensity, CO2 and nitrogen supply on lipid class composition of Dunaliella viridis. *Journal of Applied Phycology* **1998,** *10* (2), 135-144.
11. Ördög, V.; Stirk, W. A.; Bálint, P.; Aremu, A. O.; Okem, A.; Lovász, C.; Molnár, Z.; van Staden, J., Effect of temperature and nitrogen concentration on lipid productivity and fatty acid composition in three Chlorella strains. *Algal Research* **2016,** *16*, 141-149.
12. Sturm, B. S. M.; Peltier, E.; Smith, V.; deNoyelles, F., Controls of microalgal biomass and lipid production in municipal wastewater-fed bioreactors. *Environmental Progress & Sustainable Energy* **2012,** *31* (1), 10-16.
13. Emdadi, D.; Berland, B., Variation in lipid class composition during batch growth of Nannochloropsis salina and Pavlova lutheri. *Marine Chemistry* **1989,** *26* (3), 215-225.
14. Fábregas, J.; Maseda, A.; Domínguez, A.; Otero, A., The cell composition of Nannochloropsis sp. changes under different irradiances in semicontinuous culture. *World Journal of Microbiology and Biotechnology* **2004,** *20* (1), 31-35.
15. Suen, Y.; Hubbard, J. S.; Holzer, G.; Tornabene, T. G., TOTAL LIPID PRODUCTION OF THE GREEN ALGA NANNOCHLOROPSIS SP. QII UNDER DIFFERENT NITROGEN REGIMES1. *Journal of Phycology* **1987,** *23* (s2), 289-296.
16. Roberts, G. W.; Fortier, M.-O. P.; Sturm, B. S. M.; Stagg-Williams, S. M., Promising Pathway for Algal Biofuels through Wastewater Cultivation and Hydrothermal Conversion. *Energy & Fuels* **2013,** *27* (2), 857-867.
17. Gollakota, A. R. K.; Kishore, N.; Gu, S., A review on hydrothermal liquefaction of biomass. *Renewable and Sustainable Energy Reviews* **2018,** *81*, 1378-1392.

18. Beckman, D.; Elliott, D. C., Comparisons of the yields and properties of the oil products from direct thermochemical biomass liquefaction processes. *The Canadian Journal of Chemical Engineering* **1985,** *63* (1), 99-104.
19. Minowa, T.; Yokoyama, S.; Kishimoto, M.; Okakura, T., Oil production from algal cells of Dunaliella tertiolecta by direct thermochemical liquefaction. *Fuel* **1995,** *74* (12), 1735-1738.
20. Sawayama, S.; Minowa, T.; Yokoyama, S. Y., Possibility of renewable energy production and CO2 mitigation by thermochemical liquefaction of microalgae. *Biomass and Bioenergy* **1999,** *17* (1), 33-39.
21. Biller, P.; Ross, A. B., Potential yields and properties of oil from the hydrothermal liquefaction of microalgae with different biochemical content. *Bioresource technology* **2011,** *102* (1), 215-25.
22. Brown, T. M.; Duan, P.; Savage, P. E., Hydrothermal Liquefaction and Gasification of Nannochloropsis sp. *Energy & Fuels* **2010,** *24* (6), 3639-3646.
23. Ross, A. B.; Biller, P.; Kubacki, M. L.; Li, H.; Lea-Langton, A.; Jones, J. M., Hydrothermal processing of microalgae using alkali and organic acids. *Fuel* **2010,** *89* (9), 2234-2243.
24. Leow, S.; Witter, J. R.; Vardon, D. R.; Sharma, B. K.; Guest, J. S.; Strathmann, T. J., Prediction of microalgae hydrothermal liquefaction products from feedstock biochemical composition. *Green Chem.* **2015,** *17* (6), 3584-3599.
25. Li, Y.; Leow, S.; Fedders, A. C.; Sharma, B. K.; Guest, J. S.; Strathmann, T. J., Quantitative multiphase model for hydrothermal liquefaction of algal biomass. *Green Chem.* **2017,** *19*, 1163-1174.
26. Changi, S. M.; Faeth, J. L.; Mo, N.; Savage, P. E., Hydrothermal Reactions of Biomolecules Relevant for Microalgae Liquefaction. *Industrial & Engineering Chemistry Research* **2015,** *54* (47), 11733-11758.
27. Teri, G.; Luo, L.; Savage, P. E., Hydrothermal Treatment of Protein, Polysaccharide, and Lipids Alone and in Mixtures. *Energy & Fuels* **2014,** *28* (12), 7501-7509.
28. Shuping, Z.; Yulong, W.; Mingde, Y.; Kaleem, I.; Chun, L.; Tong, J., Production and characterization of bio-oil from hydrothermal liquefaction of microalgae Dunaliella tertiolecta cake. *Energy* **2010,** *35* (12), 5406-5411.
29. Duan, P.; Savage, P. E., Hydrothermal Liquefaction of a Microalga with Heterogeneous Catalysts. *Industrial & Engineering Chemistry Research* **2011,** *50*, 52-61.
30. Xu, D.; Savage, P. E., Characterization of biocrudes recovered with and without solvent after hydrothermal liquefaction of algae. *Algal Research* **2014,** *6*, 1-7.
31. Yang, Y. F.; Feng, C. P.; Inamori, Y.; Maekawa, T., Analysis of energy conversion characteristics in liquefaction of algae. *Resources, Conservation and Recycling* **2004,** *43* (1), 21-33.
32. Jena, U.; Das, K. C.; Kastner, J. R., Comparison of the effects of Na2CO3, Ca3(PO4)2, and NiO catalysts on the thermochemical liquefaction of microalga Spirulina platensis. *Applied Energy* **2012,** *98*, 368-375.
33. Fu, J.; Lu, X.; Savage, P. E., Catalytic hydrothermal deoxygenation of palmitic acid. *Energy & Environmental Science* **2010,** *3* (3), 311.
34. Imran, A.; Bramer, E. A.; Seshan, K.; Brem, G., High quality bio-oil from catalytic flash pyrolysis of lignocellulosic biomass over alumina-supported sodium carbonate. *Fuel Processing Technology* **2014,** *127*, 72-79.
35. Nguyen, T. S.; Zabeti, M.; Lefferts, L.; Brem, G.; Seshan, K., Conversion of lignocellulosic biomass to green fuel oil over sodium based catalysts. *Bioresource technology* **2013,** *142*, 353-60.

36. Ogi, T.; Yokoyama, S.-y.; Koguchi, K., Direct Liquefaction of Wood by Alkali and Alkaline Earth Salt in an Aqueous Phase. *The Chemical Society of Japan* **1985**, 1199-1202.
37. Shakya, R.; Whelen, J.; Adhikari, S.; Mahadevan, R.; Neupane, S., Effect of temperature and Na 2 CO 3 catalyst on hydrothermal liquefaction of algae. *Algal Research* **2015,** *12*, 80-90.
38. Lee, J.; Choi, D.; Kwon, E. E.; Ok, Y. S., Functional modification of hydrothermal liquefaction products of microalgal biomass using CO 2. *Energy* **2017**.
39. Roussis, S. G.; Cranford, R.; Sytkovetskiy, N., Thermal Treatment of Crude Algae Oils Prepared Under Hydrothermal Extraction Conditions. *Energy & Fuels* **2012,** *26* (8), 5294-5299.
40. Chen, W. T.; Zhang, Y.; Zhang, J.; Yu, G.; Schideman, L. C.; Zhang, P.; Minarick, M., Hydrothermal liquefaction of mixed-culture algal biomass from wastewater treatment system into bio-crude oil. *Bioresource technology* **2014,** *152*, 130-9.
41. Faeth, J. L.; Valdez, P. J.; Savage, P. E., Fast Hydrothermal Liquefaction of Nannochloropsis sp. To Produce Biocrude. *Energy & Fuels* **2013,** *27* (3), 1391-1398.
42. Jazrawi, C.; Biller, P.; Ross, A. B.; Montoya, A.; Maschmeyer, T.; Haynes, B. S., Pilot plant testing of continuous hydrothermal liquefaction of microalgae. *Algal Research* **2013,** *2* (3), 268-277.
43. Biller, P.; Sharma, B. K.; Kunwar, B.; Ross, A. B., Hydroprocessing of bio-crude from continuous hydrothermal liquefaction of microalgae. *Fuel* **2015,** *159*, 197-205.
44. Elliott, D. C.; Hart, T. R.; Schmidt, A. J.; Neuenschwander, G. G.; Rotness, L. J.; Olarte, M. V.; Zacher, A. H.; Albrecht, K. O.; Hallen, R. T.; Holladay, J. E., Process development for hydrothermal liquefaction of algae feedstocks in a continuous-flow reactor. *Algal Research* **2013,** *2* (4), 445-454.
45. Elliott, D. C.; Biller, P.; Ross, A. B.; Schmidt, A. J.; Jones, S. B., Hydrothermal liquefaction of biomass: developments from batch to continuous process. *Bioresource technology* **2015,** *178*, 147-56.
46. Xu, D.; Savage, P. E., Effect of reaction time and algae loading on water-soluble and insoluble biocrude fractions from hydrothermal liquefaction of algae. *Algal Research* **2015,** *12*, 60-67.
47. Zhou, D.; Zhang, L.; Zhang, S.; Fu, H.; Chen, J., Hydrothermal Liquefaction of Macroalgae Enteromorpha prolifera to Bio-oil. *Energy & Fuels* **2010,** *24* (7), 4054-4061.
48. Roberts, G. W.; Sturm, B. S. M.; Hamdeh, U.; Stanton, G. E.; Rocha, A.; Kinsella, T. L.; Fortier, M.-O. P.; Sazdar, S.; Detamore, M. S.; Stagg-Williams, S. M., Promoting catalysis and high-value product streams by in situ hydroxyapatite crystallization during hydrothermal liquefaction of microalgae cultivated with reclaimed nutrients. *Green Chem.* **2015,** *17* (4), 2560-2569.
49. Matsuura, Y.; Onda, A.; Yanagisawa, K., Selective conversion of lactic acid into acrylic acid over hydroxyapatite catalysts. *Catalysis Communications* **2014,** *48*, 5-10.
50. Tsuchida, T.; Sakuma, S.; Takeguchi, T.; Ueda, W., Direct Synthesis of n-Butanol from Ethanol over Nonstoichiometric Hydroxyapatite. *Industrial & Engineering Chemistry Research* **2006,** *45* (25), 8634-8642.
51. Miao, D.; Goldbach, A.; Xu, H., Platinum/Apatite Water-Gas Shift Catalysts. *ACS Catalysis* **2016,** *6* (2), 775-783.
52. Kottegoda, N.; Munaweera, I.; Madusanka, N.; Karunaratne, V., A green slow-release fertilizer composition based on urea-modified hydroxyapatite nanoparticles encapsulated wood. *Current Science* **2011,** *101* (1), 73-78.

53. Sadat-Shojai, M.; Khorasani, M. T.; Dinpanah-Khoshdargi, E.; Jamshidi, A., Synthesis methods for nanosized hydroxyapatite with diverse structures. *Acta Biomater* **2013,** *9* (8), 7591-621.
54. Sadat-Shojai, M.; Khorasani, M.-T.; Jamshidi, A., Hydrothermal processing of hydroxyapatite nanoparticles—A Taguchi experimental design approach. *Journal of Crystal Growth* **2012,** *361*, 73-84.
55. Landi, E.; Celotti, G.; Logroscino, G.; Tampieri, A., Carbonated hydroxyapatite as bone substitute. *Journal of the European Ceramic Society* **2003,** *23* (15), 2931-2937.
56. Hasegawa, M.; Doi, Y.; Uchida, A., Cell-mediated bioresorption of sintered carbonate apatite in rabbits. *The Journal of Bone and Joint Surgery. British volume* **2003,** *85-B* (1), 142-147.
57. Coto, B.; Martos, C.; Peña, J. L.; Rodríguez, R.; Pastor, G., Effects in the solubility of CaCO3: Experimental study and model description. *Fluid Phase Equilibria* **2012,** *324*, 1-7.
58. Yoshimura, M.; Sujaridworakun, P.; Koh, F.; Fujiwara, T.; Pongkao, D.; Ahniyaz, A., Hydrothermal conversion of calcite crystals to hydroxyapatite. *Materials Science and Engineering: C* **2004,** *24* (4), 521-525.
59. Ishikawa, K.; Matsuya, S.; Lin, X.; Lei, Z.; Yuasa, T.; Miyamoto, Y., Fabrication of low crystalline B-type carbonate apatite block from low crystalline calcite block. *Journal of Ceramic Society of Japan* **2010,** *118* (5), 341-344.
60. Kamitakahara, M.; Nagamori, T.; Yokoi, T.; Ioku, K., Carbonate-containing hydroxyapatite synthesized by the hydrothermal treatment of different calcium carbonates in a phosphate-containing solution. *Journal of Asian Ceramic Societies* **2015,** *3* (3), 287-291.
61. Kim, I. Y.; Ohtsuki, C., Hydroxyapatite formation from calcium carbonate single crystal under hydrothermal condition: Effects of processing temperature. *Ceramics International* **2016,** *42* (1), 1886-1890.
62. Laurencin, D.; Almora-Barrios, N.; de Leeuw, N. H.; Gervais, C.; Bonhomme, C.; Mauri, F.; Chrzanowski, W.; Knowles, J. C.; Newport, R. J.; Wong, A.; Gan, Z.; Smith, M. E., Magnesium incorporation into hydroxyapatite. *Biomaterials* **2011,** *32* (7), 1826-37.
63. Aminian, A.; Solati-Hashjin, M.; Samadikuchaksaraei, A.; Bakhshi, F.; Gorjipour, F.; Farzadi, A.; Moztarzadeh, F.; Schmücker, M., Synthesis of silicon-substituted hydroxyapatite by a hydrothermal method with two different phosphorous sources. *Ceramics International* **2011,** *37* (4), 1219-1229.
64. Tang, X. L.; Xiao, X. F.; Liu, R. F., Structural characterization of silicon-substituted hydroxyapatite synthesized by a hydrothermal method. *Materials Letters* **2005,** *59* (29-30), 3841-3846.

3 Methods

3.1 Algal Solid Cultivation

Algal biomass was the primary biomass of this study. With the scope of the research ranging from growth media and cultivation to hydrothermal reaction and product separation, it was necessary to create and manipulate both growth media and cultivation techniques for the algal biomass. Algal solids, with their respective growth media, were cultivated, harvested, and freeze-dried by our environmental engineering collaborators. The algal solid characterization explained in the subsequent paragraphs of this section were primary tasks, analyses, and the responsibility of the author. In addition, growth media data and the biomolecular content (i.e. carbohydrate, protein, and lipid) of the algal biomass that were also critical for this research were performed and shared by our collaborators. While growth media preparation and algal growth and harvesting were executed by the environmental engineering collaborators, these initial stages of this unique, third-generation biomass feedstock remained significant. Thus, a basic understanding and knowledge for how the algal solid biomass were cultivated for this research is necessary.

Algal solids that were characterized and later reacted via hydrothermal liquefaction (HTL) in this work were cultivated in three distinct types of bioreactors. The first were the open pond, pilot-scale bioreactors located at the Lawrence Municipal Wastewater Treatment Plant shown in Figure 10a. The growth media and harvesting technique for the wastewater-cultivated algal solids were discussed in the previous chapter, 2.6 *Wastewater Algal Cultivation, and Biomass Production*, as well as in prior publications.[1-2] These wastewater-cultivated algal solids provided the foundation and target for algal solids that were later cultivated in the laboratories on KU's campus. In addition to the pilot-scale, wastewater effluent-fed, open pond bioreactors, smaller

laboratory-scale light rack tanks, and bench-scale, raceway ponds depicted in Figure 10 were also utilized to cultivate algal solids for further characterization, HTL reactions, and comparison.

The first laboratory, algal bioreactors utilized for the research were 6, 15 L light rack tanks shown in Figure 10b. BG-11 media provided the basis for the growth media that the single-species, monoculture microalgae of *Chlorella kessleri* that was grown both in the light rack tanks and later raceway ponds.[3] Table 6 provides the compounds and their respective concentrations for BG-11 algal growth media. The calcium to phosphorus (Ca:P) molar ratio was the leading variable altered in the growth media between the light rack tanks and was adjusted by increasing the $CaCl_2$ concentration and maintaining the phosphorus concentration. The other features that were varied

Table 6: The various components and their respective concentrations for BG-11 algal growth media.

BASIS		TRACE METALS STOCK	
Component	**Concentration**	**Component**	**Concentration**
Formula	*mM*	*Formula*	*mM*
$NaNO_3$	17.6	H_3BO_3	46
K_2HPO_4	0.23	$MnCl_2 \cdot 4H_2O$	9
$MgSO_4 \cdot 7H_2O$	0.3	$ZnSO_4 \cdot 7H_2O$	0.77
$CaCl_2 \cdot 2H_2O$	0.24	$Na_2MoO_4 \cdot 2H_2O$	1.6
Citric Acid$\cdot H_2O$	0.031	$CuSO_4 \cdot 5H_2O$	0.3
Ferric Ammonium Citrate	0.021	$CO(NO_3)_2 \cdot 6H_2O$	0.17
$Na_2EDTA \cdot 2H_2O$	0.0027		
Na_2CO_3	0.19		
Trace Metals Stock	1 mL/L		

across multiple light rack studies were the nitrogen to phosphorus (N:P) molar ratio and the method for harvesting the algal solids. All light rack algal solids were pH controlled to approximately neutral from the regulation and continuous supply of CO_2 gas bubbled through each tank. Additionally, the algal biomass from each light rack tank were harvested during the latter, stationary growth stage, and seldomly grown at an N:P molar ratio less than 16. These growth conditions and late growth stage were to maximize biomass production and yield so that enough algal solids were available for HTL reactions.

When it came time to harvest the light rack algal solids, two dewatering techniques were implemented. The first and initial algal dewatering method involved strictly centrifuging the entire 15 L volume of growth media and algal biomass. The second dewatering technique added an extra, auto-flocculation step prior to centrifugation. This auto-flocculation step has shown to be a more efficient harvesting technique, for it greatly reduced the volume of suspended algal biomass required for centrifugation.[1, 4-6] To induce auto-flocculation the pH was increased to 10.5 or 11, depending on the observable flocculation efficiency from the operator, using a sodium hydroxide solution (NaOH). The rise in pH caused coagulants to precipitate from the growth media causing the algal cells to flocculate and settle to the bottom of the light rack tanks along with the precipitated solids. It is hypothesized, and later discussed in Chapter 4.4.1 *Inorganic Characteristics of Algal Solids*, that auto-flocculation occurred naturally in the wastewater-cultivated algal solids due to its CO_2 limitations, for besides the atmosphere, no additional CO_2 was bubbled into the open pond reactors. Thus, with increasing algal growth and limited CO_2, the pH in the open pond bioreactors was able to rise naturally.

The third and final type of algal growth bioreactor were 2, 1,200 L raceway ponds that were housed inside of a greenhouse on the roof of KU's M2SEC research facility and shown in

Figure 10c. The purpose of the raceway ponds was to provide amble algal solid samples for repeated HTL reactions. The nearly ten times greater volume allowed for previously and traditionally constant growth variables such as the N:P molar ratio of the growth media and the growth stage at which the algal solids were harvested to be experimented upon. The raceway ponds provided the means to grow the single-species, *Chlorella kessleri*, in a growth media with an N:P molar ratio less than 16 and at earlier algal growth stages, such as the exponential and transition stages, and still produce enough algal solids for multiple HTL reactions.

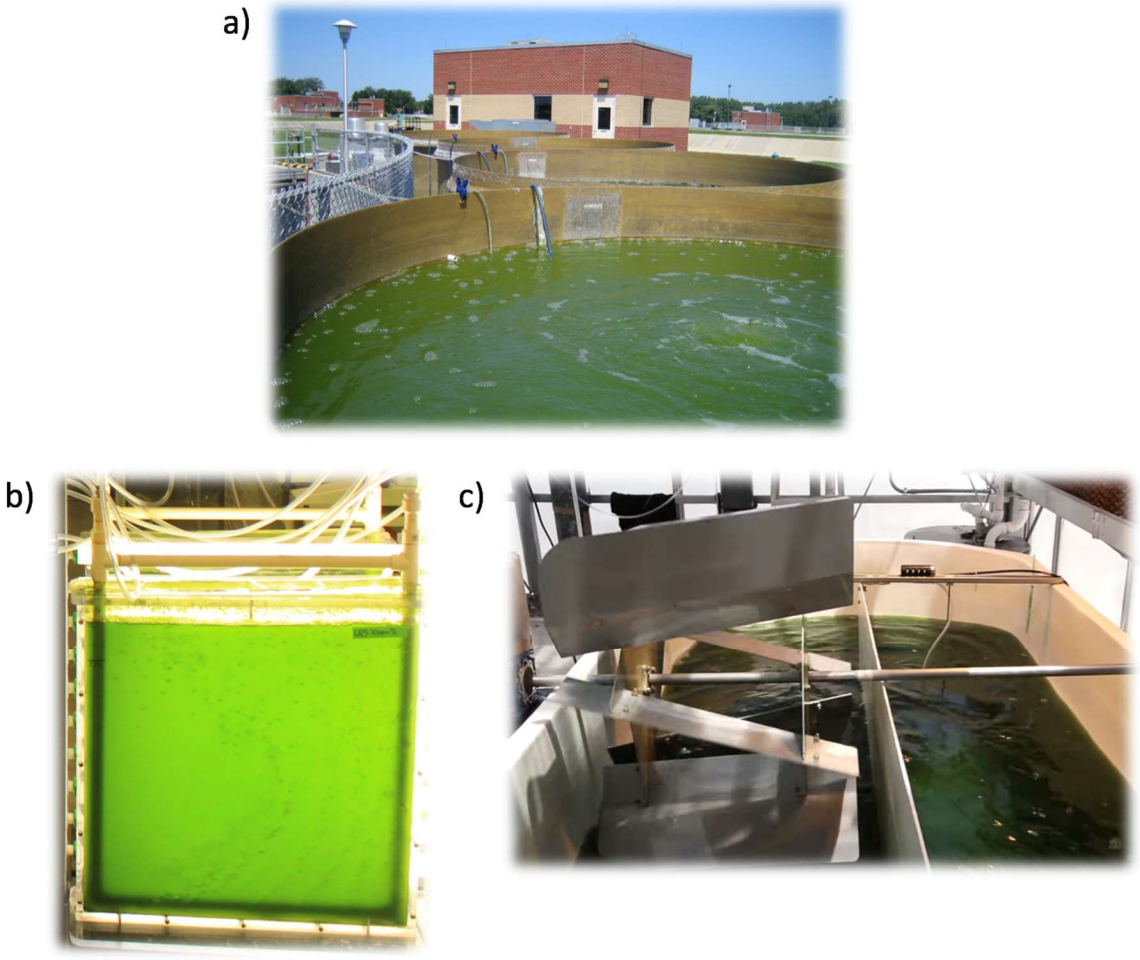

Figure 10: Photos of the various bioreactors used to cultivate algal solids researched and studied for this dissertation. a) wastewater effluent, open ponds b) light rack tank and c) greenhouse, raceway pond.

3.2 Algal Solid Proximate Thermogravimetric Analysis (TGA)

Thorough characterization of the algal solids from all three bioreactors was necessary to best understand and ultimately improve the conversion of algal solid biomass to quality, high-valued biocrude and solid products via conventional hydrothermal liquefaction. Thermogravimetric analysis (TGA) was performed in triplicate on the algal solids using a Q600 from TA Instruments. A proximate analysis method that was previously created was utilized to determine the general characteristics of the algal solids.[7] Moisture and volatile weight percentages were determined in the first, pyrolysis stage of the proximate analysis, which heated the sample to 850°C in a N_2 environment. For the second, combustion stage of the proximate analysis, the furnace was cooled to 120°C, the gas was switched to air, and the remaining solid sample was again heated to 850°C.

3.3 Algal Solid Ultimate (CHN/O) Elemental Analysis

A Perkin Elmer 2400 Elemental Analyzer provided the ultimate analysis for the algal solid biomass. Ultimate analysis included the organic – carbon (C), hydrogen (H), nitrogen (N), and oxygen (O) weight percentages for a given algal solid or biocrude sample. The elemental analyzer operated in two modes. One where C, H, and N were measured in a single run and a second where only O was measured. Triplicate runs were executed for each sample in each mode to allow for valid averages and standard deviation. Furthermore, the instrument was properly calibrated to within 0.5 wt% of the theoretical wt% of designated standard compounds.

3.4 Inorganic Analysis

Given the high, inorganic ash component of the algal solids and the high yields of HTL solids, proper measurement and analysis of the inorganic fraction for each of these samples was

critical. To determine the inorganic elements and their concentration within each sample required a two-step process: microwave acid digestion and inductively coupled plasma with optical emission (ICP-OES).

3.4.1 Microwave Acid Digestion

Characterization of the algal and HTL solids' inorganic composition was determined by microwave acid digestion followed by analysis via a Varian 725 ICP-OES. Solid samples were digested in 16HF100 rotor and vessels shown in Figure 11. Approximately 0.3 g of solids, 6 mL of nitic acid (HNO_3), and 2 mL of hydrochloric acid (HCl) were added to the vessels. Both acids used for the digestion were undiluted, concentrated, trace-metal grade acids and were handled within a fume hood. The vessels with the solid sample and concentrated acid along with a digestion blank, which included only the acid sand no solids, were then loaded into the Multiwave Pro, Anton-Paar Laboratory Microwave and digested. The purpose of the blank was to later identify any potential contaminants due to the digestion vessels. The microwave settings that allowed for complete digestion of the algal solids included a 10-minute ramp to the maximum wattage for the given number of vessels loaded, followed by a 10-minute hold, and finally a 20-minute cool down.

Once the Multiwave Pro microwave indicated the digestion method was complete and the vessels were safe to handle, they were removed from the microwave. The vessels were first purged inside a fume hood of any residual gas built up from the digestion. The internal components of the vessel and cap were inspected to ensure no residual solids remained and that a complete digestion occurred. If solids remained, the samples were re-digested. Previous digestions using the rotor and vessel 24HVT50 also displayed in Figure 11 had great difficulty in achieving complete digestion. Due to its lower pressure rating, rotor and vessels from 24HVT50 would

purge more frequently causing solids to be sprayed on the Teflon cap and walls and therefore be unable to digest completely. Incomplete digestion of the solids caused inaccurate calculations and measurements for the later ICP-OES analysis.

After a complete digestion is ensured, the concentrated acidic solution is filtered through a 0.45 μm, PTFE filter and diluted using deionized (DI) water to a 100 mL final volume. The final 100 mL acid-digested solid solution is therefore an approximately 6% HNO_3 solution. That is similar to the HNO_3 concentration of the mobile phase for the ICP-OES. Further dilutions of this acid-digested solid solution are often necessary in order to be detectable by the ICP-OES. Thus, a 1:10 and a 1:100 dilution by volume to a final volume of 10 mL of the initial 100 mL acid-

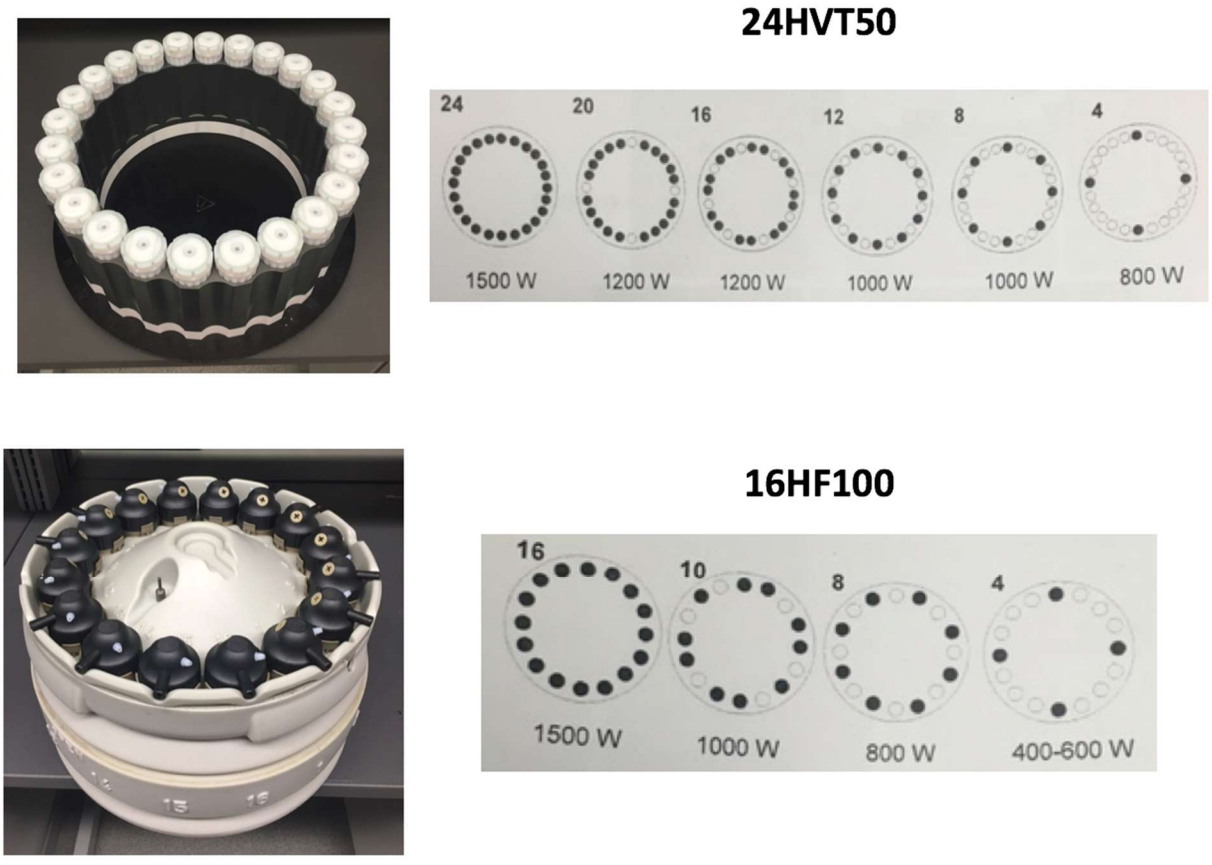

Figure 11: Two rotors and their accompanying vessels, 24HVT50 and 16HF100, were often used for the microwave acid digestion of both algal and HTL solids. The rotor and vessels 16HF100 were determined to be the ideal for complete digestion for both algal and HTL solids.

digested solid solution is performed. It is important to note that these dilutions require a premade 6% HNO_3 solution for dilution not DI water, as to not further dilute the acid concentration. In addition to the 1:10 and 1:100 dilutions, a 10 mL sample of the original 100 mL acid digested, algal solid solution is also collected along with a 10 mL sample of digestion blank, DI water, and premade 6% HNO_3 diluent in order to easily identify the cause for possible contamination during sample preparation.

3.4.2 Inductively Coupled Plasma Optical Emission Spectrometry (ICP-OES)

Within the ICP-OES software, either a new method was created, or a previously used method is opened as a template. The previous method must have the same elements required for analysis selected as well as the same standard concentrations that will be used for calibration. For the ICP-OES standard solutions, a 500 mL custom stock solution was ordered from Inorganic Ventures (Part # UKS-1). To ensure a constant matrix between the standards and the various samples that were to be analyzed through ICP-OES, the customized standard stock solution had all the same elements as BG-11 growth media. All elements and their respective concentrations within the stock standard solution are shown in Table 7. The customized standard stock solution was also 5% nitric acid (HNO_3) by volume (vol%). From the stock standard solution, 5 unique concentrations of 10, 8, 5, 3, and 1 mg/L were made by diluting the purchased standard stock solution with 5 vol% HNO_3. The dilutions were made based off volume and with respect to the 1,000 mg/L concentration of elements.

The key elements analyzed by ICP-OES were calcium (Ca) and phosphorus (P) as well as secondary elements such as magnesium (Mg), iron (Fe), and potassium (K). In addition to the

Table 7: The elements and their concentrations for the Inorganic Ventures customizable stock ICP-OES standard solution

1,000	100	10
mg/L	*mg/L*	*mg/L*
Al	B	As
Ba	La	Co
Ca	Mn	Cu
Fe	Ni	Pb
K	Zn	Sr
Mg		
Na		
P		
S		

standards, a quality control (QC) of 6 mg/L is also made from the standard, stock solution to ensure the calibration was accurate. An error of 10% or less within the calibration analysis of the standards ensured an accurately calibrated instrument. Standard solutions were remade if the calibration error for a desired element was greater than 10%.

The sequence and the sample's respective tray position along with the sample's dilution factor, solid digestion mass (i.e. ~ 0.3 grams of solid), and digestion volume (i.e. 100 mL) were

also inputted. Once all the standards, QC, digestion blank, diluents, and samples were loaded and inputted into the software, an autosampler injected each sample. The instrument measured the concentration for each selected element in each sample in triplicate. The software then calculated and reported the mg of the selected element per kg of algal solid via the previously inputted masses, volume, and dilution factors.

The relative standard deviation (RSD) from the internal triplicate that is performed automatically for each aqueous solution is also reported. Despite the RSD being reported in terms of the digested aqueous concentration, it is synonymous to the digested solid mass and can be reported as such. Thus, the ICP-OES error was known and reported. Due to lack of both algal and HTL solid sampling, triplicated digestions of the same algal or HTL solid sample were unable to be performed. Thus, the error or standard deviation due to solid digestions was unknown.

3.4.3 Fourier Transform Infrared Spectroscopy (FTIR)

Besides acid digestion and ICP-OES analysis, Fourier Transform Infrared Spectroscopy (FTIR) and provided additional, qualitative results to characterize the inorganics of the algal solids. The methods for these analyses are identical to those previously reported by Roberts et al.[7] A Varion 640-IR FTIR equipped with a Pike Technologies, GladiATR hot plate attachment helped identify key, anionic functional groups, such as carbonate (CO_3^{2-}), phosphate (PO_4^{3-}), and hydroxide (OH^-), within the algal and HTL solids. The GladiATR hot plate was held at a constant 105°C to inhibit any moisture from collecting on the sample. Meanwhile, the absorbance spectra ranged from 4,000 to 500 cm^{-1} with a sensitivity and resolution of 8 cm^{-1} and 4 cm^{-1}, respectively. The final sample spectrum was an automated average from over 250 scans of a single sample.

3.4.4 X-ray Diffraction (XRD)

Dr. Victor Day of the KU X-ray Diffractometer Laboratory located on KU's West Campus performed all single-beam, powder x-ray diffraction (XRD) of our algal and HTL solid samples. Because the XRD was a single-beam diffractomer analyzing a powder sample, a duplicate analysis of crystalline solid samples was conducted and confirmed the small sample size was representative of the entire solid sample. A Bruker Proteum diffraction system that was equipped with a Helios multilayer optics, an APEX II CCD detector, and a Bruker MicroStar microfocus rotating anode that provided the single-beam, x-ray source at 45 kV and 60 mA. The x-ray source was also monochromated CuKα radiation with a wavelength (λ) of 1.54178 Å. The diffraction data was analyzed between 20-70° 2θ and processed by the author using Bruker EVA powder diffraction software. In addition to the preloaded XRD patterns provided by the EVA software, commercial-grade minerals were analyzed to provide a better standard and more conclusive results. These minerals shown in Figure 12 included calcite (Fisher, $CaCO_3$, ACS-grade), lime (Fisher $Ca(OH)_2$, ACS-grade), silica dioxide (Alfa Aesar SiO_2, 99.5%), hydroxyapatite (HAp; Sigma-Aldrich $Ca_5(PO_4)_3OH$, ≥ 90.%), and tricalcium phosphate (TCP; Sigma-Aldrich $Ca_3(PO_4)_2$, ≥ 96.0%).

3.5 HTL Execution

Previously optimized, conventional, batch hydrothermal liquefaction was used to convert the algal biomass cultivated and harvested by our collaborators to energy-dense biocrude oil and other value-added products.[2, 10, 12] Using similar HTL reaction conditions also allowed for accurate comparison to other algae HTL results in the literature.

3.5.1 Reactor and Fluidized Sand bath

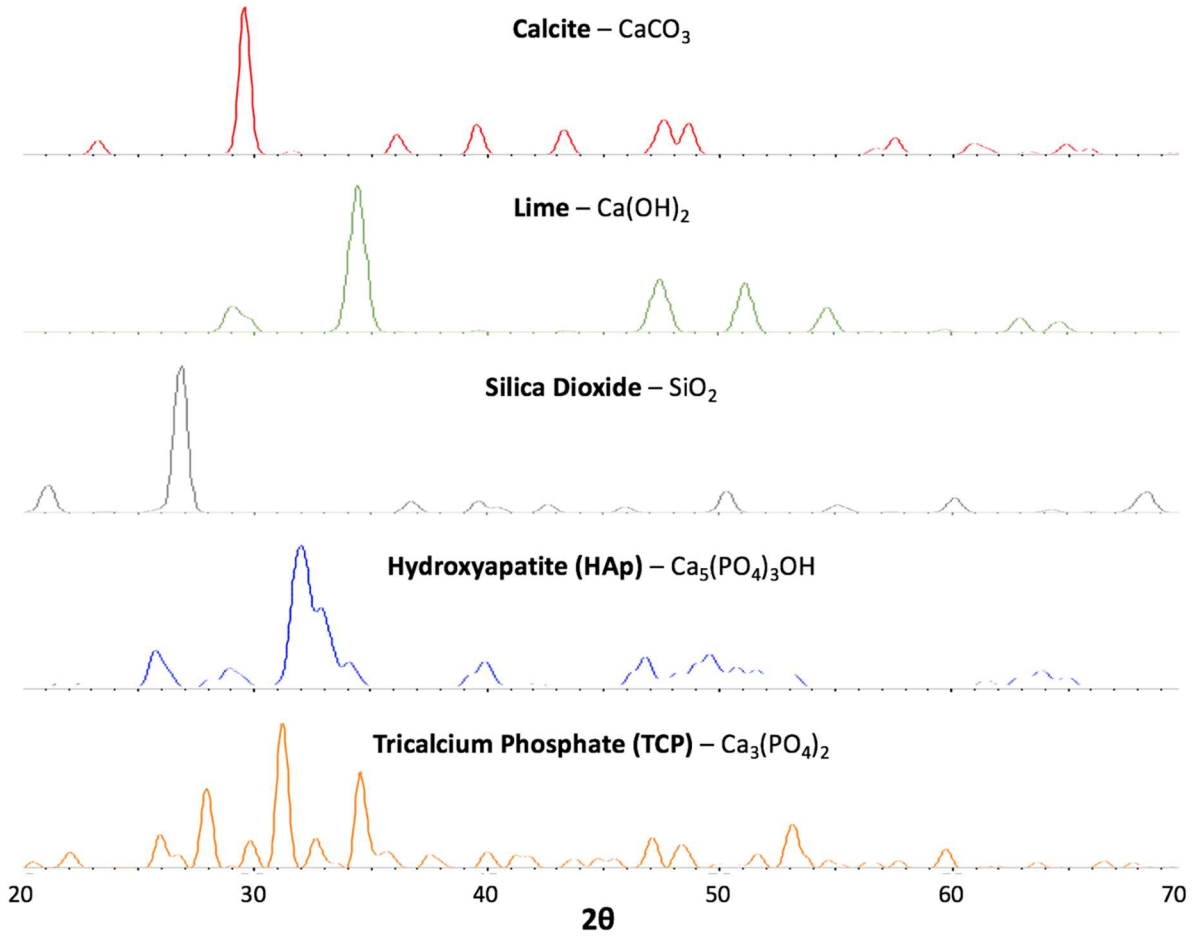

Figure 12: XRD patterns of commercial standards used to more conclusively identify the structure of algal and HTL solids.

Hydrothermal reactions were performed in a batch process using 75 mL, 4740 series Parr reactors with a high temperature, high pressure valve from High Pressure Equipment Co. (Catalog No. 30-12HF4-R-HT) shown in Figure 13a and Figure 13b. A Techne SBL-2D fluidized sand bath was used to achieve a uniform reaction temperature. The fluidized sand bath also allowed for three reactions to be conducted simultaneously. An external thermocouple was also placed near the surface of the sand bath at a similar depth as the reactor also shown in Figure 13c. The additional thermocouple is to correct for the temperature decline that occurs between the

temperature-controller thermocouple that is located near the heaters at the bottom of the sand bath and temperature near the surface where the reactors are placed. Adequate fluidization and thermal gradient of the sand is known to occur when the temperature difference between the external thermocouple and temperature-controller is approximately 10°C.

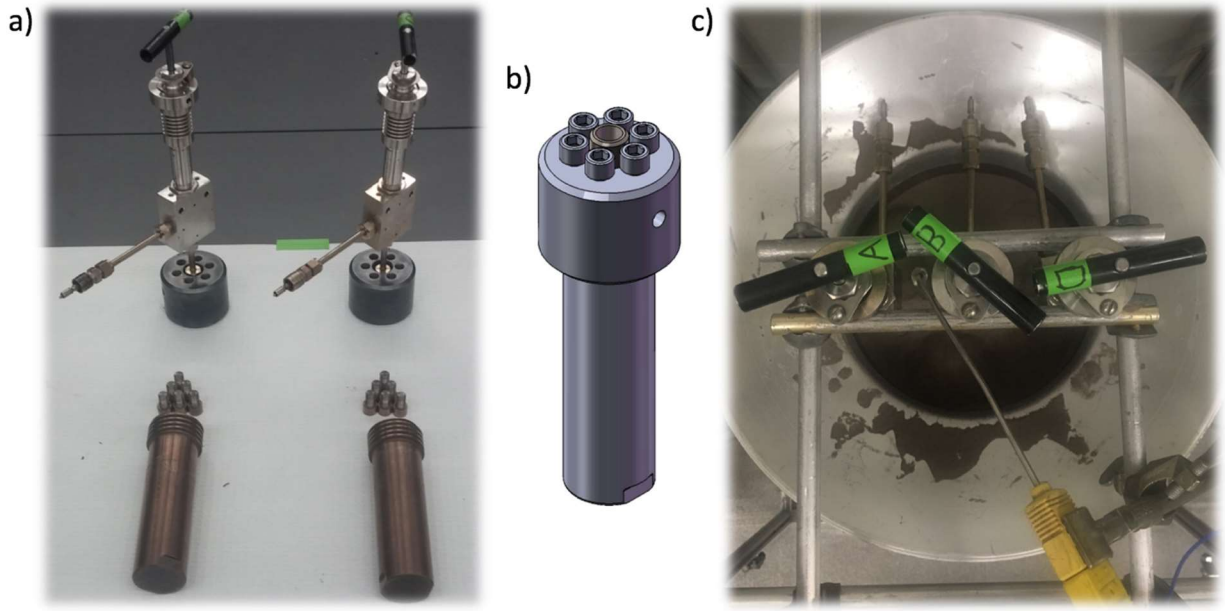

Figure 13: Photos of a) the high pressure, high temperature valves and reactor caps separated from the reactor vessel, b) The 4740 series Parr reactor vessel, cap, and hex bolts, and c) the placement for three reactors and the external thermocouple within the fluidized sand bath.

Conventional HTL reaction conditions included a 60-minute hold at a reaction temperature of 350°C. Batch reactors were loaded at room temperature; therefore, in addition to the 60-minute reaction time, reactor and reactant contents heated with the sand bath at a rate of 3-4°C/min. As the sand bath temperature rose, the air supply had to be reduced periodically to limit an excess of air flow that would cause sand to bubble out of the sand bath at an unnecessary rate. After the 60-minute hold at 350°C, the reactors were removed from the sand bath from the valve-stem, for the valve-block and reactor are too hot handle despite heat-resistant gloves, residual sand was shaken off the reactor back into sand bath, and the reactors were quenched in a bucket filled with cool,

tap-water. After all the reactors were removed from the sand bath and placed in the quenching water bucket, they were each individually rinsed and further cooled with cold tap water and air dried using compressed air. To ensure longevity of the reactor and valve, it is critical to remove as much sand from the reactor at each step and that the reactor is dry. Storing the reactors with residual sand or water can damage the reactor threading as well as the valve packing. The overall heating time for the reactors within the sand bath was approximately three hours. After drying, the reactor contents were allowed to reach equilibrium by waiting at least one hour before depressurizing the reactors and commencing product extraction. In many cases the equilibration of the reactors was done overnight.

3.5.2 Reactor Preparation

For reactor preparation, a blank, conditioning reaction at the aforementioned conditions with 30 mL DI water was performed prior to any reaction of solids. The conditioning allowed for final leak test and cleaning for the valve and reactor. If less than 85% of the initial volume loaded for the conditioning was recovered or the resulting DI water after conditioning was murky or opaque, the conditioning ultimately failed and inspection for leaks or more thorough cleaning was necessary. Typically, over 90% of the water volume was recovered and the conditioned water was clear or a translucent yellow-orange hue with minimal, visible, suspended solids. The most likely cause for leaks during conditioning or reactions were the high pressure and temperature valve not being closed completely. Prior to placing the reactors into the sand bath, the valve-stem should be inspected to ensure it is tightly turned in the clock-wise direction. Other causes for leaks include, a missing damaged graphite o-ring, which typically lasts 3-4 consecutive conditioning and HTL reactions collectively, or improper tightening of the 6 hex bolts.

Solids were often loaded at a 10 wt% of the total weight of the reactant contents. Thus, with a volume of 30 mL DI water, the total solids mass (m_{solids}) were calculated to be 3.3333 g from equation (2(2). Further adjustments can be made depending on the desired solids wt% loading or DI water volume loaded.

$$0.10 = \frac{m_{\text{ solids}}}{m_{\text{ solids}} + 30.0} \tag{2}$$

This typical 10 wt% solids loading included either all algal solids or the summation of various inorganic or biological model compounds. When loading the solids, approximately 7-10 mL of DI water were pipetted into the reactor initially. Next, approximately half of the solids volume were poured into the reactor followed by another 7-10 mL of DI water being pipetted into the reactor. When the second 7-10 mL aliquot of DI water pipetted into the reactor, it is best to attempt to rinse the sides of the reactor, so that all solids are at the bottom of the reactor. The mixture of half the solids and approximately 20 mL of the DI were then mixed with a narrow, flat spatula until homogeneous. Once the initial mixture is a uniform slurry, the remaining volume of solids are added, and another 5-7 mL of DI water are used to rinse the internal sides of the reactor. This final mixture is then stirred until a homogenous slurry is created with minimal "clumps" of solids remaining on the spatula. The remaining 5-10 mL of DI water is then used as a final rinse of the spatula and reactor.

Prior to every reaction and conditioning, a thorough cleaning of the reactor and its various parts is performed with emphasis on any threaded parts. This includes the removal of the dried, Loctite N-5000, anti-seize, threading lubricant from all hex bolts, which requires fine-point tweezers, and the reactor cap using acetone-soaked Kimwipes and Q-tips. Sand was also removed from the threading of the reactor and reactor cap using a moistened Kimwipe and compressed air.

After conditioning, the inside compartment was wiped cleaning with a paper towel and large, flat-head screwdriver and then dried with compressed air. After an HTL reaction where solids or a biocrude were produced, approximately 5-10 mL of acetone was poured into the reactor and the inside of the reactor was wiped clean with a paper towel and flat-head screw driver several times until the paper towel appeared clean. The reactor was then dried using compressed air. All reactor conditioning, loading, cleaning, and preparation steps were outlined in an HTL reaction checklist where the operated initialed and dated after the completion of each step.

3.6 HTL Product Extraction

The product extraction process after HTL can impact both product yield and properties as shown in the literature and discussed in Chapter 2.5 *Conventional, Fast-Batch, and Continuous HTL* .[8-10] The general HTL product extraction procedure best fit for all algal solid and inorganic model compound extraction is explained further. After quenching and allowing the reactors to equilibrate, the reactors were de-pressurized by opening the high-pressure valve. In the event that the gaseous product was analyzed, the reactors would be connected to an Agilent 7890B gas chromatogram thermal conductivity detector (GC-TCD) and degassed through the analyzer.

3.6.1 Aqueous co-product (ACP) Separation

The first stage of product separation separated the aqueous co-product (ACP) from the other biocrude and solid product. Thus, all the reactor products were initially poured and vacuum-filtered through a pre-massed, 70 mm diameter, Whatman GF/F glass fiber, filter paper fitted to a Buchner funnel. A 50 mL centrifuged tube was then taped to the neck of Buchner funnel and inserted into the vacuum flask to collect the ACP as shown in Figure 14a. High solid producing

reactions may inhibit the recovery of a portion of the ACP. Thus, scraping the solids with a spatula from reactor may assist ACP recovery. If excessive ACP remain in the reactor when extracting the biocrude, inflated biocrude yields of inferior quality may occur. Solids recovered on the filter paper were allowed to sit for several minutes to allow the vacuum to remove any entrapped moisture. At least 80% of the initial 30 mL volume of water were recovered in the ACP. If less than 80% of the initial volume were recovered, there is a high probability a leak occurred, and consistent reaction pressure was not achieved.

3.6.2 HTL Biocrude and Solids Separation

Once all the residual ACP was recovered from inside the reactor, the separation of solids and biocrude product ensued. The first objective of this stage was to remove all solid material from the reactor. Dichloromethane (DCM) also commonly referred to as methylene chloride was the solvent used for both extracting the solids from the reactor and separating the biocrude from algal solid HTL reactions. The reactors were rinsed with DCM and scraped with a spatula then poured over a pre-massed, gravity, Whatman #1, 150 mm diameter filter. Beneath the gravity filtration is a pre-massed, 250 mL round-bottom flask with a cork stand used to collect the DCM and biocrude solution also shown in Figure 14b. The initial tare mass of the clean, dry round-bottom flask also includes its complimentary cap and a few boiling chips. Rinsing and scraping the solids from the reactor using DCM and pouring the contents through the gravity filter was repeated until nearly all the solids were removed from the reactor.

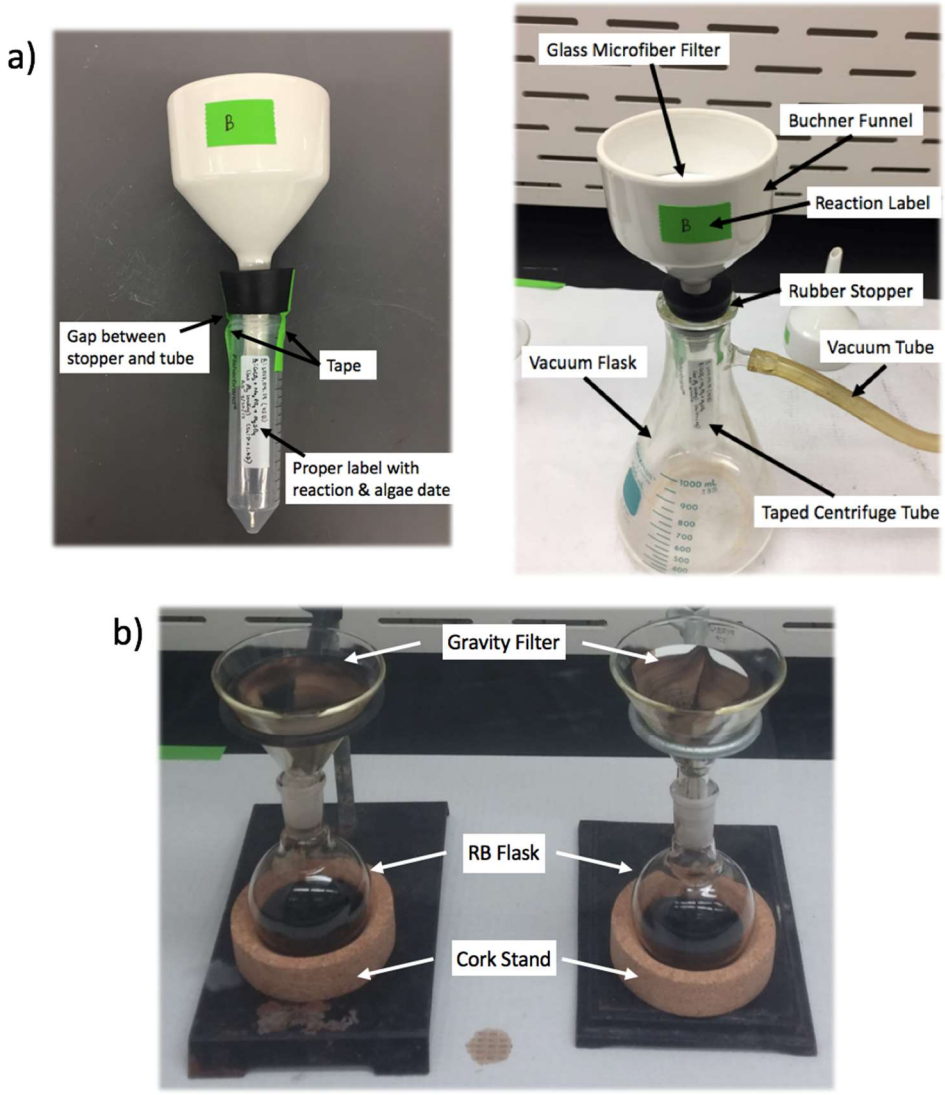

Figure 14: Photos depicting the apparatuses for a) solids and ACP separation using vacuum filtration and b) biocrude and solids separation through gravity filtration by rinsing the solids collected by each filter with DCM and collecting the biocrude and DCM solution in a round-bottom (RB) flask.

Next, the solids remaining in the Buchner funnel and on the vacuum filter from the separation of the solids and ACP were rinsed with DCM over the gravity filter paper. If necessary, solids were also scraped from the Buchner funnel as well. Repeated and continued rinsing of the solids and gravity and vacuum filter occurred ensuring all the DCM-soluble biocrude was collected. Typically, 400-500 mL of DCM was required per reactor to recover a majority of the

biocrude from conventional HTL of algal solids. Thus, DCM must be distilled off from the 250 mL round-bottom flask at least once during rinsing, and then brought back to collect the remaining biocrude. For hydrothermal reactions that did not involve algal solids or biological model compounds that did not produce an organic, biocrude product, DI water was used to extract and rinse the solid product from the reactor. These reactions included those performed on inorganic model compounds, such as calcite and trisodium phosphate, where solids and ACP were the only synthesized products from these reactions.

3.6.3 Dichloromethane (DCM) Distillation

After the filter papers and solids have been thoroughly rinsed with DCM, they are dried in a 105°C oven overnight, cooled in a desiccator, and a final mass is recorded. To measure the final biocrude mass, the DCM is distilled off until final weight percent of DCM in the biocrude is < 10 wt%. The distilling of DCM was performed using the lab-scale distillation apparatus shown in Figure 15. A water hot bath that was temperature-controlled at 55°C with mixing by a stir bar at 400 rpm heated the DCM (boiling point = 39.6°C) and biocrude solution. Meanwhile a ThermoScientific A10 refrigerated circulator cooled and pumped water at 10°C through coolant lines that were attached to an inner-rod of the distillation apparatus. This chiller rod allowed the DCM-vapor from the boiling solution to condense and drip into the catch pot. Depending on the volume of DCM and biocrude solution the round-bottom flask was slowly lowered into the hot bath. When the round-bottom flask is nearly full, the boiling can be vigorous enough that some

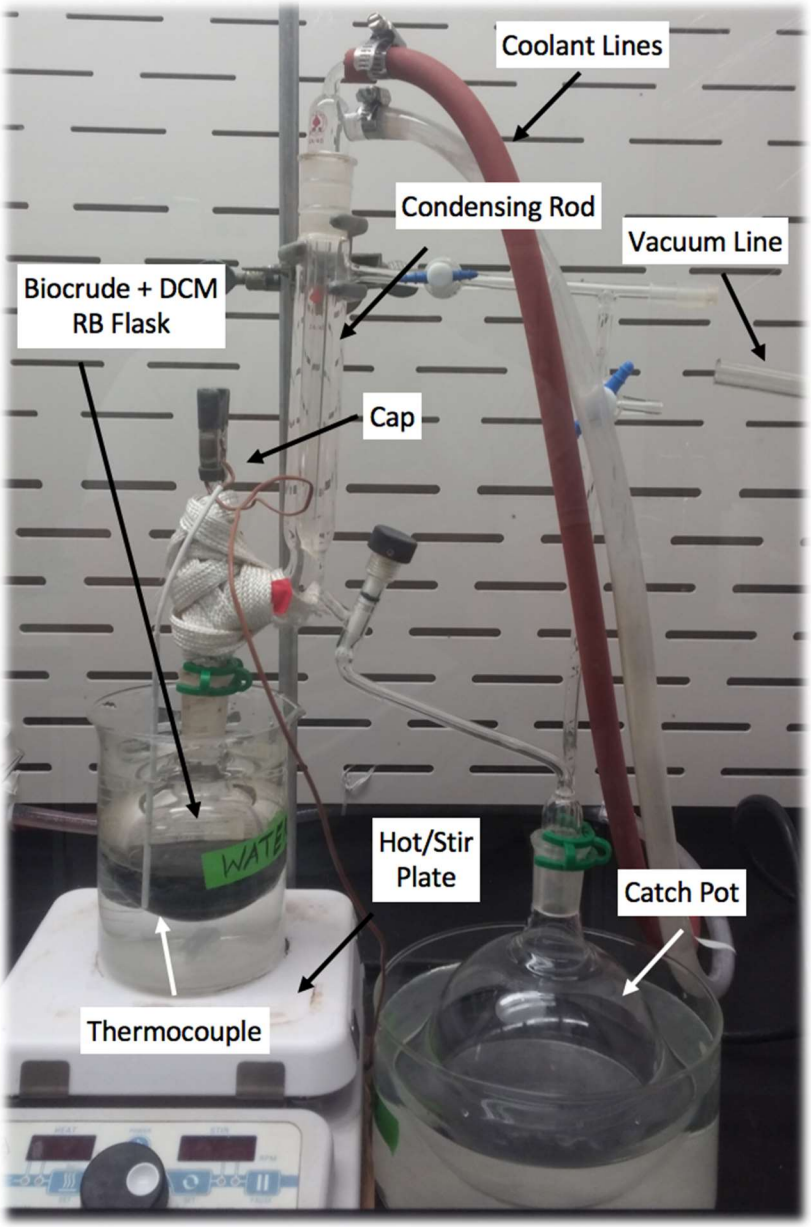

Figure 15: Lab-scale distillation apparatus used to distill and separate and safely collect the DCM, extraction solvent from the desired biocrude product.

DCM and biocrude solution boils over into the catch pot. The catch pot then needs to be emptied back into the round-bottom flask and re-boiled. Once approximately half of the DCM and biocrude solution volume remains, the entire round-bottom flask can be submerged into the hot bath.

Following a few hours and continual monitoring of the distillation, a small puddle of DCM and biocrude will remain in the biocrude. At this time, a small amount of vacuum pressure is necessary to vaporize and boil off the remaining DCM. Subtle shaking or hitting the round-bottom flask on the sides of the hot bath may be necessary to re-initiate boiling. If too much negative pressure is applied or to great of force is used when shaking the round-bottom flask and the solution is not yet thick or viscous, an unexpected, "pop" may occur from the abrupt change in stability. When this "pop" occurs, biocrude coats the upper walls of the round-bottom flask and neck of the distillation apparatus impacting yields and making it difficult to recover the biocrude for further analysis. Thus, the cap is removed, and DCM is pipetted through the opening to wash residual biocrude back to the bottom of the round-bottom flask. It takes a small amount of practice and experience to become successful at distilling the last remaining DCM solvent under vacuum.

Once the DCM and biocrude solution appears thick and viscous and the formation of bubbles is slowed but continuous under vacuum, the distillation is nearly complete. Allow the solution to remain under vacuum for 5-10 minutes, then remove the round-bottom flask from the hot bath, place the cap onto the top of the flask. Wait 30-40 minutes to let the biocrude product and round-bottom flask reach room temperature so that the final mass is recorded at a similar temperature to the initial tare mass. Once the final mass is recorded, take a sample of the biocrude using a small copper-rod and run a simulated-distillation method using the Q600 TGA. This method will report the weight percent of DCM remaining in the biocrude. If the weight percent is greater than the desired 10 wt%, the biocrude will need further distillation and a new final mass recorded. The biocrude losses from the earlier sampling should also be noted; the error will likely be minimal given the small sampling required for simulated-distillation analysis.

3.7 HTL Product Yield

After all the products had been separated and final masses of the solids and biocrude were determined, the dry weight (dw%) yields of the solid and biocrude products were calculated using the following equations. In addition, the ash free dry weight (afdw%) yield of the biocrude was also determined for continuity across algal solids with varying ash wt% and for better comparison to the literature.

$$\text{dw\% Biocrude Yield} = \frac{(1 - \text{wt\%}_{\text{DCM}})\, m_{\text{biocrude}}}{\text{algae}_{\text{afdw}}} \times 100 \quad (3)$$

$$\text{dw\% Biocrude Yield} = \frac{(1 - \text{wt\%}_{\text{DCM}})\, m_{\text{biocrude}}}{\text{algae}_{\text{dw}}} \times 100 \quad (4)$$

$$\text{dw\% Solids Yield} = \frac{m_{\text{solids}} \times \text{wt\%}_{\text{ash}}}{\text{algae}_{\text{dw}}} \times 100 \quad (5)$$

In both equations (4) and (5) algae_{dw} is the dry weight mass of algal solids loaded into the reactor while in equation (3) $\text{algae}_{\text{afdw}}$ refers to the ash-free dry weight of the algal solids. The m_{biocrude} and m_{solids} are the mass of biocrude and mass of solids, respectively, and were calculated from the difference in final and tared masses. The $\text{wt\%}_{\text{DCM}}$ represents the weight percent of DCM in decimal form (e.g. 5% would be entered as 0.05 in the equation) that remains in the biocrude after vacuum distillation and determined by the initial simulated-distillation analysis. Finally, the $\text{wt\%}_{\text{ash}}$ is the ash weight percentage, also in decimal form, of the HTL solid product that was determined by proximate analysis.

Across the literature, the method for determining ACP yields often differ while the gas yields are calculated using the ideal gas law.[11-13] For this work, the biocrude and HTL solids were the

primary product of interest. Thus, to avoid uncertainty, the ACP yield was simply the volume percent recovered from the initial DI water volume loaded. With the gaseous product being minimal, only a few reactions had their gaseous products analyzed by GC-TCD calibrated for CO_2, CO, N_2, and O_2 to confirm its composition.

3.8 Aqueous Co-product Characterization

The aqueous co-product (ACP) had little consequence to the conclusions of this dissertation. The ACP was, however, substantial to the work of our environmental wastewater collaborators who performed further experiments and tests with the ACP samples. The significance the ACP played for this dissertation was to provide an elemental balance for both the organic and inorganic material present during HTL.

Total organic carbon (TOC) and total nitrogen (TN) of the ACP were measured by our environmental engineering collaborators using a Teledyne Tekmar TORCH Analyzer owned by KU's Tertiary Oil Recovery Project (TORP). The TOC and TN results were then used to best determine a carbon and nitrogen balance on the HTL reaction. ICP-OES analysis was also performed on the ACP, and the results were reported in mg/L. From the volume of ACP collected and elemental concentration of the ACP a mass balance on the inorganic material across the HTL reaction could be calculated. Nitric acid was added to achieve a 6 vol% acidic solution that is similar to the ICP-OES carrier solution. Because of the organics present in the ACP, the solution bubbled furiously with the addition of concentrated nitric acids. The respective dilution factor from this addition of acid was determined, and then the now 6 vol% acidic ACP solution was diluted ten and hundred times with a premade 6 vol% HNO_3 solution. The purpose of the further

dilutions was to achieve a working concentration of all previously mentioned elements of interest similar to what was done the acid digested algal solid solution.

3.9 Biocrude Characterization

The biocrude product is often seen as the primary product from the hydrothermal liquefaction of algal biomass. Thus, proper analysis and characterization of the biocrude is critical and necessary for comparison to those in literature. Several of the analytical techniques to characterize the HTL biocrude product are subsequently discussed.

3.9.1 Simulated Distillation

In addition to the initial simulated-distillation analysis performed on the biocrude to confirm a final DCM weight percent, two additional simulated-distillation runs of the biocrude were conducted on the Q600 TGA to complete a triplicated analysis for statistical purposes and for calculations in future analyses. This simulated-distillation method is the same as described by Roberts et al. and estimates the weight percentage for the array of distillate fractions available within the biocrude in addition to the current weight percent of residual DCM.[7] These distillate fractions include heavy naphtha (< 193°C), kerosene (193-271°C), gasoline (271-343°C), vacuum gasoline (343-538°C), and vacuum residual (> 538°C) and were all normalized to the DCM-free, biocrude weight percentage.

3.9.2 Ultimate (CHN/O) Analysis

Similar to the ultimate analysis conducted on the algal solids, the Perkin Elmer 2400 Elemental Analyzer reported the weight percentage of carbon, hydrogen, nitrogen, and oxygen for

the biocrude oil product. Triplicated runs in both CHN- and O-mode of biocrude samples were again conducted to provide thorough statistical analysis. Due to a certain weight percentage of the biocrude product being residual DCM from distillation, normalization to the pure biocrude product were necessary for accurate results. Although, distilled biocrude samples were kept in a cool, refrigerated environment, volatization and decreases in DCM weight percent still occurred; therefore, a simulated-distillation analysis was required within twenty-four hours of performing the ultimate analysis. The following equations were used to adjust the raw weight percentage (e.g. $wt\%_{C,raw}$) originally reported from the ultimate analysis to the final, normalized, DCM-free, and more accurate weight percentage (e.g. $wt\%_{C,norm}$) of the biocrude:

$$wt\%_{C,norm} = \frac{\left(m_{raw} \times wt\%_{C,raw}\right) - \left(m_{raw} \times wt\%_{DCM} \times \frac{MW_C}{MW_{DCM}}\right)}{m_{raw}(1 - wt\%_{DCM})} \times 100 \quad (6)$$

$$wt\%_{H,norm} = \frac{\left(m_{raw} \times wt\%_{H,raw}\right) - \left(m_{raw} \times wt\%_{DCM} \times \frac{2 \times MW_H}{MW_{DCM}}\right)}{m_{raw}(1 - wt\%_{DCM})} \times 100 \quad (7)$$

$$wt\%_{N,norm} = \frac{m_{raw} \times wt\%_{N,raw}}{m_{raw}(1 - wt\%_{DCM})} \times 100 \quad (8)$$

$$wt\%_{O,norm} = \frac{m_{raw} \times wt\%_{O,raw}}{m_{raw}(1 - wt\%_{DCM})} \times 100 \quad (9)$$

The sample mass inputted into the instrument for analysis is represented by m_{raw} and the weight percentage it measured for a given element "*X*" is depicted in the equations as $wt\%_{X,raw}$. Meanwhile, the weight percent of DCM in the biocrude, measured by simulated-distillation within twenty-four hours of sampling, is shown as $wt\%_{DCM}$. The additional carbon or hydrogen due to the DCM was calculated from the mass fraction of the molecular weights of carbon (MW_C) or

hydrogen (MW_H) to the molecular weight of DCM (MW_{DCM}). Lastly, the Dulong formula shown in equation (10), allowed for an accurate estimation of the higher heating value, or energy density (MJ/kg), of the biocrude from the normalized ultimate analysis results.

$$\text{HHV (MJ/kg)} = 0.338\ \text{wt\%}_{\text{C,norm}} + 1.428\ \text{wt\%}_{\text{H,norm}} - 0.1785\ \text{wt\%}_{\text{O,norm}} \quad (10)$$

3.9.3 Gas Chromatography Mass Spectrometry (GC-MS)

To specifically identify the organic compounds and their respective prevalence within the biocrude gas chromatography mass spectrometry (GC-MS) was utilized. An Agilent series 7890B GC with an 5977A MS were utilized with identical methods reported Roberts et al. to determine the biocrude composition.[7] In addition to a single, raw biocrude sample, a single derivatized-biocrude sample were also prepared using MSFTA for each biocrude product. The derivatized samples allowed for a more accurate comparison of the long chain fatty acids that were present in several biocrude samples. The fatty acid peaks that appeared in the GC-MS spectra appeared sharper and clearer in the derivatized samples than in raw biocrude samples due to the trimethylsilyl functional substituting for the hydroxide group in the derivatized, MSTFA-added sample. For the over 100 organic compounds identified within the biocrude by the GC-MS, the compounds respective peak area and peak area percentage (% area) were reported. The % area is the automated area percentage a single compound has relative to the sum of all the compounds peak area. Thus, it provides an estimation for the prevalence of a given compound. These results were then exported to an excel VBA program that categorized the organic compounds as: saturated or unsaturated hydrocarbons, aromatics, amines, amides, nitrogen aromatics, or oxygenated compounds. The peak areas and the percent of each peak area from the total of all the peak areas (% Area) were then summed for each functional group and tabulated.

3.10 HTL Solids Characterization

The HTL solids were the most unique HTL product observed from the wastewater-cultivated and auto-flocculated algal solids. Several of the algal solid analyses were also effective methods for HTL solids. Qualitative analysis such as FTIR and XRD were helpful in identifying the composition and structure of the HTL solids. Identical FTIR and XRD methods that were used for the algal solids were found to be effective for analyzing HTL solids. Similarly, an identical proximate analysis method was utilized on the HTL solids as the algal solids using the Q600 TGA. The microwave acid digestion rotor, vessels, and method were also used on the HTL solids when there were sufficient enough yields. The same dilution and ICP-OES procedure as acid digested algal solids were also effective with the HTL solids.

Ultimate analysis of the HTL solids, however, was ineffective. Although approximately 40 wt% of the HTL solids still contained residual, volatile, and organic biocrude material, the remaining approximately 60 wt% ash content caused interferences with the Perkin Elmer 2400 Elemental Analyzer. Thus, the reported C, H, and N wt% were often imprecise for the HTL solids. Furnace and external oxygen pressure may be altered to optimize the combustion of the low-organic HTL solids. However, the high ash content accumulates within the combustion chamber of the analyzer causing more frequent and costly maintenance. Ultimate analysis of the HTL solids was ultimately discontinued. With the absence of carbon and nitrogen wt% from the HTL solids, an accurate carbon or nitrogen balance became too difficult.

3.11 Error Analysis

As mentioned in the previous individual sections, several of the biocrude and algal solid characterization analyses were performed in triplicate to allow for proper averages and standard

deviations to be calculated. The error for each analysis is represented in the respective figures and tables. With approximately 7-8 g of algal solids were produced from the light rack tanks and HTL reactions requiring 3.3333 g of algal solids per reaction, triplicate reactions could not be performed. The limited algal and HTL solid production from the light racks also limited the number microwave acid digestions conducted to one. Thus, the reproducibility of HTL product yields nor the error due to digestion of algal or HTL solids could be reported. Finally, in the raceway ponds where amble amount of algal solids were produced, the objective was to identify key growth media and growth stages for desired HTL solids and biocrude. Thus, single HTL reactions were again performed for initial proof of concept.

3.12 References

1. Sturm, B. S. M.; Lamer, S. L., An energy evaluation of coupling nutrient removal from wastewater with algal biomass production. *Applied Energy* **2011,** *88* (10), 3499-3506.
2. Roberts, G. W.; Fortier, M.-O. P.; Sturm, B. S. M.; Stagg-Williams, S. M., Promising Pathway for Algal Biofuels through Wastewater Cultivation and Hydrothermal Conversion. *Energy & Fuels* **2013,** *27* (2), 857-867.
3. Dayananda, C.; Sarada, R.; Usharani, M.; Shamala, T.; Ravishankar, G., Autotrophic cultivation of Botryococcus braunii for the production of hydrocarbons and exopolysaccharides in various media. *Biomass and Bioenergy* **2007,** *31* (1), 87-93.
4. Vandamme, D.; Foubert, I.; Muylaert, K., Flocculation as a low-cost method for harvesting microalgae for bulk biomass production. *Trends Biotechnol* **2013,** *31* (4), 233-9.
5. Vandamme, D.; Foubert, I.; Fraeye, I.; Meesschaert, B.; Muylaert, K., Flocculation of Chlorella vulgaris induced by high pH: role of magnesium and calcium and practical implications. *Bioresource technology* **2012,** *105*, 114-9.
6. Wu, Z.; Zhu, Y.; Huang, W.; Zhang, C.; Li, T.; Zhang, Y.; Li, A., Evaluation of flocculation induced by pH increase for harvesting microalgae and reuse of flocculated medium. *Bioresource technology* **2012,** *110*, 496-502.
7. Roberts, G. W.; Sturm, B. S. M.; Hamdeh, U.; Stanton, G. E.; Rocha, A.; Kinsella, T. L.; Fortier, M.-O. P.; Sazdar, S.; Detamore, M. S.; Stagg-Williams, S. M., Promoting catalysis and high-value product streams by in situ hydroxyapatite crystallization during hydrothermal liquefaction of microalgae cultivated with reclaimed nutrients. *Green Chem.* **2015,** *17* (4), 2560-2569.
8. Xu, D.; Savage, P. E., Characterization of biocrudes recovered with and without solvent after hydrothermal liquefaction of algae. *Algal Research* **2014,** *6*, 1-7.

9. Xu, D.; Savage, P. E., Effect of reaction time and algae loading on water-soluble and insoluble biocrude fractions from hydrothermal liquefaction of algae. *Algal Research* **2015,** *12*, 60-67.
10. Xu, D.; Savage, P. E., Effect of temperature, water loading, and Ru/C catalyst on water-insoluble and water-soluble biocrude fractions from hydrothermal liquefaction of algae. *Bioresource technology* **2017,** *239*, 1-6.
11. Brown, T. M.; Duan, P.; Savage, P. E., Hydrothermal Liquefaction and Gasification of Nannochloropsis sp. *Energy & Fuels* **2010,** *24* (6), 3639-3646.
12. Biller, P.; Ross, A. B., Potential yields and properties of oil from the hydrothermal liquefaction of microalgae with different biochemical content. *Bioresource technology* **2011,** *102* (1), 215-25.
13. Chen, W. T.; Zhang, Y.; Zhang, J.; Yu, G.; Schideman, L. C.; Zhang, P.; Minarick, M., Hydrothermal liquefaction of mixed-culture algal biomass from wastewater treatment system into bio-crude oil. *Bioresource technology* **2014,** *152*, 130-9.

4 Inorganic Capture

4.1 Motivation & Background

It is well-recognized that the inorganic, ash content of wastewater-cultivated algal solids is considerably higher (> 20 wt%)[1-2] than lab-grown, monoculture microalgae (< 5 wt%).[3-4] The inorganic content of wastewater-cultivated algal solids is also unique compared to the common, high ash content forms of macroalgae from marine, or saltwater, environments.[5] The ash from wastewater-cultivated algal solids is primarily composed of calcium (Ca), silica (Si), and phosphorus (P) while marine macroalgae ash is primarily sodium (Na), chloride (Cl), and potassium (K). Prior work on the hydrothermal treatment of wastewater-cultivated algal solids also indicated that the inorganic elements observed in marine macroalgae tend to remain in the aqueous co-product (ACP) after hydrothermal liquefaction (HTL) resulting in low HTL solids yield.[6] A majority of the metals and nonmetal observed in wastewater-cultivated algal solids, however, were retained in the solid phase following HTL.

The source of the inorganics in wastewater effluent is well-understood. When necessary lime, $Ca(OH)_2$, is added to adjust the pH and buffering capacity of wastewater during the treatment process. Nutrients, such as P, and silica are often included in the wastewater entering the treatment facility originating from agricultural runoff or other waste streams. How these inorganics become incorporated within the algal solids is not fully understood. It has been speculated that abundance of silica is due to the observation of diatom microalgae species within the multiple, mixed-species algal culture that cultivates in wastewater. Diatoms incorporate silica into their cell wall; however, no further empirical evidence has proven the hypothesis that the measured silica source are diatoms. Finally, although prior work revealed the presence of tricalcium phosphate, $Ca_3(PO_4)_2$ (TCP), and calcium oxide, CaO, in the ash of wastewater-cultivated algal solids, it was speculated

that these compounds were formed during the calcining or combustion of said algal solids and not via precipitation from algal cultivation or harvesting.[6]

The focus of this chapter is two-fold: 1) to further explore and quantify the inorganic species observed in wastewater-cultivated algal solids as previously mentioned and 2) the effect of the inorganics during HTL in terms of solid product both yields and structure. The fate of the inorganic species post-HTL is critical for the potential to create a high-valued, solid co-product such as a fertilizer or catalyst.

4.2 Methods and Experimental Setup

To understand the retention of inorganics from the pilot-scale, wastewater-cultivated algal solids, six lab-scale, (15L) light rack tanks were utilized (Figure 16). For simplicity, a single-strain, monoculture of *Chlorella vulgaris* was grown. The media was supplemented with a range of additional calcium and/or silica to further mimic the inorganic content of wastewater effluent. Three diatom species, *Chaetoceros*, *Cylindrotheca*, and *Skeletonema* were also grown independently to understand their inorganic structure.

In addition to altering the growth media and algal species, two dewatering or biomass harvesting methods were utilized. The first algal harvesting method was centrifuging the entire volume of the light rack tank. The second harvesting method included an auto-flocculation technique prior to centrifugation. The pH of the media was artificially increased to approximately 10.5 by the addition of concentrated sodium hydroxide (NaOH). The rise in pH causes certain solids to precipitate from the growth media. The surface charge of these precipitates differs from that of the microalgae cells causing the microalgae to coagulate, flocculate, and settle to the bottom

of the tank. Before and after photos of the auto-flocculation phenomena are shown in Figure 17. The bottom level of suspended algal solids was then further dewatered through centrifugation.

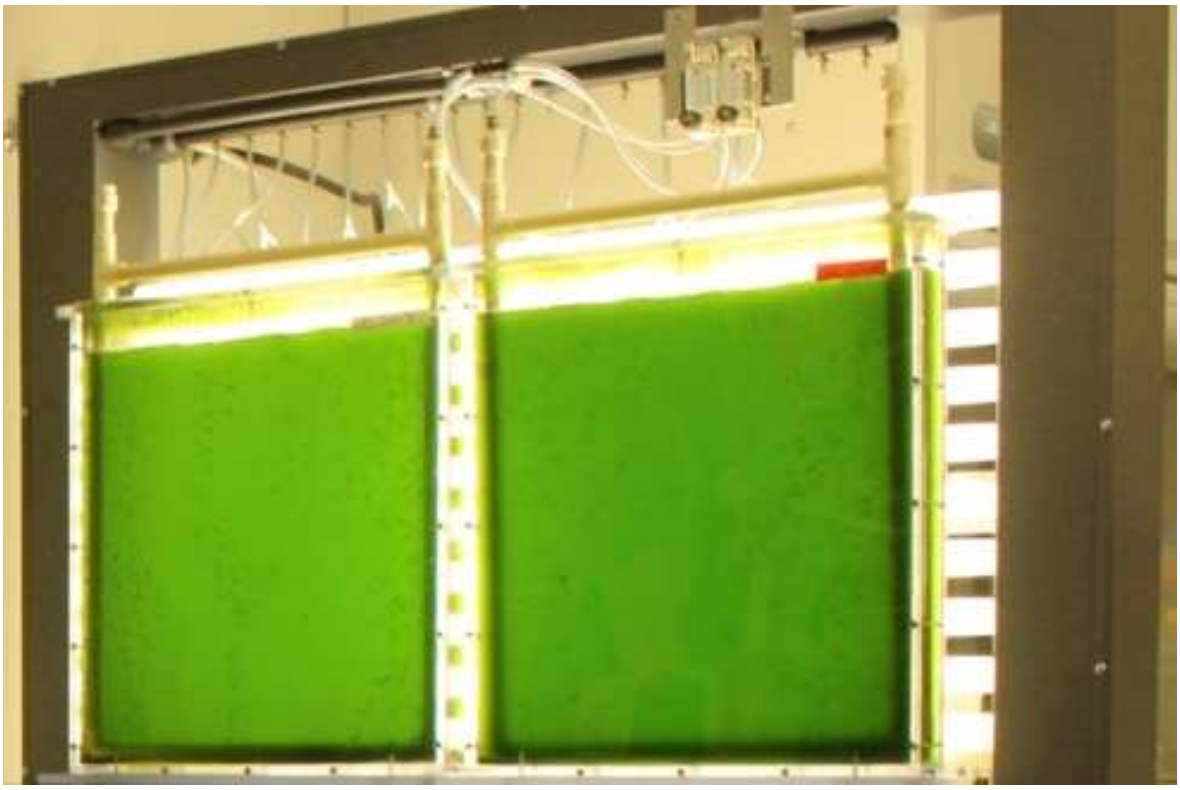

Figure 16: flat-bed, 15-liter, light rack tanks used to cultivate algal solid biomass.

The reasoning for artificially raising the pH within the light rack tanks was the higher pH observed at the pilot-scale, wastewater effluent, algal growth media by our wastewater engineering collaborators. The higher pH and auto-flocculation were able to occur naturally at the wastewater treatment facility due to the CO_2-limited nature of the growth tanks. Carbon dioxide readily dissolves (H = 29 L atm mol^{-1} at 25°C) and associates in water as carbonic acid (H_2CO_3) or bicarbonate (HCO_3^-) and ultimately lowers the pH of the water. Microalgae, however, consumes these carbonate species. Especially at later growth stages, the microalgae consume carbonate at a rate faster than atmospheric CO_2 dissolves into the media. As a result, the pH of the growth media

naturally rises inducing inorganic precipitation and microalgae auto-flocculation. This phenomena was first observed and proven in wastewater stabilization ponds by Golueke and Oswald.[7]

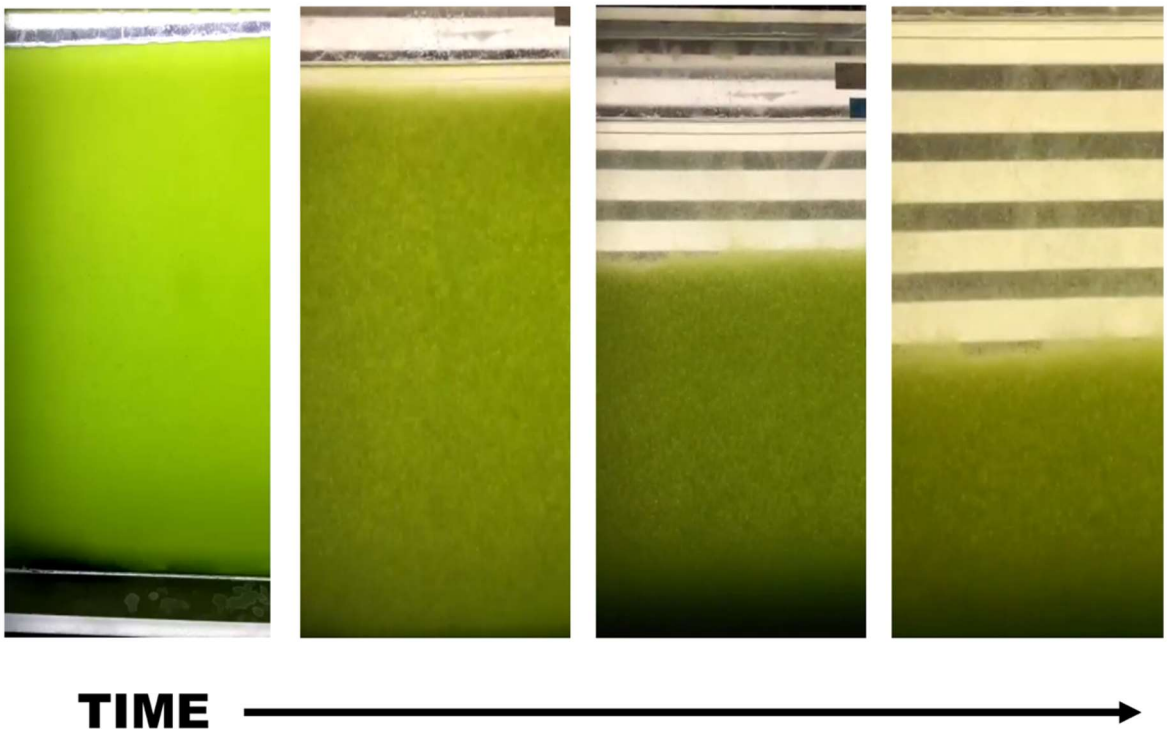

Figure 17: Four individual, time-lapse photos of algal solids auto-flocculating and naturally settling to the bottom of the light rack tank.

After harvesting the algal solids were then characterized using a variety of techniques that focused on inorganic composition and structure. A proximate analysis using a thermogravimetric analyzer (TGA) quantified the ash content. Acid, microwave digestion followed by inductively-coupled plasma optical emission spectroscopy (ICP-OES) measured the calcium, phosphorus, and other abundant metal and nonmetal elements present in the algal solids. Silica was not measured using ICP-OES, for it requires hydrofluoric acid (HF) to digest and the lab was not equipped to handle concentrated HF. Finally, Fourier Transform Infrared spectrometry (FTIR) and x-ray diffraction (XRD) provided further qualitative analysis of the inorganic compounds and structure

of the algal solids. More descriptive details of these techniques are explained in Chapter 3 *Methods*.

After algal characterization, several algal solid samples were reacted using a conventional, batch hydrothermal liquefaction (HTL) technique. The product yields were measured and quantified for each reaction. The products were further characterized with an emphasis on the fate of initial inorganics in the final HTL products. The inorganic concentrations of the ACP were measured by ICP-OES. The identical proximate method for quantifying the ash of algal solids was used for HTL solids. Then, depending on the remaining amount of solids produced during the HTL reaction, further characterization of the HTL solids was performed. Similarly, HTL solids were microwave digested in a strong acid media, diluted, and inorganic concentrations also measured by ICP-OES. Finally, XRD and FTIR provided the necessary qualitive results to better identify the inorganic structure of the HTL solids.

4.3 Collaboration

Preparing the growth media, maintaining algal growth, and harvesting the algal biomass were all overseen students under the direction of Dr. Belinda Sturm in environmental engineering. The earlier, preliminary auto-flocculation and harvesting studies were conducted by undergraduate students Emily Cook, Abigail Perkins, William O'ffill, and Ryan Magner. The later cultivation of both diatoms and *Chlorella vulgaris* were conducted by the graduate student, Sirwan Alimoradi. The role of the author for this research thrust involved the execution, training, and supervision of all the aforementioned algae characterization methods for the early, auto-flocculation study. Furthermore, I performed or oversaw all HTL reactions, product extraction and separation, and calculated all product yields. For the later diatom and fate of inorganics studies, the algae and

HTL product characterization were shared between the graduate students: Sirwan and myself. Again, my focus for the algal and HTL solids characterization was for the aforementioned methods and techniques, and those analyses and thrusts will be presented and discussed in the following sections.

4.4 Results and Discussions

4.4.1 Inorganic Characteristics of Algal Solids

The primary objective for this section was to identify how wastewater-cultivated algal solids were able to capture and retain a high inorganic content by exploring two harvesting techniques. Figure 18 displays the calcium concentration as mg Ca per dry kg of algal solids (mg/kg) from growth media varying in calcium to phosphorus (Ca:P) molar ratio. The pH signifies the two different harvesting techniques that were utilized. One harvesting technique retained the neutral, growth pH (7) and simply centrifuged the algal biomass. The second harvesting technique utilized auto-flocculation by artificially raising the pH to 10.5. Both of these harvesting techniques were compared to wastewater-cultivated algal solids.

From Figure 18, it is apparent that microalgae harvest via auto-flocculation and a higher pH captured more Ca than microalgae that was harvested at a neutral pH and then centrifuged. Additionally, the ash weight percentage of the algal solids followed the same trend. Auto-flocculated algal solids (pH = 10.5) had three to four times higher ash wt% than those that were centrifuged. The direct correlation of between algal solid calcium content (mg/kg) and ash wt% is to be expected. In addition, calcium is expected to represent the bulk of the inorganic content of the light rack algal solids,

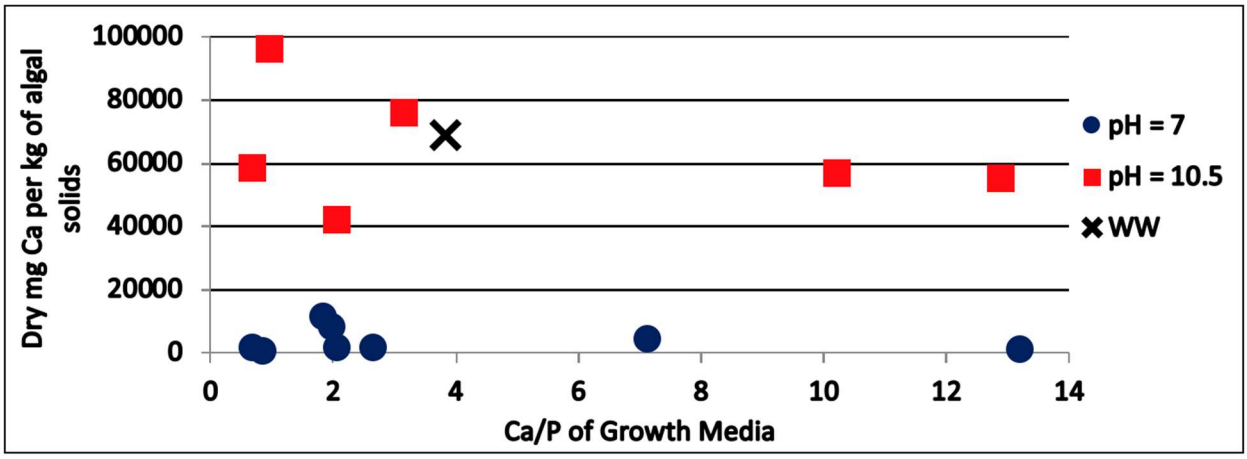

Figure 18: The measured mg of Ca per kg of dry algal solids from simply centrifuged (pH =7), auto-flocculated (pH =10.5) and wastewater (WW) cultivated samples.

Calcium concentrations ranged from 42,000 to nearly 97,000 mg/kg while the maximum Ca content for microalgae harvested at a pH of 7 was only 11,600 mg/kg. Meanwhile the Ca concentration measured in the wastewater-cultivated algal solids was 70,000 mg/kg. The Ca content of auto-flocculated and centrifuged algal solids were also not impacted by the Ca:P molar ratio of growth media, as no apparent trend appears in Figure 18. Overall, the higher amount of Ca observed in the auto-flocculated algal solids indicate the observed calcium is external of the algal cell and therefore presumed to have precipitated from solution during the auto-flocculated harvesting.

X-ray diffraction (XRD) can be used for identifying solid, crystalline compounds within the algal and HTL solid samples. Figure 19 depicts four XRD spectrums of pure calcium carbonate ($CaCO_3$), two auto-flocculated, light rack algal solids, and wastewater algal solids. It is evident that calcite, the mineral title for $CaCO_3$, is the primary crystalline structure of both auto-flocculated and wastewater algal solids. Algae harvested from the light rack, algal growth tanks and then centrifuged, depicted amorphous, or non-crystalline, solid structures from XRD. It is important to

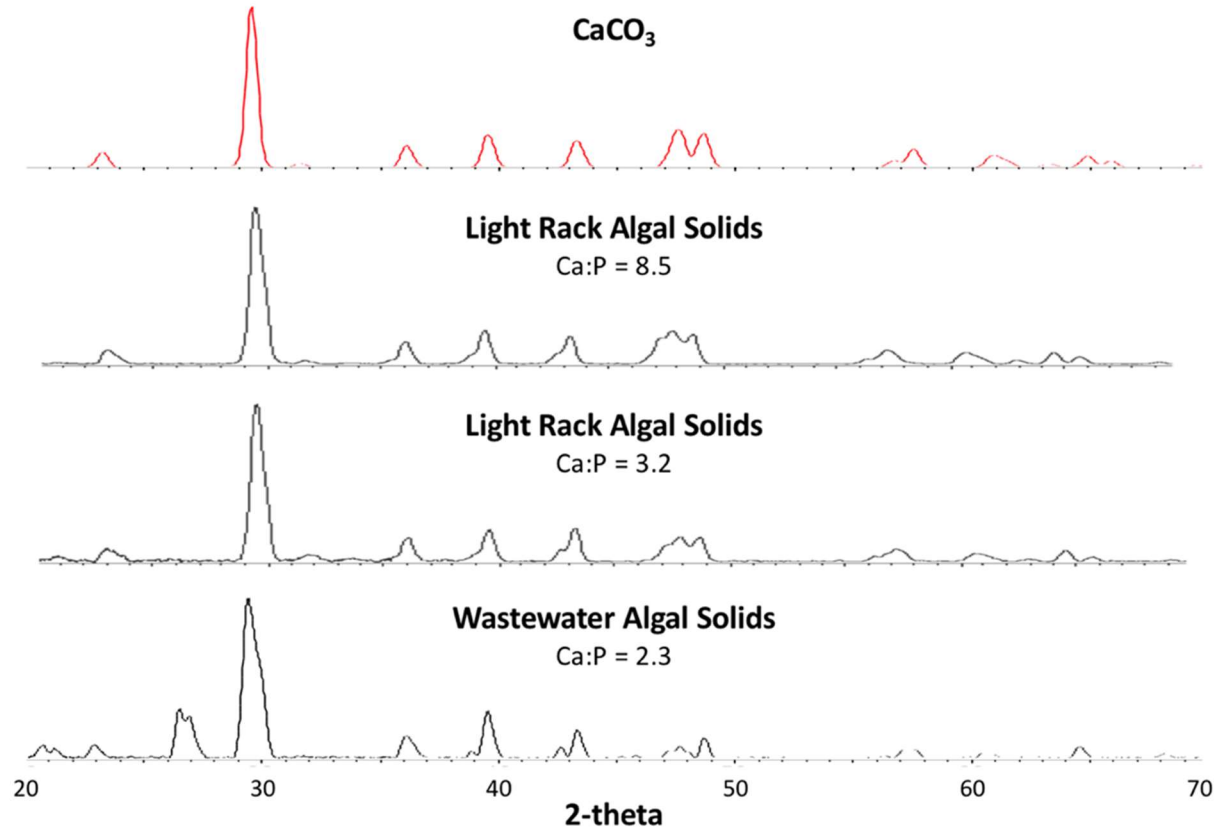

Figure 19: XRD patterns of pure calcium carbonate ($CaCO_3$) and light rack and wastewater algal solids with the corresponding Ca:P molar ratio of the algal solid samples.

note the additional peaks that appear between 20 to 22 and 26 to 28 2θ in the wastewater-cultivated algal solids that do not appear in the light rack algal solids. These peaks correspond to the primary and secondary peaks of SiO_2. These SiO_2-representative, XRD peaks differ from XRD patterns indicative of diatoms. The XRD patterns for the three aforementioned diatom species are shown in the Appendix.

With the exception of diatoms, XRD is often not performed on algal solids as they typically have a low inorganic, ash content. The clear detection of $CaCO_3$ is further evidence that calcium is precipitating from solution due to the higher pH from auto-flocculation harvesting. Chen et al. who also studied wastewater-cultivated ag also hypothesized the presence of $CaCO_3$ within the

algal solids; however, they attributed it not due to precipitation but from the presence of snail shells.[2] Prior work by Roberts et al. at KU detected calcium oxide, CaO, within the wastewater-cultivated algal solids ash which was ascribed to the presence of $CaCO_3$.[6] It is well-understood that when combusted at temperatures above 550°C, $CaCO_3$ decomposes to CaO and releases CO_2 gas.[8]

Flocculation is a practical and well-understood algal thickening technique that is associated with the surface charges of algal cells and chemical coagulants.[9] Microalgae typically has a negative surface charge due to surface carboxyl and sulphate groups.[10] Thus, an effective coagulant for microalgae would carry a positive surface charge. Auto-flocculation occurs when these coagulants appear in solution, or growth media in the case of microalgae, naturally. These coagulants typically form via precipitation, which occurs from a change in pH. Wu et al. observed an exponential increase in the flocculation efficiency of *Chlorella vulgaris* at a pH greater than 9.5.[11] They went on to hypothesize the precipitation of magnesium hydroxide, $Mg(OH)_2$, was the primary coagulant of algal growth media at the higher pH.[11].

The addition of lime and precipitation of calcium phosphate has also been theorized to cause microalgae auto-flocculation. Vandamme et al. further explored and compared the efficacy of magnesium (Mg^{2+}) and calcium (Ca^{2+}) in microalgae auto-flocculation and determined magnesium was four to five times more efficient than calcium at a pH of 10.5 or 11.[10] It is important to note that for these independent light rack and auto-flocculated algal solid tanks, the pH was artificially risen and auto-flocculation was induced during the later stationary growth stage of P-limited growth media (N:P = 109 or 545). The reason for these growth conditions was to maximize algal biomass productivity. The final phosphorus (P) concentration in the light rack tanks at the time of harvesting and auto-flocculation was therefore at ppm levels and much lower

than the previously reported ideal P-concentration (0.1-0.2 mM) for a calcium phosphate precipitation.[10]

Although no magnesium crystalline structures were detected within the algal solids by XRD analysis, the literature reports an adequate magnesium concentration (0.15 mM at a pH of 10.5) is necessary to induce auto-flocculation of algal solids.[10] It was further explained and shared by our collaborators that in light rack tanks were Mg was omitted, no auto-flocculation was observed. The significance of magnesium to induce auto-flocculation is further evident magnesium per dry kg of dry algal solids (mg/kg) within algal solids that were auto-flocculated compared to microalgae that was centrifuged. Auto-flocculated algal solids had two to three times more magnesium present than centrifuged microalgae.

In conclusion, auto-flocculation is an effective technique for dewatering algal biomass and appears to occur naturally for wastewater cultivated algal solids. Higher calcium concentrations and ash weight percentages were observed for auto-flocculated algal solids indicating the high inorganic content is external from the microalgae cell and due to solid precipitation at a higher pH. The primary crystalline structure for wastewater-cultivated algal solids and artificially, auto-flocculated algal solids was confirmed by XRD to be the mineral calcite ($CaCO_3$). Finally, magnesium, although undetected by XRD within the algal solid, has a critical role in flocculation efficacy within the growth media when harvested at low phosphorus concentrations.

4.4.2 Inorganic Characterization of HTL Solids

Flocculation has two drawbacks when it comes to commercial use. First, chemical coagulant inputs add chemical costs, but this can be avoided with auto-flocculation as previously discussed. Secondly, flocculation increases the inorganic content of the biomass, which is often

seen as problematic for fuel and/or chemical conversion and requires additional biomass pretreatment to remove. The objective of this section is to observe and discuss the structure of these inorganics from the hydrothermal conversion of high-ash algal solids.

Figure 20 depicts the XRD patterns of the resulting HTL solids produced by the algal solids previously identified in Figure 19. Calcite ($CaCO_3$) remained the primary crystalline structure for both light rack algal solids. The algal solids with the lower Ca:P molar ratio of 3.2 also had secondary peaks of tricalcium phosphate (TCP). Meanwhile the crystalline structure of the HTL solids produced from wastewater-cultivated algal solids, which had a Ca:P of 2.3, showed no significant peaks associated with calcite. The XRD pattern depicted hydroxyapatite (HAp) as the primary structure for these HTL solids while the SiO_2 peaks around 21 and 27 2θ remained from the initial algal solids. These results indicate algal solids with lower Ca:P molar ratios favor calcium phosphate as the resulting solid structure post-HTL. This is to be expected for the stoichiometric ratio of TCP and HAp are 1.5 and 1.67, respectively. It can also be hypothesized that the presence of silica may also enhance or promote the formation of calcium phosphate. This hypothesis will be further explored in Chapter 5: *Model Compounds.*

Another notable result comparing HTL solids produced from the auto-flocculated to the centrifuge algal solids was the fate of phosphorus. The auto-flocculated algal solids that had higher Ca and ash content recovered nearly 100% of the initial phosphorus in the HTL solids. Furthermore, although no apparent phosphate compounds appeared in the XRD pattern, large phosphate peaks appeared in the FTIR spectra for the HTL solids that were produced from the high-ash, high-Ca algal solids. These results are further reviewed in the independent, light rack study, *Fate of Phosphorus post-HTL*, that is discussed in the ensuing section.

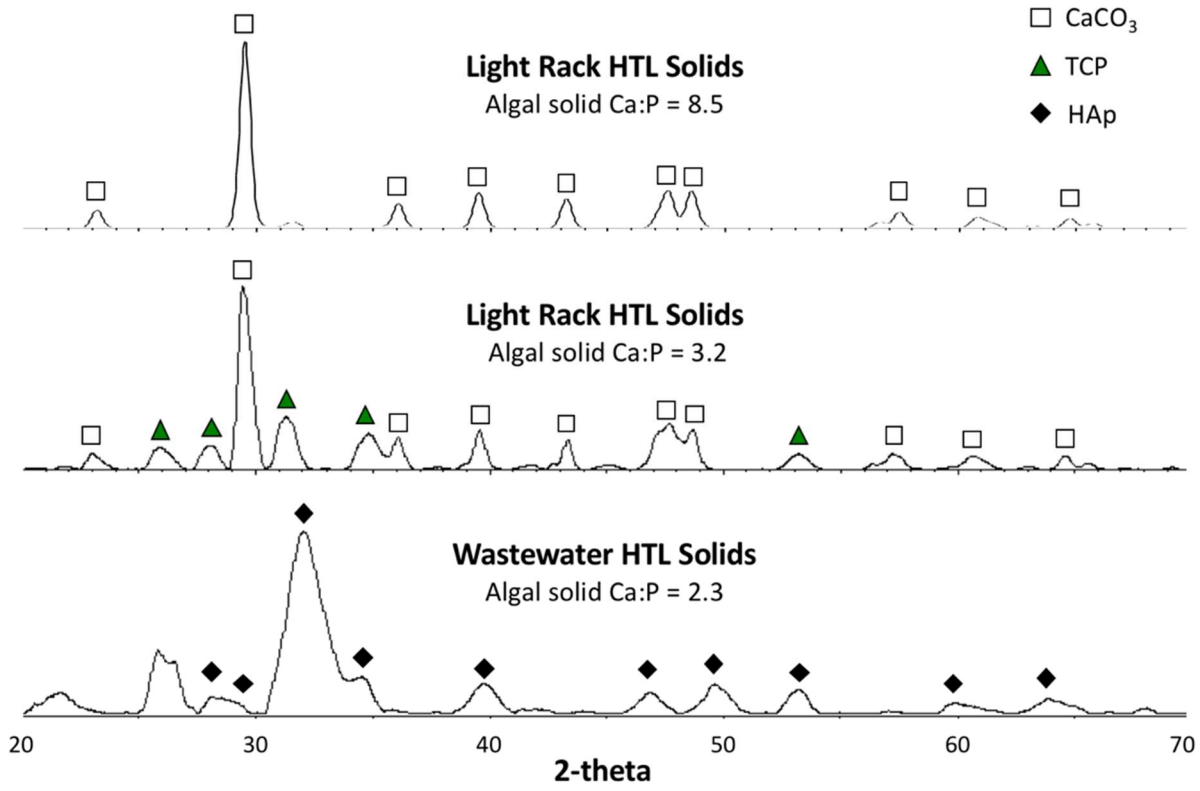

Figure 20: XRD patterns of the HTL solids produced from the algal solids represented in Figure 19. Calcite ($CaCO_3$), tricalcium phosphate (TCP), and hydroxyapatite (HAp) were all identified as the primary crystalline structures amongst the samples.

The high P-recovery in the solid product agrees with our prior work with wastewater-cultivated algal solids[6]. In contrast, HTL of monoculture, low-ash algae often reported a majority of the phosphorus remained in the aqueous phase. Many of these works focused on recycling phosphorus for subsequent, alternative algal growth media.[12-14] However, ample dilution is required due to the toxicity of the nitrogenous organic compounds also found in the aqueous HTL co-product.[15] Given the abundance of water necessary for the HTL reaction (90 wt%), the abundance of ACP recovered following the HTL reaction ($\geq$ 95 %), and the copious amount of dilution required to minimize the toxicity of N-compounds in the ACP, recycling and utilizing the ACP for further algal growth is not practical. Recovering the phosphorus in the HTL solids rather

than ACP would be more practical. Phosphorus recovered as HTL solids can serve as a catalyst or have tissue regeneration application as previously observed and reported for wastewater-cultivated algal solids.[6] Finally, solid calcium phosphates also have high agricultural fertilizer application.[16-17]

4.4.3 Fate of Phosphorus post-HTL

To further confirm the hypothesis that the higher calcium content observed in the algal solids dictated the fate of phosphorus during HTL, an additional study was conducted. Six light rack tanks were grown, and all were harvested via auto-flocculation; however, each had a different initial Ca:P molar ratio in the growth media ranging from 1.0 to 8.0. The result was a more comprehensive set of samples that best encompasses inorganic capture through auto-flocculating algal solid harvesting and the resulting HTL products. Table 8 summarizes the growth conditions, biomolecular and ash content, and the inorganic characteristics from the auto-flocculated algal solids harvested in this independent study.

The results from Table 8 agree with the preliminary, independent algal solid results from Figure 18. In general, as the molar Ca:P increased in the growth media the ash wt% and the molar Ca:P of the algal solids also tended to increase. Despite nearly double the amount of Ca and 1.4 times the amount of Mg, the algal solids from Tank 3 had a lower ash wt% than Tank 2 (6.3 versus 4.6 dw%, respectively). This discrepancy could be due to the atypical method for measuring and calculating the inorganic concentrations of the algal solids. Interferences were observed from the ICP-OES analysis of the acid-digested algal solids from this study causing imprecise and inaccurate inorganic measuring. The interferences are presumed to be from metals or inorganics

Table 8: The growth media and resulting algal solid characteristics including biomolecular (carbohydrate, protein, and lipid), ultimate (C, H, N, and O), and inorganic content along with the crystalline structure. Standard deviation depicted in ().

LIGHT RACK	MEDIA		ALGAL SOLIDS												
	Ca:P	Alkalinity	C	H	N	O	Carb.	Protein	Lipid	Ash	Ca	P	Mg	Ca:P	XRD
Tank	*mol*	*mg/L $CaCO_3$*	*dw%*	*dw%*	*dw%*	*dw%*	*dw%*	*dw%*	*dw%*	*dw%*	*mg / kg*	*mg / kg*	*mg / kg*	*mol*	*Pattern*
1	1.0	249	53.8 (0.1)	6.8 (0.1)	8.9 (0.1)	20.2 (0.3)	24.7 (3.1)	54.2 (4.2)	9.0	6.1	2,481	14,175	8,236	0.1	Amorph.
2	2.3	359	53.7 (0.02)	6.9 (0.1)	9.1 (0.04)	20.1 (0.01)	23.9 (2.3)	61.4 (3.1)	9.0	6.3	25,659	13,221	8,956	1.5	Amorph.
3	3.7	363	53.2 (0.04)	6.9 (0.02)	8.9 (0.01)	20.6 (0.2)	27.5 (3.3)	60.9 (1.0)	8.5	4.6	50,176	12,625	12,378	3.1	Amorph.
4	4.9	410	50.9 (0.1)	6.6 (0.1)	8.3 (0.03)	20.8 (0.2)	21.4 (2.8)	48.8 (1.0)	7.6	8.1	51,179	11,431	11,431	3.5	Calcite
5	5.9	410	47.7 (0.1)	6.0 (0.1)	7.7 (0.01)	20.7 (0.2)	23.9 (5.9)	46.9 (8.2)	8.8	12.3	74,150	10,613	10,631	5.4	Calcite
6	8.0	391	46.3 (0.1)	5.6 (0.1)	7.4 (0.02)	21.1 (0.3)	16.6 (4.6)	39.4 (5.2)	7.9	13.1	104,918	10,779	10,779	7.5	Calcite

Amorphous abrv. Amorph.

Carb. abrv. Carbohydrate

collected through the secondary microwave digestor borrowed from the KU Geology Department as our digestor was being repaired. The inorganic content of the algal solids was therefore back-calculated through the mass balance of the initial and final concentrations of the growth-media before and after auto-flocculation and the mass of algal solids after freeze-drying and grinding. While this indirect analysis provided a more accurate means of determining the algal solid inorganic content than the ICP-OES, the multitude of measurements and steps can occur unexpected losses and/or gains thus compounding the final error. Assumptions of the final tank volumes post-growth and before harvesting were also made to calculate the inorganic balance.

Tanks 3 and 4 also shared similar Ca and P concentrations (mg/kg) and thus similar Ca:P molar ratios; however, their crystalline structure varied greatly between being amorphous and calcite. The justification for the difference in crystalline structure can be explained through the difference in the alkalinity between the tanks. Alkalinity is a measurement of buffer capacity within a natural water body. It is measured through titration and reported as mg/L of $CaCO_3$ because carbonic acid (H_2CO_3) is often the most prominent weak acid present in natural water bodies, as well as in this study, performing the pH buffering. The total carbonate (CO_3^{2-}) present in solution is directly correlated to alkalinity when the pH is constant. Thus, algal solids from tank 4, which had an alkalinity of 410 mg/L $CaCO_3$, had a greater potential for carbonate to precipitate from solution as $CaCO_3$ during auto-flocculation than tank 3, which had an alkalinity of 363 mg/L $CaCO_3$. Water chemistry modeling to theoretically predict the carbonate concentration and inorganic compounds to precipitate from the growth media from high pH auto-flocculation of microalgae was further studied by the collaborating graduate student, Sirwan Alimoradi.

While the biomolecular content was measured and studied by the collaborator, the ultimate analysis, inorganic, ash, and overall mass balance of the algal solid biomass were a major thrust

of our collaboration. The ash-free dry weight (afdw%) mass balance from organic ultimate analysis (C, H, N, and O) was within 8% for algal solids from all six tanks. The mass balance of the biomolecular balance for the algal solids harvested from tanks 1 – 3 were also all within 6%. The balance of biomolecular content and ash wt% for the algal solids harvested from tanks 4 – 6, however, were 8 to 23% short from closing. The understated mass balance can be explained by the presence of carbonate in the algae solids leading to an underestimation of the ash wt% with TGA. During the pyrolysis and combustion of the high ash, calcite algal solids, $CaCO_3$ decomposes to CaO and emits carbon dioxide. Thus, the carbon from carbonate, often referred to and distinguished as "inorganic" carbon by environmental engineers, and two oxygen molecules are not accounted for in the ash measurement nor is measured by the conventional protein, carbohydrates, and lipids analysis leading to an incomplete balance on the algal solids. The measurement of inorganic carbon and its role in the HTL reaction is discussed in later chapters.

Figure 21 displays the dry weight yield (dw%) for the HTL solids produced by algal solids harvested from their respective tanks, and the yield of HTL solids increased with increasing calcium content of the growth media. The yield of HTL solids from the reaction of algal solids harvested from tanks 1 and 2 was less than 2 dw%. HTL solids had yields of over 17 dw% after the HTL reaction of algal solids with the highest calcium content (mg/kg). To further identify any inorganic solid transformation occurred during the HTL reaction, an inorganic balance was calculated from equation (11).

$$\%\ \text{Inorganic Recovery} = \frac{m_{\text{HTL solids}} \times \%\ ash_{\text{HTL solids}}}{m_{\text{algae}} \times \%\ ash_{\text{algae}}} \times 100 \tag{11}$$

Where m_{algae} are the mass of algal solids loaded into the reactor, $m_{HTL\ solids}$ is the mass of HTL solids recovered from the reactor, % ash_{algae} is the ash wt% of the algal solids and % $ash_{HTL\ solids}$ is the ash wt% of the HTL solids.

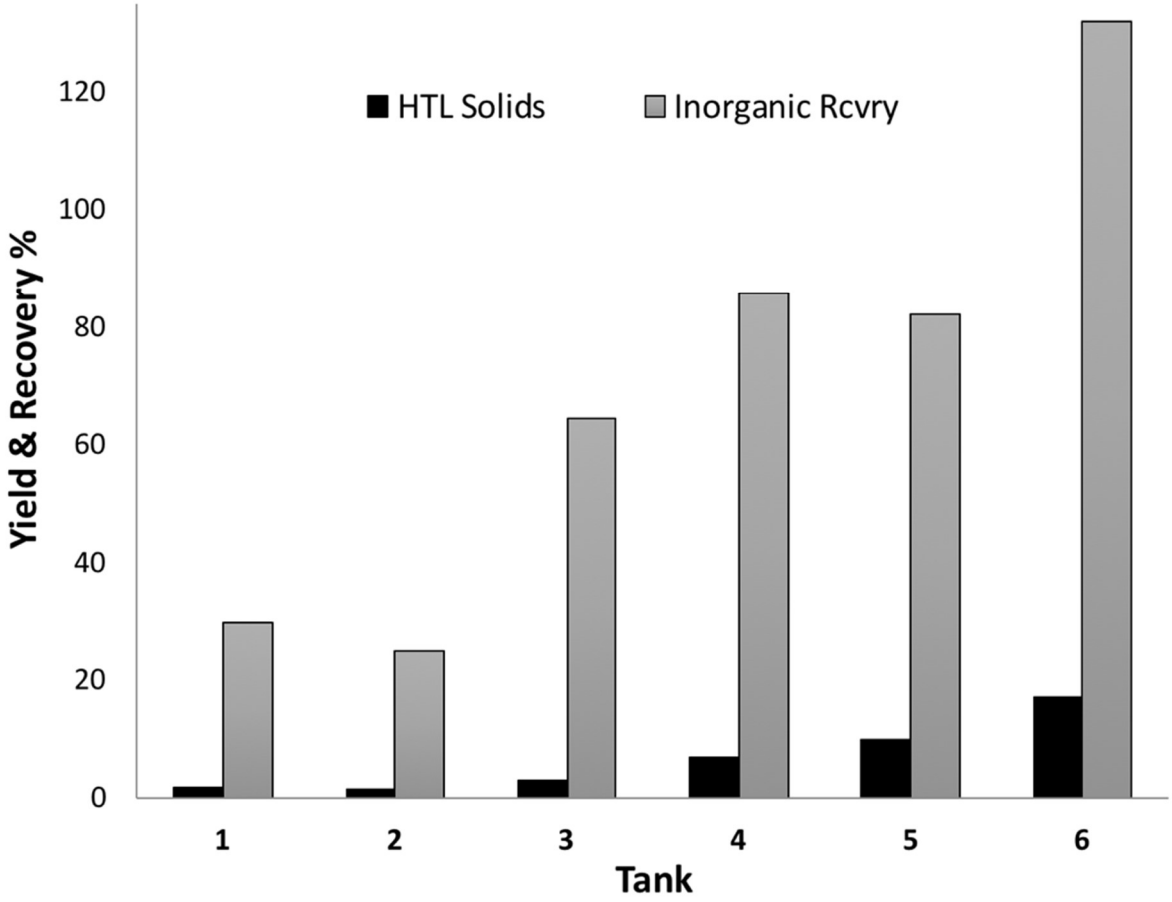

Figure 21: The dry weight (dw%) yield and inorganic recovery measured and calculated, respectively, from the HTL solids produced from the algal solids harvested their respective tanks.

The ash wt% for both the algal and HTL solids was determined using the same proximate analysis method on a TGA. Thus, the measurement of ash, or inorganic material, in both the algal and HTL solids were the same. In other words, the temperature at which the solids were ashed (850°C) ensured any remaining carbonate from to $CaCO_3$ and hydroxide from HAp was combusted. For the HTL solids it also ensured any residual biocrude that remained on the HTL solids was also combusted and removed. Overall inorganic recovery and Equation (11) provided

a broader sense of whether a change or reaction occurred during HTL between the algal and HTL solids.

Similar to the HTL solids yield and the algal solid ash and calcium content, the recovery of inorganic ash material after HTL were directly related and are shown in Figure 21. Algal solids from tanks 1 and 2 only recovered 25 - 30% of the initial inorganic content in the solid HTL product. Tank 3 algal solids saw a 65% recovery of inorganics while algal solids from tanks 4 and 5 had 86% and 82% respectively. Jiang and Savage reported the only substantial amount (> 300 ppm) of metal content present in biocrude from conventional HTL of microalgae to be sodium and iron metals.[18] Thus, the balance of the inorganics, especially those of interest in this study, are expected to be in the ACP. Algal solids harvested from tank 6, however, saw greater than 130% recovery of inorganic, ash material in the HTL solid product. This indicates a chemical transformation between the inorganic solids occurs during HTL. This transformation causes the mass of solid ash remaining after TGA proximate analysis for the HTL solids to be greater than that of the initial algal solids.

One hypothesis for this increase of inorganic ash material in the HTL solids compared to the algal solids is the capture and recovery of phosphorus (P) during the HTL reaction. Figure 22 shows the fate of phosphorus between the aqueous co-product (ACP) and the HTL solids. The phosphorus recovery in the HTL solids was less than 73% when the HTL reaction was performed on the algal solids from tank 1 – 3. This means that between 28 – 44 % of the phosphorus remained in the aqueous phase. The high amount of phosphorus in the aqueous phase is characteristic of many studies previously reported with HTL of single strain, low ash algae.[12-13, 19] In contrast to these studies, algal solids from tanks 4 - 6, saw nearly 100% of the phosphorus retained in the HTL

solids. The nearly complete recovery of phosphorus in the HTL solids agree with our previous study from wastewater-cultivated algal solids.[6]

The cause for high solid phosphorus recovery could be explained by the higher calcium loading in the growth media. Heilmann et. al. demonstrated via HTC of various animal manures, that manure with higher metal content resulted in higher levels of phosphorus being recovered in the solid product.[20] They suggested this phenomenon was due to formation of highly insoluble, phosphate salts with these metal cations which is analogous to the observed HAp in the HTL solids from wastewater-cultivated algal solids by Roberts et.al.[6, 20] In order to test this hypothesis, an additional HTL reaction was conducted by combining algal solids from tanks 1 and 2 with commercial $CaCO_3$ (Fisher Scientific). An equal mass of algal solids from tanks 1 and 2 were mixed and then doped with 0.2 g of $CaCO_3$ so that the 10 wt% solids loading to the reactor was maintained. Represented in Figure 22 as "1 & 2," this reaction resulted in 97% of the phosphorus being recovered in the HTL solids as opposed to the original 72% and 56% of the phosphorus recovered individually from tanks 1 and 2 respectively. These results confirm that the presence of precipitated calcite solids promote the recovery of P in the solid phase following HTL.

FTIR analysis provided further evidence of the presence of phosphorus and specifically, PO_4^{3-} in the HTL solids. Figure 23 shows the FTIR spectra of the solids produced from HTL of the algal solids from all six tanks. Phosphate (PO_4^{3-}) has two distinct peaks at 600 and 550 cm^{-1} and a broad peak with multiple shoulders from 900-1150 cm^{-1} which is characteristic of PO_4^{3-} stretching. All of the peaks are clearly present in the HTL solids that were produced from the algal solids harvested from tanks 4 – 6. In contrast, broad peaks that are not as distinct are observed for the HTL solids produced from the algal solids from tanks 1 - 3. Figure 23 also confirms the strong presence of carbonate in the HTL solids. Carbonate (CO_3^{2-}) peaks typically appear at 712 and 872

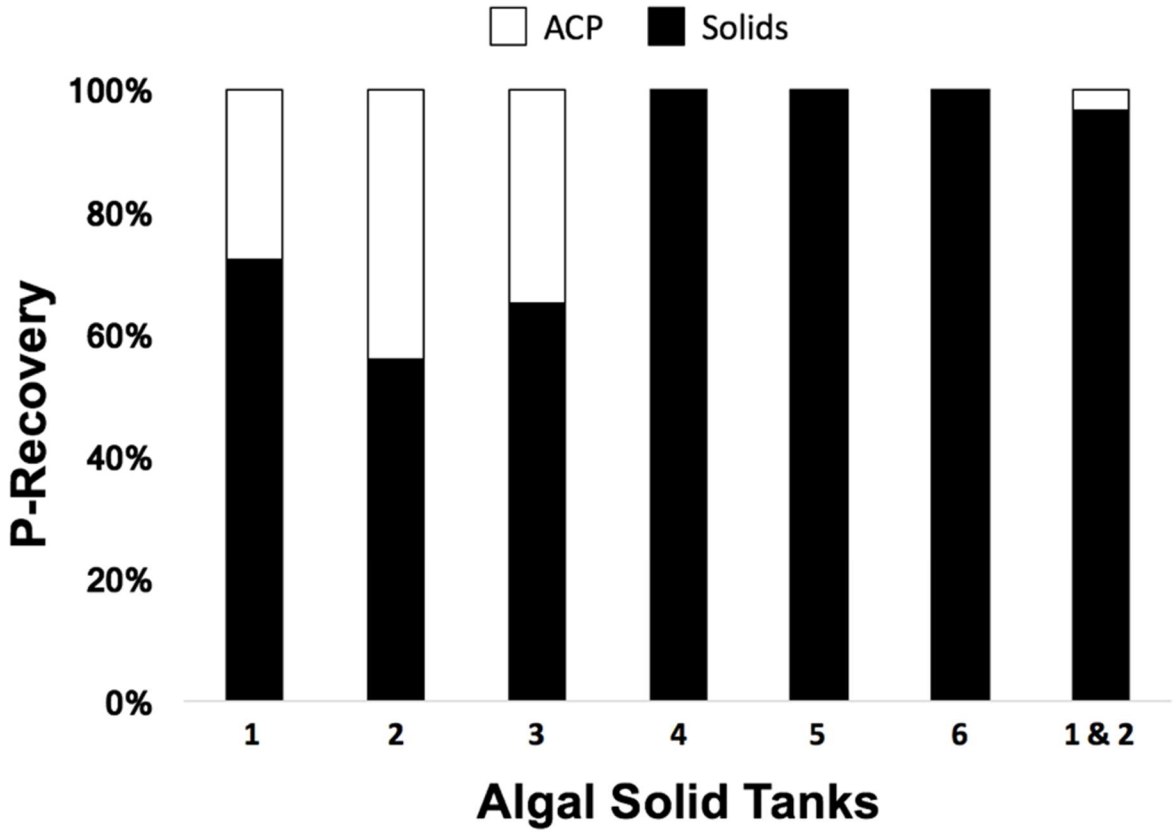

Figure 22: Phosphorus (P) recovery in the aqueous (ACP) and solid HTL products. An additional reaction involving algal solids from tanks 1 and 2 with the addition of $CaCO_3$ was also performed to further test the role of calcite on the fate of phosphorus.

cm^{-1} with a broad peak between 1150-1650 cm^{-1}. Thus, tanks 5 and 6 appear to have produced HTL solids with the greatest amount of carbonate while only a small amount in the algae harvested from tank 4. These observations of carbonate and phosphate in the HTL solids were further verified in the XRD patterns that can be seen in the Appendix. HTL solids produced by algal solids harvested from tank 1 were amorphous while XRD of HTL solids produced by algal solids from tanks 2 and 3 were unidentifiable. The HTL solids yields from these algal solids, however, were minimal (< 3 dw%) compared to the higher ash and calcite algal solids from tanks 4–6. The XRD patterns for the HTL solids synthesized by the high-ash, calcite algal solids showed both TCP and calcite as their primary structures. This combination of calcite and calcium phosphate

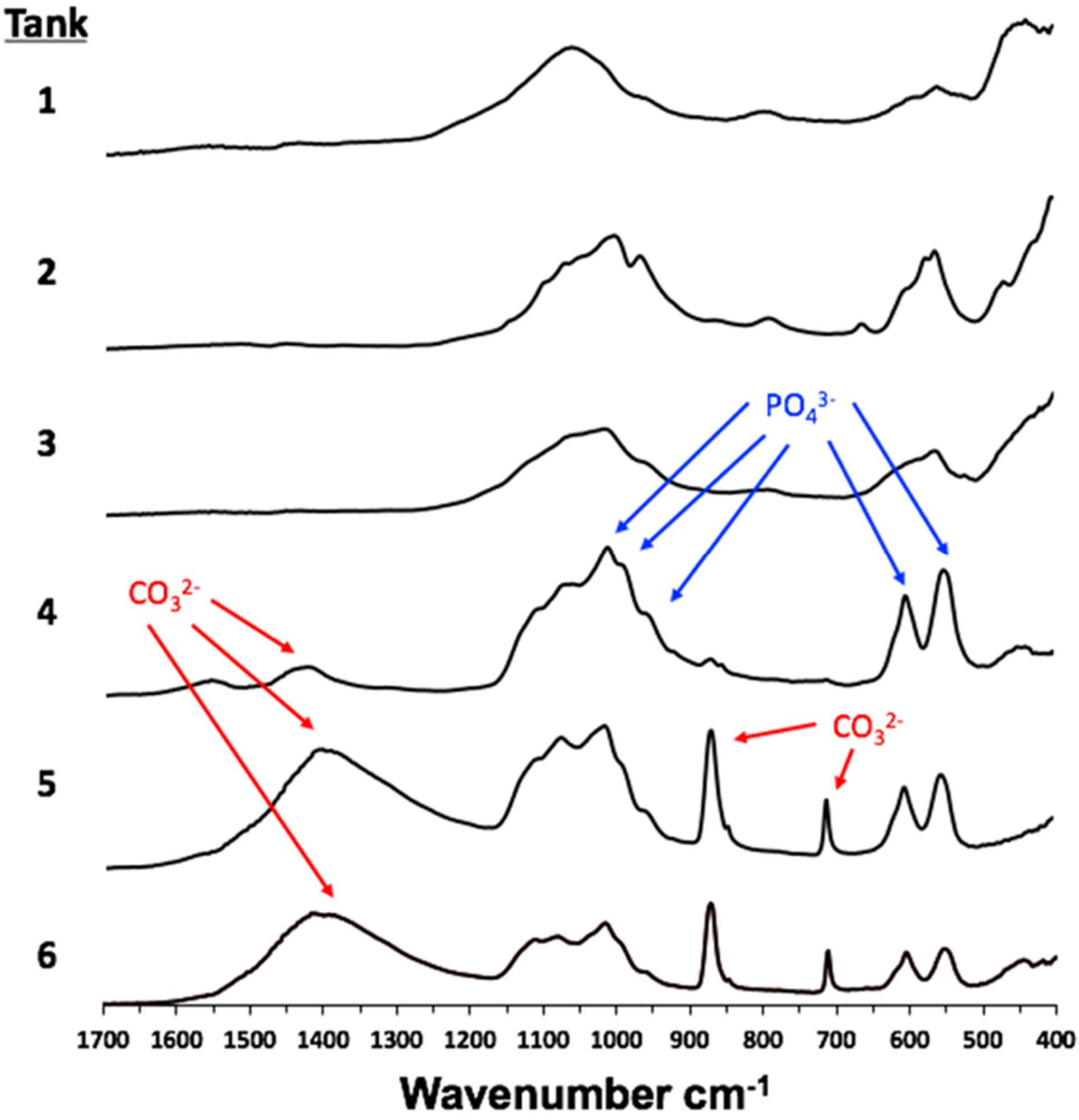

Figure 23: FTIR spectrum of the HTL solids that indicates the greater presence of both phosphate (PO_4^{3-}) and carbonate (CO_3^{2-}) ions in the HTL solids of calcite, high ash and Ca:P algal solids.

structures have been observed by several others who have identified the CO_3^{2-} and PO_4^{3-} peaks to be characteristic of substituted apatites and TCP minerals similar to what is observed in these HTL

solids.[6, 21-23] The XRD patterns for the HTL solids from all seven HTL reactions can be found in the Appendix.

The high retention of phosphate in the HTL solids from algal solids that were initially calcite, and the detection of a calcium phosphate structure for the HTL solids, lead to two possible hypotheses. First is that the solid, precipitated calcite from the auto-flocculated algal solids is transformed into calcium phosphates during HTL. The second possibility is that calcium phosphate also precipitated out during auto-flocculation; however, it remained amorphous and undetectable by XRD until after HTL. The former is explored in Chapter 5: *Model Compounds* and the later in Chapter 6: *Raceway*.

4.4.4 Inorganic in-situ HTL Catalysis

One potential application for the solids recovered from the hydrothermal liquefaction of wastewater-cultivated algal solids is catalysis. Improved or enhanced biocrude properties from HTL of high-ash, calcite algal solids compared to those that are low-ash and amorphous would further prove the *in-situ* catalytic capabilities of inorganic material within the algal solids. This section compares the properties of the biocrude extracted and analyzed from six light rack tanks from the light rack study previously discussed in Chapter 4.4.3 *Fate of Phosphorus post-HTL*. The biocrude yield and properties from the HTL reaction involving algal solids from light rack 1 and 2 that were doped with $CaCO_3$ are also discussed.

Table 9 depicts the biocrude yield, ultimate (C, H, N, and O), their various ratios relative to carbon, and the higher heating value (HHV) of the biocrude produced from the six, light rack algal solid samples. The biocrude yield was calculated in two different manners to illustrate the impact the ash wt% of the algal solids can have various means to calculate biocrude yield. The first, more

conventional way to report algal HTL biocrude yield is on a dry weight (dw%) basis. The justification for reporting yield on a dw% basis was traditional algal biomass has nominal ash content. Thus, including the mass of inorganics in traditional, low-ash microalgae did not have a large impact on the HTL biocrude dw% yields. For wastewater-cultivated and auto-flocculated algal solids with higher calcium content, the added mass due to inorganics can cause the HTL biocrude dw% to be lower and dissimilar to low-ash algal solids. Table 9 shows this discrepancy of dw% biocrude yields between low- and high-ash algal solids well. Low-ash algal solids that were harvested from light rack tanks 1-3 had a biocrude yield of 40-48 dw% while the higher ash algal solids harvested from tanks 4-6 had a lower biocrude yield of 35-38 dw%. Calculating the biocrude yield on an afdw% basis helps eliminate said discrepancy where the biocrude yields for five out of the six tanks were between 40-44 afdw%. HTL biocrude yields of microalgae are typically in the upper-30's to lower-40's, and calculating the yields on an ash free dry weight basis aids in equal comparison amongst low- and high-ash algal biomass.[1-3, 24]

The addition of $CaCO_3$ to low-ash algal solids harvested from light rack tanks 1 and 2 lowered the biocrude yield from 43.5 and 51.1 afdw% without $CaCO_3$, respectively, to 38.5 afdw% with $CaCO_3$. The added inorganics and higher HTL solids yield can entrap biocrude on the HTL solids. Thus, the greater HTL solids present, the more residual oil can be collected on the HTL solids, and not collected in the biocrude product. Furthermore, Biller and Ross did observe sodium carbonate Na_2CO_3 increase the biocrude yields of carbohydrate model compounds such as glucose and starch. They also observed an increase in biocrude yield was also observed from the addition of Na_2CO_3 with *Porphyridium cruentum*. A strain of microalgae that was 40 wt% carbohydrate.

It is hypothesized that when dissociated, $CaCO_3$ would have a similar impact for high carbohydrate algal solids. The carbohydrate content of the algal solids harvested from the light

rack tanks were less than a quarter of the mass for algal solids harvested from tanks 1 and 2. Also, XRD of the HTL solids from this HTL reaction that was doped with $CaCO_3$ showed the HTL

Table 9: The resulting biocrude yield, carbon (C), hydrogen (H), nitrogen (N), and oxygen (O) content as well as its higher heating value (HHV) for the six HTL reactions involving algal solids from the six light rack tanks. The HTL additional reaction and biocrude properties of algal solids from tanks "1 & 2" that were doped with $CaCO_3$ are also shown. Standard deviation depicted in ().

LIGHT RACK	BIOCRUDE									
	YIELD		C	H	N	O	H/C	N/C	O/C	HHV
Tank	*dw%*	*afdw%*	*wt%*	*wt%*	*wt%*	*wt%*	*mol*	*mol*	*mol*	*MJ/kg*
1	40.7	43.5	79.3 (0.8)	8.7 (0.2)	5.7 (0.1)	7.0 (0.3)	1.31	0.062	0.066	38.0
2	47.8	51.1	80.0 (0.8)	10.2 (0.1)	5.1 (0.1)	6.5 (0.2)	1.52	0.054	0.061	40.4
3	41.4	43.7	79.6 (0.4)	10.6 (0.2)	5.4 (0.1)	6.7 (0.1)	1.58	0.059	0.063	40.8
4	37.8	41.4	78.2 (0.4)	9.4 (0.1)	5.3 (0.1)	6.5 (0.2)	1.43	0.058	0.062	38.6
5	35.4	40.4	78.3 (0.9)	9.8 (0.1)	5.3 (0.1)	5.7 (0.1)	1.49	0.058	0.055	39.4
6	37.2	42.7	78.6 (1.1)	8.8 (0.4)	5.4 (0.1)	6.9 (0.2)	1.33	0.059	0.066	37.8
1 & 2	34.5	38.5	76.6 (0.1)	10.5 (0.2)	5.2 (0.1)	9.1 (0.1)	1.63	0.059	0.089	39.3

solids remained $CaCO_3$. Thus, the added $CaCO_3$ may not have had as great of impact on the biocrude yield, as it did not dissociate completely during the reaction.

Ultimate analysis provides are a large overview of the general composition of the biocrude product. The carbon content of the biocrude produced from HTL on the algal solids from all of the tanks was near 79 ± 0.7 wt%. Similarly, no large variation in the nitrogen content of the biocrude was observed from the six auto-flocculated algal solids. The average nitrogen content

for all six biocrudes produced was 5.4 ± 0.2 wt%. Similarly, the average oxygen content for the biocrude was 6.5 ± 0.5 wt% with algal solids from tank 5 producing the biocrude with the lowest at 5.7 wt%. The hydrogen content of the biocrude had the highest variance ranging from 8.7 to 10.6 wt%. The N/C and O/C molar ratios were both near 0.06 for the all biocrude products despite varied Ca and biomolecular content. This lower O/C and N/C molar ratios are typical for HTL biocrude from algae where the ACP was separated prior to the addition of extraction solvent (DCM).[6, 25-26]

The H/C molar ratio, however, varied from 1.31 to 1.59 with the lowest biocrude H/C molar ratios appearing from the algal solids with the lowest (tank 1) and highest (tank 6) calcium additions to the growth media. No obvious trend was observed between the addition of calcium to the growth media or algal solid Ca:P molar ratio and the final biocrude H/C molar. The potential causes for an undistinguishable trend across the six algal solids and their resulting biocrude H/C molar ratio is two-fold: 1) varying biomolecular content and ultimate elemental analysis (C, H, N, and O) among the algal solids and 2) varying initial and final inorganic compounds in the algal and HTL solids, respectively, that may act as catalyst and enhance or vary the biocrude composition and properties *in-situ*.

The first potential cause, varying algal biomolecular content and ultimate elemental analysis, fundamentally dictate the biocrude properties and composition.[3, 27-28] The variables that effect these algal properties are the initial N:P molar ratio in the growth media and growth stage at which the algae is harvested. Both these were algal growth variables were held constant for this study, yet the biomolecular content and ultimate analysis varied amongst the algal solids (Table 8). Our collaborators explained the variance in biomolecular content being caused by the loss of bioavailable phosphorus from precipitation. The additional calcium in tanks 4 – 6 could exceed

the saturation point causing phosphorus to precipitate from solution as calcium phosphate at the neutral pH held during growth. Thus, the decrease in the aqueous and bioavailable phosphorus can vary the algal biomolecular and ultimate elemental composition and therefore the HTL biocrude properties.

The second cause for varying biocrude properties could be due to *in-situ* catalysis performed by the inorganics. Calcite was the primary structure for the high ash and high calcium algal solids. Additionally, algal solids from tank 4 created HTL solids with TCP structure. Both calcite and TCP can have catalytic properties. However, given the varying biomolecular content it is difficult to clearly and concisely identify the cause for varying biocrude properties. Analysis from the HTL reaction of algal solids from tanks 1 and 2 that was doped of $CaCO_3$ provided some explanation. When $CaCO_3$ was doped into the reactor, the highest H/C molar ratio of 1.65 was achieved in the biocrude. Thus, the $CaCO_3$ observed in the algal solids may be having an *in-situ* catalytic effect on the biocrude in addition or with exception to the calcium phosphates observed in the HTL solids. This hypothesis is explored and discussed further in the ensuing chapters.

Jena et al. saw a similar increase in the H/C ratio as well as the highest C and H recovery in the biocrude from HTL reactions that were doped with Na_2CO_3.[29] They hypothesized that Na_2CO_3 dissociates at the subcritical water conditions of HTL and the presence of algal macromolecules create OH^- and $HCOO^-$ ions that further decompose the algal hydrocarbon macromolecules to the biocrude product.[29] The presence of Na_2CO_3 has also been hypothesized to promote a water-gas shift reaction that produces a higher amount of CO_2 and H_2 gas during the HTL of biomass.[24, 29-31] The greater presence of CO_2 and H_2 gas can further enhance, improve, and upgrade biocrude properties *in-situ*.[32-34] A similar phenomena could also be occurring from the addition and presence of $CaCO_3$ in the algal solids.

A key difference between the potential, *in-situ*, $CaCO_3$ catalysis observed in this study and the common alkali metal carbonate salt Na_2CO_3 is that $CaCO_3$ is more insoluble in water (6.17×10^{-4} g/100 mL water at 20°C) than the Na_2CO_3 (21.5 g/100 mL). Thus, the dissociation of $CaCO_3$ is most likely the rate-limiting step in the possible *in-situ* catalysis of the biocrude oil. However, Coto et. al. demonstrated that while the solubility of $CaCO_3$ decreases with higher temperatures, it dramatically increases with higher pressures of CO_2 and presence of other ions.[35] Thus, the presence of the other inorganic ions and high pressure CO_2 that is known to be produced by from the decomposition of the organic, biomolecules of algal biomass can promote $CaCO_3$ dissociation. With the dissociation of $CaCO_3$, a similar *in-situ* catalysis and water-gas shift reaction as proposed by Jena et al. with Na_2CO_3 may be occurring and enhancing the biocrude properties.

Comparison of the distillate fractions for the various biocrude samples from this study indicates that the different calcium loadings in the growth media did not greatly impact distillate or boiling point distribution for the biocrude. Figure 24 compares the distillate fractions of the biocrude produced from this study to biocrude produced from wastewater-cultivated algal solids. The most abundant distillation fraction for all biocrude samples was the vacuum gas fraction (343-538°C) at 35.65 ± 4.8 wt%, followed by kerosene (193-271°C) at 21.83 ± 2.8 wt% and vacuum residual (>538°C) fractions at 19.26 ± 1.5 wt%. The least abundant fractions were the gasoline (271-343°C) and heavy naphtha fraction (<193°C) at 10.81 ± 2.2 wt% and 11.55 ± 1.1 wt%, respectively.

This distribution for the given distillation fractions, Vacuum Gasoline > Kerosene > Vacuum Residue > Heavy Naphtha, is similar to what we have previously reported and observed for HTL on wastewater-cultivated algae.[6] In addition, 90 wt% or higher of the biocrude distilled off by 600°C. By comparison, Chen et al. observed approximately 16-32 wt% residual in the

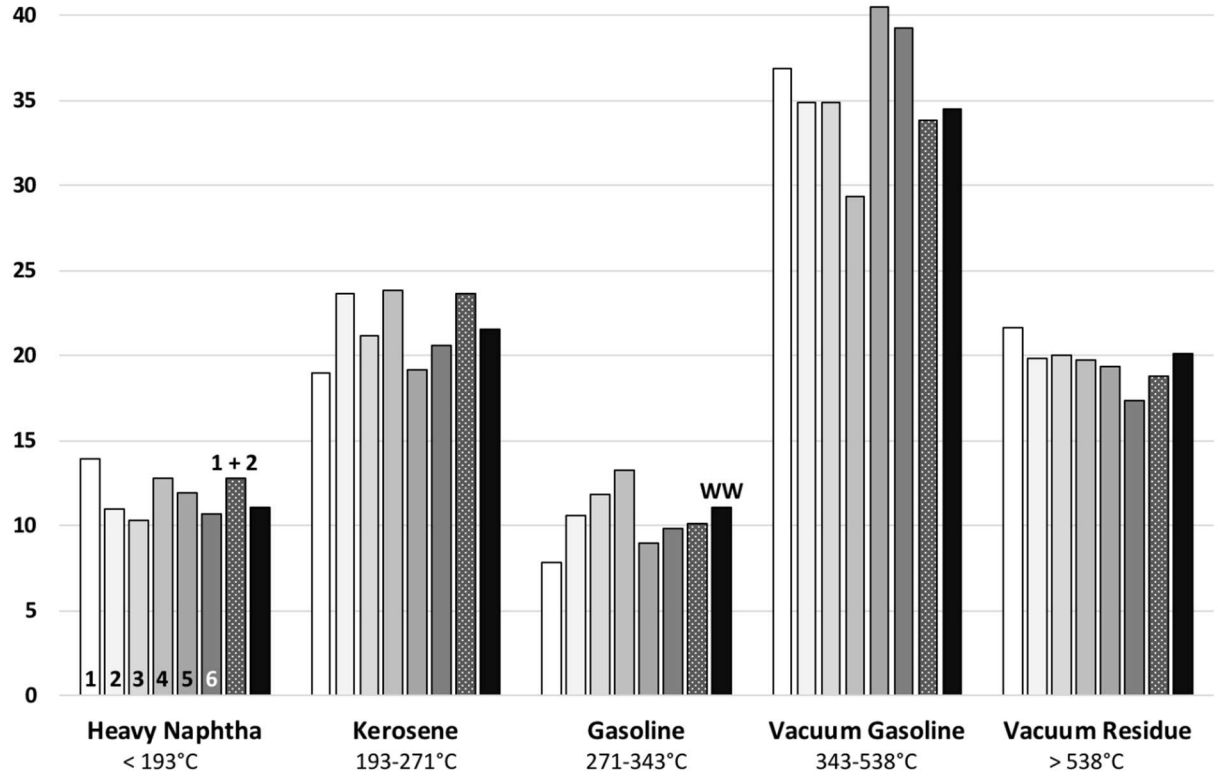

Figure 24: The distribution of distillate fractions from the biocrude produced from algal solids harvest from light rack tanks 1 – 6. Biocrude from the $CaCO_3$ doped reactions with algal solids from tanks 1 and 2 and wastewater are repesented by "1 + 2" and "WW," respectively.

simulated distillation of their biocrude product at 600°C.[2, 30] Similarly, Roussis et al. observed only 77% of their initial HTL biocrude to distilled off by 550°C. It was not until after a 450°C secondary thermal treatment that their biocrude product showed similar distillate properties to the biocrude fractions in this study.[36] Biocrude products that have a greater amount of light distillate fractions, such as those that appear in this study, are more desirable because less refining and upgrading is required for the product to be used in existing infrastructure.

The most noteworthy changes in the distillate fractions occurred in the Vacuum Gasoline fraction. Biocrude produced from algal solids harvested from tanks 5 and 6 had the highest Vacuum Gasoline fraction at 39-40 wt%. These algal solids also displayed the highest presence of calcium carbonate. The biocrude produced from wastewater-cultivated algal solids that also

showed high amount of calcium carbonate and the algal solids from tanks 1 and 2 that were doped with $CaCO_3$ had much lower Vacuum Gasoline distillate fractions (33-34 wt%). Additionally, the Vacuum Gasoline fraction was the least (29 wt%) in the biocrude produced by algal solids from tank 4. This biocrude also had higher wt% for the lighter distillate fractions (i.e. Heavy Naphtha, Kerosene, and Gasoline). These algal solids from tank 4 also the sole algal solids that produced TCP in the HTL solids. The distribution of other distillate fractions amongst the biocrude created from the assortment of algal solids were mixed. The variance in distillation results can again be contributed to the varying biomolecular content and/or the inorganic structures amongst the algal solids. Subsequent chapters are aimed to better isolate these variables to identify their effect on biocrude properties and HTL solid structures.

Gas chromatography-mass spectrometry (GC-MS) can further assist and more specifically identify the potential *in-situ* catalysis performed by the inorganics captured during auto-flocculation. Table 10 reports the organic compounds and functional groups observed by GC-MS analysis and groups them into four, common categories for biocrude analysis: aliphatic, aromatic, nitrogen (N-) compounds, and oxygen (O-) compounds. The number of distinguishable (MS probability $\geq$ 90%) peaks for a given compound or functional group along with their relative peak area to the entire spectra (% area) are both shown. The GC-MS % area is directly correlated to the concentration or abundance of said compound in the biocrude.

The most prevalent compounds found in the biocrude were various C_{16} compounds. This includes C_{16} alkane and alkene derivatives as well as hexadecanoic acid and hexadecanamide. Phenols and cyclic N-compounds such as indoles, pyrazine, pyrrole, pyridine, quinoline, and pyrrolidinone were also present due to the high protein content of all six algal solids. Ideally, the biocrude would be composed of long- and short-chain hydrocarbons along with some cyclic-

and/or aromatic functional groups. An absence or minimal amount of nitrogen and oxygen, (i.e. N- and O-compounds) is also preferred.

Given the abundance of C_{16} compounds, the chemistry of interest is the transformation of C_{16} amides and acids to alkane and alkene derivatives. Biocrude produced from algal solids harvested from tank 1 had the highest amount of hexadecanoic acid and also had the highest algal lipid content amongst the algal solids. When $CaCO_3$ was added the HTL reaction with algal solids from tanks 1 and 2, however, the C_{16} acid content dropped from 15.2 and 9.9 % area in the biocrude produced by algal solids harvested from tanks 1 and 2 respectively to 6.1 % area in the biocrude produce when algal solids from tanks 1 and 2 were doped with $CaCO_3$. The total amide peak area, composed of C_{16} and greater amides, in the biocrude produced by the independent algal solids from tanks 1 and 2 were 8.5 and 9.6 % respectively and decreased similarly to 5.5 % area when these algal solids were reacted together and with the addition of $CaCO_3$. These results are indication that $CaCO_3$ may aid in the reduction of C_{16} acids and amides; however, the supplementation of other C_{16} compounds, such as alkanes or alkenes, from these reductions was not observed in the $CaCO_3$-doping reaction. The % area of C_{16} alkane, alkene, and their derivatives in the biocrude from the $CaCO_3$-doped HTL reaction with algal solids from tanks 1 and 2 (18.4 % area) was in between the biocrude from the independent HTL reactions of tank 1 and 2 algal solids (20.6 and 16.3 % area respectively). Aromatic compounds, such as phenol and its derivatives, however did increase in the biocrude where the HTL reaction was doped with $CaCO_3$ (10.7 % area) compared to the independent HTL reactions and biocrude from algal solids from tanks 1 and 2 that were 9.0 and 6.5 % area respectively. N-cyclic compounds in the biocrude also increased slightly to 3.2 % area when $CaCO_3$ was added externally to the reaction in comparison to the

Table 10: Key organic compounds and functional groups identified by GC-MS analysis of the biocrude produced by algal solids harvested from their respective tanks and the supplementary HTL reaction of algal solids from tanks 1 & 2 that were doped with CaCO3 in the column labeled "1 & 2."

	1		2		3		4		5		6		1 & 2	
	Peaks	*% Area*	*Peaks*	*% Area*	*Peaks*	*% Area*	*Peaks*	*% Area*	*Peaks*	*% Area*	*Peaks*	*% Area*	*Peaks*	*% Area*
ALIPHATICS	**14**	**20.64**	**10**	**16.33**	**12**	**22.90**	**12**	**16.28**	**9**	**12.44**	**11**	**16.09**	**13**	**18.39**
Alkane + Deriv.	5	3.02	2	1.57	3	2.18	3	1.38	1	0.54	3	1.30	5	2.70
Alkene + Deriv.	9	17.62	8	14.76	9	20.72	9	14.90	8	11.90	8	14.79	8	15.69
AROMATICS	**8**	**8.99**	**8**	**6.47**	**7**	**8.68**	**8**	**6.70**	**7**	**4.62**	**10**	**9.19**	**10**	**10.74**
Phenol + Deriv.	4	4.62	2	2.65	2	4.16	2	2.73	2	2.07	3	4.35	4	5.15
p-Cresol	1	2.68	1	1.85	1	2.32	1	1.39	1	1.27	1	1.85	1	2.43
Naphthalene Deriv.	3	1.69	3	1.36	3	1.93	3	1.83	2	0.82	3	1.70	3	2.58
N-COMPOUNDS	**17**	**16.08**	**18**	**16.47**	**16**	**18.46**	**17**	**12.46**	**18**	**14.87**	**21**	**13.64**	**15**	**13.41**
Amides	3	8.51	3	9.60	3	9.53	3	5.32	3	7.58	3	5.31	3	5.52
Indole + Deriv.	1	1.37	1	1.51	1	1.74	1	1.31	1	1.31	1	1.38	1	1.08
Indole Deriv.	5	3.55	5	2.49	4	3.42	3	2.10	4	2.50	3	2.65	4	3.63
N-cyclic Compounds	8	2.65	9	2.87	8	3.77	10	3.73	10	3.48	14	4.30	7	3.18
O-COMPOUNDS	**7**	**18.58**	**4**	**13.72**	**5**	**8.29**	**4**	**18.72**	**5**	**11.80**	**7**	**18.70**	**5**	**12.53**
Hexadecanoic Acid	1	15.21	1	9.94	1	4.53	1	7.25	1	2.15	1	10.90	1	6.14
Octadecanoic Acid	1	1.04	1	2.69	1	1.61	1	10.18	1	7.30	1	6.27	1	3.78
Cyclic Ketone	3	1.91	2	1.09	3	2.15	2	1.29	2	1.12	3	1.27	2	0.65

Derivative abrv. Deriv.
Nitrogen abrv. N
Oxygen abrv. O

biocrude produced from the independent HTL reactions of algal solids harvested from tanks 1 and 2 that had 2.7 and 2.9 % area respectively.

The observation of an increase in phenols and N-cyclic compounds as opposed to the C_{16} alkane and alkene derivatives in the biocrude agrees with the biocrude ultimate analysis. Although substantial decreases in amides were observed from the GC-MS analysis of these biocrudes, the N wt% remained unchanged when $CaCO_3$ was doped to the HTL reaction of low-ash algal solids from tanks 1 and 2. Thus, the expected nitrogen loss from the reduction of amides must remain in the biocrude product such as in N-cyclic compounds as observed in the GC-MS analysis. The O wt% of the biocrude increased substantially (9.1 wt%), however, when $CaCO_3$ was doped to the HTL reaction of tank 1 and 2 algal solids. The biocrude from the independent HTL reactions of tank 1 and 2 algal solids were 7.0 and 6.5 wt% respectively. Thus, a substantial increase of phenolic or O-compounds would be expected in the biocrude from tank 1 and 2 algal solids that were doped with $CaCO_3$; however, the GC-MS results indicate the opposite.

The literature also has mixed reports of the proposed C_{16} chemistry between the acids and amides. Biller et al. who doped various microalgae species with sodium carbonate (Na_2CO_3), which is hypothesized to have a similar, water-gas shift catalytic impact as calcium carbonate, observed both octanoic (C_{18}) acid and hexadecanamide both disappear from the biocrude product and heptadecane appear when Na_2CO_3 was added to the HTL of *Chlorella sp*.[3] Jena et al. also experimented with addition of Na_2CO_3 and TCP to the HTL of *Spirulina sp*. microalgae; however, they observed the opposing results to Biller et al. The addition of Na_2CO_3 more than doubled the carboxyl acid area%.[29] The amide area% also increased and the alkane area% also decreased.[29] However, the addition of TCP did notably decrease the amide concentration of the biocrude.[29]

Given the numerous components present during the HTL from the varying biomolecular content of algal biomass, isolating, understanding and/or predicting the catalytic impact of a hetero- or homogeneous catalysts can be difficult. A series HTL reactions of single algal model compounds, carbohydrates, proteins, and lipids, with individual, observed inorganic compounds, such as $CaCO_3$, TCP, and HAp, can provide further clarity of the *in-situ* catalytic effect of high calcium and high ash algal solids.

4.5 Conclusions

It is apparent from this work that the increased inorganic, ash content in algal solids is from the precipitation of calcium and magnesium solids. The precipitation is a side effect of the auto-flocculation and higher pH harvesting technique. Compared to algal solids that were harvested at a neutral pH and centrifuged, the inorganic, more specifically the calcium, content from the auto-flocculated solids are substantially higher. These results indicate that the ash and calcium content observed in these algal solids are external of the algal cell. Also, the cause for the higher inorganic, calcium content was due to a chemical phenomenon, precipitation, and not the result of a biological one. X-ray diffraction confirmed the primary crystalline-structure of the algal solids was the mineral calcite ($CaCO_3$). Furthermore, the increase of calcium present in the algal solid also increased the solid recovery of phosphorus from 70% to nearly 100% in the HTL solids. Although only one HTL solid sample showed an indication of a calcium phosphate structure (TCP), FTIR further confirmed the presence of both phosphate and carbonate in HTL solids produced by high ash, calcite algal solids.

The biocrude displayed promising properties but lacked a clear trend or pattern to the inorganic structure observed with the HTL solids. These positive biocrude properties included

low N/C and O/C and high H/C molar ratios for the biocrude. The distillate fractions of the biocrude were also favorable with lower Vacuum Gasoline and higher Heavy Naphtha, Kerosene, and Gasoline distillate fractions from algal solids harvested from tank 4. These algal solids were also the only algal solids that produced TCP in the HTL solids. Finally, the biocrude composition was also mixed and varied amongst the algal solid samples. An increase in C_{16} alkane and alkene derivatives and decrease C_{16} acids and amides were observed when HTL reactions of low-ash algal solids from were doped with $CaCO_3$. However, given the varying biomolecular content of the algal solids, it was difficult to concluded if these changes in biocrude composition was due to the inorganics or the biomolecular composition of the algal solids.

4.6 Reference

1. Roberts, G. W.; Fortier, M.-O. P.; Sturm, B. S. M.; Stagg-Williams, S. M., Promising Pathway for Algal Biofuels through Wastewater Cultivation and Hydrothermal Conversion. *Energy & Fuels* **2013,** *27* (2), 857-867.
2. Chen, W. T.; Zhang, Y.; Zhang, J.; Yu, G.; Schideman, L. C.; Zhang, P.; Minarick, M., Hydrothermal liquefaction of mixed-culture algal biomass from wastewater treatment system into bio-crude oil. *Bioresource technology* **2014,** *152*, 130-9.
3. Biller, P.; Ross, A. B., Potential yields and properties of oil from the hydrothermal liquefaction of microalgae with different biochemical content. *Bioresource technology* **2011,** *102* (1), 215-25.
4. Valdez, P. J.; Nelson, M. C.; Wang, H. Y.; Lin, X. N.; Savage, P. E., Hydrothermal liquefaction of Nannochloropsis sp.: Systematic study of process variables and analysis of the product fractions. *Biomass and Bioenergy* **2012,** *46*, 317-331.
5. Zhou, D.; Zhang, L.; Zhang, S.; Fu, H.; Chen, J., Hydrothermal Liquefaction of Macroalgae Enteromorpha prolifera to Bio-oil. *Energy & Fuels* **2010,** *24* (7), 4054-4061.
6. Roberts, G. W.; Sturm, B. S. M.; Hamdeh, U.; Stanton, G. E.; Rocha, A.; Kinsella, T. L.; Fortier, M.-O. P.; Sazdar, S.; Detamore, M. S.; Stagg-Williams, S. M., Promoting catalysis and high-value product streams by in situ hydroxyapatite crystallization during hydrothermal liquefaction of microalgae cultivated with reclaimed nutrients. *Green Chem.* **2015,** *17* (4), 2560-2569.
7. Golueke, C. G.; Oswald, W. J., Surface Properties and Ion Exchange in Algae Removal. *Journal (Water Pollution Control Federation)* **1970,** *42* (8), R304-R314.
8. Rodriguez-Navarro, C.; Ruiz-Agudo, E.; Luque, A.; Ortega-Huertas, A. B. R.-N. M., Thermal decomposition of calcite: Mechanisms of formation and textural evolution of CaO nanocrystals. *American Mineralogist* **2009,** *94* (4), 578-593.

9. Vandamme, D.; Foubert, I.; Muylaert, K., Flocculation as a low-cost method for harvesting microalgae for bulk biomass production. *Trends Biotechnol* **2013,** *31* (4), 233-9.
10. Vandamme, D.; Foubert, I.; Fraeye, I.; Meesschaert, B.; Muylaert, K., Flocculation of Chlorella vulgaris induced by high pH: role of magnesium and calcium and practical implications. *Bioresource technology* **2012,** *105*, 114-9.
11. Wu, Z.; Zhu, Y.; Huang, W.; Zhang, C.; Li, T.; Zhang, Y.; Li, A., Evaluation of flocculation induced by pH increase for harvesting microalgae and reuse of flocculated medium. *Bioresource technology* **2012,** *110*, 496-502.
12. Zhang, L.; Lu, H.; Zhang, Y.; Li, B.; Liu, Z.; Duan, N.; Liu, M., Nutrient recovery and biomass production by cultivating Chlorella vulgaris 1067 from four types of post-hydrothermal liquefaction wastewater. *Journal of Applied Phycology* **2015,** *28* (2), 1031-1039.
13. Biller, P.; Ross, A. B.; Skill, S. C.; Lea-Langton, A.; Balasundaram, B.; Hall, C.; Riley, R.; Llewellyn, C. A., Nutrient recycling of aqueous phase for microalgae cultivation from the hydrothermal liquefaction process. *Algal Research* **2012,** *1* (1), 70-76.
14. Ramos-Tercero, E. A.; Bertucco, A.; Brilman, D. W. F., Process Water Recycle in Hydrothermal Liquefaction of Microalgae To Enhance Bio-oil Yield. *Energy & Fuels* **2015,** *29* (4), 2422-2430.
15. Pham, M.; Schideman, L.; Scott, J.; Rajagopalan, N.; Plewa, M. J., Chemical and biological characterization of wastewater generated from hydrothermal liquefaction of Spirulina. *Environ Sci Technol* **2013,** *47* (4), 2131-8.
16. Liu, R.; Lal, R., Synthetic apatite nanoparticles as a phosphorus fertilizer for soybean (Glycine max). *Sci Rep* **2014,** *4*, 5686.
17. Kottegoda, N.; Munaweera, I.; Madusanka, N.; Karunaratne, V., A green slow-release fertilizer composition based on urea-modified hydroxyapatite nanoparticles encapsulated wood. *Current Science* **2011,** *101* (1), 73-78.
18. Jiang, J.; Savage, P. E., Influence of process conditions and interventions on metals content in biocrude from hydrothermal liquefaction of microalgae. *Algal Research* **2017,** *26*, 131-134.
19. Ekpo, U.; Ross, A. B.; Camargo-Valero, M. A.; Williams, P. T., A comparison of product yields and inorganic content in process streams following thermal hydrolysis and hydrothermal processing of microalgae, manure and digestate. *Bioresource technology* **2016,** *200*, 951-60.
20. Heilmann, S. M.; Molde, J. S.; Timler, J. G.; Wood, B. M.; Mikula, A. L.; Vozhdayev, G. V.; Colosky, E. C.; Spokas, K. A.; Valentas, K. J., Phosphorus reclamation through hydrothermal carbonization of animal manures. *Environ Sci Technol* **2014,** *48* (17), 10323-9.
21. Kamitakahara, M.; Nagamori, T.; Yokoi, T.; Ioku, K., Carbonate-containing hydroxyapatite synthesized by the hydrothermal treatment of different calcium carbonates in a phosphate-containing solution. *Journal of Asian Ceramic Societies* **2015,** *3* (3), 287-291.
22. Ishikawa, K.; Matsuya, S.; Lin, X.; Lei, Z.; Yuasa, T.; Miyamoto, Y., Fabrication of low crystalline B-type carbonate apatite block from low crystalline calcite block. *Journal of Ceramic Society of Japan* **2010,** *118* (5), 341-344.
23. Arahira, T.; Maruta, M.; Matsuya, S., Development and characterization of carbonate apatite/β-tricalcium phosphate biphasic cement. *Materials Letters* **2017,** *194*, 205-208.
24. Brown, T. M.; Duan, P.; Savage, P. E., Hydrothermal Liquefaction and Gasification of Nannochloropsis sp. *Energy & Fuels* **2010,** *24* (6), 3639-3646.
25. Xu, D.; Savage, P. E., Characterization of biocrudes recovered with and without solvent after hydrothermal liquefaction of algae. *Algal Research* **2014,** *6*, 1-7.

26. Xu, D.; Savage, P. E., Effect of reaction time and algae loading on water-soluble and insoluble biocrude fractions from hydrothermal liquefaction of algae. *Algal Research* **2015,** *12*, 60-67.
27. Changi, S. M.; Faeth, J. L.; Mo, N.; Savage, P. E., Hydrothermal Reactions of Biomolecules Relevant for Microalgae Liquefaction. *Industrial & Engineering Chemistry Research* **2015,** *54* (47), 11733-11758.
28. Leow, S.; Witter, J. R.; Vardon, D. R.; Sharma, B. K.; Guest, J. S.; Strathmann, T. J., Prediction of microalgae hydrothermal liquefaction products from feedstock biochemical composition. *Green Chem.* **2015,** *17* (6), 3584-3599.
29. Jena, U.; Das, K. C.; Kastner, J. R., Comparison of the effects of Na2CO3, Ca3(PO4)2, and NiO catalysts on the thermochemical liquefaction of microalga Spirulina platensis. *Applied Energy* **2012,** *98*, 368-375.
30. Chen, W.-T.; Qian, W.; Zhang, Y.; Mazur, Z.; Kuo, C.-T.; Scheppe, K.; Schideman, L. C.; Sharma, B. K., Effect of ash on hydrothermal liquefaction of high-ash content algal biomass. *Algal Research* **2017,** *25*, 297-306.
31. Ogi, T.; Yokoyama, S.-y.; Koguchi, K., Direct Liquefaction of Wood by Alkali and Alkaline Earth Salt in an Aqueous Phase. *The Chemical Society of Japan* **1985**, 1199-1202.
32. Lee, J.; Choi, D.; Kwon, E. E.; Ok, Y. S., Functional modification of hydrothermal liquefaction products of microalgal biomass using CO 2. *Energy* **2017**.
33. Duan, P.; Savage, P. E., Hydrothermal Liquefaction of a Microalga with Heterogeneous Catalysts. *Industrial & Engineering Chemistry Research* **2011,** *50*, 52-61.
34. Zhao, B.; Wang, Z.; Liu, Z.; Yang, X., Two-stage upgrading of hydrothermal algae biocrude to kerosene-range biofuel. *Green Chemistry* **2016,** *18* (19), 5254-5265.
35. Coto, B.; Martos, C.; Peña, J. L.; Rodríguez, R.; Pastor, G., Effects in the solubility of CaCO3: Experimental study and model description. *Fluid Phase Equilibria* **2012,** *324*, 1-7.
36. Roussis, S. G.; Cranford, R.; Sytkovetskiy, N., Thermal Treatment of Crude Algae Oils Prepared Under Hydrothermal Extraction Conditions. *Energy & Fuels* **2012,** *26* (8), 5294-5299.

5 Model Compounds

5.1 Motivation & Background

There are several organic and inorganic reagents during the hydrothermal liquefaction (HTL) reaction of algal solids. Thus, it is difficult to clearly identify and understand the cause of certain results and observations given the multitude of variables that could have an effect. To reduce the variability from these reagents, HTL was performed on individual inorganic and biological model compounds. While many of the control experiments have been performed and discussed in the literature, few have combined the areas of hydrothermal synthesis of calcium phosphate material and hydrothermal liquefaction of algae for biocrude production. The aim of this chapter is to report and discuss the successes and shortcomings from some of the first trials and iterations of a combined inorganic and biological model compound study.

As discussed in Chapter 2.7 *Hydrothermal Synthesis of HAp*, calcium phosphate minerals, such as hydroxyapatite (HAp; $Ca_5(PO_4)_3OH$) and tricalcium phosphate (TCP; $Ca_3(PO_4)_2$) are commonly used for biomaterial applications pertaining to cellular generation of bone and teeth tissue.[1-3] Furthermore, HTL of algal biomass has also shown great promise in creating an enhanced biocrude product.[4-5] No research, however, has been reported on the simultaneous hydrothermal synthesis of these calcium phosphates as catalysts for upgrading HTL biocrude from algae. Biological model compounds such as carbohydrates, amino acids, and lipids have been utilized to better control the morphology and structure of calcium phosphate materials during hydrothermal synthesis.[3, 6-8] The resulting organic, biocrude product, however, was never characterized or reported. Additionally, a variety of external, heterogeneous catalysts have been added to HTL reactions of algae to improve the biocrude properties.[9-11] These studies, however, never explored

the great inorganic or catalytic synthesis potential of hydrothermal treatment as the other calcium phosphate, biomaterial fields have demonstrated.

The thrust of this chapter has three main parts. The first is to understand the solid and inorganic synthesis occurring from the inorganic molecules observed in the high ash, high calcium auto-flocculated, and wastewater-cultivated algal solids reported in Chapter 4: *Inorganic Capture*. The second portion is dedicated to identifying effective quantitative measures of these inorganic compounds in both the algal and HTL solids. Accurate quantification or a general estimate of the inorganic compounds present will allow further understanding of the inorganic chemistry taking place during HTL. The final segment of this chapter includes the first inorganic and biological model compound experimentation of simultaneous, inorganic synthesis with *in-situ* catalytic biocrude upgrading. Within this final portion, the potential enhancement of biocrude properties from either the final, HTL solid product, or from the energy absorbed or released from the synthesis of the HTL solids are trialed. The aid of biological model compounds has on the synthesis of calcium phosphate solids is also investigated.

5.2 Methods and Experimental Setup

Because calcite was the primary observed inorganic in both the algal and HTL solids, it is the primary calcium reagent used in this chapter. Calcite is the common, mineral nomenclature for the XRD-observed calcium carbonate ($CaCO_3$) present in wastewater-cultivated and auto-flocculated algal solids. Calcium hydroxide, $Ca(OH)_2$, and calcium chloride (Fisher $CaCl_2$, ACS-grade) were also used for more homogeneous and uniform HAp formations for later comparison and catalytic studies. Trisodium phosphate (Fisher $Na_3PO_4 \cdot 12H_2O$, ACS-grade) was the sole phosphate reagent for the study, for it provided a soluble, inorganic form of phosphate. While a

majority of the aqueous phosphate that is observed in the HTL of algae is from biological components such as ATP and DNA, trisodium phosphate eliminates any additional variances these biological compounds may have.

GNC Soy protein (no additive flavoring), glucose Fisher ≥ 98.0%), and palmitic acid (Sigma Aldrich C_{16}, 90%)) were the primary protein, carbohydrate, and lipid biological model compounds respectively for this chapter. Soy protein has been used recurrently as a protein model compound in algal HTL studies.[9, 12] Glucose has also been used frequently in the literature allowing for an ease of comparison and identification in biocrude yields and property improvements.[9, 13] Palmitic acid was used because it is well-understood to be the primary fatty acid present in an algal biomass.[13-14] Lastly, tetradecanamide was also hydrothermally reacted with additional, potential, catalytic upgrading reactions performed due to the interest and significance of amide chemistry and reduction in the HTL biocrude product.

For all hydrothermal reactions, conventional HTL reaction techniques were utilized: 10 wt% solids loading, 350°C, and a 60-minute reaction time with a 3-4 °C/min temperature ramp. X-ray diffraction helped in identifying the resulting HTL solid structure and scanning electron microscopy (SEM) showed their general morphology. ICP-OES quantified the inorganic recovery in the aqueous and solid HTL products while a new, thermogravimetric method for more accurately and precisely quantifying the weight percentage of carbonate (CO_3^{2-}) in algal and HTL solids was also intensively explored. Gas chromatography-mass spectrometry (GC-MS) was the primary biocrude analysis to observe and understand any changes in biocrude composition. Further details on these analyses is explained in Chapter 3: *Methods*.

The collection of these inorganic and biological reagents was then reacted, and their products analyzed based off of the three objectives: 1) inorganic synthesis 2) inorganic

quantification and 3) biocrude improvement. For the first objective the various calcium compounds, $CaCO_3$, $Ca(OH)_2$, and $CaCl_2$, were each reacted hydrothermal with Na_3PO_4 at Ca:P molar ratios ranging from 1.00 to 2.33. The resulting HTL solids were then examined via XRD and SEM while ICP-OES provided a means to balance the Ca and P for the reaction. In addition, low-ash algae and SiO_2 were also added to $CaCO_3$ + Na_3PO_4 reactions to observe their effect on the final HTL solid structure.

From objective one came the need to more accurately quantify or estimate the inorganic compounds present in the algal and HTL solids. These inorganic compounds included $CaCO_3$ and calcium phosphate materials such as HAp and/or TCP. Thermogravimetric analysis provided such quantification for both algal and HTL solid samples. The method for how $CaCO_3$ and calcium phosphate materials were distinguished and quantified by TGA is further explained in the discussion. However, to verify the method it was trialed with both pure $CaCO_3$ and mixtures of $CaCO_3$ and glucose at varying concentrations.

For the final objective, the algal biological model compounds were first hydrothermally reacted independent of any inorganic solids. These reactions tested their viability to produce a biocrude product and to provide a baseline or control for further reactions. After the initial control reactions, the biological model compounds best suited for biocrude production were trialed with commercial HAp, silica, and HAp precursors. Further details of the experimental procedure and analyses are explained in the discussion.

5.3 Collaboration

A majority of the reactions and product analysis for this chapter were conducted by the author and the chemical engineering, undergraduate research assistants under the author's training

and supervision. Intermittently, low-ash, algal biomass that was remaining from the previous light rack studies were utilized. Again, the cultivation of the biomass was overseen by our collaborator, Dr. Belinda Sturm while the proximate and elemental analysis of the algal biomass were performed by the primary author.

The collaborating graduate student, Sirwan Alimoradi, also aided in the water chemistry modeling necessary for the calculation of the theoretical, total carbonate present in auto-flocculated, light rack algal solids. Furthermore, Sirwan further identified additional, potential algal biomolecules from high-ash, auto-flocculated algal solids. The potential HTL biocrude products from these new algal biomolecules were then reviewed and discussed by the author.

5.4 Results and Discussions

5.4.1 Hydroxyapatite Synthesis from Calcite

The foundational inorganic reaction was the conversion of calcite to calcium phosphates such as HAp and TCP. Thus, calcite was initially reacted solely with trisodium phosphate at Ca:P molar ratios ranging from 1.00 to Ca:P molar ratio observed in the wastewater-cultivated algal solids of 2.33. Figure 25 depicts the XRD of the HTL solids created from these reactions. The peak indicative of calcite is located on the left between 29.0 and 30.5 2θ, and its intensity does not change with increasing Ca:P molar ratio. Peaks indicative of HAp appear between 31.5 and 35.0 2θ and their intensity decreases as Ca:P molar ratio increases.

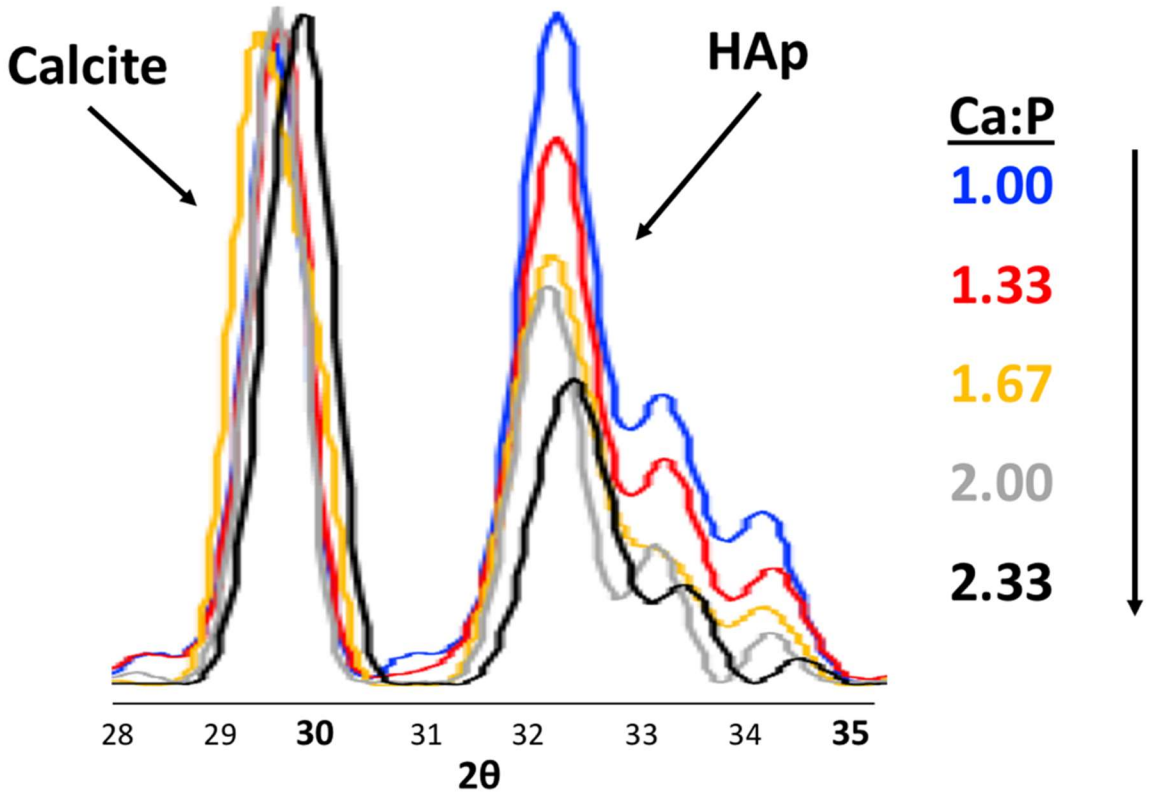

Figure 25: XRD patterns of HTL solids produced by calcite ($CaCO_3$) and trisodium phosphate (Na_3PO_4) loaded at Ca:P molar ratios from 1.00 to 2.33.

These results indicate that when calcite is in the presence of an aqueous form of phosphate, at conventional HTL conditions with no other inorganic or biological components lower Ca and higher P loading promote hydrothermal synthesis of HAp. The HTL reaction with a similar Ca:P molar ratio of the wastewater-cultivated algal solids (2.33) had the smallest presence of an HAp structure and therefore presumably the lowest conversion of calcite to HAp. This differs greatly from the XRD of in the HTL solids produced by wastewater-cultivated algal solids where a nearly complete and homogenous HAp structure was observed in the XRD pattern. The only additional, structural peaks observed in the HTL solids of wastewater-cultivated algal solids were indicative

of SiO_2, which also appeared in the original algal solids. Thus, additional variables must be playing a role to promote this synthesis of HAp from calcite.

Recall Figure 19 from Chapter 4.4.1 *Inorganic Characteristics of Algal Solids* where algal solid XRD patterns were compared between those that were auto-flocculated and cultivated in light rack growth tanks to those that were cultivated in wastewater. The single difference between the auto-flocculated and wastewater-cultivated algal solid XRD patterns was the extraneous, secondary peaks between 20 to 22 and 26 to 28 2θ in the wastewater-cultivated algal solids that did not appear in the auto-flocculated, light rack algal solids. These peaks were indicative of SiO_2 and appeared secondary to calcite in the wastewater-cultivated algal solids and HAp in the resulting HTL solids. Unlike the light rack cultivated and artificially auto-flocculated algal solids however, no remnants of the original calcite structure were observed in the HTL solids from wastewater-cultivated algal solids. The ensuing hypothesis was then that the secondary structural XRD peaks of SiO_2 that were observed in the wastewater-cultivated algal solids, but did not appear in the light rack cultivated, auto-flocculated algal solids, were promoting the synthesis of calcium phosphates hydrothermally.

The literature also supports this hypothesis where silica can act as a "seed-crystal" for the formation of calcium phosphates hydrothermally through an intermediate-step were calcium silicates, xonotlite and tobermorite, are formed.[15-17] Another set of reactions were, therefore, conducted where silicon dioxide (Alfa Aesar, SiO_2, ≥ 99.5%) was added at various amounts to the calcite and trisodium phosphate hydrothermal reaction with a constant 2.33 Ca:P molar ratio. The silica mass that was added and the XRD patterns of the resulting HTL solids are shown in Figure 26. As more silica was added the appearance and intensity of HAp and calcium phosphate structures increased. While minimal to no changes in structure were observed when 1 mg of SiO_2

was added, the primary peak for HAp between 31.5 and 33.5 2θ became the most dominant diffraction peak for HTL solids that were produced from the addition of 10 and 50 mg of SiO_2. When 100 mg of SiO_2 was added, both the number and intensity of peaks indicative of HAp grew in intensity compared to the control with 0 mg of SiO_2.

There were a few, supplementary peaks from the HTL solids where 10 and 50 mg of SiO_2 that did not match or align with any of the structures of the inorganic model compounds. These

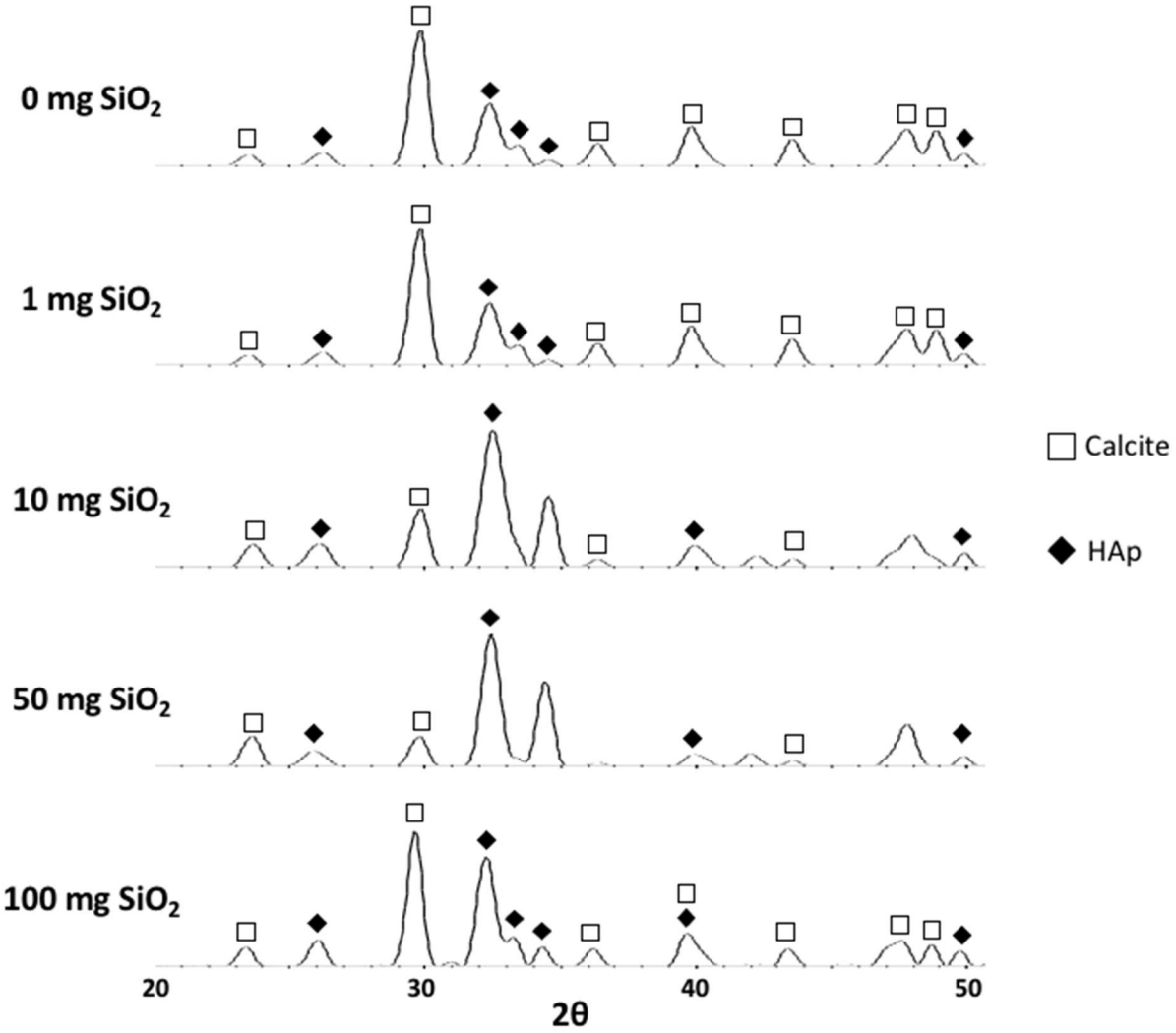

Figure 26: XRD patterns of HTL solids produced from hydrothermally reacting calcite and trisodium phosphate at a constant Ca:P molar ratio of 2.33 with the addition of SiO_2 at various masses to promote HAp or other calcium phosphate structures as detected by XRD.

unidentifiable peaks appeared at 34.5, 42, and 48 2θ. The peak at 34.5 2θ had the greatest intensity amongst the three peaks, and it is approximately the second-most intense peak in the 10 and 50 mg of SiO_2 HTL solid XRD patterns. Given its diffraction angle and intensity relative to the other peaks, this peak does not fit a HAp structure. A peak of similar intensity does appear as a secondary peak for TCP and serves as the primary peak for $Ca(OH)_2$. However, overall the additional, supplementary peaks necessary to conclude the presence of a TCP or $Ca(OH)_2$ structure within these HTL solids were absent. The XRD patterns of these and other inorganic model compound structures used to identify the HTL solid products can be found in Figure 12.

Silicon dioxide was then added and hydrothermally reacted with previously auto-flocculated, light rack algal solids where a calcium phosphate structure was detected in the XRD pattern of the HTL solids. The purpose of these reactions was to further conclude that SiO_2 promotes and increases the formation calcium phosphate structures in the HTL solids in the presence of an algal biomass. The results showed even greater promise for the conversion of calcite to calcium phosphates and are shown in Figure 27. The primary calcite peaks became secondary to the HAp and TCP peaks after 0.30g of SiO_2 was added to the reaction. Furthermore, the calcite peaks nearly disappeared when the light rack algal solids were doped with 0.45g of SiO_2. The one drawback was that as more SiO_2 was added, a broad, unidentifiable peak appeared between 20 and 24 2θ and its insanities grew. Thus, it is expected that this peak is related to some form of silica in combination with calcium and phosphate.

While the XRD results from the addition of SiO_2 were promising, they were not identical to the nearly uniform or homogeneous HAp or TCP structured HTL solids that were observed from

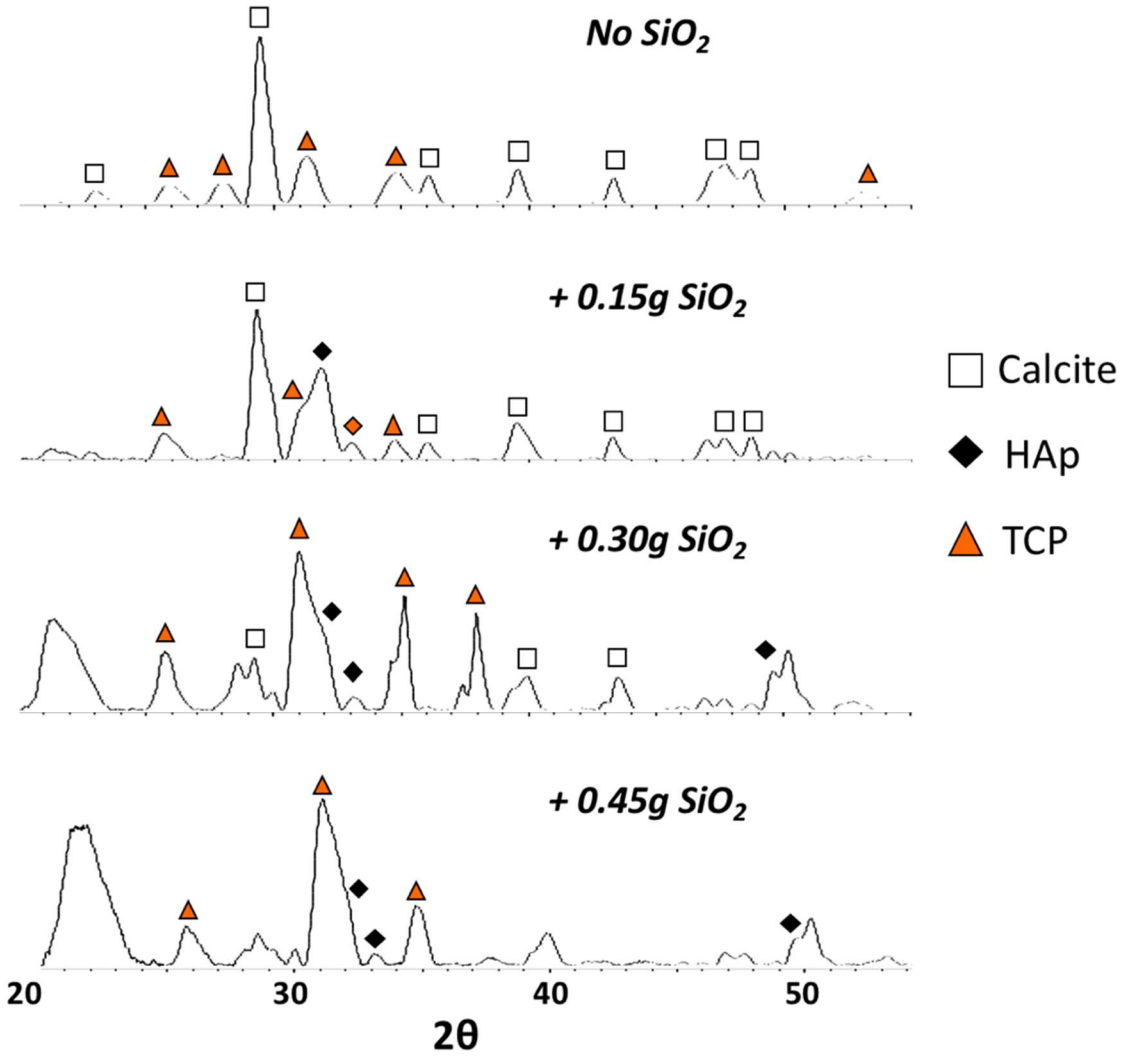

Figure 27: XRD patterns of HTL solids produced from HTL-reacted auto-flocculated, light rack algal solids that were later doped with increasing amounts of SiO_2 and a greater presence of calcium phosphate structures were observed in the HTL solid product.

HTL solid product from wastewater-cultivated algal solids as seen in Figure 28. Initial attempts to completely imitate the inorganic, solid transformations observed with the HTL of wastewater-cultivated algal solids were encouraging yet unsuccessful. The original, solid, crystalline structure detected from XRD of both wastewater-cultivated and auto-flocculated algal solids harvested from high calcium and high alkalinity growth media was calcite ($CaCO_3$). Minimal HAp or TCP structures, however, were detected from the hydrothermal treatment of calcite and trisodium

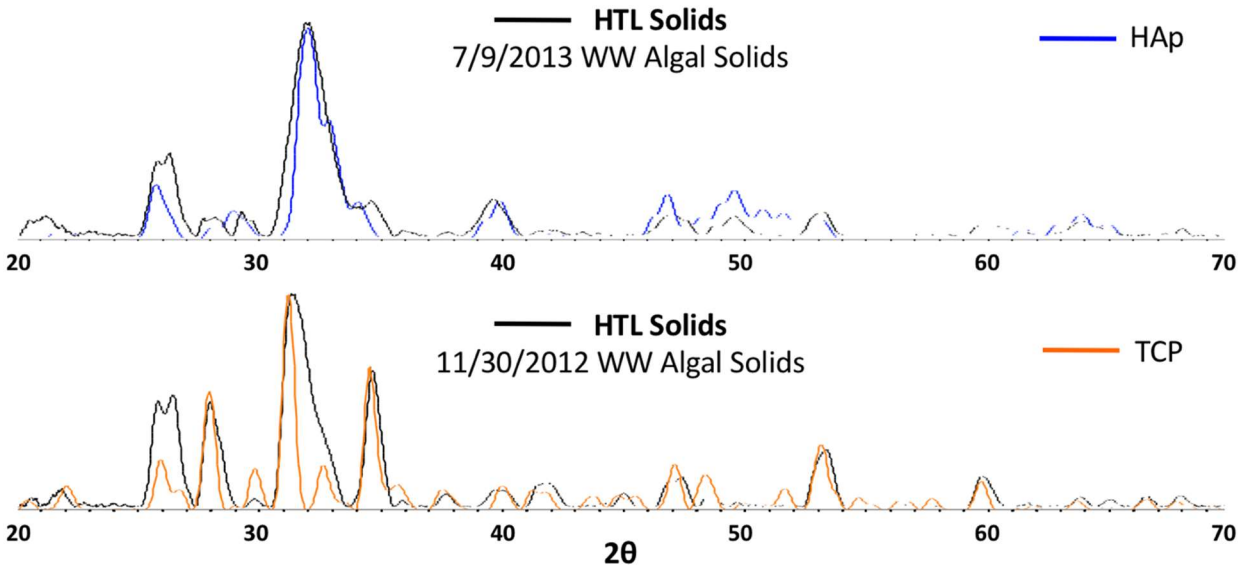

Figure 28: XRD patterns of HTL solids (black) that were produced by wastewater-cultivated algal solids that were harvested on two different dates and that display two distinct calcium phosphate structures HAp and TCP. For comparison XRD patterns from commercial HAp and TCP compounds are overlaid in blue and orange respectively.

phosphate at conventional HTL conditions. The addition of silica as SiO_2 promoted the presence of calcium phosphate structure in the HTL solids. However, complete calcite conversion nor a uniform calcium phosphate structure in the HTL solids were observed. The addition of soluble magnesium as $MgSO_4$ to the calcite and trisodium phosphate reaction also had less of an impact on the HTL solid structure than silica. The following research thrust was then to understand the mechanism and potential rate-determining step for the hydrothermal conversion of calcite to calcium phosphate.

5.4.2 Calcite Solubility

The first hypothesis was that the dissociation of calcite was the rate-limiting step due to its low solubility, especially at higher temperatures. Others have shown complete conversion and

homogeneous HAp structure in the XRD pattern from calcite using various soluble phosphate compounds, milder temperatures, and longer reaction times than conventional HTL conditions.[18-22] Furthermore, Sadat-Shojai et al. reviewed and summarized the various methods for HAp synthesis and concluded that for most HAp synthesis methods, including hydrothermal synthesis, the initial steps include free calcium (Ca^{2+}) and phosphate (PO_4^{3-}) ions.[23] To confirm solubility is a key and that HAp synthesis is achievable with inorganic reagents at conventional HTL conditions, more soluble forms of calcium were reacted. Calcium hydroxide (1.73 g/L at 20°C) and calcium chloride (74.5 g/L at 20°C) were reacted with trisodium phosphate at a Ca:P molar ratio of 1.67 and conventional HTL conditions (350°C; 60 min.) and compared to the original calcite HTL reactions at the same Ca:P molar ratio.

The resulting HTL solids and their structure via XRD are shown Figure 29 and confirm the hypothesis that solubility has a critical role in the hydrothermal synthesis of HAp. The HTL solids from calcium chloride, the most soluble form of calcium. Figure 29 confirms complete conversion to an HAp XRD pattern. Calcium hydroxide also had considerable, but not complete, conversion to HAp. The presence of $Ca(OH)_2$ remained along with a noticeable amount of calcite peaks. The presence of calcite is unusual, as no carbon was added or inputted to the reactors. This carbon is most likely due to CO_2 that enters the reactor during purging. Both calcium hydroxide and calcium chloride are orders of magnitude more soluble in water than calcite, and both showed a greater presence of an HAp structure in their XRD patterns and therefore greater conversion than calcite.

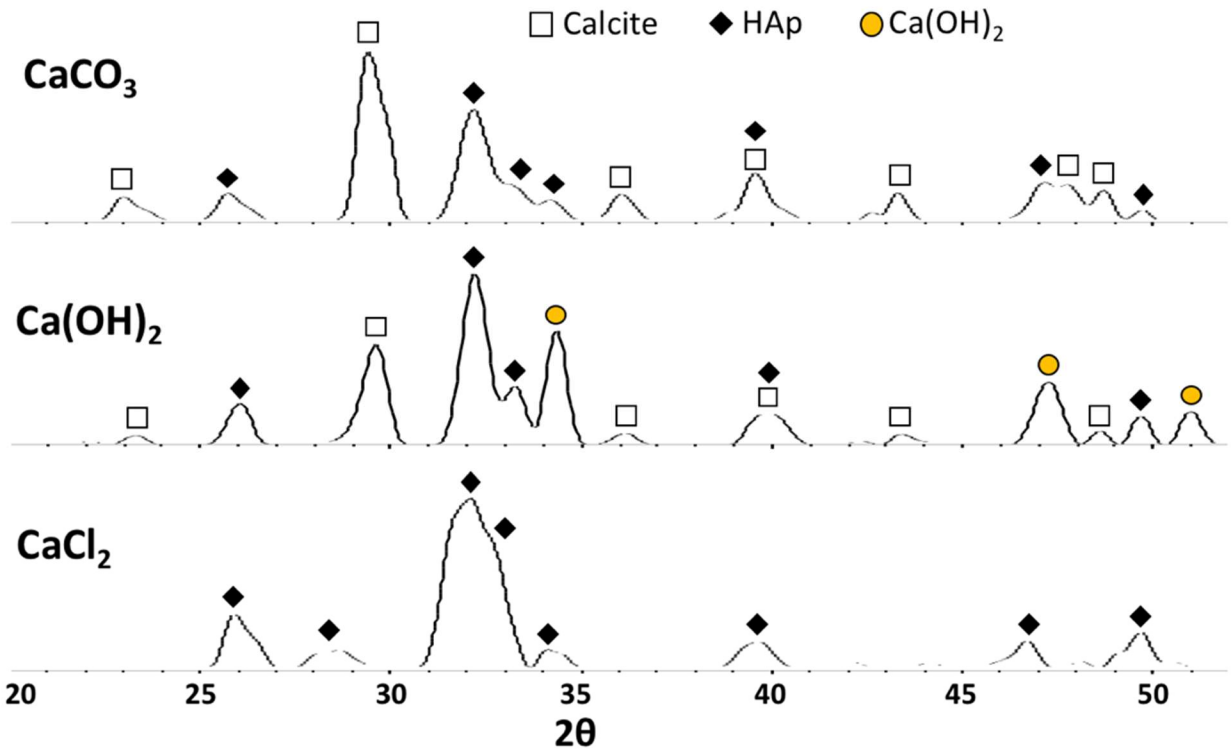

Figure 29: XRD patterns of solid products formed from conventional HTL reactions of various calcium reagents and trisodium phosphate at an identical Ca:P molar ratio of 1.67.

Scanning electron microscopy (SEM) of these HTL solids provided further insight into the complete and partial conversion observed between the different calcium model compounds. The morphologies of the varying calcite and calcium phosphate HTL solids from initial calcite, calcium chloride, and auto-flocculated algal solids are shown in Figure 30. HTL solids produced from calcium chloride and had a uniform HAp structure in their XRD pattern and their solid morphology are shown in Figure 30a where distinct nano-rods can be seen. Meanwhile, Figure 30b shows the morphology of the HTL solids produced from calcite where the XRD pattern showed the primary structure to be calcite and the secondary structure to be HAp. A closer look at the surface of the primary structure observed in Figure 30b displays what appears to be the initiation of small nano-rod structures on the calcite crystal's surface. The formation of HAp nano-rods on the calcite

surface agrees with what others in the literature have observed.[18, 21-22] Furthermore, it is hypothesized the reaction of $CaCO_3$ to HAp occurs on the surface because this is where the initial and necessary free Ca^{2+} ions appear and available PO_4^{3-} bond to.

With the SEM images and literature supporting the hypothesis that the dissociation of $CaCO_3$ is the rate-limiting step for the hydrothermal formation of HAp, a greater understanding of the variables impacting the solubility of $CaCO_3$ is necessary. While very few explored the solubility of calcite at conventional HTL conditions, Coto et al. experimented and modeled the

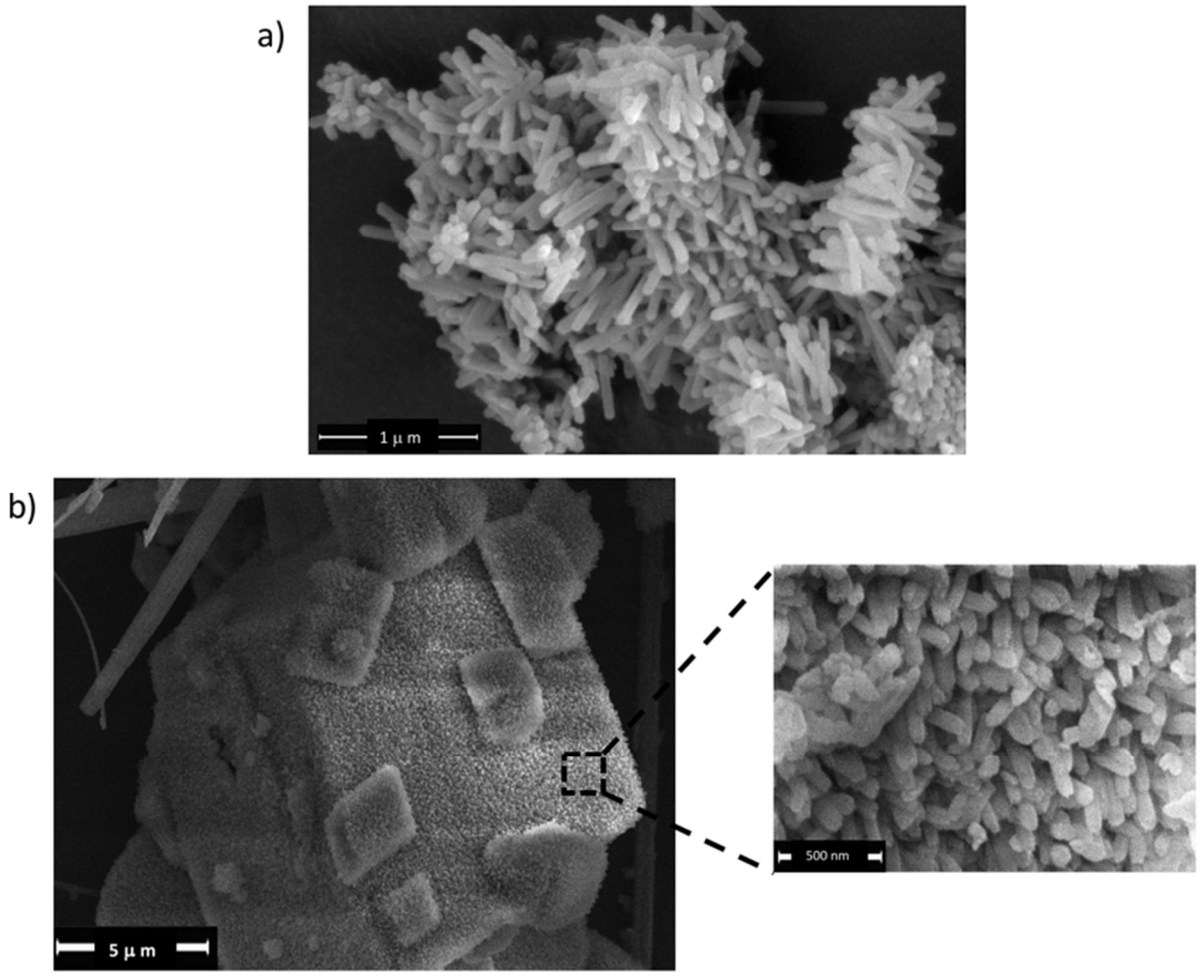

Figure 30: SEM images of HTL solids produced from (a) calcium chloride, and (b) calcite.

solubility of $CaCO_3$ with several similar key variables at more moderate conditions.[24] The first variable was the presence of additional ions in solution. An optimum concentration between 2-3 M of sodium chloride was found to enhance the dissociation of $CaCO_3$ and increase the concentration of free Ca^{2+} measured in solution by more than three times the control that had no NaCl.[24] Shi et al. further explored and modeled the beneficial impact various ions have on the dissociation of calcite at elevated temperatures including: Na^{+}, HCO_3^{-}, B^{3+}, Br^{-}, SO_4^{-2}, Si^{4+}, and Cl^{-}.[25]

The variable that has been seen to have the largest effect on increasing the solubility and dissociation of calcite is the partial pressure of carbon dioxide (CO_2).[24, 26] This is due in large part to the equilibrium relationship between CO_2, water, and $CaCO_3$ as shown in equation (12). Given this relationship, a greater presence of CO_2 causes the equilibrium to shift to the left and therefore promote the dissociation of $CaCO_3$. It is well-accepted and understood that CO_2 is produced during

$$Ca^{2+} + 2HCO_3^{-} \leftrightarrow CaCO_3(s) + CO_2 + H_2O \qquad (12)$$

the HTL reaction of algal biomass.[10, 27-28] The abundance of CO_2 during HTL is further verified by the composition of the gaseous product from HTL of wastewater-cultivated algal solids. Gas chromatography with thermal conductivity detection (GC-TCD) calibrated for CO_2 reported was 70-80 vol% of the gaseous product from HTL of wastewater-cultivated algal solids was CO_2 from calibrated. Thus, the carbon present from the algal components may be the critical component for calcite dissociation and calcium phosphate formation during HTL.

Low-ash, light rack microalgae was therefore added to the hydrothermal reactions of calcite and trisodium phosphate to provide CO_2 that would enhance the dissolution of calcite during the HTL reaction remained. The concern for using high-ash algal solids as the organic, biomass, or

CO_2 source is the additional inorganics within the algal solids could interfere and provide false-positive, calcium phosphate HTL solids. Unfortunately, minimal amounts of low-ash, microalgae remained in stock following previous HTL reactions. Thus, equal amounts (0.8-0.9), of low-ash algal biomass was added to four calcite and trisodium phosphate reactions at molar Ca:P ranging between 1.33 and 2.33. This allowed the carbon to calcium (C:Ca) molar ratio to vary between 5.3 and 6.1 despite the minimal amount of algal biomass.

The XRD results for the HTL solids produced from the hydrothermal reaction of calcite and trisodium phosphate with or without the addition of low-ash algae are shown in Figure 31. For all four reactions the presence of calcite structure increased, seen between 29-30 2θ, or the presence of an HAp structure decreased, seen between 31-35 2θ, from the addition of algal biomass according to the XRD results. This opposes the original hypothesis that the addition of algal biomass would enhance or increase the HAp structure observed by the XRD. Furthermore, the control reactions of calcite and trisodium phosphate were repeated at the same Ca:P molar ratios and mass loadings as the reactions and results shown in Figure 25; however, the previous XRD results were not reproducible. The trend where a lower Ca:P molar ratio produced HTL solids that had a higher intensity of HAp than calcite peaks as seen in Figure 25 was not observed from these duplicate hydrothermal reactions. The lack of reproducible and unexpected results led to the exploration for other methods to more precisely quantify the hydrothermal conversion of calcite to trisodium phosphate.

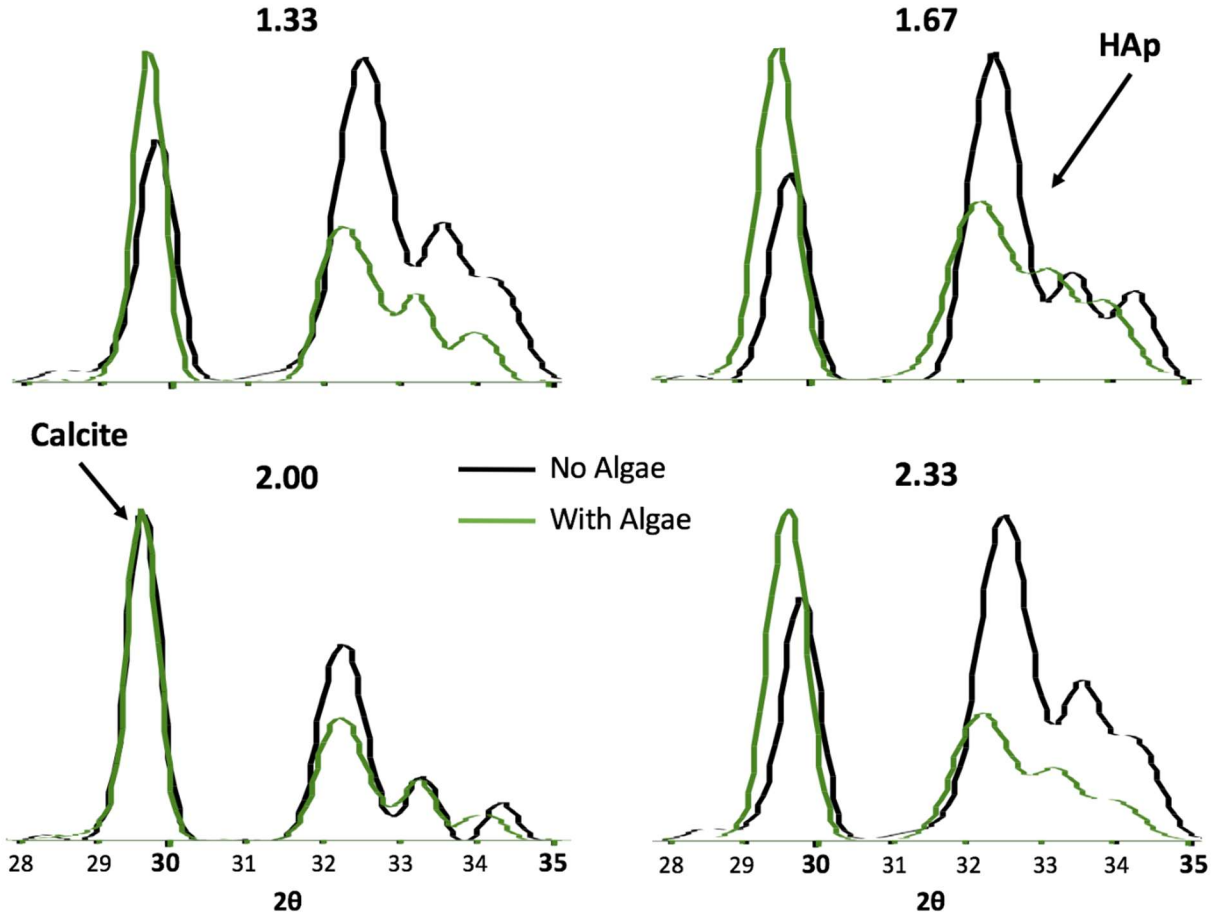

Figure 31: XRD patterns of the HTL solids produced from the hydrothermal reaction of calcite and trisodium phosphate at Ca:P ratios ranging from 1.33 to 2.33 (black). Low-ash algal solids were also added to these reactions (green) to observe the change HTL solid structure between calcite and the desired HAp.

5.4.3 Enhanced Quantification of Inorganic Conversion

Although others have used XRD and FTIR for quantifying the presence of compounds within a sample, these techniques are primarily used for qualitative results. Understanding the chemistry, mechanism, and rate-determining step aids in finding methods for better quantifying the conversion of calcite to calcium phosphates hydrothermally. The first alternative method was based upon the *Fate of Phosphorus post-HTL* discussed in the previous chapter. With the apparent phase change from aqueous to solid phosphate occurring during the HTL reaction, one could

quantify the conversion of calcite from the amount of phosphorus recovered in the solids. Through ICP-OES analysis of the ACP and HTL solid product, a balance and determination of the fate of initial phosphorus can be differentiated and quantified amongst the HTL solid and aqueous products.

Utilizing the fate of phosphorus to determine the conversion of calcite to calcium phosphate assumes the transformation of aqueous to solid phosphate is quick and immediate after a dissociation of calcite and free Ca^{2+} ions become present. This assumption is validated from the previous solubility study including the hydrothermal reaction of calcium chloride and trisodium phosphate shown in Figure 29. Calcium chloride was the most soluble form of calcium in that study, and it was also the only calcium salt to have a uniform, homogeneous HAp structure from the XRD pattern of the resulting HTL solids. The complete, HAp structure in the HTL solids indicates aqueous phosphate quickly bonds to aqueous and free Ca^{2+} ions from the soluble calcium chloride to form a final, solid, HAp product.

Figure 32 shows the percent of P that was recovered as a solid from the HTL reactions of calcite and trisodium phosphate with or without the addition of low-ash microalgae. It compares the impact that equal amounts of the low-ash microalgae have on select Ca:P molar ratios. For all four Ca:P molar ratios, the addition of algae increased the solid P recovery in the HTL solids. A decrease of P concentration was also observed in the ACP from HTL reactions with algae as opposed to without. The overall balance of for P on nearly all the HTL reactions were near 90 %. Only two reactions had the P-balance closer to 80% where small losses of either ACP or HTL solids during the extraction were noted. These results confirm that the presence of algal biomass aids in the dissociation of calcite during the HTL reaction and promotes the recovery of P in the HTL solids.

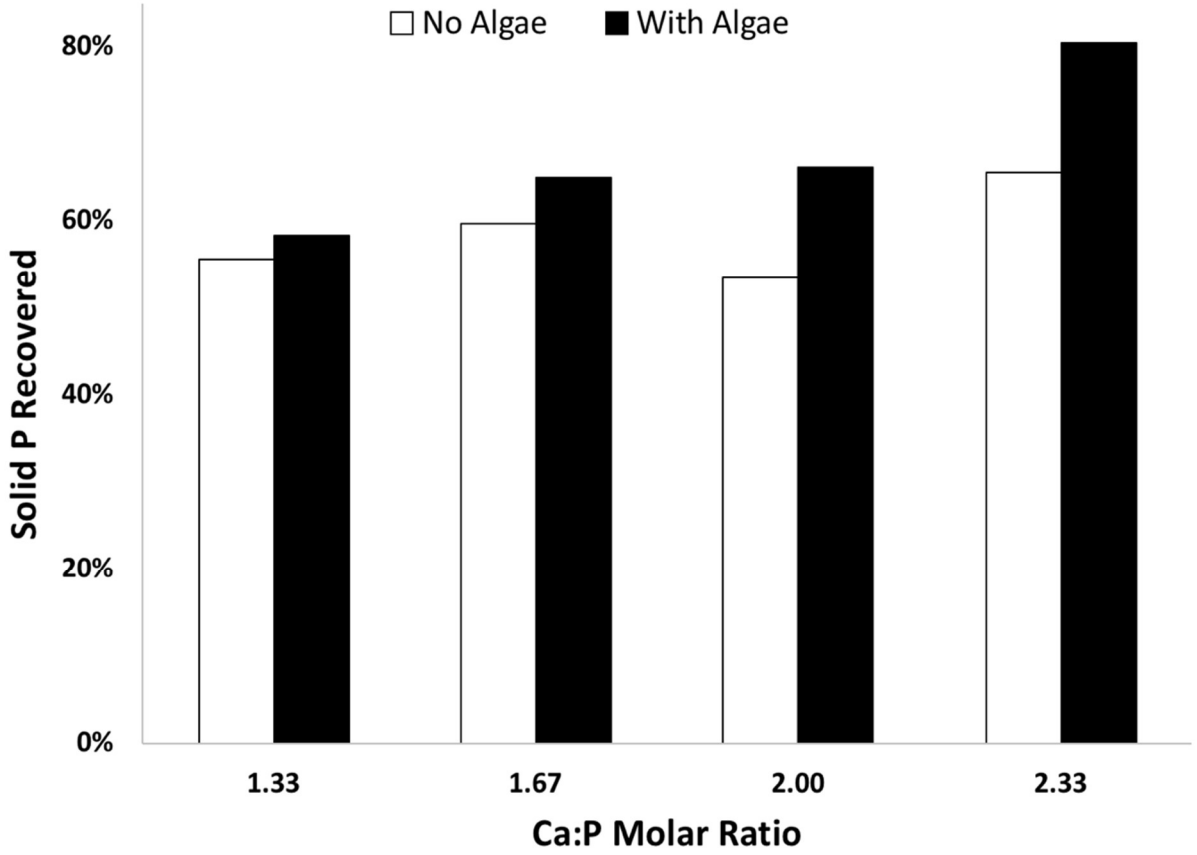

Figure 32: The percent of phosphorus (P) recovered in the HTL solids from the reaction of calcicte and trisodium phosphate at varying Ca:P molar ratios both in the absence (white) and presence (black) of low-ash algal biomass.

Furthermore, the difference in P-recovery between reactions with and without low-ash algae increased with the Ca:P molar ratio. In other words, only an additional 2.7% of P was recovered in the HTL solids when algae were added to the calcite and trisodium reaction at a Ca:P molar ratio of 1.33. Meanwhile, the greatest amount of P was recovered in the HTL solids (80.4%) where when low-ash algae was added to an overall Ca:P molar ratio of 2.33, and this was an increase of 14.8% of solid P recovered in comparison to the calcite and trisodium phosphate reaction without algae.

With similar masses of low-ash algae being added to the reaction and algae being harvested from the same light rack growth tank, the carbon to calcium (C:Ca) molar ratio decreased with increasing Ca:P molar ratio. For example, the lowest C:Ca molar ratio was 5.3 at the highest Ca:P molar ratio was 2.33. Similarly, the C:Ca molar ratio was the highest at 6.7 when the Ca:P molar ratio was the smallest of 1.33. Previous reports from the literature would indicate that a higher C:Ca molar loading and therefore higher potential for CO_2 would favor greater calcite dissociation and P recovery.[24-25] However, the results from Figure 32 contradict this theory. The C:Ca molar ratio loaded to these model compound HTL reactions were between 5.3 and 6.7 while the C:Ca molar ratio of the wastewater-cultivated and auto-flocculated, light rack algal solids were at least 18.8 and 14.5 respectively. Thus, the calcite, trisodium phosphate, and algae HTL reactions may have been carbon-limited compared to the HTL reactions involving wastewater-cultivated algal solids. This carbon-limitation hypothesis is supported by the C:Ca molar ratio being approximately three times less in the model compound reactions compared to the wastewater-cultivated algal solid reactions. Higher C:Ca molar ratios were not achievable due to the lack of low-ash algal biomass remaining in stock. The effect of C:Ca molar ratio has on the final HTL solid structure will be explored and discussed in the ensuing Chapter 6: *Raceway*.

A complimentary quantifying technique to the addition or recovery of solid phosphorus for measuring the hydrothermal conversion of calcite to calcium phosphate is evaluating the loss of carbonate. According to the theorized mechanism, phosphate must replace carbonate to achieve the desired calcium phosphate product. Thermogravimetric analysis (TGA) has great promise for not only distinguishing between calcium phosphate and calcium carbonate, but more accurately and precisely quantifying the amount of carbonate represented in an algal or HTL solid sample.

Figure 33 best depicts this distinction and measurement of carbonate via TGA. On the left of Figure 33 shows the mass degradation of $CaCO_3$ and HAp, and after being thermally treated to 850°C in a purely nitrogen environment. HAp degrades very little losing less than 10 wt%. Calcium carbonate, conversely, losses over 40 wt% between 600 and 800°C. This distinction is further evident when comparing the derivative weight (wt% min^{-1}) of the thermal degradation of

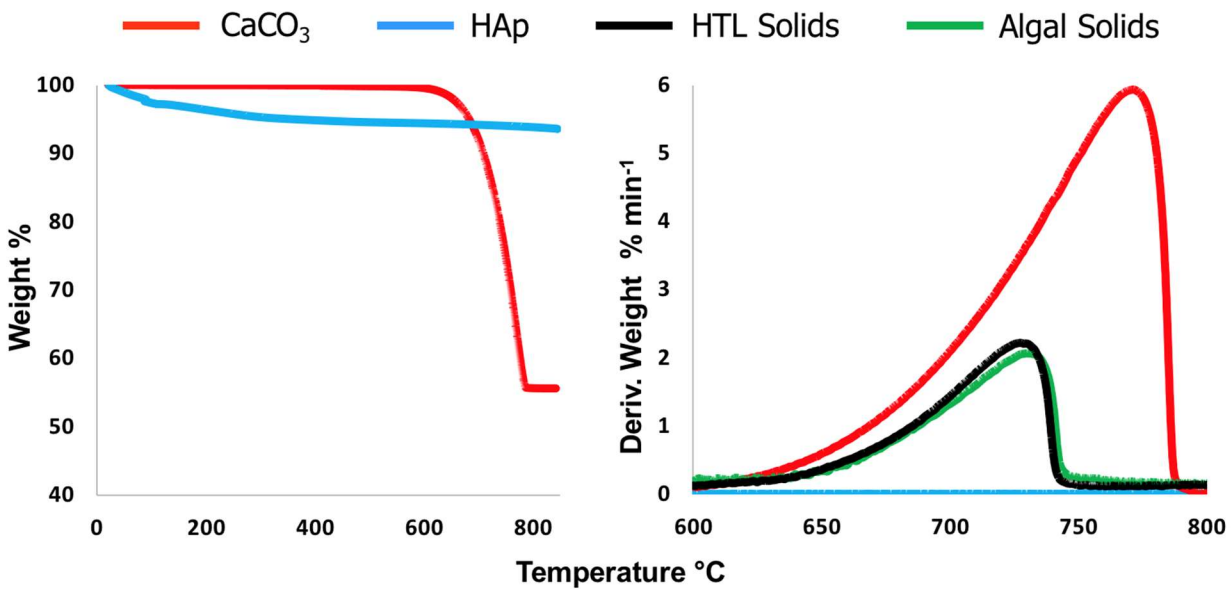

Figure 33: Thermal gravimetric analysis (TGA) of key inorganic model compounds, algal, and HTL solids. Overall wt% change (left) shows the clear distinction between $CaCO_3$ and HAp from TGA while the derivative weight (right) provides clear means to calculate the mass of inorganic carbon in both the algal and HTL solid samples.

these solid samples shown on the right of Figure 33. HAp appears as flat line along the x-axis because no substantial change in wt% is observed. Calcium carbonate, algal and HTL solids, however display a large peak between 600 and 800°C representing the mass lost from the volatilization of CO_2 gas from the $CaCO_3$ solid leaving only CaO ash.

Measuring the amount of carbonate in the initial solid sample can then be calculated by first determining the mass of CO_2 emitted. This is done by calculating the difference in wt%

between the starting and final temperatures when the wt% change occurred. The starting and final temperatures are determined through the derivative wt% where the initial temperature is the far-left end of the peak and the final temperature is the far-right. For example, in Figure 33 the difference in observed total wt% between 600 and 750°C would be used to quantify the mass of CO_2 emitted from $CaCO_3$ in the algal and HTL solid samples. The $CaCO_3$ peak has a wider temperature range, 600–800°C because it has a much greater wt% of $CaCO_3$ compared to the algal and HTL solid samples. Once the mass of CO_2 loss is determined, simple stoichiometry from the equilibrium expression for the degradation of $CaCO_3$ to CaO shown in equation (13) will determine the mass of carbonate (i.e. inorganic carbon)

$$\mathrm{CaCO_3(s)} \leftrightarrow \mathrm{CaO(s)} + \mathrm{CO_2(g)} \qquad (13)$$

present in the algal and HTL solids. Comparing the loss or addition of inorganic carbon between the initial, auto-flocculated algal solids and final HTL solids is critical in not only determining the conversion efficiency of calcite to calcium phosphate, but also the potential for *in-situ* catalysis and biocrude upgrading from the proposed water-gas shift reaction.

Table 11 compares the TGA-calculated, using the previously mentioned method, and the theoretical weight percentage of carbonate both for commercial calcium carbonate and for the light rack algal solids previously discussed in Table 8 from Chapter 4.4.3 *Fate of Phosphorus post-HTL*. While the theoretical weight percent of $CaCO_3$ can be determined using simple stoichiometry, our collaborator used water chemistry modeling of the growth media to determine the theoretical carbonate weight percentage of the light rack algal solids. The water chemistry model correlates pH and alkalinity to determine a total carbonate (CO_3^{2-}) concentration present in the growth media. Furthermore, our collaborator confirmed that the algal growth media was carbonate-limited and

calcium-abundant when the algal solids were auto-flocculated. Thus, when the algal light rack tanks were auto-flocculate at a pH of 11, all of the carbonate in the growth media would precipitate

Table 11: Comparison of the TGA-calculated and the theoretical CO_3 wt% for commercial $CaCO_3$ and light rack (LR) algal solids discussed in Table 8 from Chapter 4.4.3 *Fate of Phosphorus post-HTL.*

SAMPLE	MEDIA		SOLIDS				
	Ca	Alkalinity	Ash	XRD	Theo. CO_3	TGA CO_3	% Error
	mg/L	*mg/L $CaCO_3$*	*wt%*	*Pattern*	*wt%*	*wt%*	*%*
$CaCO_3$	-	-	55.0	Calcite	**60.0**	**59.9**	**0.1**
LR 1	9.2	249	6.0	Amorph.	**n.d.**	**2.03**	**-**
LR 2	19.0	359	6.2	Amorph.	**3.44**	**1.93**	**43.9**
LR 3	28.8	363	4.6	Amorph.	**6.91**	**1.95**	**71.8**
LR 4	38.0	410	8.0	Calcite	**8.17**	**2.88**	**64.8**
LR 5	44.5	410	12.1	Calcite	**11.41**	**4.47**	**60.8**
LR 6	57.2	391	12.9	Calcite	**15.11**	**7.08**	**53.1**

Light Rack abrv. LR
Theoretical abrv. Theo.
Non-detectable abrv. n.d.
Amorphous abrv. Amorph.

out of solution as $CaCO_3$. The total carbonate concentration determined from the water chemistry modeling would therefore be the theoretical mass of carbonate in the algal solids. Finally, with a total mass of freeze-dried algal solids harvested from each tank, a theoretical weight percentage of carbonate for the algal solids could be determined.

For pure calcium carbonate, the TGA method for calculating carbonate weight percentage (wt%) was within 0.1% error of the theoretical or stoichiometric carbonate weight percent of $CaCO_3$. However, when the TGA-calculated method for determining the carbonate weight percent was applied to the light rack algal solids samples, it was discovered that the TGA-calculated carbonate weight percent was nearly half the theoretical carbonate weight percent that

was determined by our collaborator using a water chemistry model. Thus, the TGA-calculated weight percent carbonate had a 44-72% error compared to the theoretical carbonate weight percent. The trend of increasing carbonate weight percentage with increasing, initial calcium concentration for each tank continued for both the theoretical and TGA-calculated carbonate weight percentage. Thus, the TGA method for calculating the carbonate weight percentage for algal solids may need optimizing to become more accurate for measuring carbonate in algal solids. Further investigation of the proximate analysis of the algal solids on the TGA was then explored.

The prior TGA-calculated method for determining carbonate weight percentage only considered the pyrolysis stage of the proximate analysis conducted for solid samples. After the furnace reaches 850°C during pyrolysis, it cools to 120°C, switches the furnace gas supply from N_2 to air, and begins a second temperature ramp again to 850°C. This second stage of the proximate analysis measures the combustible material present in the solid sample. While less than 1 wt% loss was observed from the second-stage, combustion of pure $CaCO_3$, a 5 to 15 wt% loss from combustion was observed in all algal solid samples. It is hypothesized that the remaining carbonate that would reduce the error between TGA-calculated and theoretical carbonate remains in the combustible, non-volatile material of the algal solids.

The hypothesis that further weight loss due to CO_3 from $CaCO_3$ is based upon the equilibrium relationship between $CaCO_3$, CaO, and CO_2, and the development of Calcium-Looping for CO_2 capture. Calcium-Looping is the continuous and reversible process of the release and recapture of CO_2 gas from the $CaCO_3$ and CaO solid, respectively.[29-30] There was no indication that CO_2 was being recaptured on the algal solid, for no increase in mass was observed during the pyrolysis or combustion of algal solid samples on the TGA. Furthermore, gaseous N_2 and air were flown through the TGA furnace at 100 mL/min during pyrolysis and combustion,

respectively. It was presumed that the flow rate was significant enough and the CO_2 concentration in the compressed air was minimal enough that the furnace was vacated of enough CO_2 to not impact the $CaCO_3$ and CO_2 equilibrium. This presumption, however, neglected the abundance of additional solid carbon from the algal biomass. Thus, the hypothesis was further refined to include that the presence of additional, solid, organic material with $CaCO_3$ delayed the release of CO_2 from the $CaCO_3$.

To test this hypothesis various mixtures of $CaCO_3$ and glucose were prepared then analyzed via the same TGA, proximate method as the previous algal solids. Proximate analysis on the TGA were also done on pure samples of $CaCO_3$ and glucose as controls. Initially pure glucose was difficult to run on the TGA, as it expanded when thermally treated. When 15 mg or more were loaded into the TGA sample pan, the glucose would expand, come in contact with the roof of the furnace and push down on the sample beams causing gross errors and incomplete results. Two masses of pure glucose were tested, 6.5 mg and 10.6 mg, for reproducibility. The glucose and $CaCO_3$ mixtures were prepared in two different manners. The first was a *premixed* 5 g mixture where glucose/$CaCO_3$ solids were added at a respective 50/50 and 75/25 wt% combination and shaken vigorously to ensure homogeneity. The second mixture was a single 50/50 wt% glucose and $CaCO_3$; however, approximately 10 mg of glucose and $CaCO_3$ were *preloaded* separately into the TGA sample pan. While this method ensured exact 50/50 wt% was analyzed, the miniature size of the TGA sample pan inhibited proper mixing. To distinguish between the two methods for prepare glucose and $CaCO_3$ mixtures, they are further referred to as premixed or preloaded mixtures.

The TGA, derivative weight results for glucose, $CaCO_3$, and mixtures of the two can be seen in Figure 34. The top figure depicts the pyrolysis stage of the proximate analysis while the

bottom shows the combustion stage. The pyrolysis derivative weight percent peaks are as to be expected. For the two, 6.5 and 10.6 mg, pure glucose runs shown in solid and dotted green lines, respectively a large peak appears near 230°C with two shoulder peaks between 270-290°C and 370°C. These same peaks also appear in all three glucose and $CaCO_3$ mixture runs and align with their respective loadings. The pure glucose samples had the largest of these derivative weight percent peaks followed by the 75/25 wt% glucose/$CaCO_3$ premixed mixture shown in black. Lastly, the two 50/50 wt% mixtures that were premixed or preloaded into the TGA sample pan, shown by a solid and dotted-gray line respectively, had the least yet similar derivative weight peak heights and areas within the same temperature range of the previous pure glucose sample and the glucose and $CaCO_3$ mixtures.

The previously identified derivative weight percent peak indicative of CO_2 loss from $CaCO_3$ between 600-800°C during pyrolysis also appears for proximate analysis runs of $CaCO_3$ and glucose and $CaCO_3$ mixtures. The relative peak heights and peak areas also trend with the premixed and preloaded mixtures. The largest derivative weight percent peak occurs with the pure $CaCO_3$ sample shown in red. The next largest peaks appeared from the solid and dotted gray lines representing the premixed and preloaded 50/50 glucose and $CaCO_3$ mixtures. The greater discrepancy between these peak heights and areas at this temperature range indicate how the solid-solid mixtures are prepared do impact the proximate analysis results. This discrepancy is explored in greater detail when the calculations for the actual carbonate mass loaded and TGA-calculated carbonate mass is compared later. The premixed 75/25 wt% glucose/$CaCO_3$ mixture had the smallest derivative weight percent peak height and area at the 600-800°C range during pyrolysis. The overall comparison between the controls and mixtures depict a clear distinction between the derivative weight percent peaks representative of glucose and $CaCO_3$ during pyrolysis.

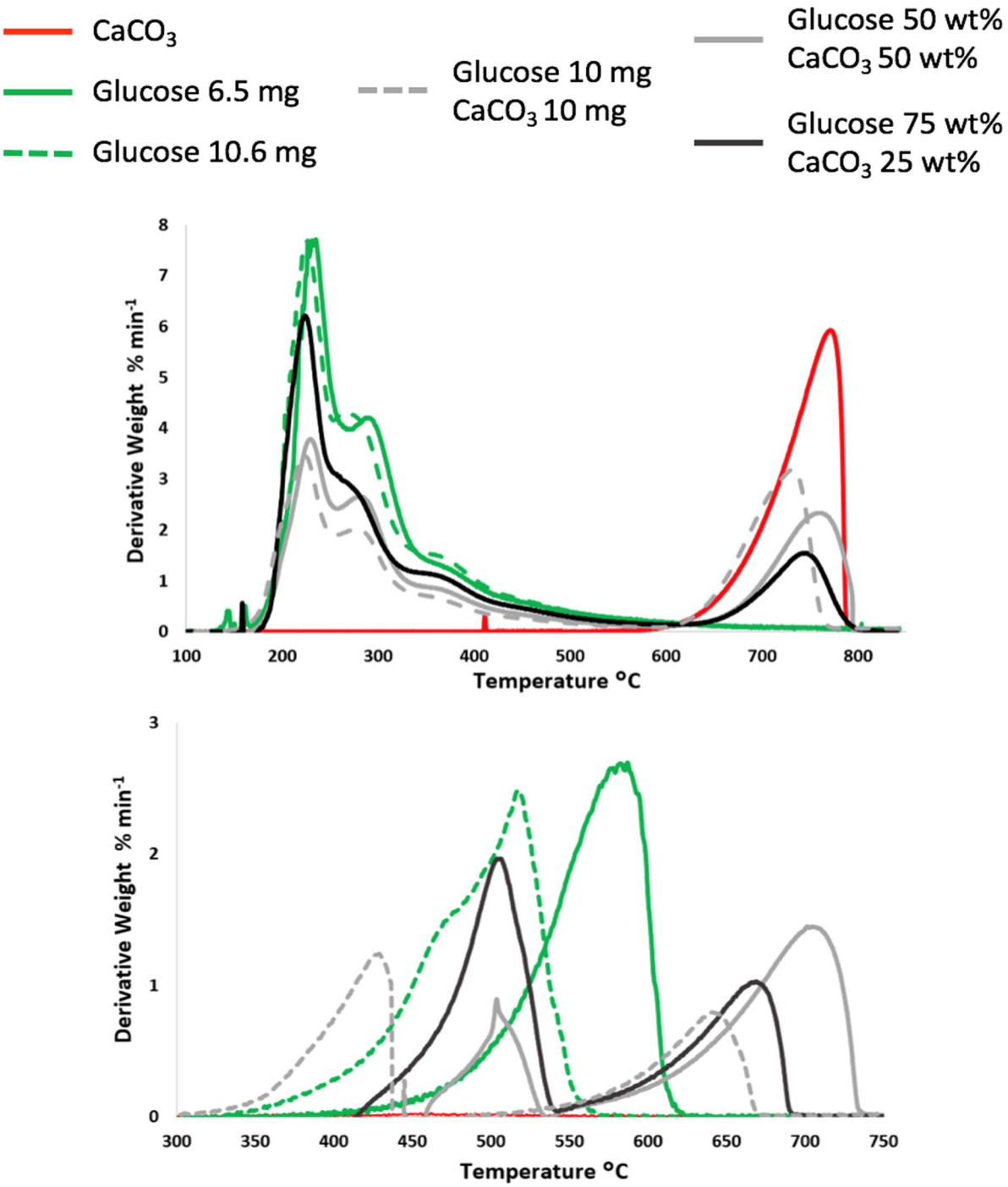

Figure 34: Derivative weight % results from the proximate analysis including the initial pyrolysis stage (top) and the final combustion stage (bottom). Samples included pure CaCO3 and pure glucose at two different mass loadings (6.5 and 10.6 mg); two premixed, 5-gram mixtures of glucose/CaCO3 at 50/50 and 75/25 wt% respectively; and finally, a preloaded mixture of 10 mg of glucose and CaCO3 each.

The second stage of the proximate analysis on the TGA is combustion, and the combustion of the aforementioned samples and mixtures appear at the bottom of Figure 34. As previously mentioned, pure $CaCO_3$ has no change in weight during this combustion stage. Derivative weight percent for the pure glucose and glucose/$CaCO_3$ mixtures, therefore only appeared between 300-750°C during the combustion stage. Pure glucose samples had a single large peak appear at different temperature ranges depending on the mass loading. At a higher, 10.6 mg solid loading, this single, broad, derivative weight peak appeared between 325-575°C while at 6.5 mg loading this peak shifted to be between 400-625°C. Meanwhile, glucose/$CaCO_3$ mixtures had two distinct derivative weight percent peaks appear. The one apparent derivative weight percent peak shared by all mixtures appeared between 550-750°C. This peak is presumed to be the hypothesized delayed combustion of the remaining carbonate from $CaCO_3$, for it did not appear in any pure glucose or $CaCO_3$. The results for the premixed glucose/$CaCO_3$ mixtures also show this peak grow as the weight percentage of $CaCO_3$ increased from 25 wt% shown in black to 50 wt% shown in gray. The preloaded 50/50 wt% mixture, meanwhile, had the smallest derivative weight percent peak appear at this temperature range.

It is presumed that the lack of missing for the preloaded mixture caused may have caused derivative weight percent peak to shift and appear between 300-440°C. Given the pure, 10.6 mg sample of glucose also began combusting at this temperature and a larger, it is assumed that the earlier, complete combustion of the glucose occurred due to the method for which the sample was loaded. The premixed 75/25 and 50/50 wt% glucose/$CaCO_3$ mixtures also had a broad peaks appear between 400-500°C and 450-500°C shown in solid black and gray lines in Figure 34, respectively. The temperature ranges and derivative weight peaks for theses premixed mixtures agree and fit with pure, 10.6 mg of glucose loading shown as a dotted-green line. Thus, one may

conclude the later derivative weight percent peaks appearing between 550-750°C are due to a delayed combustion of $CaCO_3$.

The hypothesis that an additional solid, organic material may delay the release of CO_2 from $CaCO_3$ during proximate analysis on TGA is confirmed. First, the derivative weight percent peaks between approximately 500-750°C appeared only in glucose/$CaCO_3$ mixtures and were not previously seen in the proximate analysis of pure $CaCO_3$ or pure glucose. Further evidence that these peaks were indicative of $CaCO_3$ and not glucose was that their size and area grew with greater, premixed $CaCO_3$ wt%. This additional loss of carbonate during combustion was not originally accounted for in the TGA-calculated carbonate weight percentage and therefore could explain the underestimated carbonate weight percentage when compared to the theoretical water chemistry carbonate weight percent for the algal solids .

Table 12 again compares the TGA-calculated mass of carbonate to the actual and theoretical amounts of carbonate from the three different glucose and $CaCO_3$ mixtures. For these calculations the hypothesized weight percent of carbonate due to the delayed combustion of $CaCO_3$ that occurs between approximately 500-750°C is calculated identically as it was for pyrolysis. The difference in weight percentage that occurs at the beginning (T1) and final (T2) temperatures as seen by the derivative weight percent peaks is assumed to be the loss of CO_2 from $CaCO_3$. The weight percent of CO_3 is then calculated from the weight percent of CO_2 using their molar masses and the stoichiometry from equation (). The total carbonate weight percent calculated from pyrolysis and from the sum of pyrolysis and combustion are compared to the actual carbonate weight percent that was loaded with each sample.

Table 12: The actual loaded and TGA-calculated carbonate weight percentages from both pyrolysis and later combustion of three glucose and $CaCO_3$ mixtures

LOADING				PYROLYSIS				COMBUSTION			TOTAL	
Glucose	$CaCO_3$	Mixture	CO_3	T1	T2	CO_3	Error	T1	T2	CO_3	CO_3	% Error
wt%	*wt%*	*Method*	*wt%*	*°C*	*°C*	*wt%*	*%*	*°C*	*°C*	*wt%*	*wt%*	*%*
50	**50**	Pre-Mixed	30.0	600	800	28.6	4.6	540	740	3.7	44.7	49.1
50	**50**	Pre-Loaded	30.4	600	800	34.0	11.6	495	675	1.5	41.0	34.6
75	**25**	Pre-Mixed	21.0	600	800	17.8	15.4	540	700	1.5	27.0	28.8

The sum of the pyrolysis and combustion carbonate weight percentages, however, overestimated the actual carbonate weight percentages for the glucose and $CaCO_3$ mixtures. A carbonate weight percent of 44.7 and 41.0 wt% were calculated for the 50/50 wt% premixed and preloaded glucose/$CaCO_3$ mixtures, respectively. The actual carbonate weight percent of the 50/50 premixed and preloaded mixtures were 30.0 and 30.4 wt%, respectively. Similarly, the premixed 75/25 wt% glucose/$CaCO_3$ mixture had only 21.0 wt% carbonate, but the combined pyrolysis and combustion carbonate weight percent totaled 27.0 wt%. The summation of the carbonate from both pyrolysis and combustion resulted in 28.8-49.1% error from the actual, theoretical amount.

The carbonate weight percentages of the mixtures from pyrolysis calculations alone, however, were more accurate with errors ranging from 4.6-15.4% compared to the actual and theoretical amount. Calculations from the pyrolysis stage of TGA measured 28.6 wt% of the actual 30.0 wt% carbonate in the premixed 50/50 wt% glucose/$CaCO_3$ mixture. The premixed 25/75 wt% glucose/$CaCO_3$ similarly measured 17.8 wt% from pyrolysis, TGA calculations compared to the actual 21.0 wt% carbonate loaded. It was only the preloaded 50/50 wt% glucose/$CaCO_3$

mixture that the pyrolysis, TGA calculations overestimated the carbonate weight percent at 34.0 wt% as opposed to the actual 30.4 wt%. This overestimation may be due to the lack of mixing and therefore glucose and $CaCO_3$ layering within the sample pan disrupting and interfering with the thermal degradation of $CaCO_3$ during the analysis. The underestimations in the premixed mixtures may be due to the hypothesized, delayed combustion of $CaCO_3$; however, including the additional combustion peaks observed with these mixtures caused for an overestimation of carbonate. Thus, the additional weight loss observed during the combustion of glucose and $CaCO_3$ mixtures between 500-750°C is not due to $CaCO_3$ alone and may be from a glucose and $CaCO_3$ char. Further investigation to the thermal degradation of $CaCO_3$ and biological model compounds is necessary to better distinguish both the source and resulting gases of the observed weight loss both during pyrolysis and combustion stages of proximate analysis.

In conclusion, the presence of solid organic material such as glucose or algal biomass disrupts the thermal degradation of $CaCO_3$. This disruption creates additional weight loss and derivative weight percent peak to appear during the combustion of an organic and $CaCO_3$ solid between 500-750°C. This additional weight loss, however, overestimates the actual carbonate weight percent of the solid sample indicating the weight lost during combustion is not just CO_2 from $CaCO_3$. Meanwhile, the CO_2 weight loss observed during pyrolysis alone accounted for nearly 85% or more of the initial carbonate in a glucose and $CaCO_3$ mixture. Thus, the additional organic solids may cause the complete degradation of $CaCO_3$ to be delayed and later combusted during the second stage of proximate analysis. However, a majority of the carbonate is still lost during pyrolysis with less error than the summation of the loss during pyrolysis and combustion.

5.4.4 HTL of Organic and Biological Model Compounds

The third and final research thrust was to discern if the previously identified inorganic compounds were acting as some sort of catalyst and impacting the biocrude properties and composition *in-situ*. Control experiments and HTL reactions of major biological compounds were first necessary to distinguish key differences when inorganic model compounds were added. The first control HTL reactions involved glucose, soy protein, and tetradecanamide. After singular reactions of each, it was determined that traditional HTL product extraction techniques were not optimum for HTL of several of these biological model compounds. The premise, therefore, is to present the preliminary findings and hypotheses to better guide future work on the *in-situ* catalysis from wastewater-cultivated or auto-flocculated algal solids.

The preliminary HTL reactions of glucose yielded an abundance of a solid, char product. This solid, char product differed from the previous, calcium phosphate, HTL solids. The char resembled that of combusted wood where it was black, light, and flaky. Because of the abundance and light, flaky nature of the char, substantial losses were occurred while extracting and drying the solids. Thus, accurate, solids yields were unobtainable. The biocrude yield from the independent, glucose HTL reaction was also inadequate for further analysis. Additional techniques and experience to optimize the HTL product extraction from carbohydrates that are high char producing are also required.

A high char and low biocrude yield are characteristic of HTL of pure carbohydrates. High solid char yields from HTL of carbohydrates such as glucose and starch were observed by Biller and Ross who also concluded carbohydrates had the smallest impact on the overall biocrude yield.[9] Teri et al. also reported starch and cellulose to have the highest solids yield and the lowest biocrude yield when reacted independently.[12] Biocrude yields increased by approximately 10 wt% and 30

wt%, however, when these carbohydrates were reacted with other biological compounds such as protein and lipids, respectively.[12] Biller and Ross also observed an increase in biocrude yield from HTL of glucose and starch when the Na_2CO_3 was added externally and went on to hypothesized that Na_2CO_3 is selective to the decarboxylation of carbohydrates.[9]

It is, therefore, hypothesized that the $CaCO_3$ observed in the wastewater-cultivated and auto-flocculated algal could provide similar catalysis as Na_2CO_3. Preliminary results from HTL of whole algal solids, however, support this hypothesis, as biocrude yields from wastewater and auto-flocculated algal solids are comparable to other, low-ash and high lipid, monocultures on an ash-free dry weight (afdw%) basis.[9, 27, 31] The hypothesized cause for the comparable biocrude yields from the wastewater-cultivated and auto-flocculate algal solids, despite their low lipid content, is that the $CaCO_3$ selectively and more efficiently converted the 16-25 dw% of carbohydrates to the desired biocrude product. Chen et al. further confirmed the benefit high-ash and carbonate content algal solids have on increasing the biocrude yield.[32] Glucose and $CaCO_3$ HTL reactions were unable to be performed because a substantial amount of repairs were required on the high pressure and high temperature valves on the HTL reactors. Repeated use caused sand from the heated sand bath to damage the packing and threading of the valves leading to potential leaks and incomplete reactions. Additionally, a total solids loading that is comparable to the conventional HTL parameters and yet produces enough biocrude for analysis needs to be determined. Similarly, the optimum C:Ca molar ratio for the HTL reaction of glucose and $CaCO_3$ could also be identified.

The second model compound of interest was tetradecanamide (Alfa Aesar, TDA, 98%). Although this fatty acid amide is not a primary biological compound observed in microalgae, C_{16} and C_{18} amides are primary N-compounds observed in the biocrude after HTL of microalgae.

Roberts et al. further hypothesized that the acid-base properties of the HAp observed in the HTL solids could reduce these fatty acid amides to aliphatic and aromatics via amines and nitriles.[31] Thus, control HTL reactions of just tetradecanamide and HTL reactions doped with commercial HAp were performed.

The initial control reactions of tetradecanamide also produced unexpected results. A noticeable biocrude product was not observed. Instead, the primary product was a white, greasy, solid that, for the most part was not soluble in the organic extraction solvent, dichloromethane. The tetradecanamide wt% loaded and overall mass loading was adjusted while other reaction conditions, temperature and time, were held constant in an attempt to better convert the tetradecanamide solid to a biocrude product while maintaining conventional HTL conditions. All attempts, however, resulted in the same white, greasy, solid product. Continuing with the hypothesis that HAp may also enhance the depolymerization of the C_{14} fatty acid amide, commercial HAp was added at 15, 25, and 35 wt% relative to the tetradecanamide that was also added. The total solids loaded for the reaction, HAp and tetradecanamide, remained the conventional 10 wt%. The GC-MS results for the DCM-soluble fraction are shown in Figure 35.

Only two distinct peaks appeared in the GC-MS results from the DCM-soluble product that was produced via the HTL of tetradecanamide alone and with the addition of HAp. These two peaks were identified to be the original tetradecanamide (TDA) and the presumed product tetradecanitrile (TDN). The conversion of an amide to a nitrile agrees with the previously hypothesized mechanism in the literature that report this conversion to be the initial step for the reduction of long chain amides.[31, 33-34] This conversion of TDA to TDN is further quantified by comparing the ratio of peak areas in each spectrum shown to the right of Figure 35. The ratio of TDA to TDN peak area in each GC-MS spectra decreases with the addition more HAp from 23.8

in the control to 0.1 when 35 wt% HAp was added to the reaction. It, therefore, may be concluded that HAp does assist the conversion of TDA to TDN during HTL despite the lack of an apparent biocrude product.

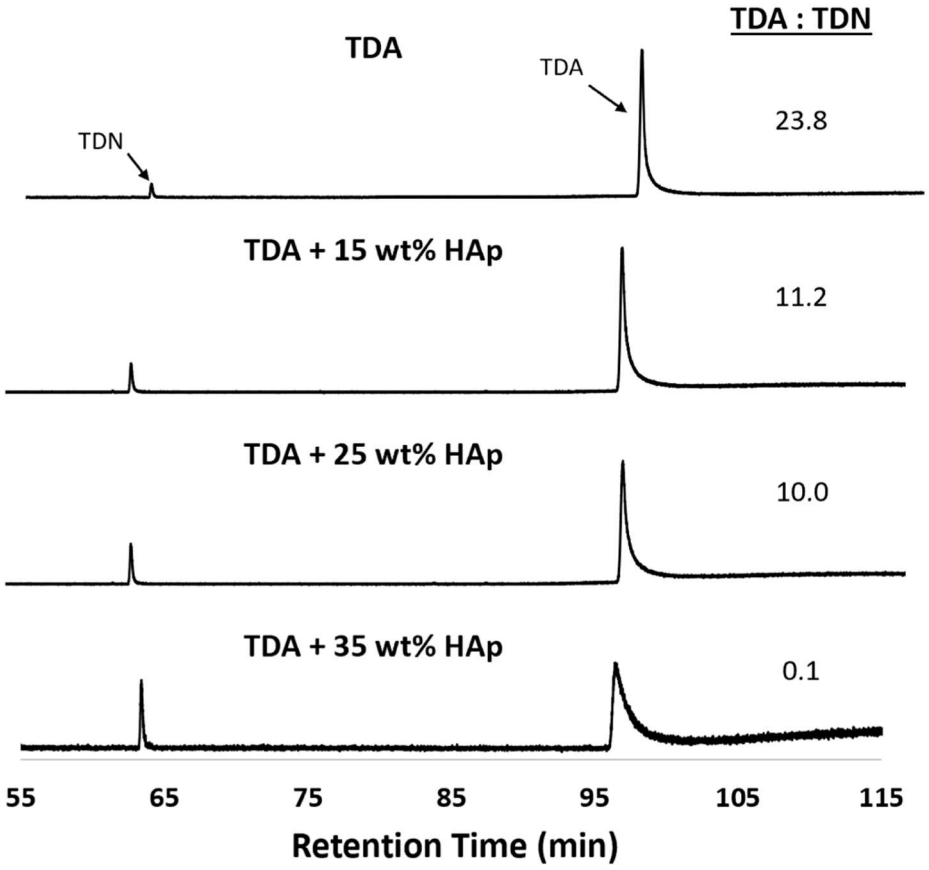

Figure 35: GC-MS results of the DCM-soluble fraction from the HTL product of tetradecanamide (TDA) and various doping of commercial HAp. The two distinct peaks represented are the initial reactant, TDA, and the presumed product, tetradecanitrile (TDN). The ratio of their peak areas (TDA:TDN) are represented on the right.

HTL of palmitic acid produced an identical white, solid product as HTL of tetradecanamide, and many in the literature have observed the similar results through the HTL of long chain compounds. Changi et al. has provided the most comprehensive review for the HTL of biological compounds and notes larger fatty acids ($\geq C_{16}$) are stable at the subcritical water

conditions. Thus, independently, the long chain compounds do not decompose into the desired, biocrude product during HTL while smaller fatty acid chains ($\leq C_{12}$) will.[13] Watanabe et al. best characterized the reaction mechanism for the conversion and HTL of long chain fatty acids to be decarboxylation of the fatty acid to ketones and ultimately alkanes and alkenes.[35] A variety of catalysts were trialed. Cobalt chloride ($CoCl_2$) and alkali bases, NaOH and KOH, were favorable for increasing the pentadecane yield from the hydrothermal deoxygenation of palmitic acid. Yields increased from 0.62 ± 0.23 in the control to 2.1 ± 0.02, 7.1 ± 1.0, and 5.5 ± 2.3 from approximately 10 wt% loading of $CoCl_2$, NaOH, and KOH respectively and reaction time of 17-18 hours. Few however have experimented with the recently identified $CaCO_3$ or calcium phosphate solids from wastewater-cultivated and auto-flocculated algal solids. The preliminary results for these inorganics are also promising. As discussed in Chapter 4.4.4: *Inorganic in-situ HTL Catalysis*, both long chain fatty acids and amides peak areas decreased in the biocrude that was doped with $CaCO_3$ and had high phosphate recovery in the HTL solids.

Although $CaCO_3$ and HAp showed great potential for upgrading or enhancing the biocrude product through *in-situ* catalysis, a more encompassing hypothesis remained. It had yet to be determined the exact cause of the *in-situ* catalysis. One potential catalytic source was the final HTL solid, calcium phosphate products, such as HAp or TCP. Each have shown to have catalytic properties in the literature.[36-38] A second potential cause for the *in-situ* biocrude upgrade could be from the energy absorbed or released from the apparent inorganic conversion to calcium phosphates. Finally, the presence of additional, solid material could be enhancing the biocrude product.

To test these hypotheses regarding the *in-situ* HTL biocrude upgrading four distinct HTL reactions were conducted. The first HTL reaction (A) was a control that included only soy protein.

Prior reactions indicated soy protein to be viable biological model compound for many reasons. First soy protein produced a feasible amount of biocrude product for analysis when loaded 15 wt% solids. Soy protein had also been previously tested in the literature to allow for further comparison.[12] The second reaction (B) included soy protein doped with commercial HAp at 25 wt% relative to the soy protein mass. The third HTL reaction (C) included soy protein with $CaCl_2$ and Na_3PO_4. The total mass of $CaCl_2$ and Na_3PO_4 was also 25 wt% relative to the soy protein mass while the Ca:P molar ratio was 1.67. Previous inorganic hydrothermal synthesis reactions had shown these calcium and phosphate reagents and loading conditions promote HAp synthesis. In addition, the HAp synthesized from the HTL reaction of $CaCl_2$ and Na_3PO_4 also had a greater nano-structure than the commercial HAp when viewed by SEM. It is well-documented that a nano-structure can also be more advantageous for catalysis for several reasons.[39] The fourth and final HTL reaction (D) involved soy protein doped with inert silica also at 25 wt% relative to the soy protein loading. The purpose of the silica was to provide an inert solid in the reaction to further conclude the HAp was serving as an active catalyst, and it was not just the presence of a solid material that was changing the biocrude composition. Calcium carbonate was omitted because it had only recently been discovered to be the primary calcium-species present in the algal solids. In addition, the necessary loading conditions and C:Ca molar ratio to ensure a complete conversion of $CaCO_3$ to HAp have yet to be discovered.

The amide peak areas observed from the GC-MS analysis of the biocrude produced from these four reactions (A through D) are shown in Figure 36. The control and HTL reaction doped with $CaCl_2$ and Na_3PO_4, reactions A and C respectively, had the highest amide peak area percentage with 9.2 and 11.1 % area, respectively. The results from these two reactions indicate that the synthesis of HAp from $CaCl_2$ and Na_3PO_4 do not have an impact on the amide content of

the HTL biocrude. The HTL reactions of soy protein doped with commercial HAp and inert silica, however, had noticeably less amide peak area percentages of 7.1 and 7.0 % area, respectively. The results of these reactions are displayed in Figure 36 as reactions B and D, respectively. The decrease in amide % area for both HAp and silica indicate that the presence of additional solids

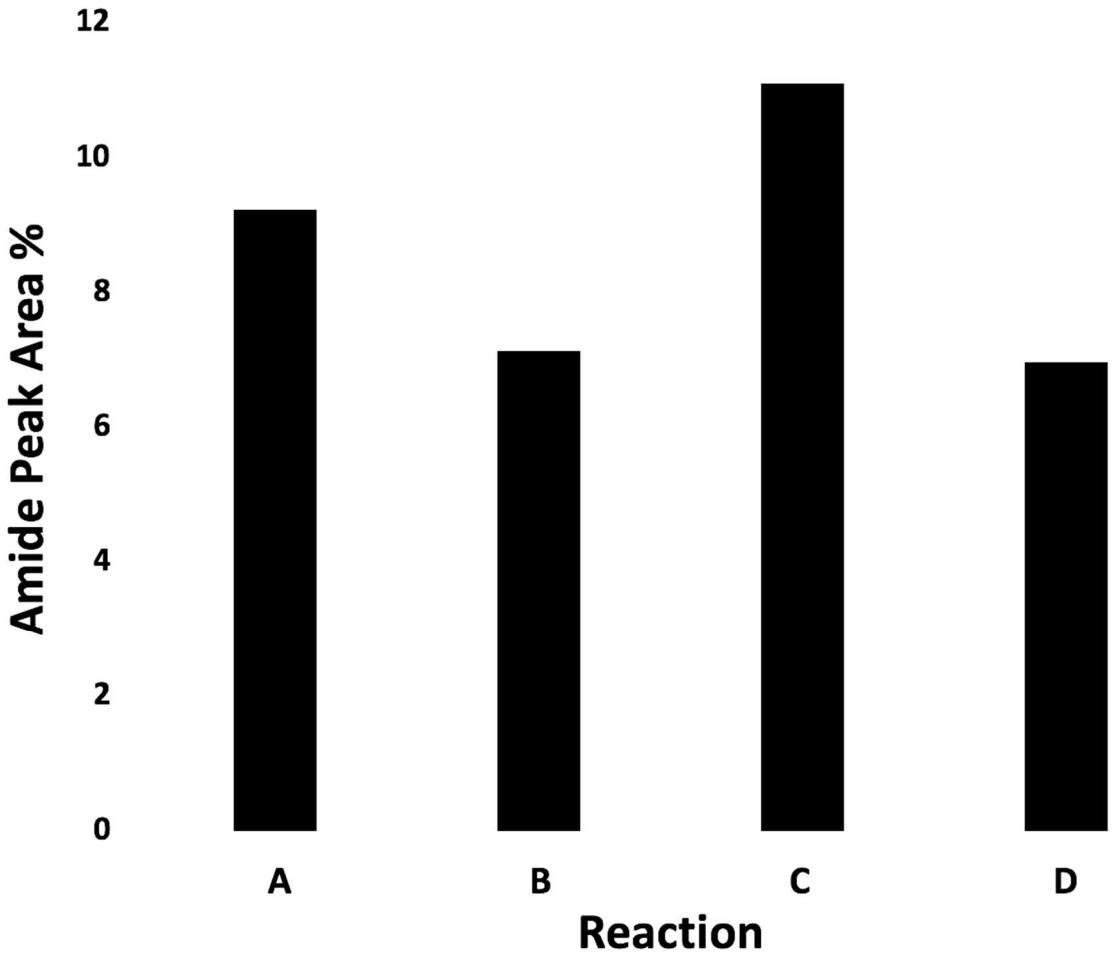

Figure 36: The total amide peak area percentage observed from the GC-MS analysis of the biocrude produced from four independent HTL reactions. First, an HTL reaction was a control of just soy protein (A). Second, an HTL reaction included soy protein and commercial HAp (B). Third, an HTL reaction of soy protein with $CaCl_2$ and Na_3PO_4 that formed HAp HTL solids during the HTL reaction (C).. The fourth and final HTL reaction included soy protein and inert silica solid (D).

rather than the potential, catalytic active sights of HAp may be causing the reduction in amides and enhancing the biocrude product.

5.5 Conclusions

Although calcite ($CaCO_3$) was the previously identified, primary crystalline structure of both the wastewater-cultivated and auto-flocculated, the resulting HTL solids appeared as either two distinct calcium phosphate structures, HAp or TCP, according to XRD. Inorganic model compound hydrothermal reactions were therefore performed using commercial calcite and trisodium phosphate (Na_3PO_4) at various Ca:P molar ratios and conventional HTL conditions. Initially, calcite remained a primary structure of the HTL solids product with the secondary structure being HAp. Additionally, the intensity of the HAp structure in the XRD pattern increased with decreasing Ca:P ratio.

Given the high, elemental substitution observed in the calcium phosphate HTL solids from the HTL of wastewater-cultivated algal solids, silica and magnesium were also added to the calcite and trisodium phosphate reactions. Small amounts of silica (SiO_2), from 0.01 to 0.45 grams, added to the initial inorganic model compound reactions altered the final HTL solid structure dramatically. Large decreases of the primary, calcite, XRD peaks and large increases in both HAp and, unidentifiable but, presumably silicate peaks appeared when additional silica was doped to the reaction. These results, where an increase in calcium phosphate structures was observed in the XRD patterns of HTL solids when doped with silica, also occurred when silica was added to auto-flocculated algal solids that originally produced HTL solids with calcite and a small presence of TCP in the XRD.

Complete conversion of the calcite to a nearly uniform HAp or TCP structure, as observed with the wastewater-cultivated algal solids however, was never achieved. Mechanistic studies of how calcite could be converted to calcium phosphates hydrothermally were explored. Calcium compounds with a wide-range of solubility were hydrothermally reacted and indicated that the dissociation of calcite to be the rate-determining step for the hydrothermal synthesis of calcium phosphates. SEM images further proved this dissociation occurs on the calcite surface as this is where the nano-rod morphology, characteristic of HAp, appeared. Besides the presence of additional ions to assist and promote the dissociation of calcite, carbon dioxide (CO_2) can also drastically improve the solubility of calcite given their equilibrium relationship. Carbon dioxide is present in the HTL of algal solids due to the decomposition of the organic biomass provided by the algae; therefore, the calcite and trisodium phosphate hydrothermal reaction was doped with low-ash algae. Improvements to the conversion of calcite to calcium phosphate from the presence of algae were inconclusive from XRD of the HTL solids. Thus, alternative methods for more accurately and precisely quantifying this conversion were explored.

The transformation of calcite to calcium phosphate requires the exchange of carbonate (CO_3^{2-}) for phosphate (PO_4^{3-}) within the solid structure. Thus, the recovery of solid phosphorus (P) and/or loss of soluble, aqueous P are quantifiable analyses for the conversion of calcite to calcium phosphates. For all Ca:P molar ratios between calcite and trisodium phosphate that were tested, the addition of algae increased the solid P-recovery indicating a higher conversion of calcite to calcium phosphate. The highest recovery occurred at the highest Ca:P molar ratio loading, which was also the lowest C:Ca molar ratio. This was not to be expected given the inverse, equilibrium relationship between CO_2 and $CaCO_3$. In other words, a higher C:Ca molar ratio would indicate a greater amount of CO_2 relative to $CaCO_3$, and the equilibrium relationship would

dictate more calcite would dissociate and more phosphate be recovered. Because of the opposing result, the C:Ca molar ratio is an area of interest for further reactions.

With the ability to measure P-recovery, the ability to measure carbonate loss was explored. The proximate, thermogravimetric analysis (TGA) provided a clear distinction between $CaCO_3$ and calcium phosphate solids. Solid calcium carbonate thermally degrades solid calcium oxide (CaO) between 600-800°C with the change in mass being stoichiometrically proportional to the loss of CO_2 gas from the degradation reaction. This change in weight causes a large peak to appear in the derivative weight percentage that also appeared in calcite-detectable HTL and algal solids. Accurate and precise measurements and calculations for the amount of carbonate in pure solid calcite were obtainable using $CaCO_3$ to CaO and CO_2 stoichiometry and the observed weight loss from the TGA. When this same method was applied to algal solids, the TGA-calculated result for the mass of carbonate did not agree with the theoretical mass of carbonate determined from the water chemistry of the growth media and harvesting pH. Further investigation of the thermal degradation of calcite in the presence of biological model compounds, such as glucose, indicated an additional stage of decomposition during the combustion phase of the proximate analysis. Although initial results were able to begin to isolate derivative weight peaks from glucose and $CaCO_3$, accurate and precise measurements of carbonate using the same TGA weight loss and stoichiometry were unachievable. The results, however, did provide great promise and expansion for the potential, TGA-derived method for quantifying biomolecular and carbonate content of algal solids.

The final thrust of the inorganic and biological model compound study was to observe the potential catalytic impact the inorganics had during the HTL of algae based upon changes or improvements to the biocrude composition. Initially, it was difficult to find a biological model

compound that produced an adequate biocrude product after HTL. Carbohydrates, such as glucose and starch, yielded an abundant, primarily solid char product that was light and flaky. Meanwhile, long-chain fatty acids and amides, like palmitic acid (C_{16}) and tetradecanamide (C_{14}), yielded primarily a white, greasy solid after HTL that was not soluble in dichloromethane (DCM). GC-MS analysis of the small fraction of DCM-soluble product obtained from the tetradecanamide reaction showed the presence of tetradecanitrile in addition to the initial reactant. The addition of commercial HAp to the HTL reaction of tetradecanamide showed a greater appearance of the presumed product, tetradecanitrile, than the reactant in the DCM-soluble, organic product.

Soy protein at an increased 15 wt% solids loading provided enough of a biocrude product for analysis. Thus, a control with three additional HTL reactions were performed where soy protein was doped with 1) HAp, 2) silica, and 3) $CaCl_2$ and Na_3PO_4. No reduction of peak area percentage for long chain amides were observed in the GC-MS analysis between the control and the doping of $CaCl_2$ and Na_3PO_4 indicating the synthesis of HAp from these reactants caused the change in amide concentration in the biocrude. The amide concentration in the biocrude did, however, decrease between the control and addition of HAp and silica. The reduction from both HAp and silica indicate the presence of a solid during HTL may be the cause for the reduction of long chain amides in the biocrude rather than catalytic active sites from the HAp.

5.6 References

1. Neria, I. S.; Kolen'ko, Y. V.; Lebedev, O. I.; Tendeloo, G. V.; Gupta, H. S.; Guitian, F.; Youshimura, M., An Effective Morphology Control of Hydroxyapatite Crystals via Hydrothermal Synthesis. *Crystal Growth & Design* **2009,** *9* (1), 466-474.
2. Earl, J. S.; Wood, D. J.; Milne, S. J., Hydrothermal synthesis of hydroxyapatite. *Journal of Physics: Conference Series* **2006,** *26*, 268-271.
3. Cao, H.; Zhang, L.; Zheng, H.; Wang, Z., Hydroxyapatite Nanocrystals for Biomedical Applications. *J. Phys. Chem.* **2010,** *114* (43), 18352-18357.

4. Roberts, G. W.; Fortier, M.-O. P.; Sturm, B. S. M.; Stagg-Williams, S. M., Promising Pathway for Algal Biofuels through Wastewater Cultivation and Hydrothermal Conversion. *Energy & Fuels* **2013,** *27* (2), 857-867.
5. Guo, Y.; Yeh, T.; Song, W.; Xu, D.; Wang, S., A review of bio-oil production from hydrothermal liquefaction of algae. *Renewable and Sustainable Energy Reviews* **2015,** *48*, 776-790.
6. Cui, H.; Liu, H.; Qin, J.; Li, Y.; Tang, H.; Yang, X., Hydrothermal synthesis and characterisation of glutamine-modified rod-like hydroxyapatite nanoparticles. *Micro & Nano Letters* **2012,** *7* (12), 1292-1295.
7. Ma, M. G., Hierarchically nanostructured hydroxyapatite: hydrothermal synthesis, morphology control, growth mechanism, and biological activity. *Int J Nanomedicine* **2012,** *7*, 1781-91.
8. Nathanael, A. J.; Han, S. S.; Oh, T. H., Polymer-Assisted Hydrothermal Synthesis of Hierarchically Arranged Hydroxyapatite Nanoceramic. *Journal of Nanomaterials* **2013,** *2013*, 1-8.
9. Biller, P.; Ross, A. B., Potential yields and properties of oil from the hydrothermal liquefaction of microalgae with different biochemical content. *Bioresource technology* **2011,** *102* (1), 215-25.
10. Jena, U.; Das, K. C.; Kastner, J. R., Comparison of the effects of Na2CO3, Ca3(PO4)2, and NiO catalysts on the thermochemical liquefaction of microalga Spirulina platensis. *Applied Energy* **2012,** *98*, 368-375.
11. Duan, P.; Savage, P. E., Hydrothermal Liquefaction of a Microalga with Heterogeneous Catalysts. *Industrial & Engineering Chemistry Research* **2011,** *50*, 52-61.
12. Teri, G.; Luo, L.; Savage, P. E., Hydrothermal Treatment of Protein, Polysaccharide, and Lipids Alone and in Mixtures. *Energy & Fuels* **2014,** *28* (12), 7501-7509.
13. Changi, S. M.; Faeth, J. L.; Mo, N.; Savage, P. E., Hydrothermal Reactions of Biomolecules Relevant for Microalgae Liquefaction. *Industrial & Engineering Chemistry Research* **2015,** *54* (47), 11733-11758.
14. Fu, J.; Lu, X.; Savage, P. E., Catalytic hydrothermal deoxygenation of palmitic acid. *Energy & Environmental Science* **2010,** *3* (3), 311.
15. Berg, U.; Donnert, D.; Weidler, P. G.; Kaschka, E.; Knoll, G.; Nüesch, R., Phosphorus removal and recovery from wastewaterby tobermorite-seeded crystallisation of calcium phosphate. *Water Science & Technology* **2006,** *53* (3), 131.
16. Maeda, H.; Ishida, E. H.; Kasuga, T., Hydrothermal preparation of tobermorite incorporating phosphate species. *Materials Letters* **2012,** *68*, 382-384.
17. Shaw, S.; Clark, S. M.; Henderson, C. M. B., Hydrothermal formation of the calcium silicate hydrates, tobermorite (Ca5Si6O16(OH)2·4H2O) and xonotlite (Ca6Si6O17(OH)2)- an in situ synchrotron study. *Chemical Geology* **2000,** *167*, 129-140.
18. Kamitakahara, M.; Nagamori, T.; Yokoi, T.; Ioku, K., Carbonate-containing hydroxyapatite synthesized by the hydrothermal treatment of different calcium carbonates in a phosphate-containing solution. *Journal of Asian Ceramic Societies* **2015,** *3* (3), 287-291.
19. Ishikawa, K.; Matsuya, S.; Lin, X.; Lei, Z.; Yuasa, T.; Miyamoto, Y., Fabrication of low crystalline B-type carbonate apatite block from low crystalline calcite block. *Journal of Ceramic Society of Japan* **2010,** *118* (5), 341-344.

20. Kim, I.-Y.; Kikuta, K.; Ohtsuki, C., Formation of Oriented Hydroxyapatite Rods by Hydrothermal Treatment of Calcite Single Crystal. *Korean Journal of Materials Research* **2012,** *22* (8), 397-402.
21. Yoshimura, M.; Sujaridworakun, P.; Koh, F.; Fujiwara, T.; Pongkao, D.; Ahniyaz, A., Hydrothermal conversion of calcite crystals to hydroxyapatite. *Materials Science and Engineering: C* **2004,** *24* (4), 521-525.
22. Kim, I. Y.; Ohtsuki, C., Hydroxyapatite formation from calcium carbonate single crystal under hydrothermal condition: Effects of processing temperature. *Ceramics International* **2016,** *42* (1), 1886-1890.
23. Sadat-Shojai, M.; Khorasani, M. T.; Dinpanah-Khoshdargi, E.; Jamshidi, A., Synthesis methods for nanosized hydroxyapatite with diverse structures. *Acta Biomater* **2013,** *9* (8), 7591-621.
24. Coto, B.; Martos, C.; Peña, J. L.; Rodríguez, R.; Pastor, G., Effects in the solubility of CaCO3: Experimental study and model description. *Fluid Phase Equilibria* **2012,** *324*, 1-7.
25. Shi, W.; Kan, A. T.; Zhang, N.; Tomson, M., Dissolution of Calcite at Up to 250 °C and 1450 bar and the Presence of Mixed Salts. *Industrial & Engineering Chemistry Research* **2013,** *52* (6), 2439-2448.
26. Loos, D.; Pasel, C.; Luckas, M.; Schmidt, K. G.; Herbell, J.-D., Experimental investigation and modelling of the solubility of calcite and gypsum in aqueous systems at higher ionic strength. *Fluid Phase Equilibria* **2004,** *219* (2), 219-229.
27. Brown, T. M.; Duan, P.; Savage, P. E., Hydrothermal Liquefaction and Gasification of Nannochloropsis sp. *Energy & Fuels* **2010,** *24* (6), 3639-3646.
28. Ross, A. B.; Biller, P.; Kubacki, M. L.; Li, H.; Lea-Langton, A.; Jones, J. M., Hydrothermal processing of microalgae using alkali and organic acids. *Fuel* **2010,** *89* (9), 2234-2243.
29. Grasa, G. S.; Abanades, J. C., CO2 Capture Capacity of CaO in Long Series of Carbonation/Calcination Cycles. *Industrial & Engineering Chemistry Research* **2006,** *45* (26), 8846-8851.
30. Dieter, H.; Hawthorne, C.; Zieba, M.; Scheffknecht, G., Progress in Calcium Looping Post Combustion CO2 Capture: Successful Pilot Scale Demonstration. *Energy Procedia* **2013,** *37*, 48-56.
31. Roberts, G. W.; Sturm, B. S. M.; Hamdeh, U.; Stanton, G. E.; Rocha, A.; Kinsella, T. L.; Fortier, M.-O. P.; Sazdar, S.; Detamore, M. S.; Stagg-Williams, S. M., Promoting catalysis and high-value product streams by in situ hydroxyapatite crystallization during hydrothermal liquefaction of microalgae cultivated with reclaimed nutrients. *Green Chem.* **2015,** *17* (4), 2560-2569.
32. Chen, W.-T.; Qian, W.; Zhang, Y.; Mazur, Z.; Kuo, C.-T.; Scheppe, K.; Schideman, L. C.; Sharma, B. K., Effect of ash on hydrothermal liquefaction of high-ash content algal biomass. *Algal Research* **2017,** *25*, 297-306.
33. Roussis, S. G.; Cranford, R.; Sytkovetskiy, N., Thermal Treatment of Crude Algae Oils Prepared Under Hydrothermal Extraction Conditions. *Energy & Fuels* **2012,** *26* (8), 5294-5299.
34. Bai, X.; Duan, P.; Xu, Y.; Zhang, A.; Savage, P. E., Hydrothermal catalytic processing of pretreated algal oil: A catalyst screening study. *Fuel* **2014,** *120*, 141-149.
35. Watanabe, M.; Iida, T.; Inomata, H., Decomposition of a long chain saturated fatty acid with some additives in hot compressed water. *Energy Conversion and Management* **2006,** *47* (18-19), 3344-3350.

36. Stošić, D.; Bennici, S.; Sirotin, S.; Calais, C.; Couturier, J.-L.; Dubois, J.-L.; Travert, A.; Auroux, A., Glycerol dehydration over calcium phosphate catalysts: Effect of acidic–basic features on catalytic performance. *Applied Catalysis A: General* **2012,** *447-448*, 124-134.
37. Daorattanachai, P.; Khemthong, P.; Viriya-Empikul, N.; Laosiripojana, N.; Faungnawakij, K., Conversion of fructose, glucose, and cellulose to 5-hydroxymethylfurfural by alkaline earth phosphate catalysts in hot compressed water. *Carbohydrate research* **2012,** *363*, 58-61.
38. Matsuura, Y.; Onda, A.; Yanagisawa, K., Selective conversion of lactic acid into acrylic acid over hydroxyapatite catalysts. *Catalysis Communications* **2014,** *48*, 5-10.
39. Zaera, F., Nanostructured materials for applications in heterogeneous catalysis. *Chem Soc Rev* **2013,** *42* (7), 2746-62.

6 Raceway

6.1 Motivation & Background

The fabrication of biocrude or HTL solids that imitated the properties or structure, respectively, of the HTL products from wastewater-cultivated algal studies were unsuccessful from inorganic and biological model compounds reactions (Chapter 5: *Model Compounds*) nor reactions involving auto-flocculated algal solids cultivated in light rack tanks (Chapter 4: *Inorganic Capture*). The final research thrust was a cumulative study across over twenty algal solid samples that were cultivated in bench-scale, raceway ponds. The greatest advantage the larger raceway ponds provided over the previous light rack growth tanks was the ability to cultivate and produce more algal solids. The larger cultivation volume allowed algal solids to be cultivated in growth media and conditions that do not maximize algal biomass productivity, yet it allowed enough algal solids to be harvested to be properly characterized and reacted. For example, algal solids could be harvested during the early stages of growth for both nitrogen- and phosphorus-limited media and the large volume of the raceway allowed there to be enough algal solid biomass for ample testing.

By altering the limiting nutrient in the media and varying the growth stage at which the algal solids were harvested, the main independent variable of the raceway study became the phosphorus (P) compounds within the algal solids. The previous focus was on the calcium and converting calcite to calcium phosphate, for calcite was the primary structure observed in the wastewater-cultivated algal solids and HAp was the primary structure of the resulting HTL solids. However, based upon the water chemistry modeling and research done by our collaborator, the N-limited media of wastewater effluent (N:P = 13.5) would cause calcium phosphates to be more favorable to precipitate during auto-flocculation than calcite.

The precipitation of phosphates was inhibited in prior light rack growth tanks in order to amplify biomass productivity. By harvesting at later growth stages in P-limited media (N:P > 16), algal growth was maximized but left minimal aqueous phosphorus available to precipitate with the algal solids when the pH was increased for auto-flocculation. Thus, despite calcium phosphate being more thermodynamically favorable than calcite to precipitate from the growth media, it was negligible or undetectable in the algal solids due to the marginal concentration of aqueous phosphorus remaining in the light rack algal tanks when auto-flocculation was artificially induced. The phosphorus accumulated by the microalgae is used to synthesize biological compounds such as DNA, ATP, and phospholipids within algal cell. This type of phosphorus was referred to as *bio-P* and was the primary form of phosphorus in previous studies. The alternate form of phosphorus would be *solid-P*, and this form of phosphorus would form via precipitation from the aqueous forms of calcium and phosphorus that remain in the growth media when the pH is artificially increased, and auto-flocculation is induced. Thus, the leading hypothesis was that increasing the amount of solid-P in the algal solids by inducing auto-flocculation at earlier growth stages and in growth media with excess-P, and therefore limited in nitrogen (N-limited; N:P < 16), the algal solids would be more favorable to creating calcium phosphates in the HTL solids.

The original theory behind this bio- vs. solid-P hypothesis was initially proposed by the collaborating graduate student, Sirwan Alimoradi. In addition to attempting to recreate the biocrude properties and HTL solids structure observed by wastewater-cultivated algal solids, the secondary objective for the author was to empirically prove or disprove the hypothesis that a greater proportion of solid-P than bio-P promotes a calcium phosphate in the HTL solids. The final hypothesis of this raceway study was to identify any possible *in-situ*, catalytic changes in biocrude properties from varying HTL solid structures.

6.2 Methods and Experimental Setup

To vary the amount of aqueous phosphorus remaining in the growth media at the time of harvesting and auto-flocculation, our collaborator proposed growing microalgae in nitrogen-limited (N-limited) growth media in addition to the established, P-limited. Furthermore, auto-flocculation and algal solid harvesting would occur at all major growth stages: exponential, transition, and stationary. The 2, 1,200 L raceway ponds allowed for sufficient algal solids for HTL reactions and characterization to be harvested at the lesser algal production growth conditions and stages.

Figure 37 best illustrates the algal growth curve amongst the N-limited and P-limited raceways. Optical density measured by our collaborator best measures algal growth production. For N-limited media the maximum optical density achieved during the stationary phase was 0.4, and it was achieved within 20 days of growth. For P-limited media, approximately three times greater algal production was achieved in this growth media. Furthermore, the final stationary growth stage was achieved within 36 days for P-limited media.

Excess phosphorus that remains in the growth media also varies among the N- and P-limited media and their respective growth stages. Figure 37 also shows the percent of excess phosphorus remaining in the growth media. The excess of phosphorus is then captured through precipitation and auto-flocculation. These precipitated phosphorus solids were referred to as solid-P in the algal solids as opposed to bio-P, which is phosphorus accumulated by the algal cell for molecular, biological compounds such as DNA, ATP, and phospholipids. The theoretical bio-P and solid-P percent was determined by measuring the aqueous phosphorus concentration at the time of harvesting. The amount the phosphorus concentration decreased from the initial concentration

was assumed to be accumulated by the algal biomass and reported as the theoretical bio-P percent. Meanwhile, the remaining aqueous phosphorus measured in the growth media was assumed to completely precipitate from solution when the pH was increased to 11 and auto-flocculation was artificially induced. Thus, the measured aqueous phosphorus concertation remaining in the growth media when auto-flocculation was induced was reported as the theoretical solid-P percent.

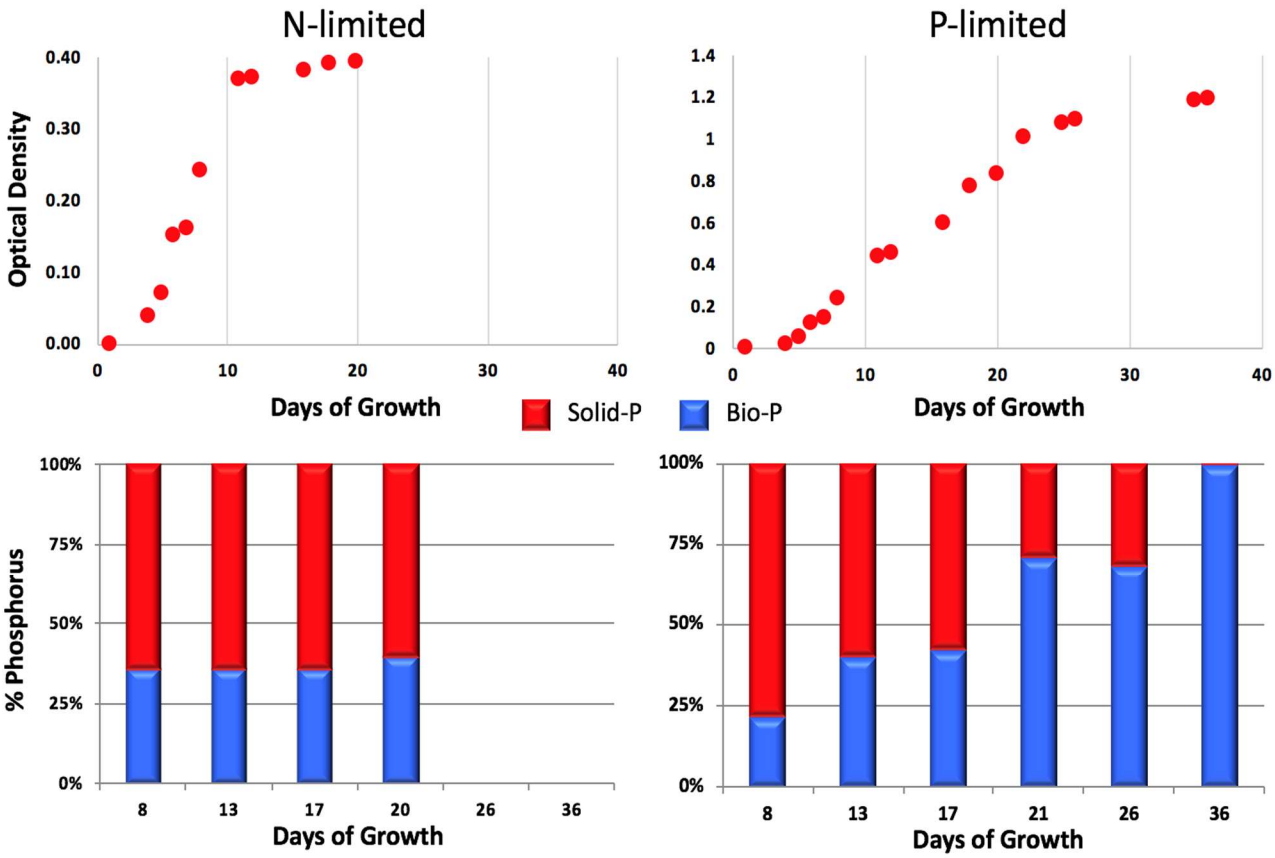

Figure 37: Algal growth curves (top) for the N-limited (left) and P-limited (right) raceway growth media. The proportion of theoretical solid-P (red) and bio-P (blue) for the respective growth medias are also shown on the bottom.

While varying the speciation of phosphorus within the algal solid was paramount for this study, varying the total Ca:P was an additional independent variable controlled for this study. To vary and control the Ca:P molar ratio of the algal solids harvested from the raceways, 50 L of the

microalgae and growth media were removed from the 1,200 L raceway ponds to an external tank where the auto-flocculation occurred. While the proportion of solid-P and bio-P were expected to change within the respective growth media and growth stages, the total P and total Ca was not expected to change from the initial Ca and P concentrations. Thus, the necessary amount of lime, $Ca(OH)_2$, was added to the external tanks to vary and achieve the desired Ca:P molar ratio. The pH was then increased to 11 from the addition of concentrated sodium hydroxide (NaOH). The rise in pH caused algal solids to auto-flocculate within the external tank and settle to the bottom of the tank where they were removed, centrifuged, and freeze-dried.

At each growth stage, 3, 50 L samples were taken from the raceway and auto-flocculated to produce a low, medium, and high algal solid Ca:P molar ratio that was between 1.0-3.0. The various algal solid samples harvested from the two raceway ponds and their respective growth stages are best summarized in Table 13 and Table 14. It should be noted that the transition growth stage of the P-limited media occurred so rapidly that only one algal solid harvesting could occur. The shift in growth stages in the N-limited media, however, was much slower. Thus, an additional growth stage could be harvested at the initial exponential stage. They are distinguished and referred to as early and late exponential growth stages. Lastly, a final algal solid sample was harvested from the P-limited raceway during the stationary-stage where the pH was not artificially raised and therefore auto-flocculation did not occur. The microalgae and growth media that remained in the raceway were simply centrifuged and freeze-dried.

6.3 Collaboration

For this research thrust, the cultivation, auto-flocculation, and harvesting of the raceway algal solids were overseen and executed by our environmental engineering collaborators while the

HTL reactions of these algal solids and the extraction and of the final HTL products were overseen or executed by the author. Algal characterization and analysis were distributed between the author and collaborator. The biomolecular and inorganic content were measured by the collaborator while the proximate, ultimate, FTIR, and XRD analysis were overseen or conducted by the author. The HTL product analyses were also distributed amongst the author and collaborator. The complete biocrude analyses, simulated distillation, GC-MS, and ultimate analysis, were overseen or conducted by the author. Total organic carbon, total nitrogen, and inorganic content using ICP-OES of the ACP were completed by our collaborator in addition to further environmental studies of the HTL ACP. Acid digestion and ICP-OES analysis for the final inorganic content of the HTL solids were also performed by our collaborator. Proximate analysis and XRD of the HTL solids were all conducted or overseen by the author. All subsequent insight and conclusions drawn by the data collected by the author and collaborator are unique to the author unless otherwise stated.

6.4 Results and Discussions

6.4.1 Algal Solid Characterization and Evidence of Amorphous Calcium Phosphate

Table 13 and Table 14 depict the algal characteristics for the algal solids harvest from the N-limited (N:P = 10) and P-limited growth (N:P = 25) media, respectively. The biomolecular content of the algal solids were measured once in duplicate at each growth stage because the growth media's N:P molar ratio and growth stage dictate the biomolecular content the most.[1-2] Thus, the biomolecular content was assumed to be constant across the often, three algal solid samples harvested from the same growth media and growth stage. Despite the variance in growth media and growth stage the biomolecular content of the *Chlorella kessleri*, algal solids consisted

mostly of proteins (28-46 dw%), followed by carbohydrates (10-16 dw%), and lastly lipids (2-18 dw%). The only algal solids that did not have the biomolecular trend of proteins > carbohydrates > lipids were algal solids harvested from P-limited media during the stationary growth stage. In this media and growth stage the lipid and carbohydrate content were 17.9 and 16.3 dw%. The variance for the lipid content, however, was also the greatest at ± 7.0 dw% for the P-limited, stationary algal solids.

The ultimate analysis is complimentary to the biomolecular content of the algal solids. Thus, the variances in the average hydrogen (H) and nitrogen (N) dw% were ± 1.1% or less across the three algal solid samples harvested in the same growth media and the same growth stage. The minimal variation in the average H and N dw% further verifies the assumption that the biomolecular and organic content did not vary across algal solids harvested from the same growth media and at the same growth stage. Larger variations in the average oxygen (O) of ± 1.3-1.5 dw% occurred amongst the three algal solid samples harvested at the exponential stages of both N-limited (Table 13) and P-limited (Table 14). This variation could be due to the inorganic carbon, or carbonate (CO_3), mass that is captured during auto-flocculation. The variance in the average dw% carbon (C) was even greater for the algal solids harvested at the same growth stage and growth media ranged from ± 1.2-3.0 dw% across both raceway ponds. Further analysis of the carbonate weight percent and its role with other inorganic elements and inorganic solid structure is discussed in greater detail later in the chapter.

Overall, the CHN dw% of the algal solids in P-limited media increased at later growth stages while the O dw% decreased. The CHN and O dw% were the highest, however, at the last harvest from P-limited media that was not auto-flocculated. This global increase in CHN and O dw% is due to the decrease in ash dw% from approximately 40-50 dw% ash in auto-flocculated

algal solids to 24 dw% in the algal solids that were not auto-flocculated. Algal solids cultivated in N-limited media followed a similar trend. CHN and O dw% increased in the algal solids at each successive growth stage while the ash dw% decreased. This inverse trend is due to the increasing and accumulating biomass that is also occurring in the raceway at later growth stages. A greater amount of biomass due to continuing algal growth leads to greater dw% of biomolecules and organic compounds and less dw% of inorganics or ash.

Ultimate analysis and biomolecular content essentially provide thoroughness and background information for the later HTL products. The primary algal characteristics of interests for this work are the inorganic elements. The ash dry weight percent of the auto-flocculated algal solids harvested from N-limited media were similar ranging from 41.1 to 48.6 dw%. Similarly, the addition of lime at three increasing amounts resulted in three distinct mg of Ca per kg of algal solids (mg/kg Ca) at the exponential and stationary growth stages. For the exponential stage the mg/kg Ca increases from approximately 115,000 to 181,000 mg/kg Ca. At the stationary phase, the mg/kg Ca also increased from approximately 118,500 to 151,500 mg/kg Ca. The final algal solids harvested from the N-limited media that were not auto-flocculated had less than half the mg/kg Ca (approx. 50,000 mg/kg) than the lowest mg/kg Ca from auto-flocculated algal solids in N-limited media.

Table 13: Ultimate, inorganic, and biomolecular content of the algal solids cultivated from the **N-limited** raceway pond and harvested at three distinct growth stages: exponential (Exp), transition (Trans), and stationary (Stat). Standard deviation depicted in ().

Growth	C	H	N	O	Ash	Ca	P	Mg	Ca:P	Carb.	Protein	Lipid
Stage	*dw%*	*dw%*	*dw%*	*dw%*	*dw%*	*mg/kg*	*mg/kg*	*mg/kg*	*mol*	*dw%*	*dw%*	*dw%*
Exp.	27.0 (0.2)	3.5 (0.2)	3.7 (0.1)	21.1 (0.4)	45.1	114,934	75,767	29,578	**1.17**			
Exp.	27.2 (0.3)	3.5 (0.1)	3.6 (0.04)	22.4 (0.3)	44.4	138,744	64,132	27,213	**1.67**	11.3 (1.1)	31.8 (0.3)	2.5 (1.6)
Exp.	25.1 (0.2)	2.7 (0.2)	3.3 (0.01)	24.1 (0.2)	44.7	180,809	54,710	24,433	**2.55**			
Trans.	27.5 (0.2)	2.5 (0.1)	4.0 (0.1)	20.0 (0.1)	46.9	135,660	80,950	32,929	**1.29**	11.8 (1.0)	31.0 (0.2)	4.2 (0.1)
Stat.	31.0 (0.1)	4.7 (0.2)	4.2 (0.1)	20.5 (0.4)	41.1	118,535	74,977	27,449	**1.22**			
Stat.	27.5 (0.2)	4.2 (0.2)	3.7 (0.2)	21.0 (0.2)	46.0	133,856	67.050	24,463	**1.54**	12.1 (0.1)	28.6 (1.2)	8.7 (0.01)
Stat.	25.8 (0.1)	3.9 (0.3)	3.3 (0.1)	21.4 (0.1)	48.6	151,579	66,181	25,554	**1.77**			
Stat.[a]	43.1 (0.6)	5.7 (0.1)	6.4 (0.2)	22.6 [b]	24.3	50,552	47,587	6,265	**0.82**			

Exponential abrv. Exp.
Transition abrv. Trans.
Stationary abrv. Stat.
[a] Algal solids were centrifuged, not auto-flocculated
[b] Calculated by difference

Table 14: Ultimate, inorganic, and biomolecular content of the algal solids cultivated from the **P-limited** raceway pond and harvested at four distinct growth stages: early and late exponential, transition, and stationary. Standard deviation depicted in ().

Growth	C	H	N	O	Ash	Ca	P	Mg	Ca:P	Carb.	Protein	Lipid
Stage	*dw%*	*dw%*	*dw%*	*dw%*	*dw%*	*mg/kg*	*mg/kg*	*mg/kg*	*mol*	*dw%*	*dw%*	*dw%*
Early Exp.	29.2 (0.5)	3.2 (0.2)	5.1 (0.1)	19.5 (0.3)	40.5	104,142	69,893	27,204	**1.15**			
Early Exp.	29.0 (0.5)	3.3 (0.2)	4.6 (0.1)	21.0 (0.1)	41.0	126,039	56,177	23,589	**1.74**	10.4 (0.2)	36.8 (1.6)	4.1 (0.2)
Early Exp.	25.1 (1.6)	2.1 (0.2)	3.7 (0.4)	22.2 (1.2)	43.1	152,037	46,921	21,006	**2.51**			
Late Exp.	36.8 (0.8)	5.5 (0.1)	5.9 (0.2)	22.9 (0.2)	31.2	69,916	52,342	15,622	**1.03**			
Late Exp.	36.9 (0.4)	5.0 (0.3)	5.9 (0.1)	23.6 (0.1)	30.4	87,935	46,248	15,175	**1.47**	13.6 (0.01	43.8 (2.0)	15.2 (2.1)
Late Exp.	31.7 (0.6)	3.3 (0.2)	4.7 (0.2)	25.6 (0.2)	26.6	125,584	37,025	17,437	**2.62**			
Trans.	39.9 (0.3)	5.4 (0.2)	6.2 (0.03)	24.3 (0.4	26.0	69,463	40,629	9,770	**1.32**			
Trans	37.6 (1.4)	4.8 (0.2)	5.7 (0.2)	25.7 (0.1)	28.9	82,594	32,148	11,127	**1.99**	16.5 (2.4)	45.5 (0.9)	10.5
Trans.	37.9 (0.4)	4.9 (0.1)	5.8 (0.1)	25.8 (0.3)	27.2	93,338	31,544	7,119	**2.29**			
Stat.	47.7 (0.1)	6.5 (0.3)	7.7 (0.1)	24.5 (0.2)	14.5	34,118	23,511	6,380	**1.12**			
Stat.	42.7 (0.4)	5.6 (0.2)	6.6 (0.1)	25.8 (0.1)	19.6	71,399	19,745	8,018	**2.80**	16.3 (0.7	43.8 (1.7)	17.9 (7.0)
Stat.	42.5 (0.9)	5.4 (0.3)	6.5 (0.2)	26.0 (0.5)	19.5	7,155	20,475	6,449	**2.91**			

The mg/kg P in the algal solids, meanwhile, tended to trend indirectly with the addition of lime at each individual growth stage. A slight decrease from approximately 76,000 to 55,000 mg/kg P in the exponential phase and from approximately 75,000 to 66,000 mg/kg P in the stationary phase of N-limited growth media. This trend is to be expected given the total P in the growth media was held constant during growth and only Ca was added as lime during harvesting. The overall total algal solid mass was increasing from the addition of lime while the initial P content in the growth media was held constant. Thus, the mg/kg P would decrease from the addition of more Ca or lime to the growth media. Algal solids that were not auto-flocculated had the least amount of mg/kg P compared to the auto-flocculated algal solids grown in N-limited media at 47,500 mg/kg P.

Algal solids from the P-limited media had identical trends in the mg/kg Ca and P as the algal solids harvested from the N-limited media. As the mg/kg Ca increased within each of the four growth stage from P-limited media, the mg/kg P decreased. Dissimilar to the N-limited media, however, the overall mg/kg Ca and P within the algal solids decreased with each successive growth stage. The highest mg/kg of Ca and P occurred in the early exponential stage of the P-limited media with approximately 152,000 mg/kg Ca and 70,000 mg/kg P. Meanwhile, the lowest Ca and P content occurred in the later stationary stage with approximately 7,000 mg/kg Ca and 20,000 mg/kg P. The justification and cause for the decrease in mg/kg Ca and P with later growth stages of P-limited media is identical to the similarly observed decrease in ash dw%. As previously noted in Chapter 2: *Literature Review*, P-limited media is preferred for biomass productivity, thus a greater amount of organic, algal biomass was produced in the P-limited raceway than the N-limited raceway. Algal biomass accumulates during growth, and with the exception to the small amount of lime added to vary the Ca:P molar ratio, the inorganics remained constant relative to the

increasing algal biomass, which causes a decrease in ash dw% and inorganic mg/kg at later growth stages. The differentiation between organic and inorganic solids between the N-limited and P-limited raceways is further explored with quantification and classification of bio-P, solid-P, and inorganic carbon (CO_3) within the algal solids.

Although prior TGA methods for measuring carbonate in algal solids did not agree with actual or theoretical weight percentage, their trends across several algal solid samples were similar. Furthermore, previous inorganic and biological model compound studies showed a large majority ($\geq$ 85%) of the carbonate was present during the pyrolysis stage of the proximate analysis. Thus, the carbonate measured during pyrolysis from the TGA proximate analysis was the assumed carbonate mass for the algal solids harvested from the raceways and reported in Table 15 and Table 16. It is also known from prior XRD of auto-flocculated solids that the form of carbonate within the algal solids is calcite ($CaCO_3$). Thus, stoichiometry can provide the mass of calcium associated with the measured carbonate mass (% Ca as $CaCO_3$). The mass of calcium calculated to be $CaCO_3$ was, however, only a fraction of the total calcium in the algal solids that was measured by acid digestion and ICP-OES analysis. Water chemistry modeling conducted by our collaborator reported that TCP (pK_{sp} = 26.0) was more than three times more thermodynamically favorable to precipitate from the growth media than calcite (pK_{sp} = 8.5) given the pH and various elemental concentrations. Thus, the remaining calcium mass that was not measured and calculated to be calcite was presumed to be an amorphous form of calcium phosphate (% Ca as $Ca_x(PO_4)_y$).

The greatest evidence opposing the hypothesis that the aqueous phosphorus remaining in the growth media was precipitating as an amorphous form of calcium phosphate during auto-flocculation was very thermodynamically unstable. Crystalline, calcium phosphate structures, such as HAp and TCP, that are detectable by XRD are much more thermodynamically favorable

to precipitate. When open to the atmosphere, solid, amorphous calcium phosphate will immediately hydrate to HAp from the moisture in the air.[3-4] Thus, precipitation, the most common method for synthesizing calcium phosphate solids, is not practical unless done in organic, hydrophobic solutions. Although difficult to synthesize artificially, amorphous calcium phosphate is prevalent in nature and are observed both in teeth and the exoskeleton of marine invertebrates. It has, therefore, become well-known that biological components, specifically pyrophosphates such as ATP, aid in the stability of amorphous calcium phosphate.[3-6] In addition, carbonate and magnesium are also large ionic stabilizer for amorphous calcium phosphate.[3, 5, 7] Pyrophosphates, carbonate, and magnesium are all in abundance in auto-flocculated algal solids; therefore, it is more evident and likely that stable amorphous calcium phosphate could be present in the auto-flocculated algal solids. To test this hypothesis, the ash after proximate analysis from the TGA was collected and analyzed by XRD.

The results of these TGA-calculated carbonate weight percentages and the resulting percent of calcium as calcite or as calcium phosphate for algal solids harvested from N-limited media are shown in Table 13. In addition, the algal solid structure as observed by XRD for the N-limited algal solids are also summarized. The solid structure of the algal solids harvested from the N-limited media were either amorphous or calcite. Amorphous, non-crystalline algal solids were observed when the calcium content (mg/kg) for the algal solids was the lowest for the respective growth stage in N-limited media. These amorphous algal solids also had the least carbonate wt% according to TGA at only 1-2 dw%. The percent of the total calcium in the algal solids that would be associated with the TGA-measured carbonate was therefore also minimal (< 10%). The percent of the remaining calcium that is assumed to be calcium phosphate based off water chemistry modeling was therefore maximized (> 90%). For this assumption to be valid, an abundance of

aqueous phosphorus must remain in the growth media when these amorphous algal solids were harvested in order for more solid-P to precipitate from solution. According to Figure 37, this correlation holds true. N-limited media had more than 60% of the initial and total phosphorus remaining in solution throughout every growth stage.

To provide further empirical evidence that amorphous forms of calcium phosphate existed within the algal solids, XRD analysis was performed on the ash collected after proximate analysis on the TGA. It can be seen from Table 15 that the primary structure observed in the XRD pattern of the N-limited, algal solid, TGA-ash was TCP for a majority of the algal solids harvested from N-limited media. Algal solids that were not auto-flocculated were one of two exceptions where lime was the primary structure observed in the TGA-ash as opposed to TCP. The second exception were the algal solids harvested during the exponential growth stage with the highest calcium content (Table 13) that also had lime as the primary XRD structure in the TGA-ash. These high calcium, exponential algal solids, however, also had the highest dw% carbonate of all the other algal solids harvested from N-limited media. Thus, the calculated amount of calcium assumed to be calcium phosphate was also the least at 51.4% Ca. Overall, the observance of lime over TCP in the TGA-ash of these algal solids agree with calculated percent of calcium assumed to be calcium phosphate.

The assumption that the remaining calcium within the algal solids that was not determined to be associated with calcite was indeed calcium phosphate is further verified by the XRD patterns of their respective TGA-ash. For all the auto-flocculated algal solids that had their percent of total calcium to be 70% or more as calcium phosphate also had TCP or HAp to be the primary structure in their respective TGA-ash XRD pattern. This included algal solids that originally appeared as amorphous or as calcite in their original XRD analysis. Thus, the agreeance between the observed

XRD patterns from the TGA-ash of the N-limited algal solids and the calculated amount of calcium as calcium phosphate empirically proves the original two hypotheses. The first hypothesis was that the remaining, aqueous phosphorus would precipitate as amorphous calcium phosphate. The second was that using the dw% of carbonate measured during pyrolysis stage or proximate analysis, one can estimate the proportion of calcium as calcite and calcium phosphate within auto-flocculated algal solids.

Algal solids harvested from the P-limited media further verified the agreement between the calculated percent of calcium as calcium phosphate and the XRD pattern of the algal solid TGA-ash. Shown in Table 16, it can be seen that algal solids harvested from P-limited media had a greater amount of carbonate (dw% CO_3) in the algal solids as the calcium content of the algal solids increased (Table 13). The direct relationship between calcium content and carbonate dw% is shared by both P-limited and N-limited media. Unlike N-limited media, however, the theoretical amount of solid-P decreases as algal growth progresses in P-limited media (Figure 37). Thus, a greater variance in the calcium as calcite or calcium phosphate occurred between the different growth stages. The percent of calcium as calcium of phosphate, however, followed the same trend as the theoretical amount of solid-P for the P-limited algal solids. The amount of solid-P decreased as algal growth progress in P-limited media. Likewise, the calculated percent of calcium as calcium phosphate deceases from 52-74% in the early exponential phase to 11-28% in the stationary phase. The continued direct relationship between the theoretical amount of solid-P and the percent of calcium as calcium phosphate further verifies the method for using the TGA-measured carbonate weight percent to empirically estimate the proportion of calcite and calcium phosphate within an algal solid sample.

The TGA-ash structure observed by XRD agreed with the calculated percent of calcium as calcium phosphate for algal solids harvested at the early and late exponential stage as well as the transition stage for P-limited algal solids. For example, in the early exponential phase a 52-74% of calcium was calculated to be calcium phosphate. The primary XRD patterns for the TGA-ash of these algal solids were TCP and HAp. At the late exponential stage, the percent of calcium as calcium phosphate had a similar range between 50-69%. The primary structure in the TGA-ash of

Table 15: The TGA-measured dw% of CO_3 in the algal solids cultivated in **N-limited** media. The percent of total calcium associated with said CO_3 as $CaCO_3$ was determined stoichiometrically and the balance as some form of calcium phosphate ($Ca_x(PO_4)_y$). The XRD structure of the algal solid and the primary and secondary structure from the algal solid, TGA-ash are also represented.

Growth	CO_3	$CaCO_3$	$Ca_x(PO_4)_y$	Algal Solid XRD	Algal Solid Ash XRD	
Stage	*dw%*	*% Ca*	*% Ca*	*Pattern*	*Primary*	*Secondary*
Exp.	1.8	8.7	91.3	Amorph.	TCP	Lime
Exp.	7.2	27.6	72.4	Calcite	TCP	Lime
Exp.	16.8	48.6	51.4	Calcite	Lime	TCP
Trans.	1.8	7.2	92.8	Amorph	TCP	u.i.
Stat.	1.1	6.0	94.0	Amorph.	TCP	-
Stat.	4.5	18.8	81.2	Calcite	TCP	-
Stat.	4.5	15.8	84.2	Calcite	HAp	-
Stat.*	1.1	11.2	88.8	Calcite	Lime	-

*Algal solids were centrifuged, not auto-flocculated
Unidentifiable abrv. u.i.

NOTE: The N-limited algal solids listed in Table 15 are in the same order as Table 13 with calcium content of the algal solids increasing in each growth stage as one descends the table.

the P-limited, late exponential stage algal solids were TCP and lime. The observance of lime as the primary XRD structure and TCP as the secondary structure for the TGA-ash occurred in the algal solids where the calculated percent of calcium as calcium phosphate was the lowest for the late exponential stage at 50.5%. The nearly equal distribution of calcium as calcite and calcium phosphate that was calculated by the CO_3 dw% determined by TGA again agrees with qualitative XRD results that show a combination of lime and TCP in the algal solid ash.

The unison of the calculated amount calcium phosphate and the observed primary structure from the XRD of the algal solids' TGA-ash continues into the transition phase. Algal solids that were calculated to have 61.2% of its total calcium as calcium phosphate had TCP as its primary and sole XRD pattern in its TGA-ash. At 15% calcium as calcium phosphate in the algal solid the primary and sole structure was lime in the TGA-ash. Finally, the third algal solid sample harvested during the transition phase had 28.9% calcium as calcium phosphate, and the TGA-ash of these algal solids appeared primarily as lime with a secondary XRD pattern of TCP.

The final growth stage, stationary, for P-limited algal solids showed the greatest deviation between the calculated amount of calcium as calcium phosphate and the primary and secondary structures of their TGA-ash. For example, algal solids with the lowest and highest calcium content were calculated to have 28 and 20% of its total calcium as calcium phosphate. The primary structure of the TGA-ash for both these algal solids, however, was TCP. The algal solids with the median calcium content did show agreeance between the calculated amount of calcium as calcium phosphate of only 10.6% and a primary lime solid structure in its TGA-ash. During the final, stationary phase of P-limited media, algal biomass production is at its maximum while the theoretical amount of solid-P is minimal. The abundance of organic biomass and nominal amount

phosphorus available for precipitation can cause the discrepancy between the calculated amount of calcium phosphate and the observed primary structure in the algal solids' TGA-ash.

Table 16: The TGA-measured dw% of CO_3 in the algal solids cultivated in **P-limited** media. The percent of total calcium associated with said CO_3 as $CaCO_3$ was determined stoichiometrically and the balance as some form of calcium phosphate ($Ca_x(PO_4)_y$). The XRD structure of the algal solids and the primary and secondary structure from the algal solid, TGA-ash are also represented.

Growth	CO_3	$CaCO_3$	$Ca_x(PO_4)_y$	Algal Solid XRD	Algal Solid Ash XRD	
Stage	*dw%*	*% Ca*	*% Ca*	*Pattern*	*Primary*	*Secondary*
Early Exp.	4.9	26.1	73.9	Amorph.	TCP	-
Early Exp.	8.3	34.9	65.1	Calcite	TCP	-
Early Exp.	14.0	47.7	52.3	Calcite	HAp	Lime
Late Exp.	3.8	30.8	69.2	Amorph.	TCP	-
Late Exp.	6.7	40.7	59.3	Calcite	TCP	-
Late Exp.	12.2	49.5	50.5	Calcite	Lime	TCP
Trans.	5.2	38.8	61.2	Calcite	TCP	-
Trans	13.7	85.0	15.0	Calcite	Lime	-
Trans.	13.1	71.0	28.9	Calcite	Lime	TCP
Stat.	4.8	72.0	28.0	Calcite	TCP	Lime
Stat.	12.7	89.4	10.6	Calcite	Lime	TCP
Stat.	11.7	80.0	20.0	Calcite	TCP	Lime

NOTE: The **P-limited** algal solids listed in Table 16 are in the same order as Table 14 with calcium content of the algal solids increasing in each growth stage as one descends the table.

The observance of TCP and HAp in the TGA-ash of the raceway-cultivated algal solids confirms the hypothesis that the inorganic structure within the algal solids is a combination of calcite and amorphous calcium phosphate. Roberts et al. had also viewed TCP as the primary structure from the ash of algal solids cultivated in wastewater that was also N-limited media (N:P = 13.5).[8] It was also shown that the thermal treatment of HAp up to 700-900°C caused the solid to dehydrate to HAp.[8] Thus, after proximate analysis of the algal solids that achieves 850°C both during pyrolysis and combustion, one would expect the amorphous calcium phosphate within the algal solids to appear as TCP in the algal solid TGA-ash. The dehydration of HAp to TCP, however, is reversible, and TCP can be rehydrated to HAp.[9] Due to mechanical issues with the XRD the raceway-cultivated algal solid TGA-ash were analyzed months after they had been ashed. Ample time in an ambient, humid atmosphere would cause the TCP from the algal solid TGA-ash to rehydrate to HAp. Thus, the appearance HAp within the TGA-ash from P-limited, early exponential algal solids would be expected.

Lime was an additional structure observed in the TGA-ash from raceway-cultivated algal solids. However, Roberts et al. observed calcium oxide as a secondary structure to TCP from the ash of wastewater-cultivated algal solids.[8] From equation 13, it is well-understood that thermal treatment of calcium carbonate above 600°C results in the emission of CO_2 gas and a calcium oxide solid. Similar to TCP, however, calcium oxide has the potential to rehydrate as lime.[10] Thus, the extended period of time the TGA-ash samples from the raceway-cultivated algal solids remained in at ambient, humid conditions as the XRD was being repaired would cause the hydration of calcium oxide to lime.

6.4.2 Amorphous Calcium Phosphate to HTL Solids

Although only three unique solid structures, calcite, lime, and amorphous, were observed in the algal solids with varying bio- and solid-P proportions, a variety of calcium phosphate and calcite structures were observed in the HTL solids. The primary and secondary structures observed by XRD for these HTL are summarized in Table 17. In addition to the observed XRD patterns, the percent of calcium associated with calcium phosphate, TCP or HAp, is also reported in Table. The percent of calcium in the HTL solids was calculated based off the total calcium measured in the HTL solids and the weight percent of carbonate measured by TGA identical to how the percent calcium was calculated in the algal solids.

The percent of calcium as calcium phosphate that was calculated for the HTL solids agreed with a majority of the primary structures observed by XRD. Algal solids harvested from the N-limited media created HTL solids that were primarily calcium phosphate, either HAp or TCP. In addition, the percent of calcium that was calculated and assumed to be associated with calcium phosphate was 87% or higher in these HTL solids whose primary structure was calcium phosphate. Thus, confirming the assumption that the calcium not associated with carbonate as calcite was likely calcium phosphate.

The exception to this agreement between HTL solid structure and percent of calcium as calcium phosphate were HTL solids produced by algal solids that were harvested in the exponential phase of the N-limited media that also had the highest calcium content. Only 53.6% of the total calcium in the HTL solids were determined to be compounded as calcium phosphate, yet the primary structure is reported as HAp. The XRD pattern of these HTL solids shown in Figure 38, however, shows equal representation between the primary calcite and HAp peaks.

Table 17: The primary and secondary XRD structures for the resulting HTL solids, respective to the algal solids shown in Table 15 and Table 16. To compliment the XRD results, the calculated percent of calcium as calcium phosphate also reported.

N-LIMITED				P-LIMITED			
Growth	**$Ca_x(PO_4)_y$**	**XRD**		**Growth**	**$Ca_x(PO_4)_y$**	**XRD**	
Stage	*% Ca*	*Primary*	*Secondary*	*Stage*	*wt% Ca*	*Primary*	*Secondary*
Exp.	94.7	HAp	-	**Early Exp.**	78.1	TCP	-
Exp.	91.4	HAp	-	**Early Exp.**	90.0	HAp	-
Exp.	53.6	HAp	Calcite	**Early Exp.**	68.7	Calcite	HAp
Trans.	90.0	HAp	-	**Late Exp.**	95.7	TCP	-
Stat.	91.9	TCP	-	**Late Exp.**	90.2	TCP	Calcite
Stat.	92.2	TCP	Calcite	**Late Exp.**	32.0	Calcite	HAp
Stat.	87.4	HAp	-	**Trans.**	92.9	TCP	-
Stat.*	90.4	TCP	-	**Trans**	56.2	Calcite	TCP
				Trans.	43.8	Calcite	TCP
				Stat.	93.6	TCP	-
				Stat.	19.9	Calcite	TCP
				Stat.	25.7	Calcite	TCP

* Algal solids were centrifuged, not auto-flocculated

Thus, nearly 50/50 proportion of calcium phosphate and calcite, as determined from the TGA-measured carbonate of the HTL solids again appears accurate.

The HTL solids produced from algal solids harvested from P-limited media had a greater variety in both structure and percent of calcium as calcium phosphate overall. At the early and late exponential phase, a greater observance of calcium phosphate structures and calcium as calcium phosphate occurred at the lowest and median algal solid calcium content. During these same growth stages and at the highest calcium content for each stage, calcite became the primary structure. In addition, the early and late exponential algal solids that had the highest mg/kg of calcium in P-limited media produced HTL solids with a minimal 68.7 and 32% calcium as calcium

phosphate, respectively. Meanwhile, the percent of calcium as calcium phosphate in the HTL solids from the early and late exponential algal solids with the median and lowest mg/kg of were near 80% or at and above 90%.

Algal solids harvested during the later growth stages, transition and stationary, of P-limited media had the largest range of calcium as calcium phosphate from 19.9 to 93.6%. Similar to the previous, earlier growth stages, the algal solids from the later growth stages with the lowest

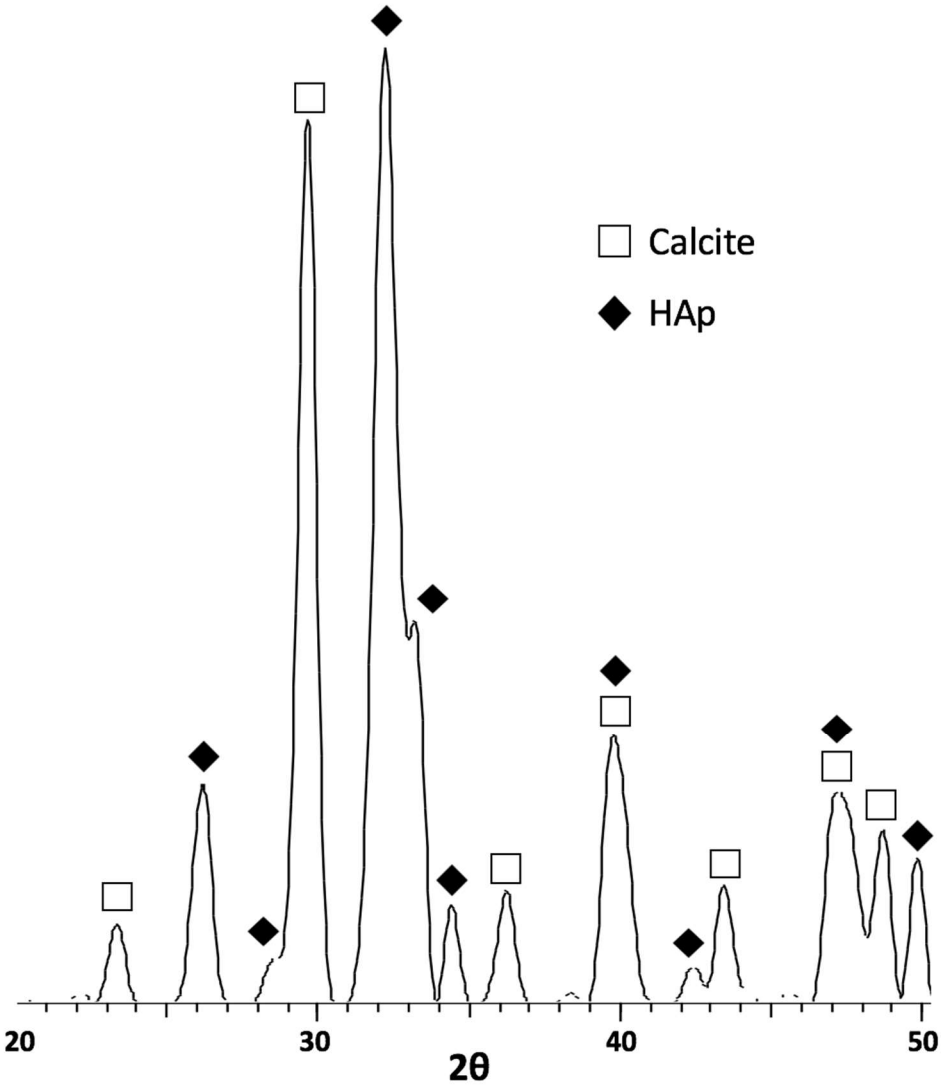

Figure 38: XRD pattern of the HTL solids produced from algal solids harvested during the exponential phase in N-limited media and had the highest calcium content compared to the algal solids harvested in identical media and growth stage.

calcium content created HTL solids with the highest percent of calcium as calcium phosphate both above 90%. The primary structure for these HTL solids produced from algal solids with a lower calcium content and later growth stage in P-limited media were also both TCP. It was at the median and highest, algal solid, calcium concentrations that the amount of calcium as calcium phosphate in the HTL solids were minimized to 43.8% and lower. The exception was the HTL solids from the transition-stage algal solids with median calcium content that had 77.9% calcium as calcium phosphate. Despite the high percentage of calculated calcium as calcium phosphate, the primary structure for these HTL solids remained calcite. The primary structure for the HTL solids was also calcite for the remainder of the median and high calcium content algal solids that were harvested during the transition and stationary stages from P-limited media.

The previous tables have demonstrated the correlation and agreement between the calculate percent of calcium as calcium phosphate and the primary, inorganic structure of the algal or HTL solids as observed by XRD. Thus, Figure 39 compares the initial percent of calcium as calcium phosphate in the algal solids to the later percent of calcium as calcium phosphate in the final HTL solids. It can be seen from Figure 39 that algal solids that had a majority of calcium as calcium phosphate initially ($\geq$ 60%) produced HTL solids that were also primarily calcium phosphate ($\geq$ 74%). The sole outlier to this trend occurs with algal solids harvested during the stationary stage of P-limited media. The percent calcium as calcium phosphate in these algal solids was 28.0% while the HTL solids had 93.6% of its calcium as calcium phosphate.

The presumed cause for this outlier is associated with the biomass to inorganic solids ratio that is best characterized by the carbon to calcium molar ratio (C:Ca). Recall from Chapter 5: *Model Compounds* that the rate determining step for the hydrothermal synthesis of calcium phosphate from calcite was the dissociation of calcite. Furthermore, additional CO_2 created by the

algal biomass during the reaction, shifted the equilibrium in favor $CaCO_3$ dissociation. Thus, a greater amount of biomass to calcite, or C:Ca molar, ratio would promote greater $CaCO_3$ dissociation. The C:Ca for the P-limited, stationary algal solids harvested for this raceway study and as seen as an outlier in Figure 39 was 46.7. The C:Ca of the additional P-limited algal solids that had a similar percent of calcium as calcium phosphate (15.0 and 28.9%) but produced HTL solids with minimal amount calcium as calcium phosphate (56.2 and 43.8% respectively) were only 15.2 and 13.6 respectively. Similarly, the C:Ca molar ratio of prior model compound HTL reaction were merely 5.3-6.7. Thus, the outlier observed in Figure 39 leads to the potential C:Ca molar ratio required to hydrothermal convert algal solids that are initially, primarily calcite to calcium a phosphate.

Figure 39 also depicts that a majority of the algal solids that resulted in HTL solids that were primarily calcium phosphate were harvested from N-limited media. In addition, further analysis of the algal solids harvested from P-limited media that produced similar, calcium phosphate HTL solids also appeared to be harvested in the early and late exponential and the transition growth stage. The common precursor these algal solids also share is the high probability for theoretical solid-P to be captured from the growth media during auto-flocculation of the algal solid. In summary, the aqueous phosphorus that remains in the growth media, either from N-limited media or the early growth stages of P-limited media, results in amorphous calcium phosphate to be captured within the algal solid during auto-flocculation. The amorphous form of calcium phosphate in the algal solids are undetectable by XRD. However, after conventional HTL, the calcium phosphate structure becomes apparent.

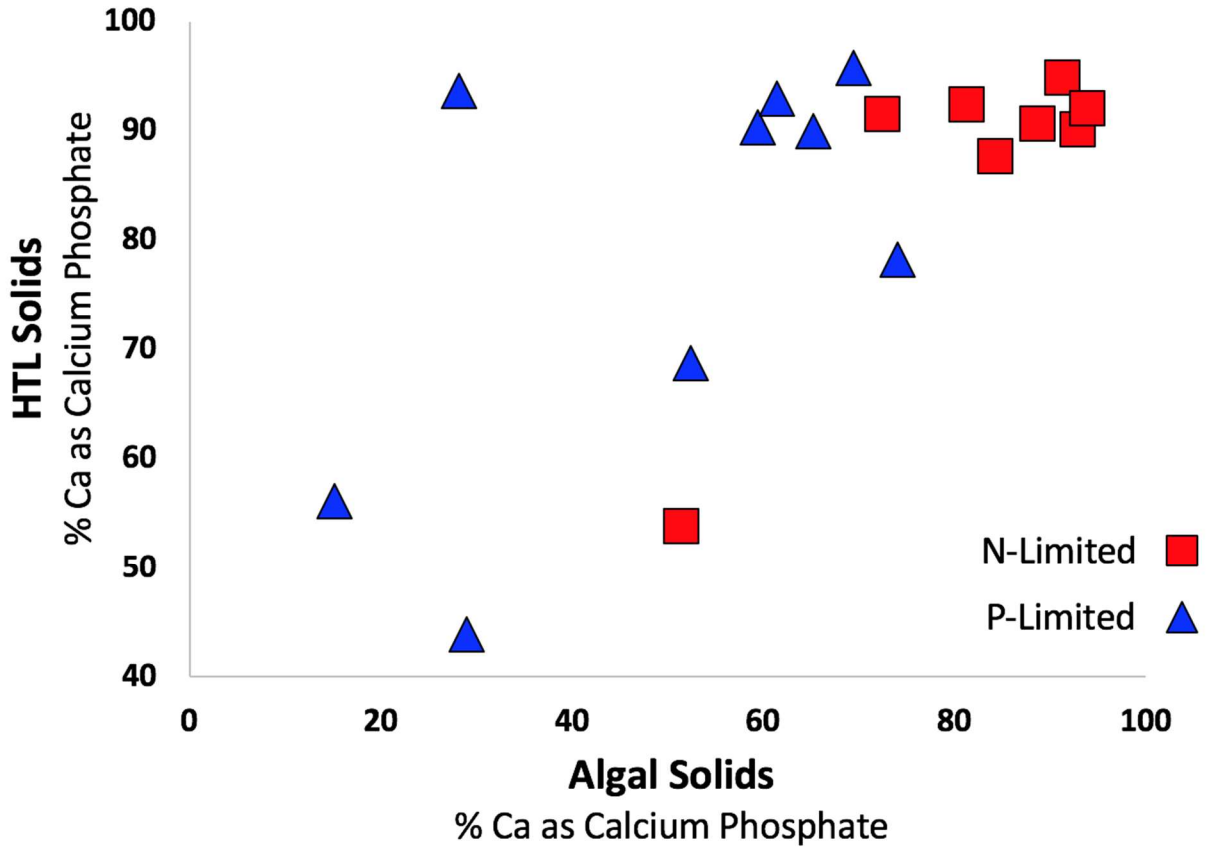

Figure 39: A comparison of the calculated percent of calcium as calcium phosphate between the initial algal solids that were cultivated in two types of media, N- and P-limited, and their final HTL solids.

The conclusion that the observance of uniform calcium phosphates in the HTL solids is caused by the precipitation of aqueous phosphorus that remains in the growth media from the rise in pH during auto-flocculation can be applied to previous wastewater-cultivated algal solids. Similar to the several of the auto-flocculated algal solids cultivated in the raceway, wastewater-cultivated algal solids showed calcite as a primary crystalline structure. The resulting HTL solids from these calcite algal solids, however, were uniform HAp or TCP. XRD of the ash for both the wastewater- and raceway-cultivated algal solids revealed the presence of solid calcium phosphate that was formerly amorphous in the original algal solid. In addition, calculating the percent of calcium as calcium phosphate from the TGA-measured carbonate weight percentage aided in

confirming the presence of amorphous calcium phosphate in wastewater- and raceway-cultivated algal solids. The uniform calcium phosphate HTL solids that were formed from these amorphous calcium phosphate algal solids varied between HAp and TCP. The growth media and algal solids explain why uniform calcium phosphates were observed in the HTL solids. However, the cause for the differing HAp or TCP structure seen in these HTL solids were uncertain.

To investigate potential causes of HAp or TCP structure in the HTL solids previous, key independent variables were investigated. The algal and HTL solids depicted in Figure 40 represent the algal and HTL solids that were determined to initially be a primarily amorphous calcium phosphate in the algal solids followed by having primarily calcium phosphate in the HTL solids. In other words, Figure 40 further investigates the calcium phosphate structure of the algal and HTL solids depicted in the upper-righthand corner of Figure 39.

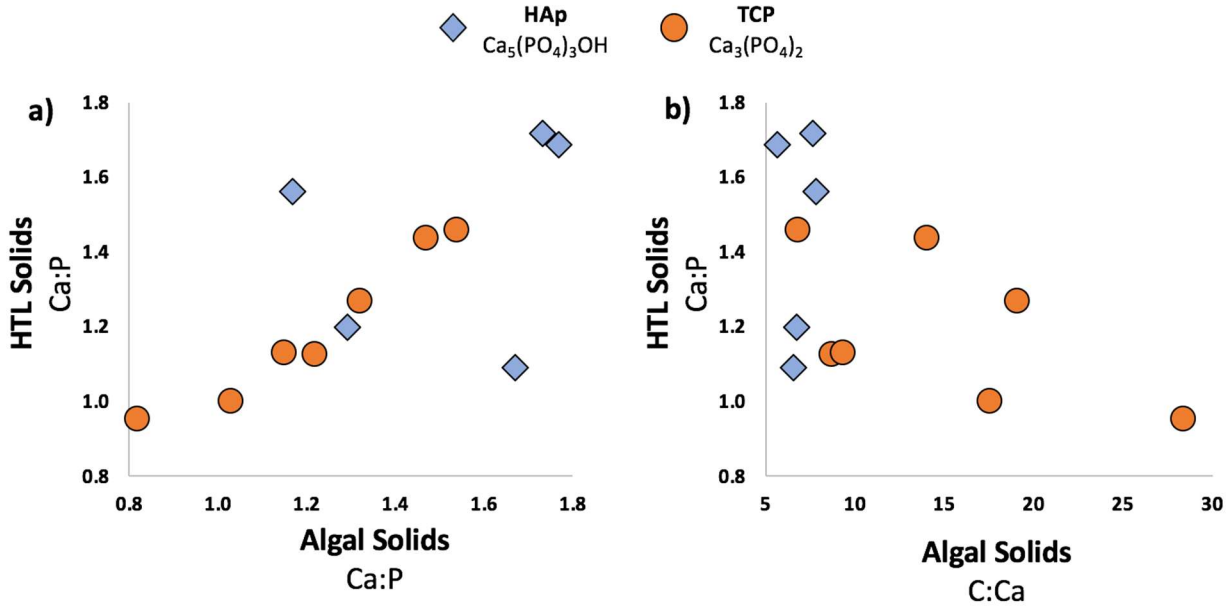

Figure 40: The calcium phosphate structure, HAp or TCP, of the HTL solids depending on the Ca:P or C:Ca molar ratio of the initial algal solids.

The first independent variable was the Ca:P molar ratio of the algal solids compared to the HTL solids and the resulting XRD structure of the HTL solids shown in Figure 40a. For algal

solids that produced HTL solids that were TCP, a linear trend appears indicating the Ca:P molar ratio of the algal solids was similar to that of the final HTL solids. Meanwhile, algal solids that formed HAp HTL solids appeared more scattered when comparing their respective Ca:P molar ratios. The scattering of HAp structure in Figure 40a is indicative of the common, ion-substitution that can occur within the HAp surface.[11-13] Thus, a wide range of Ca:P molar ratios may appear in HAp HTL solids. The phenomenon of ion-substitution within the HAp crystal is further observed by the maximum Ca:P molar ratio achieved by HAp and TCP HTL solids. For TCP HTL solids the maximum Ca:P molar ratio was approximately 1.5. That is the stoichiometric ratio of TCP. At Ca:P molar ratios that were greater than 1.5, only HAp HTL solids were observed.

The Ca:P molar ratio of the algal and HTL solids provided some clarity to the resulting calcium phosphate structure in the HTL solids. The second independent variable investigated was the ratio of biomass to inorganics, which is best summarized by the C:Ca molar ratio of the algal solids shown in Figure 40b. HTL solids that had a uniform TCP structure had a wide-range of C:Ca molar ratios from 6.8-28.4. Meanwhile, the C:Ca molar ratio of the algal solids that resulted in HTL solids with a uniform HAp structure were all below 8.0 and averaged 6.9 ± 0.9. It is hypothesized that the C:Ca molar ratio impacts the pH of the HTL reaction. The reaction pH then impacts the calcium phosphate structure in the HTL solids. It has been previously mentioned in terms of enhanced calcite dissociation that additional biomass, or higher C:Ca molar ratio, causes a greater amount of CO_2 gas to be produced during the reaction. An increase in the partial pressure of CO_2 during the reaction can also lower the pH from the added CO_2 reacting with the water to create carbonic acid (H_2CO_3). Thus, causing the reaction media to become more acidic. The appearance of a HAp structure in the HTL solids from algal solids with a C:Ca molar ratio less

than 8 therefore implies a more basic reaction media to be favorable for the synthesis of HAp HTL solids.

The optimum pH for the hydrothermal synthesis of HAp is often debated in the literature.[14-17] Goto et al. best reviewed the effect of pH on the calcium phosphate structure, which is described as a dissociation of phosphate (PO_4^{3-}) from TCP and the substitution of hydroxide (OH^-) in its place.[16] The cause for discrepancy regarding the optimum pH is that under hydrothermal conditions this mechanism can appear favorable in both acidic or basic conditions. Under acidic conditions, H^+ ions aid in removing phosphate ions from the crystal creating vacancies for hydroxide ions from the subcritical conditions to fill. Under basic conditions, an abundance of OH^- ions assist in the potential mass transfer limitations of these hydroxide ions filling vacancies on the solid surface.

The pH of reaction media during HTL of algae is difficult to measure given the high temperature and pressures. It is often difficult for models to predict the pH as well given the thermodynamically instability of subcritical water. The ion product (K_w), which is the ratio of the concentration of H^+ ions to OH^- ions, i.e. $[H^+] / [OH^-]$, however, has been reported to increase from 10^{-14} to 10^{-11} under subcritical conditions indicating a more acidic media. This agrees with the observations of Goto et al. who observed the pH to decrease to approximately 5 in the ACP after the hydrothermal synthesis of HAp from TCP.[16] However, Biller et al. observed a more alkaline pH of 9 in the ACP after HTL of microalgae.[18] They attributed the higher pH to the greater presence of ammonium in the ACP from HTL of microalgae.[18] Ammonia forms due to the degradation of algal proteins during HTL.[19] The pH and ammonium concentration of the ACP from the wastewater- or raceway-cultivated algal solids were not measures following the HTL reactions, for at the time pH was not considered a critical variable for the morphology and structure

of the HTL solids. Further investigation into the properties of the ACP following the HTL of auto-flocculated algal solids is therefore recommended.

6.4.3 HTL Solids and Biocrude Yield

To the best of the author's knowledge this was the first representation of HTL solids and biocrude yield properties based on the growth media and stage that algal solids were cultivated. The scope of prior work on the HTL of algae initiated with a pre-cultivated algal biomass and its biomolecular content. Thus, similar to previous Tables and Figures the HTL solids and biocrude yield along with the biocrude properties are shown in respect to the growth media and growth stage the algal solids were cultivated in. Figure 41 depicts the biocrude and HTL solids yield from an ash free dry weight (afdw%) and dry weight basis (dw%), respectively, for the algal solids grown and harvested from N- and P-limited media, top and bottom figures respectively. Similar to previous tables, the results for each respective growth stage are shown in increasing Ca content within the algal solids.

As expected, as majority of HTL solids yield increased with increasing Ca content in the algal solids at each respective growth stage. The two exceptions to this trend occurred during the early exponential and transition growth stages of P-limited media. The maximum HTL solids yield was 55.6 dw% and came from auto-flocculated algal solids harvested at the stationary stage of N-limited media. The auto-flocculated algal solids that had the lowest HTL solids yield of 14.9 dw% occurred at the stationary stage of P-limited media. Algal solids that were not auto-flocculated and harvested during the stationary stage of N-limited media also had minimal HTL solids yield at 15.9 dw%. It was well-known and discussed in Chapter 4: *Inorganic Capture* that

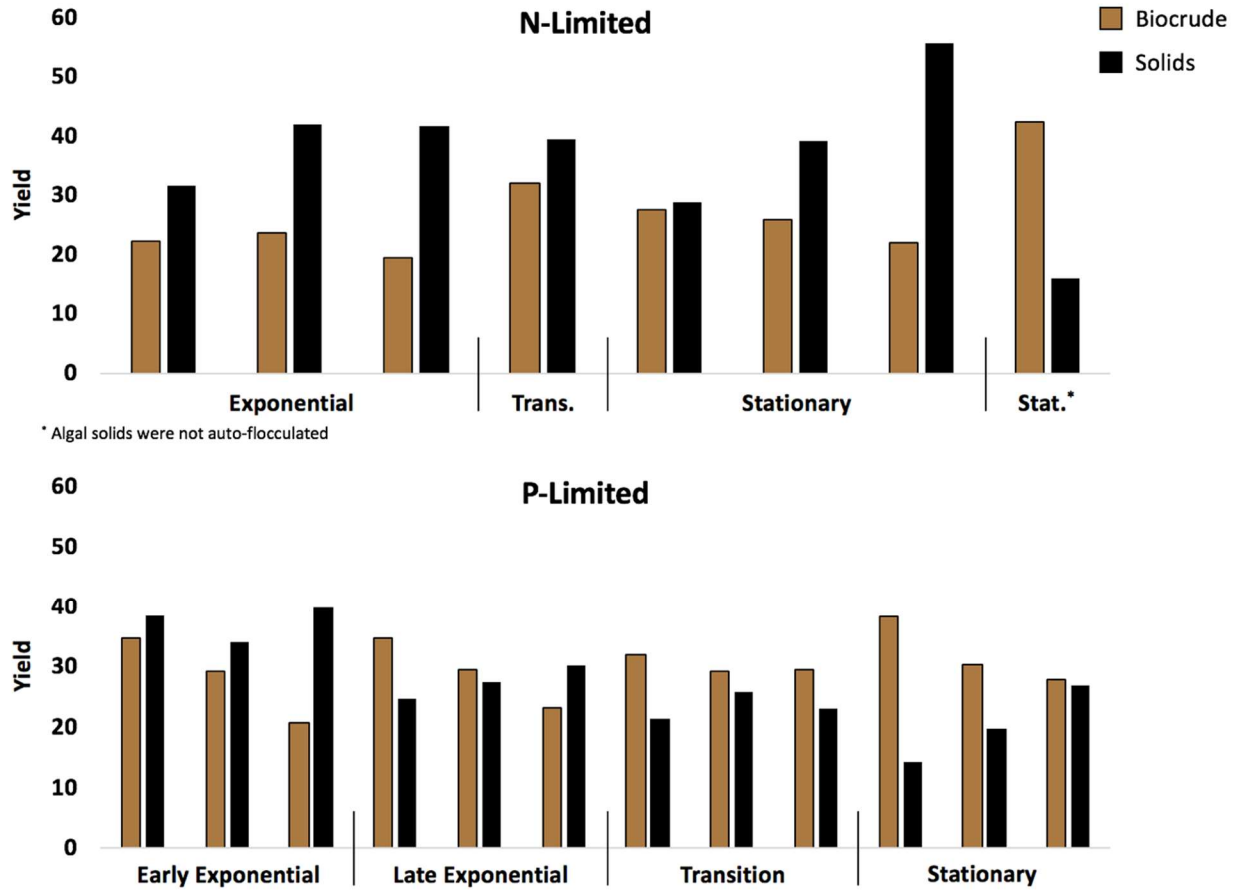

Figure 41: The biocrude (afdw%) and HTL solids (dw%) yields produced from algal solids harvested in N- and P-limited raceway ponds (top and bottom, respectively) and were harvested at distinct growth stages.

auto-flocculation enhances the recovery of inorganic molecules within the algal solids due to precipitation from the growth media.

As a whole, N-limited algal solids that were auto-flocculated produced a greater amount of HTL solids at an average of 39.8 ± 8.6 dw% than P-limited algal solids which averaged 27.2 ± 7.5 dw%. P-limited algal solids produce a lesser amount of HTL solids given the higher biomass to ash ratio of the algal solids. It is well understood that P-limited media produces a greater amount of algal biomass than N-limited media. Similarly, harvesting at later growth stages also maximizes algal biomass productivity. Thus, in this raceway-study where the inorganic content was constant

while the algal biomass varied, a lower ash wt% was observed in the P-limited media and later growth stages. Finally, the HTL solids yield is often directly correlated to the algal solids' ash wt%.

In comparison to the algal solids cultivated in the light rack and discussed in *Fate of Phosphorus post-HTL* section of Chapter 4.4.3, the HTL solids yields from the N- and P-limited raceways were much higher. The highest HTL solids yield was 17.7 dw% from the light rack cultivated algal solids shown in Figure 21. Similarly, the HTL solids yield of previous wastewater-cultivated algal solids was approximately 25 dw%. Both HTL solids yields are less than the previously stated, average HTL solids yields from the raceway-cultivated, N- and P-limited media, 39.8 and 27.2 dw% respectively.

The biocrude yield between N- and P-limited on an afdw% basis was more comparable to one another than the HTL solids, yet they were still significantly different ($p < 0.05$). The average biocrude yield from N-limited algal solids was 24.7 ± 4.2 afdw% while P-limited algal solids were 29.9 ± 4.8 afdw%. These biocrude yields are substantially lower than biocrude yields observed from the previous light rack study shared in Table 9. Similarly, biocrude yields in the mid- to upper-20's observed from this raceway study on an afdw% basis is less than the biocrude yields in the upper-30's and lower-40's observed in the literature. The cause for the smaller, limited biocrude yields observed in both the N- and P-limited raceway-cultivated algal solids is the extensive amount residual biocrude that could not be rinsed by the extracting solvent, DCM, and that remained on the HTL solids. On average, 22.3 ± 5.2 wt% of the HTL solids was residual biocrude oil. Thus, the greater amount of HTL solids, the greater amount of residual biocrude oil was entrapped to them. The higher HTL solids yields observed in the raceway-cultivated algal

solids in comparison to both the light rack and wastewater-cultivated algal solids explains the lower biocrude yields.

6.4.4 Biocrude Properties

Ultimate analysis of the biocrude provides a general oversight on the quality of biocrude. Table 18 summarizes the ultimate properties of the biocrude produced from algal solids cultivated in N-limited media. For auto-flocculated algal solids harvested from N-limited media the carbon and hydrogen wt% remained constant at 76.7 ± 0.6 dw% and 10.9 ± 0.2 dw% respectively across the different growth stages. Algal solids that were not auto-flocculated had the highest carbon wt% at 79.2 wt%. They also had the most optimum higher heating value (HHV) of 41.3 MJ/kg. The greater HHV is due to the lowest oxygen content of all biocrudes. However, the oxygen wt% may have been underestimated because it was calculated by difference for this biocrude sample rather than measured due to ongoing maintenance and repairs on the CHN/O Elemental Analyzer.

The oxygen dw% amongst the biocrude produced from N-limited media was the highest during the single algal solid sample harvested during the transition growth stage at 10.4 wt%. Meanwhile the oxygen content of the biocrude was less at the exponential and stationary growth stage at 8.3 ± 0.3 wt% and 7.8 ± 0.04 wt%, respectively. Meanwhile, the nitrogen content of the biocrude produced from N-limited algal solids decreased with later growth stages, from 5.4 ± 0.1 dw% at the exponential stage to 4.8 ± 0.05 dw% at the stationary stage.

Table 18: Ultimate (CHN/O) analysis and HHV of the HTL biocrude oil produced from **N-limited** growth media.

GROWTH	BIOCRUDE							
	C	H	N	O	H/C	N/C	O/C	HHV
Stage	*wt%*	*wt%*	*wt%*	*wt%*	*mol*	*mol*	*mol*	*MJ/kg*
Exp.	77.1 (0.4)	10.7 (0.3)	5.4 (0.1)	8.6 (0.3)	1.65	0.060	0.084	39.8
Exp.	76.7 (0.5)	10.9 (0.4)	5.6 (0.02)	8.2 (0.03)	1.69	0.063	0.081	40.0
Exp.	77.3 (0.2)	10.8 (0.3)	5.3 (0.03)	8.1 (0.1)	1.66	0.059	0.078	40.1
Trans.	76.2 (0.4)	11.1 (0.2)	5.1 (0.01)	10.4 (0.5)	1.73	0.057	0.102	39.7
Stat.	77.1 (0.2)	10.5 (0.1)	4.8 (0.04)	7.9 (0.2)	1.63	0.053	0.077	39.7
Stat.	76.8 (0.1)	11.1 (0.6)	4.9 (0.01)	7.8 (0.1)	1.72	0.054	0.076	40.4
Stat.	75.7 (0.4)	10.9 (0.3)	4.8 (0.01)	7.8 (0.1)	1.71	0.054	0.077	39.7
Stat. [a]	79.2 (0.8)	10.9 (0.6)	4.5 (0.1)	5.5 [b]	1.63	0.048	0.052	41.3

[a] Algal solids were not auto-flocculated
[b] Calculated by difference

Table 19 summarizes the ultimate properties of the biocrude produced by algal solids harvested in P-limited media. The HHV of the biocrude from P-limited algal solids was comparable to the biocrude from N-limited algal solids near 40 MJ/kg. The highest biocrude HHV was 42.4 MJ/kg from P-limited algal solids harvested during the transition growth stage. The higher carbon and hydrogen content of 78.2 and 12.2 wt%, respectively, that was observed in the biocrude from P-limited, transition algal solids are the cause for the maximized HHV. Unlike biocrude produced from N-limited algal solids the CHN/O wt% of the biocrude produced from P-limited algal solids were more scattered across the various growth stages. Indicating that the

growth stage from algal solids cultivated in P-limited media does not impact the ultimate, CHN/O properties of the resulting HTL biocrude.

Simulated distillation is another analytical technique that provides a broad overview of the distillate fractions present in the biocrude. The top of Figure 42 compares the division of distillate

Table 19: Ultimate (CHN/O) analysis and HHV of the HTL biocrude oil produced from **P-limited** growth media.

GROWTH	BIOCRUDE							
	C	H	N	O	H/C	N/C	O/C	HHV
Stage	*wt%*	*wt%*	*wt%*	*wt%*	*mol*	*mol*	*mol*	*MJ/kg*
Early Exp.	77.2 (0.2)	11.1 (0.1)	4.9 (0.04)	8.2 (0.1)	1.71	0.055	0.080	40.5
Early Exp.	76.8 (0.3)	10.8 (0.2)	4.7 (0.1)	8.3 (0.1)	1.68	0.052	0.081	40.0
Early Exp.	75.9 (0.2)	11.3 (0.2)	5.4 (0.05)	8.7 (0.4)	1.78	0.061	0.086	40.0
Late Exp.	77.0 (0.5)	11.3 (0.2)	4.9 (0.1)	8.5 (0.1)	1.75	0.054	0.083	40.7
Late Exp.	77.2 (0.2)	11.1 (0.6)	4.9 (0.1)	8.4 (0.1)	1.71	0.054	0.081	40.4
Late Exp.	76.8 (0.2)	11.8 (0.3)	5.3 (0.02)	8.0 (0.1)	1.83	0.059	0.079	41.3
Trans.	77.6 (0.2)	11.7 (0.2)	4.7 (0.1)	8.3 (0.3)	1.79	0.052	0.080	41.4
Trans	77.7 (0.2)	12.2 (0.2)	4.7 (0.02)	8.1 (0.2)	1.87	0.052	0.078	42.2
Trans.	78.2 (0.2)	12.2 (0.1)	4.8 (0.03)	8.3 (0.1)	1.86	0.053	0.080	42.4
Stat.	77.1 (0.4)	11.5 (0.2)	4.7 (0.04)	8.6 (0.1)	1.78	0.053	0.084	40.9
Stat.	76.2 (0.2)	11.6 (0.8)	5.2 (0.01)	9.8 (0.3)	1.81	0.058	0.096	40.6
Stat.	77.6 (0.4)	11.2 (0.5)	4.8 (0.01)	8.6 (0.1)	1.72	0.053	0.083	40.7

fractions amongst the biocrude produced from algal solids cultivated in N-limited growth media at various growth stages. The vacuum gasoline fraction (343-538°C) was the largest fraction amongst all growth stages of N-limited media at 42-47 wt% of the biocrude. The second largest distillate fraction for 6 out of the 8 biocrude products was the kerosene fraction (271-343°C) from the N-limited algal solids and made up 15-20 wt% of the biocrude. Algal solids from the transition and the stationary growth stage that were not auto-flocculated from N-limited media produced a biocrude where the vacuum residual (>538°C) had a greater distillate fraction than the kerosene fraction. The third most abundant distillate fraction for each of the N-limited algal solids was the heavy naphtha fraction (<193°C) with a range of 7.6-11.9 wt% of the biocrude. The gasoline distillate fraction was the least abundant of the biocrude from each of the N-limited algal solids with range of 7.5-10.1 wt%.

The bottom of Figure 42 compares the division of distillate fractions amongst the biocrude produced from algal solids harvested at different growth stages in P-limited media. Analogous to N-limited algal solids the vacuum gasoline fraction was the most abundant distillate fraction at41-46 wt% of the biocrude produced from algal solids cultivated in P-limited media. The kerosene distillate fraction was the second most abundant fraction for each biocrude sample ranging from 18-22 wt%. The heaviest fraction, vacuum residual, was a close third with 12-18 wt% of the biocrude. Depending on the growth stage, heavy naphtha and gasoline were the next most abundant distillate fractions. A majority of the biocrude produced from the early and late exponential phase had a greater amount of heavy naphtha than gasoline fraction ranging from 9-12 and 8-14 wt%, respectively. At the later transition and stationary growth stages the gasoline fraction was greater at 10-15 wt% of the biocrude as opposed to the 6-9 wt% in the heavy naphtha.

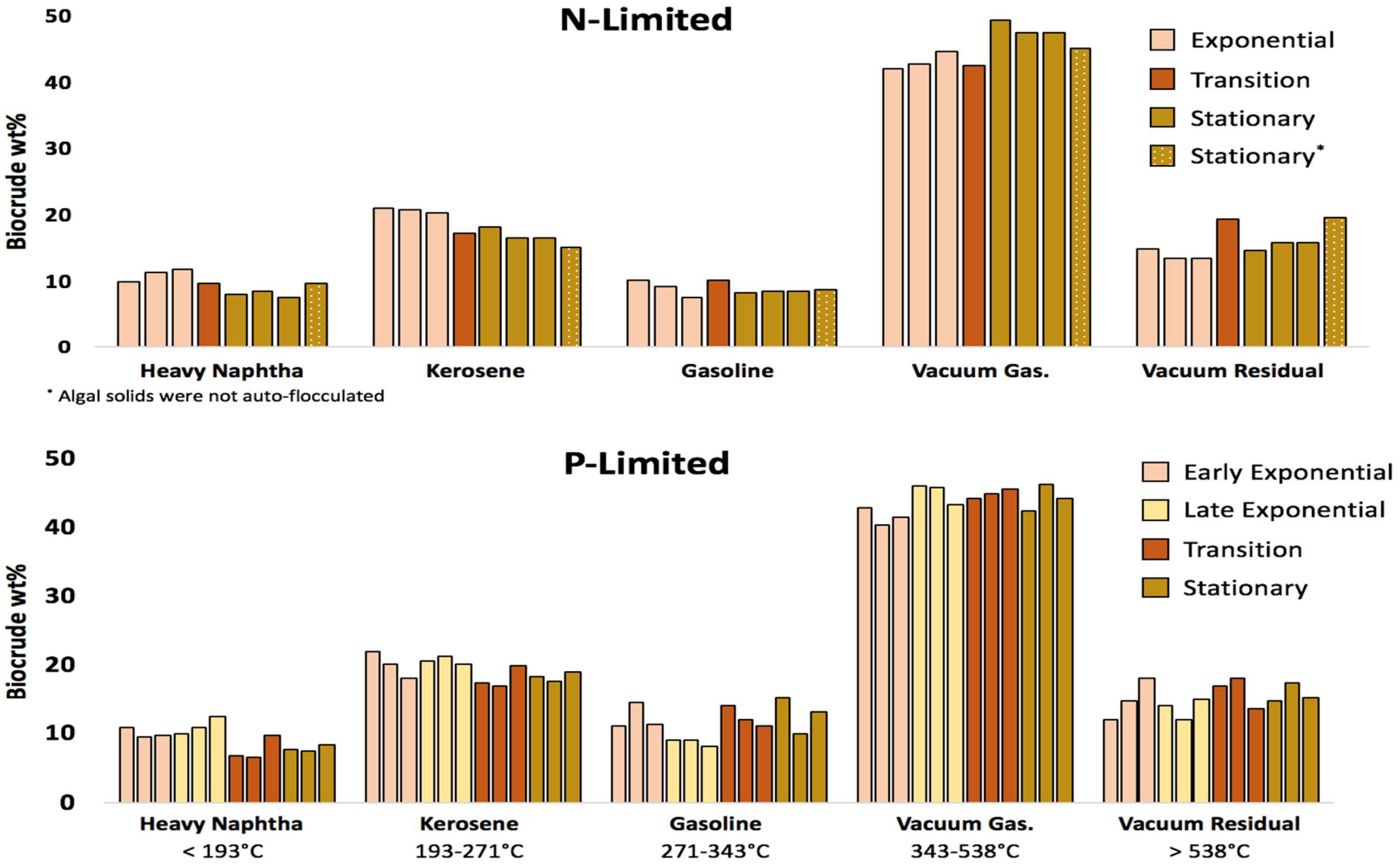

Figure 42: Simulated distillation fractions of the biocrude produced from algal solids cultivated in N-limited (top) and P-limited (bottom) media and harvested at various growth stages.

A biocrude oil with lighter distillate fractions, such as heavy naphtha, kerosene, and gasoline, are more advantageous for refining Thus, biocrude produced form algal solids harvested at earlier growth stages, such as the exponential and transition stages, for both N- and P-limited algal solid would be optimum for refinement to high-value products. The cause for a heavier biocrude product at the later growth stages is due long carbon chain molecules, such as lipids, that become more prevalent in the algal solid at later growth stages as seen in Table 13 and Table 14. Overall, 90 wt% or more of the biocrude samples from N-limited algal solids could be distilled off at 600°C or less. Having 90 wt% or more of the biocrude being distilled off at 600°C less is agreeable with biocrude produced from auto-flocculated algal solids cultivated in light racks and discussed in the previous Chapter 4: *Inorganic Capture* and wastewater-cultivated algal solids.[8]

Gas Chromatography-Mass Spectrometry (GC-MS) analysis conveyed the composition of the biocrude samples, and thus confirmed the abundance or scarcity of heavier compounds in the biocrude samples. Figure 43 shows the common functional groups observed in the biocrude samples from N- (top) and P-limited (bottom) algal solids harvested at their various growth stages. The biocrude from algal solids cultivated in N-limited and P-limited media were both primarily composed of C_{15} and C_{16} saturated and unsaturated compounds. Although there was a great deal of variance in the amount of saturated and unsaturated hydrocarbons in the biocrude from algal solids harvested at the later, stationary growth stage in P-limited media, a general trend of increasing saturated and unsaturated hydrocarbons in the biocrude from algal solids harvested at the later growth stages tends to occur. With these hydrocarbons being long chain, $> C_{15}$ hydrocarbons and their various derivatives, they certainly add to the heavier distillate fractions of the biocrude. Thus, the observance of a greater amount of C_{15} and C_{16} saturated and unsaturated hydrocarbons in the biocrude from algal solids harvested at the later growth stages in Figure 43

agrees with the increase in heavier distillate fractions also observed from these algal solids in Figure 42.

Comparing biocrude produced from algal solids cultivated in N- versus P-limited media, P-limited algal solids produced a biocrude with greater amount of C_{16} carboxylic acid and amide compounds than algal solids that were cultivated in N-limited media. Lipids and proteins in the algal solid have been identified as the source of long chain carboxylic acids and amides in HTL biocrude.[19-21] Given the limitation of N nutrients, a lesser dw% of protein was observed in the algal solids cultivated in N-limited media as opposed to P-limited (see Table 13 and Table 14). The lower protein content from N-limited algal solids therefore caused a decrease in long chain amides. Recall from Chapter 4.4.4 *Inorganic in-situ HTL Catalysis*, which explains and discusses the biocrude compounds that result from HTL of common algal biomolecules in greater detail, that a lower amide concentration in the biocrude is preferred for future upgrading and refining of the biocrude. Similar to proteins, lipids are the common source for long chain fatty acid compounds in the biocrude after HTL. P-limited media also produced algal solids with a greater amount of lipids than algal solids that were cultivated in N-limited media. Thus, the greater abundance of long chain fatty acids in the biocrude from P-limited algal solids as opposed to N-limited algal solids can also be explained by their respective algal solid lipid content. The biocrude from cultivated from N- and P-limited media in the raceway also showed a great deal of agreement with biocrude produced from previous wastewater (N-limited) and light rack (P-limited) studies. Roberts et al. reported a lower amide concentration in the biocrude produced from wastewater-cultivated algal solids when compared to other HTL biocrude products reported in the literature.[22]

Figure 43: Biocrude composition as per the GC-MS peak area percentage for common biocrude functional groups. Biocrude was produced from HTL of algal solids cultivated in N- and P-limited media and harvested at varying growth stages.

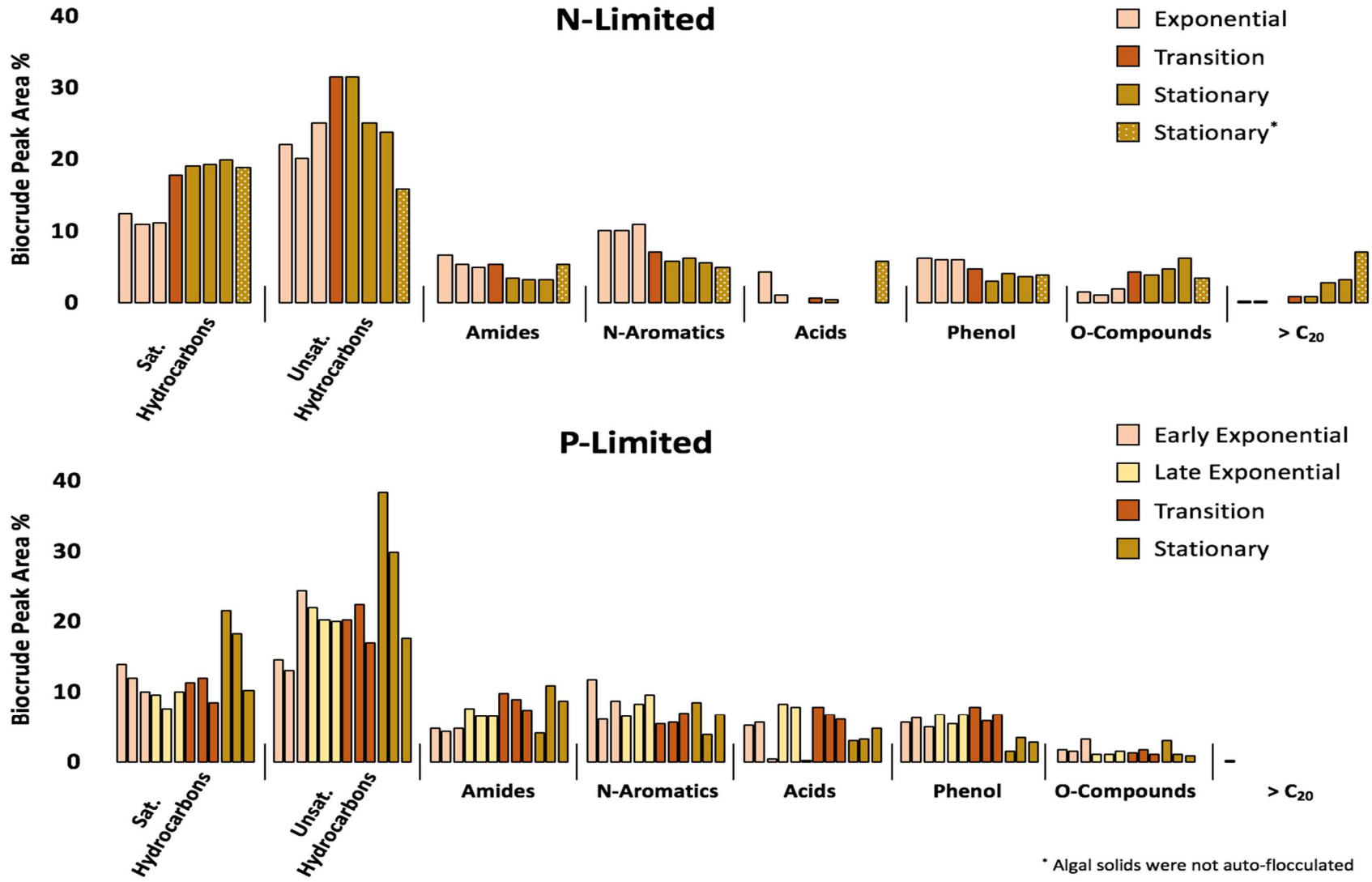

Furthermore, the biocrude produced from these N-limited, wastewater-cultivated algal solids also had a large amount of $>C_{20}$ hydrocarbons appear in its GC-MS spectra. These $>C_{20}$ compounds had not been observed in biocrude products from the previous light rack study (see Chapter 4.4.4 *Inorganic in-situ HTL Catalysis*) or other literature reports.[20, 23-27] Similar biocrude $>C_{20}$ compounds only appeared in biocrude produced from the raceway-cultivated algal solids that were harvested at the later, stationary growth stage of P-limited media. Figure 43 therefore provides strong evidence that algal growth media and the growth stage at the time of algal solid harvesting will impact the biocrude composition.

The reason algal growth media and growth stage have a large impact on the biocrude composition is because they also have a large impact on the biomolecular content of algal. The growth media and growth stage impacting the algal biomolecular content and these biomolecules impacting the HTL biocrude composition are both supported by the literature.[19-21] A major hypothesis still remains, and that is that the HTL solids have a catalytic impact on the biocrude product. Without a low-ash or low-HTL solid yielding algal biomass as a control for comparison nor the tested reproducibility and variance of a biocrudes' composition for an algal solid cultivated at identical growth media and stages, it is difficult to definitively conclude the catalytic role the various HTL solids structures observed from this study had on biocrude composition. Figure 43, however, does provide promise that changes in the biocrude composition may be occurring due to the HTL solids. A high degree of variance in the saturated and unsaturated hydrocarbon content of the biocrude from N- and P-limited algal solids harvested at the stationary stage could be due to the varying inorganic content within those algal solids. For at the same growth stage and media, the biomolecular content of the algal solid is shown to be constant, and therefore only the inorganic content is varying.

Improved biocrude quality due to the inorganic HTL solids can be better seen from the broader properties of the biocrude. A Van Krevelen diagram is often used to compare a crude oil's H/C and O/C molar ratio.[22] Higher H/C and lower O/C molar ratios in the biocrude is desired for it to serve as a renewable alternative to current petroleum crude oil.[26, 28] Figure 44 is a Van Krevelen diagram of the biocrude produced from the algal solids cultivated from the N- and P-limited raceway ponds. They are further categorized by the respective solid structure that appeared in their complimenting HTL solids, HAp, TCP, or calcite ($CaCO_3$). Analogous to Table 18 and Table 19, there was little variance in the biocrudes, O/C, nor the N/C, molar ratio from the algal solids cultivated in raceway ponds. There was a great deal of variance, however, in the biocrudes' H/C molar ratio. In addition, when the biocrudes' H/C molar ratio is compared to the complimentary HTL solid structure a trend appears. Biocrude where HAp HTL solids were formed tended to have a lower H/C molar ratio (Avg. 1.69). HTL solids that were predominantly TCP also had a biocrude product that had a slightly higher H/C molar ratio at an average of 1.72. Finally, HTL solids that remained primarily calcite, or $CaCO_3$, had the highest H/C molar ratio, averaging 1.82, in its complimentary biocrude product. Thus, there was a significant difference ($p < 0.05$) between the average H/C molar ratio of the biocrude where calcite was the primary HTL solid structure as opposed to when calcium phosphate was the primary HTL solid structure. The significant increase in H/C ratio in the biocrude suggests calcite may be a more beneficial inorganic structure than calcium phosphate for *in-situ* HTL biocrude upgrading.

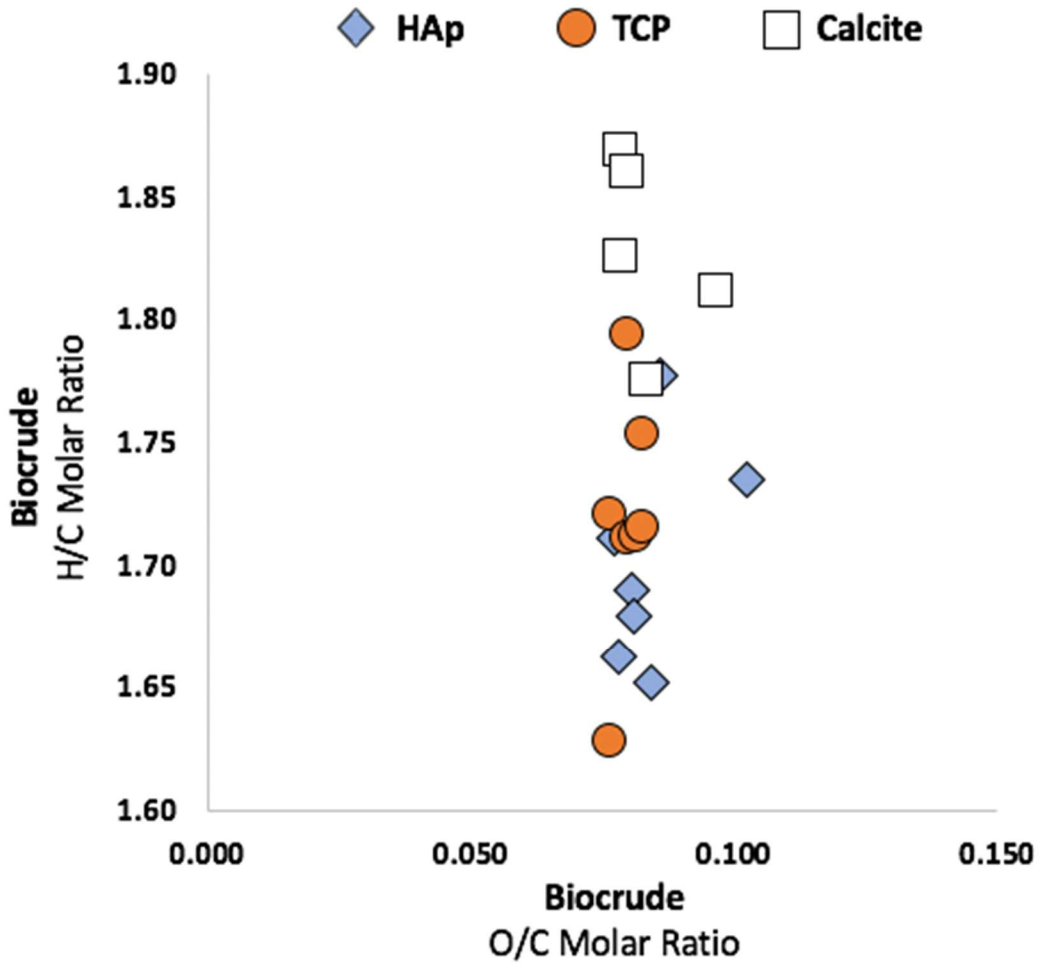

Figure 44: Van Krevelen diagram comparing the H/C vs. O/C molar ratio of the biocrude product in comparison to the complimentary HTL solid structure observed by XRD.

6.5 Conclusion

Varying the algal growth media between N- and P-limited as well as the growth stage at which the algal solids were auto-flocculated and harvested, helped identify the justification for the calcium phosphate structure in the HTL solids and other key biocrude properties. The original hypothesis was that excess phosphorus that remains aqueous in N-limited, algal growth media precipitates from solution as solid, amorphous calcium phosphate and therefore undetectable by XRD. Given the high, thermodynamic instability of amorphous calcium phosphate in both

aqueous and open, ambient environments, the likelihood of it being in auto-flocculated algal solids seemed scarce. However, literature supports that biological pyrophosphates such as ATP in addition to other inorganic species such as carbonate and magnesium, all of which are abundant in the algal solids, stabilize the amorphous calcium phosphate structure. The appearance of HAp, TCP, and lime in XRD patterns of the ash from the algal solids also aided in confirming the presence of solid calcium phosphate in combination with calcite within the algal solids.

The XRD of the algal solid ash empirically confirmed the presence of calcium phosphate in the algal solids. However, to determine if this impacted the structure of the HTL solids, a method to quantify the proportion of calcite to calcium phosphate within the algal solids was desired. Despite some inaccuracies between the theoretical amount of carbonate, which was based off the water chemistry of the growth media, and the proximate thermal analysis for quantifying carbonate in algal solids discussed in Chapter 5.4.3 Enhanced Quantification of Inorganic Conversion, both appeared to correspondingly trend together. Thus, using the same TGA-method to quantify carbonate in the algal solids the mass of calcium associated with that carbonate was determined stoichiometrically as $CaCO_3$. The balance of calcium remaining in the algal solids was then assumed to be calcium phosphate. Comparing the percent of calcium as calcium phosphate with the theoretical amount of solid-P as calcium phosphate, both values also trended analogously with one other.

Furthermore, the final HTL solids structure also corresponded directly with the theoretical solid-P, and percent of calcium as calcium phosphate in the algal solids. HTL solids that had uniform calcium phosphate structures, either HAp or TCP based off XRD, were observed from algal solids with high, theoretical solid-P and high percent of calcium as calcium phosphate. In conclusion, the presence of excess phosphorus in the algal growth media at the time of auto-

flocculation results in amorphous calcium phosphate in the algal solids and crystalline HAp or TCP in the HTL solids. N-limited or early-stage P-limited growth media with an abundance of calcium are therefore the optimum growth media and stages for the observance of HAp or TCP in the HTL solids.

To understand the biomass traits that distinguished HAp from TCP structures in the HTL solids, both the Ca:P and C:Ca molar ratio were examined. HTL solids that were TCP tended to have equal Ca:P molar ratios as their initial algal solids. Meanwhile, HAp structured HTL solids Ca:P molar ratios did not correspond to their initial algal solid Ca:P molar ratio and appeared scattered. In addition, TCP HTL solids did not exceed a Ca:P molar ratio greater than its stoichiometric Ca:P molar ratio of 1.5. The highly substituted nature of HAp, however, allowed the HTL solids to have a Ca:P molar ratio of nearly 1.8. The C:Ca molar ratio provides a proportion of biomass to inorganics on a mole basis. HAp structures in the HTL solids were only observed at a C:Ca molar ratio less than 8. It is hypothesized that the higher amount of carbon from the biomass results in a reaction media that is more acidic. At HTL reaction conditions, the biomass decomposes to CO_2 gas. The CO_2 gas reacts then with the aqueous reaction media creating carbonic acid. Greater investigation to the role of C:Ca molar ratio and pH on the calcium phosphate structure of HTL solids are therefore recommended.

The HTL solids yields from the N- and P-limited raceway ponds were higher than the previously wastewater- or light rack-cultivated HTL solids yields at an average 38.9, 27.2, 25.5, and 17.7 dw%, respectively. This vast increase in HTL solids yield minimized the biocrude yield to an average of 24.7 afdw% from N-limited algal solids and 29.9 afdw% from P-limited algal solid. The decline in biocrude yield is due to the residual biocrude that is left on the HTL solids during the extraction. Approximately 25 wt% of the HTL solids is residual biocrude that cannot

be washed off the HTL solids with DCM. Thus, the greater HTL solids yield, the greater amount of biocrude is lost.

The algal growth media and growth stage also had a large impact on the biocrude properties. This is to be expected as algal growth media and stage dictate the biochemical content of the algal solids, which in turn impact the biocrude properties. Previous wastewater-cultivated algal solids produced a biocrude that had a low amide content and the appearance of > C_{20} hydrocarbons that made it unique to other algal, HTL biocrude reported in the literature. Experimenting with role of growth media and growth stage revealed similar traits, low amide content and > C_{20} hydrocarbons, in the biocrude from P-limited, stationary algal solids. These growth conditions are similar to that which was observed from in the wastewater-cultivated algal solids. Thus, the growth media and growth stage at which the algal solids are harvested have a role in the quality and characteristics of the resulting HTL biocrude.

The final hypothesis was to observe any *in-situ*, catalytic changes in the biocrude due to the varying calcite or calcium phosphate HTL solids. Large variances in the saturated and unsaturated hydrocarbon composition occurred in several of the biocrude samples produced from algal solids in the same growth media and harvested at the same growth stage. Algal solids from identical growth media and growth stages have the most similar biochemical content. Thus, only the inorganic fraction is varying and be the potential cause for changes in the biocrudes' hydrocarbon composition. Further investigation of the biocrudes' H/C molar ratios also indicated that HTL solids that remained calcite also created a biocrude product with significantly higher H/C molar ratios at 1.83 than biocrudes where HAp or TCP HTL solids were observed. Thus, it is hypothesized that $CaCO_3$ has a greater *in-situ* catalytic impact on the biocrude than the previously proposed calcium phosphates.

6.6 References

1. Rhee, G. Y., Effects of N:P atomic ratios and nitrate limitation on algal growth, cell composition, and nitrate uptake 1. *Limnology and Oceanography* **1978,** *23* (1), 10-25.
2. Chen, M.; Tang, H.; Ma, H.; Holland, T. C.; Ng, K. Y.; Salley, S. O., Effect of nutrients on growth and lipid accumulation in the green algae Dunaliella tertiolecta. *Bioresource technology* **2011,** *102* (2), 1649-55.
3. Combes, C.; Rey, C., Amorphous calcium phosphates: synthesis, properties and uses in biomaterials. *Acta Biomater* **2010,** *6* (9), 3362-78.
4. Lai, R.-H.; Dong, P.-J.; Wang, Y.-L.; Luo, J.-B., Redispersible and stable amorphous calcium phosphate nanoparticles functionalized by an organic bisphosphate. *Chinese Chemical Letters* **2014,** *25* (2), 295-298.
5. Blumenthal, N. C.; Betts, F.; Posner, A. S., Effect of carbonate and biological macromolecules on formation and properties of hydroxyapatite. *Calcified Tissue Research* **1975,** *18* (1), 81-90.
6. Blumenthal, N. C.; Betts, F.; Posner, A. S., Stabilization of amorphous calcium phosphate by Mg and ATP. *Calcified Tissue Research* **1977,** *23* (1), 245-250.
7. Boskey, A. L.; Posner, A. S., Magnesium stabilization of amorphous calcium phosphate: A kinetic study. *Materials Research Bulletin* **1974,** *9* (7), 907-916.
8. Roberts, G. W.; Sturm, B. S. M.; Hamdeh, U.; Stanton, G. E.; Rocha, A.; Kinsella, T. L.; Fortier, M.-O. P.; Sazdar, S.; Detamore, M. S.; Stagg-Williams, S. M., Promoting catalysis and high-value product streams by in situ hydroxyapatite crystallization during hydrothermal liquefaction of microalgae cultivated with reclaimed nutrients. *Green Chem.* **2015,** *17* (4), 2560-2569.
9. Hurle, K.; Neubauer, J.; Goetz-Neunhoeffer, F., Hydration mechanism of partially amorphized beta-tricalcium phosphate. *Acta Biomater* **2017,** *54*, 429-440.
10. Ramachandran, V. S.; Sereda, P. J.; Feldman, R. F., Mechanism of Hydration of Calcium Oxide. *Nature* **1964,** *201*, 288.
11. Kamitakahara, M.; Nagamori, T.; Yokoi, T.; Ioku, K., Carbonate-containing hydroxyapatite synthesized by the hydrothermal treatment of different calcium carbonates in a phosphate-containing solution. *Journal of Asian Ceramic Societies* **2015,** *3* (3), 287-291.
12. Tang, X. L.; Xiao, X. F.; Liu, R. F., Structural characterization of silicon-substituted hydroxyapatite synthesized by a hydrothermal method. *Materials Letters* **2005,** *59* (29-30), 3841-3846.
13. Aminian, A.; Solati-Hashjin, M.; Samadikuchaksaraei, A.; Bakhshi, F.; Gorjipour, F.; Farzadi, A.; Moztarzadeh, F.; Schmücker, M., Synthesis of silicon-substituted hydroxyapatite by a hydrothermal method with two different phosphorous sources. *Ceramics International* **2011,** *37* (4), 1219-1229.
14. Neria, I. S.; Kolen'ko, Y. V.; Lebedev, O. I.; Tendeloo, G. V.; Gupta, H. S.; Guitian, F.; Youshimura, M., An Effective Morphology Control of Hydroxyapatite Crystals via Hydrothermal Synthesis. *Crystal Growth & Design* **2009,** *9* (1), 466-474.
15. Sadat-Shojai, M.; Khorasani, M. T.; Dinpanah-Khoshdargi, E.; Jamshidi, A., Synthesis methods for nanosized hydroxyapatite with diverse structures. *Acta Biomater* **2013,** *9* (8), 7591-621.
16. Goto, T.; Kim, I. Y.; Kikuta, K.; Ohtsuki, C., Comparative study of hydroxyapatite formation from

alpha- and beta-tricalcium phosphates under hydrothermal conditions. *Journal of the Ceramic Society of Japan* **2012,** *120* (4), 131-137.
17. Loo, S. C.; Siew, Y. E.; Ho, S.; Boey, F. Y.; Ma, J., Synthesis and hydrothermal treatment of nanostructured hydroxyapatite of controllable sizes. *J Mater Sci Mater Med* **2008,** *19* (3), 1389-97.
18. Biller, P.; Ross, A. B.; Skill, S. C.; Lea-Langton, A.; Balasundaram, B.; Hall, C.; Riley, R.; Llewellyn, C. A., Nutrient recycling of aqueous phase for microalgae cultivation from the hydrothermal liquefaction process. *Algal Research* **2012,** *1* (1), 70-76.
19. Changi, S. M.; Faeth, J. L.; Mo, N.; Savage, P. E., Hydrothermal Reactions of Biomolecules Relevant for Microalgae Liquefaction. *Industrial & Engineering Chemistry Research* **2015,** *54* (47), 11733-11758.
20. Biller, P.; Ross, A. B., Potential yields and properties of oil from the hydrothermal liquefaction of microalgae with different biochemical content. *Bioresource technology* **2011,** *102* (1), 215-25.
21. Teri, G.; Luo, L.; Savage, P. E., Hydrothermal Treatment of Protein, Polysaccharide, and Lipids Alone and in Mixtures. *Energy & Fuels* **2014,** *28* (12), 7501-7509.
22. Roberts, G. W.; Fortier, M.-O. P.; Sturm, B. S. M.; Stagg-Williams, S. M., Promising Pathway for Algal Biofuels through Wastewater Cultivation and Hydrothermal Conversion. *Energy & Fuels* **2013,** *27* (2), 857-867.
23. Brown, T. M.; Duan, P.; Savage, P. E., Hydrothermal Liquefaction and Gasification of Nannochloropsis sp. *Energy & Fuels* **2010,** *24* (6), 3639-3646.
24. Xu, D.; Savage, P. E., Characterization of biocrudes recovered with and without solvent after hydrothermal liquefaction of algae. *Algal Research* **2014,** *6*, 1-7.
25. Duan, P.; Savage, P. E., Hydrothermal Liquefaction of a Microalga with Heterogeneous Catalysts. *Industrial & Engineering Chemistry Research* **2011,** *50*, 52-61.
26. Ross, A. B.; Biller, P.; Kubacki, M. L.; Li, H.; Lea-Langton, A.; Jones, J. M., Hydrothermal processing of microalgae using alkali and organic acids. *Fuel* **2010,** *89* (9), 2234-2243.
27. Xu, D.; Savage, P. E., Effect of reaction time and algae loading on water-soluble and insoluble biocrude fractions from hydrothermal liquefaction of algae. *Algal Research* **2015,** *12*, 60-67.
28. Roussis, S. G.; Cranford, R.; Sytkovetskiy, N., Thermal Treatment of Crude Algae Oils Prepared Under Hydrothermal Extraction Conditions. *Energy & Fuels* **2012,** *26* (8), 5294-5299.

7 Conclusions and Future Work

Renewable and sustainable means are necessary to meet the rise in food, energy, and water demand with the rise in global population. Previous work at the University of Kansas has identified an effective means for recovering nutrients, such as nitrogen and phosphorus, from wastewater effluent through algal growth and cultivation. Further treatment of these wastewater-cultivated algal solids via hydrothermal liquefaction (HTL) converts the algal biomass to an energy-dense biocrude oil while retaining over 95% the phosphorus in the HTL solid product.[1] The phosphorus-dense HTL solid is therefore ideal for future fertilizer application. The removal of nutrients from wastewater effluent by algal cultivation and the conversion of these algal solids to a biocrude oil and solid phosphorus fertilizer make this work an ideal nexus of water, energy, and food, respectively.

A fundamental knowledge for this discovery, however, still remained. Understanding the chemistry and reaction conditions involved to recover almost all the phosphorus as a solid while producing a higher-quality biocrude oil allows for future reproducibility and optimization. The following sections introduce major findings and conclusions to the capture of inorganics in the algal and HTL solids, how these inorganics may impact biocrude characteristics, and lastly how algal growth media and growth stage can vary the inorganic structure in the algal and HTL solids as well as the biocrude composition and properties. Finally, the suggested areas and paths for future work to further expand the fundamental knowledge or resolve any remaining unanswered questions are also addressed.

7.1 Inorganic Capture

A unique feature of the algal solids cultivated from wastewater effluent was their high inorganic content. Previous findings indicated that the inorganic composition of the wastewater-cultivated algal solids was primarily silica, calcium, and phosphorus.[2] It was known that the high amount of calcium in the wastewater effluent was due to the addition of lime to the treatment plant to control the alkalinity, or buffer capacity, of the effluent. Finally, phosphorus is a key nutrient for algal growth; therefore, the high phosphorus content was considered natural and necessary for biological growth.[2] Further investigation determined that the dewatering technique to harvest the algal solids, known as auto-flocculation, was the primary cause for the inorganic content.

The aqueous ions present in algal growth media, provide the necessary precursors to form effective coagulants for algal cells. These coagulants form when the pH of the growth media is increased to 10 or 11, precipitate from solution, and cause the algal solids auto-flocculate. By dewatering and harvesting algal solids at a neutral and basic pH, the algal solids that were harvested at the higher pH and auto-flocculated had 2-4 times the ash wt% and nearly 40 times the calcium content compared to algal solids that were harvested at a neutral pH. The observation of higher calcium in the auto-flocculated algal solids confirmed the hypothesis that the calcium was external of the algal cell.

X-ray diffraction further identified the crystalline structure of the auto-flocculated and wastewater-cultivated algal solids to be calcite ($CaCO_3$). Moreover, the greater presence of calcium as calcite in the algal solids aided in the phosphorus recovery in the HTL solids. Algal solids that were crystalline and calcite recovered over 99% of the initial phosphorus while amorphous algal solids or algal solids that were not auto-flocculated recovered at most 72%. Despite the similar calcite crystalline structure and the high recovery of phosphorus in the HTL

solids for both the wastewater-cultivated and crystalline, auto-flocculated algal solids, their resulting HTL solid structure was divergent. The crystalline structure of the HTL solids produced from the initial lab-grown, crystalline, auto-flocculated algal solids remained calcite. Meanwhile, the wastewater-cultivated algal solids produced HTL solids that had a calcium phosphate structure primarily, either hydroxyapatite (HAp), $Ca_5(PO_4)_3OH$, or tricalcium phosphate (TCP), $Ca_3(PO_4)_2$.

7.2 Model Compounds

Following the successful understanding and explanation for the capturing of inorganics both in the algal and HTL solids, a greater understanding for the observed structure of calcium phosphates in the HTL solids of wastewater-cultivated algal solids was necessary. To assist in eliminating or bettering controlling the additional variables created by the growth of algal biomass, inorganic and organic model compounds were reacted hydrothermally at identical, conventional, HTL conditions. Given calcite was the perceived, primary, Ca structure from XRD, commercial $CaCO_3$ and trisodium phosphate (Na_3PO_4) were reacted at Ca:P molar ratios similar to that of wastewater-cultivated algal solids (2.33) and the stoichiometric molar ratios of TCP (1.5) and HAp (1.67).

The XRD patterns of the HTL solids resulting from these hydrothermal synthesis reactions depicted a combination of calcite and HAp structures of varying relative intensities. The XRD patterns and relative intensities between calcite and HAp, however, could not be duplicated from identical, independent reactions. In addition, a nearly uniform HAp or TCP structure, as seen in the HTL solids produced by wastewater-cultivated algal solids, were never observed from the HTL reactions of calcite and Na_3PO_4 alone. The addition of silica as SiO_2, however, increased the intensity of the HAp peaks within the HTL solids of calcite and Na_3PO_4 reactions. Silica also

amplified the appearance of calcium phosphate structures in the HTL solids from lab-grown, auto-flocculated, crystalline algal solids. While XRD provided qualitative results for differentiating calcite and calcium phosphate structures in algal and HTL solids, more quantitative means were desired.

Thermogravimetric analysis (TGA) could distinguish the loss of carbonate from solid $CaCO_3$. Between 600-800°C CO_2 is lost and becomes calcium oxide (CaO). With the change in mass due to the loss of CO_2 provided by the TGA, stoichiometry allowed for the mass of carbonate to be calculated. For pure $CaCO_3$ this method, had less than 1% error compared to theoretical mass of carbonate. This error increased to 50-70% when applied to algal solids and the theoretical amount of carbonate as determined by water chemistry by our collaborator. Additional TGA experiments with glucose and $CaCO_3$ mixtures determined that the presence of additional, organic biomass caused a delay in the thermal degradation of $CaCO_3$ and release of CO_2, to CaO. Overall, a majority of the CO_2 from $CaCO_3$ was lost during the initial pyrolysis stage, and the calculated mass of carbonate trended analogously with the water chemistry or theoretical amount of carbonate. Thus, the TGA method for estimating the amount of $CaCO_3$ in algal and HTL solids was determined to be applicable for future measurements.

The final research thrust from the model compound study was to observe any changes in the biocrude product due to the previously observed calcium phosphate HTL solids. One manner to test this hypothesis was the addition of commercial HAp with commercial tetradecanamide (TDA), a C_{14} chain amide similar to the C_{16} amide commonly observed in algal, HTL biocrude. Although little biocrude was produced, the DCM soluble fraction of the organic HTL product showed a greater conversion of TDA to tetradecanitrile (TDN) from GC-MS analysis with increased HAp loading. Upon review, the literature supports the claim that long chain

hydrocarbons > C_{14} are stable under hydrothermal conditions and when reacted independently, do not decompose to a biocrude product.[3-4] Thus, palmitic acid, the most common, C_{16} fatty acid observed algal HTL biocrude, would also not be feasible to react via HTL independently. Carbohydrate model compounds, such as glucose and starch, also favored a solid, char product rather than a liquid biocrude which is in agreement with the literature.[5-6] Soy protein, a common nutritional supplement, however was able to produce a viable biocrude product for analysis when loaded at 15 wt% solids as opposed to usual 10 wt%.

Soy protein underwent HTL both independently and with the addition of commercial HAp, silica, or $CaCl_2$ and Na_3PO_4 which formed HAp *in-situ* of the HTL reaction. Comparing the biocrude results between the control, just soy protein, and the three, external solids were inconclusive in terms of their amide concentration within the biocrude. Further adjustments to the external solids loading that are reasonable to the ash content of previously auto-flocculated algal solids could lead to more dramatic changes in the biocrude composition. Also, previous results have indicated that calcite ($CaCO_3$) can have an impact on biocrude properties. Thus, it is recommended that various calcite loadings also be investigated. Finally, there is a great deal of discrepancy across the literature to the effect various heterogeneous catalysis have on the biocrude product.[5, 7-10] Thus, ample amounts of external solids, algal biomass, and model compounds are recommended to allow for replication and reproducibility surrounding the external solids. Multiple HTL reactions will allow for proper statistical analysis of the biocrude products and would add key conclusions to inconsistencies in the literature.

7.3 Raceway

The final study of this dissertation entails algal solids cultivated in 2, 1,200 L raceway ponds with N- and P-limited growth media. Cultivation, auto-flocculation, and harvesting was all done by the collaborating environmental engineering student, Sirwan Alimoradi. The original hypothesis proposed by our collaborator was altering the proportion of P assimilated into the algal cell, or bio-P, and the phosphorus that would precipitate out of solution as calcium phosphate during auto-flocculation, solid-P would impact the final structure of the HTL solids. The objective of the primary author was therefore to find empirical means distinguish and quantify the bio-P and solid-P within the algal solid and to prove or disprove the hypothesis of whether the bio- to solid-P ratio effected HTL solid structure.

XRD of the algal solids cultivated in N- and P-limited media from the raceways continued to appear as amorphous or calcite. No appearance of crystalline calcium phosphate was observed. TCP, HAp, and lime, however, were all observed in the TGA ash of the various auto-flocculated algal solids cultivated in both N- and P-limited media. The XRD results from the algal solids' ash are in agreement with XRD pattern of the ash from wastewater-cultivated algal solid observed by Roberts et al.[1] The observance of calcium phosphate structures in the algal solid ash rather than the algal solid indicate that amorphous calcium phosphate precipitates from solution and is captured with the algal solids. Although thermodynamically unfavorable, the literature supports the stability of amorphous calcium phosphate in the presence of pyrophosphates, such as biological ATP, carbonate, and magnesium.[11-13] All three of which are in abundance in the algal solids.

In addition to confirming the presence of precipitated amorphous calcium phosphate within the algal solids, an estimate of the amount of solid-P was also desired for further confirmation. Estimation on the amount of amorphous calcium phosphate, or solid-P, was done using the

previous TGA-method for measuring the mass of carbonate in the algal solid sample. Similar to the previous agreement between trends of the TGA-measured and theoretical mass of carbonate in the algal solids, there was also agreement between the trends for the percent of calcium as calcium phosphate and the theoretical amount of solid-P in the algal solids. Furthermore, the algal solids that showed the highest amount of solid-P and highest estimated amount of calcium as calcium phosphate also showed calcium phosphate as the primary structure of the algal solids' ash.

The agreement between the theoretical solid-P and the calculated percent of calcium as calcium phosphate within the algal solid and the calcium phosphate structure of the algal solid ash continued for the HTL solids' structure. HTL solid samples that had a uniform or primary structure of TCP or HAp also had the estimated percent of calcium as calcium phosphate well-over 50%. Thus, the algal growth media and stage at which the algae are auto-flocculated are the central variables that dictate the presence of calcium phosphates in the HTL solids. Algal solids that were harvested in N-limited media or harvested during the early growth stages of P-limited media create have excess phosphorus remaining in solution. This excess phosphorus than precipitates from solution during auto-flocculation as amorphous calcium phosphate that is stabilized by the other algal and inorganic components. Following HTL, these calcium phosphates become crystalline HAp or TCP. This conclusion also agrees with the N-limited growth conditions of wastewater-cultivated algal solids and the observed HAp structure in the HTL solids by Roberts et al.[1]

Preliminary findings for the distinctions between HAp or TCP structures within the HTL solids were also observed. The Ca:P molar ratio of the algal and HTL solids were equal and ≤ 1.5 when TCP HTL solids formed. HTL solids that were HAp had Ca:P molar ratios that were more scattered in comparison their initial algal solid Ca:P molar ratio. Algal solids that had Ca:P molar ratios greater than the stoichiometric Ca:P ratio of TCP (1.5) also only produced HAp HTL solids.

The C:Ca molar ratio also provided further insight to the distinction between HAp or TCP HTL solids. HTL solids that were HAp were only observed when the C:Ca ratio was less than 8.0. It is hypothesized the amount of carbon in the HTL reaction impacts the pH of the aqueous reaction media through the production of CO_2. Furthermore, the role of organic carbon as CO_2 during HTL is the most intriguing aspect for future research. A continuing hypothesis is that gaseous CO_2 from algal biomass benefits $CaCO_3$ dissociation. The release of free Ca^{2+} could then promote water-gas shift reactions that improve biocrude properties and solid phosphorus recovery *in-situ*. Experimenting with various C:Ca molar ratios via HTL of calcite and algae or other biological model compounds is highly encouraged. Subsequent estimations of calcite dissociation and biocrude composition are key results to investigate.

Altering the algal growth media and growth stage not only impacts the inorganic structure of auto-flocculated algal solids but the organic, biomolecular content as well. Thus, variances in biocrude properties from HTL of the algal solids cultivated in the raceways were also observed. To the best of the author's knowledge, this raceway, HTL study is the first algal HTL biocrude study with the scope of algal growth media and growth stage to HTL biocrude properties. Gas chromatography mass spectrometry (GC-MS) provided a detailed composition of the biocrude oil produced from the raceway-cultivated algal solids. Saturated and unsaturated hydrocarbons were the primary component of HTL biocrude from N- and P-limited algal solids totaling 25-50% of the biocrude's GC-MS peak area. A greater amount of these hydrocarbons was observed in biocrude produced by algal solids harvested at later growth stages of both N- and P-limited media. In addition, the algal solids at later, stationary growth stages had a higher lipid content than those harvested during the exponential phase. Thus, the added lipid content produced at later algal

growth stages produces an HTL biocrude product with greater, long chain, saturated and unsaturated hydrocarbons.

Previous distinctions between mixed-culture, wastewater-cultivated algal solids and the lab-grown, low-ash, monoculture algae cited in the literature were less long chain amides and hydrocarbon chains that were > C_{20} in the HTL biocrude from wastewater-cultivated algal solids.[2] It was previously hypothesized that these results were due the abundant HAp HTL solids. However, the growth media and stage variables from the raceway study indicated algal solids from N-limited media that were harvested at the later stationary growth stage also produced biocrude with these distinctions. The results lead to the possible conclusion that the algal growth media from the wastewater-cultivated algal solids may have played a larger role than the HTL solids in reduction of long chain amides and increase in C_{20} hydrocarbons in the biocrude.

A large amount of variance in the biocrudes composition was still observed, however, from algal solids harvested at identical growth stages and in the same growth media. Thus, only the inorganic component was varied and may have a substantial impact on the biocrude composition. A comparison of various biocrudes' H/C molar ratio and the respective HTL solid structure indicates that higher and more favorable H/C molar ratios were achieved in biocrudes where the complimentary HTL solid structure was $CaCO_3$ as opposed to HAp or TCP. The higher biocrude H/C results from $CaCO_3$ HTL solids further supports the former hypothesis surrounding HTL of calcite in algal solids. Investigating the role of calcite both as *in-situ* catalyst for biocrude upgrading and for calcium phosphate synthesis during HTL are key drivers for future and continued work of high ash, auto-flocculated algal solids.

7.4 References

1. Roberts, G. W.; Sturm, B. S. M.; Hamdeh, U.; Stanton, G. E.; Rocha, A.; Kinsella, T. L.; Fortier, M.-O. P.; Sazdar, S.; Detamore, M. S.; Stagg-Williams, S. M., Promoting catalysis and high-value product streams by in situ hydroxyapatite crystallization during hydrothermal liquefaction of microalgae cultivated with reclaimed nutrients. *Green Chem.* **2015,** *17* (4), 2560-2569.
2. Roberts, G. W.; Fortier, M.-O. P.; Sturm, B. S. M.; Stagg-Williams, S. M., Promising Pathway for Algal Biofuels through Wastewater Cultivation and Hydrothermal Conversion. *Energy & Fuels* **2013,** *27* (2), 857-867.
3. Changi, S. M.; Faeth, J. L.; Mo, N.; Savage, P. E., Hydrothermal Reactions of Biomolecules Relevant for Microalgae Liquefaction. *Industrial & Engineering Chemistry Research* **2015,** *54* (47), 11733-11758.
4. Fu, J.; Lu, X.; Savage, P. E., Catalytic hydrothermal deoxygenation of palmitic acid. *Energy & Environmental Science* **2010,** *3* (3), 311.
5. Biller, P.; Ross, A. B., Potential yields and properties of oil from the hydrothermal liquefaction of microalgae with different biochemical content. *Bioresource technology* **2011,** *102* (1), 215-25.
6. Teri, G.; Luo, L.; Savage, P. E., Hydrothermal Treatment of Protein, Polysaccharide, and Lipids Alone and in Mixtures. *Energy & Fuels* **2014,** *28* (12), 7501-7509.
7. Duan, P.; Savage, P. E., Hydrothermal Liquefaction of a Microalga with Heterogeneous Catalysts. *Industrial & Engineering Chemistry Research* **2011,** *50*, 52-61.
8. Jena, U.; Das, K. C.; Kastner, J. R., Comparison of the effects of Na2CO3, Ca3(PO4)2, and NiO catalysts on the thermochemical liquefaction of microalga Spirulina platensis. *Applied Energy* **2012,** *98*, 368-375.
9. Ross, A. B.; Biller, P.; Kubacki, M. L.; Li, H.; Lea-Langton, A.; Jones, J. M., Hydrothermal processing of microalgae using alkali and organic acids. *Fuel* **2010,** *89* (9), 2234-2243.
10. Shakya, R.; Whelen, J.; Adhikari, S.; Mahadevan, R.; Neupane, S., Effect of temperature and Na 2 CO 3 catalyst on hydrothermal liquefaction of algae. *Algal Research* **2015,** *12*, 80-90.
11. Lai, R.-H.; Dong, P.-J.; Wang, Y.-L.; Luo, J.-B., Redispersible and stable amorphous calcium phosphate nanoparticles functionalized by an organic bisphosphate. *Chinese Chemical Letters* **2014,** *25* (2), 295-298.
12. Blumenthal, N. C.; Betts, F.; Posner, A. S., Effect of carbonate and biological macromolecules on formation and properties of hydroxyapatite. *Calcified Tissue Research* **1975,** *18* (1), 81-90.
13. Blumenthal, N. C.; Betts, F.; Posner, A. S., Stabilization of amorphous calcium phosphate by Mg and ATP. *Calcified Tissue Research* **1977,** *23* (1), 245-250.

8 Appendix

8.1 Reaction and Product Separation Sheets

Figure 45 and Figure 46 are the reaction and product separation sheets that provided a checklist for the preparation, execution, and product separations of the HTL reactions. They also served as physical, hand-written documentation of the reaction conditions and product masses.

Reaction Date: **Algae:**

Reactor: 75 A B C D 450 1.2

Valve: A B C D E F G H

	Initials	*Date*
Conditioning		
Milli-Q Water added (mL): _____	_____	_____
Preliminary Leak Test: ☐	_____	_____
Water Collected (mL): _____	_____	_____
Recovered (%): _____	_____	_____
Reactor Loading		
Milli-Q Water to be added (mL): _____	_____	_____
Algae Mass (g): _____	_____	_____
Algae Moisture (wt%): _____	_____	_____
Algae Ash (wt%): _____	_____	_____
Secondary Leak Test: ☐	_____	_____
Purge with N_2 (x3) : ☐	_____	_____
Cooling Water: ☐		
Reaction Conditions		
Time Reactor Began Heating: _____	_____	_____
Time Reaction Started: _____	_____	_____
Time Reactor Removed: _____	_____	_____
Reaction RAMP Time (min.): _____	_____	_____
Reaction HOLD Time (min.): _____	_____	_____
Reaction Temperature (°C) _____	_____	_____
Reaction Pressure (psi) _____	_____	_____
Reaction Mixing (rpm) _____	_____	_____
Final Temperature (°C): _____	_____	_____
Final Pressure (psi): _____	_____	_____
Extraction Preparation		
Vacuum Filter Paper – 110°C Oven: ☐	_____	_____
Gravity Filter Paper – 110°C Oven: ☐	_____	_____

Comments:
Write on back

Figure 45: HTL reaction preparation checklist

Reaction Date:		**Algae:**	
RB Flask (with boiling chips and cap; without base)		*Initials*	*Date*
Tare Mass (g): _____		_____	_____
Final Mass (g): _____		_____	_____
Crude GC Sample Prepared (mg): _____	☐	_____	_____
Derivatized GC Sample Prepared (mg): _____	☐	_____	_____
Vacuum Filtration (Whatman #5)			
Tare Mass (g): _____		_____	_____
Final Mass (g): _____		_____	_____
Gravity Filtration (Whatman #1)			
Tare Mass (g): _____		_____	_____
Final Mass (g): _____		_____	_____
Aqueous Co-Product (ACP)			
ACP Collected (mL): _____		_____	_____

Comments:

Figure 46: HTL product separation checklist

8.2 Diatom XRD

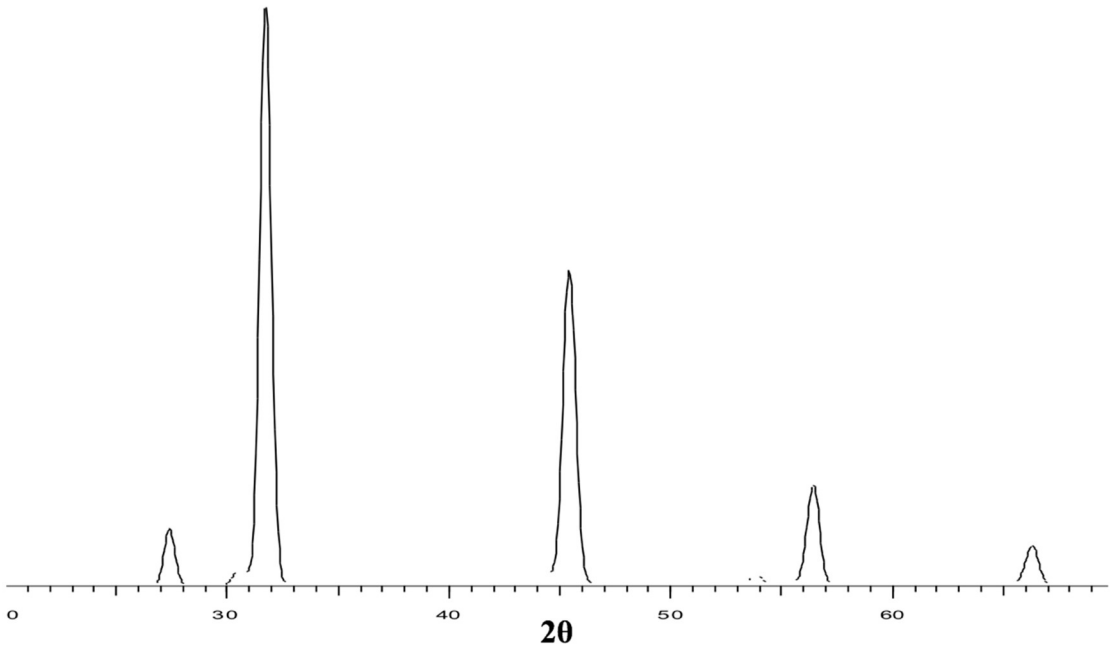

Figure 47: XRD pattern of diatom *Chaetoceros* that was cultivated in the light rack.

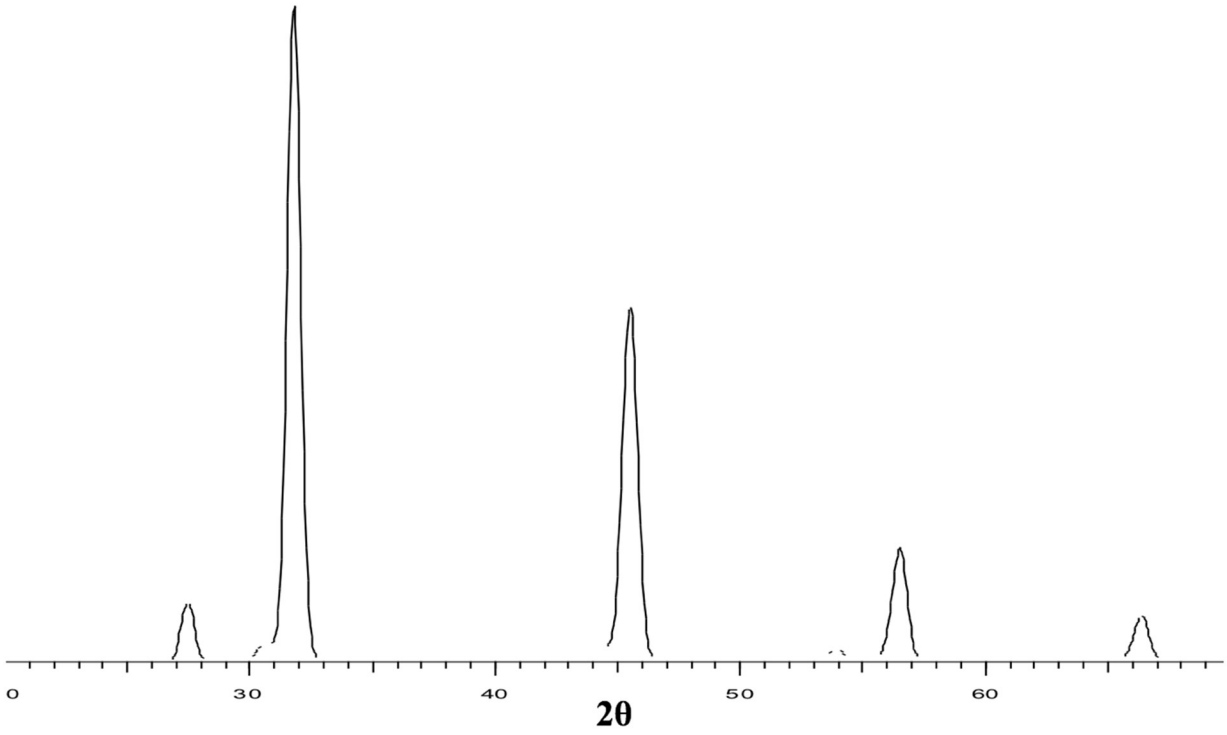

Figure 48: XRD pattern of diatom *Cylindrotheca* that was cultivated in the light rack.

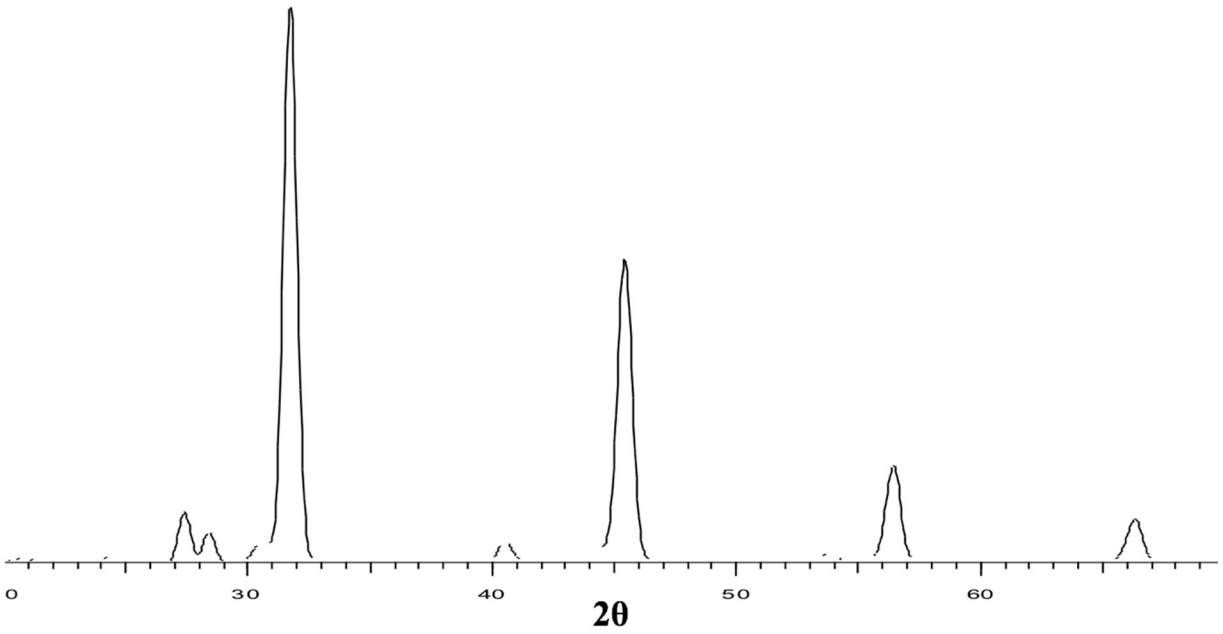

Figure 49: XRD pattern of the diatom Skeletonema that was cultivated in the light rack.

8.3 Light Rack Algal and HTL Solids XRD

The following figures are XRD patterns for algal solids cultivated and auto-flocculated in light rack tanks discussed in Chapter 4.4.3: *Fate of Phosphorus post-HTL*. The following figure then shows the XRD pattern of the algal solids' respective HTL solids structure.

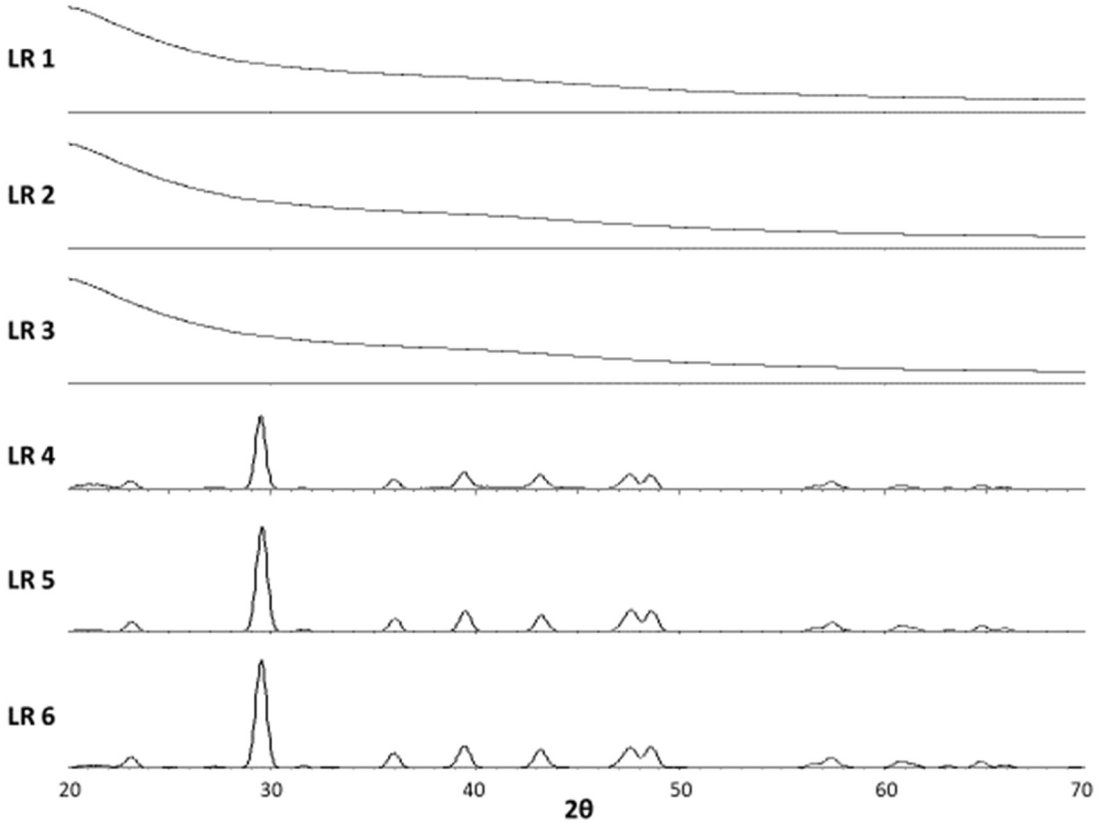

Figure 50: XRD diffraction patterns of algal solids cultivated in light racks and discussed in Chapter 4.4.3: *Fate of Phosphorus post-HTL*.

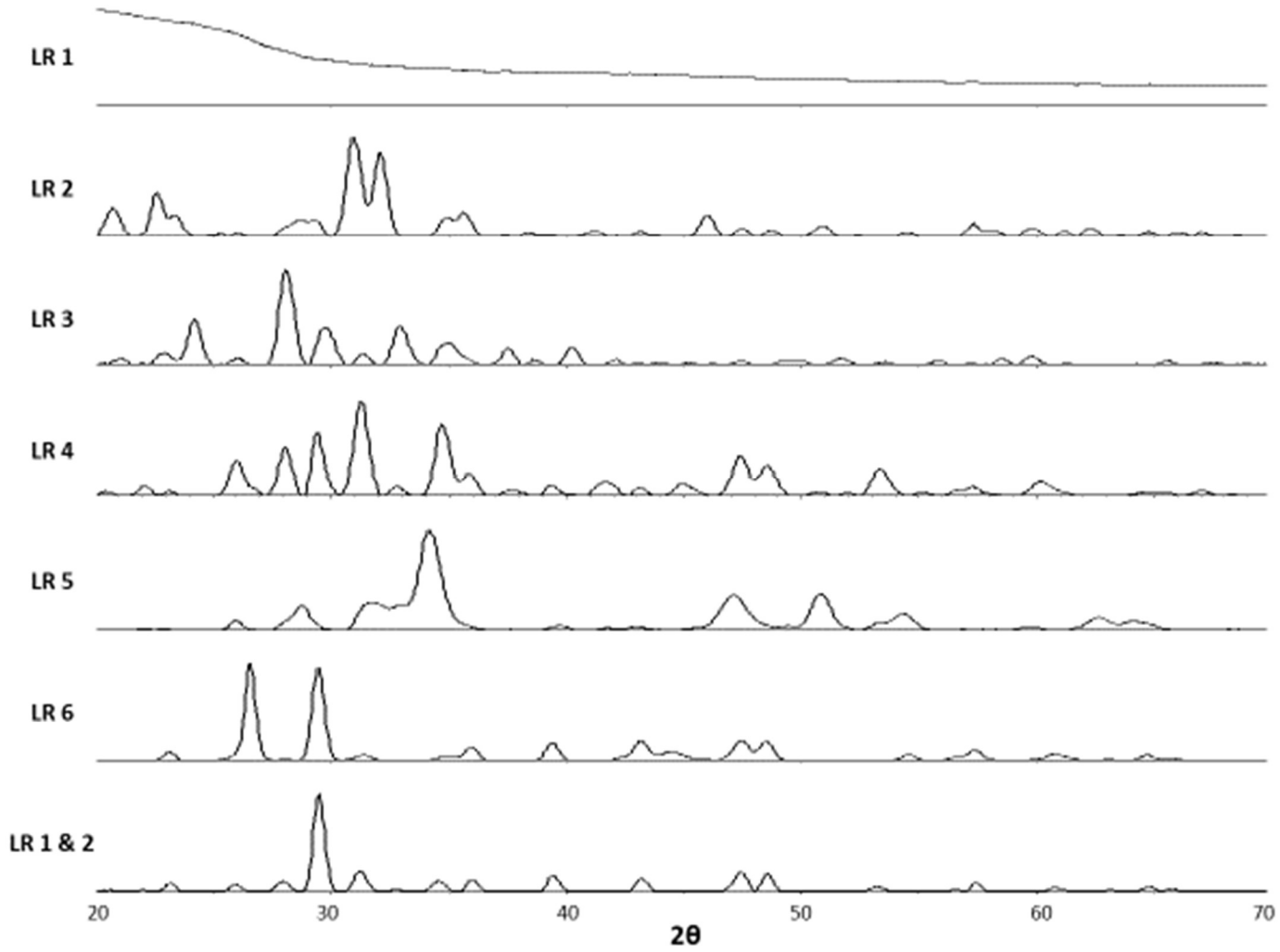

Figure 51: XRD patterns of the HTL solids produced from the light rack algal solids discussed in Chapter 4.4.3: *Fate of Phosphorus post-HTL*.

8.4 N-Limited Raceway Algal Solid, Algal Ash, and HTL Solids XRD

The following figures are the XRD patterns of algal solids cultivated and harvested from the N-limited raceway pond. Their respective TGA ash and HTL solids XRD patterns are also shown in the respective figures.

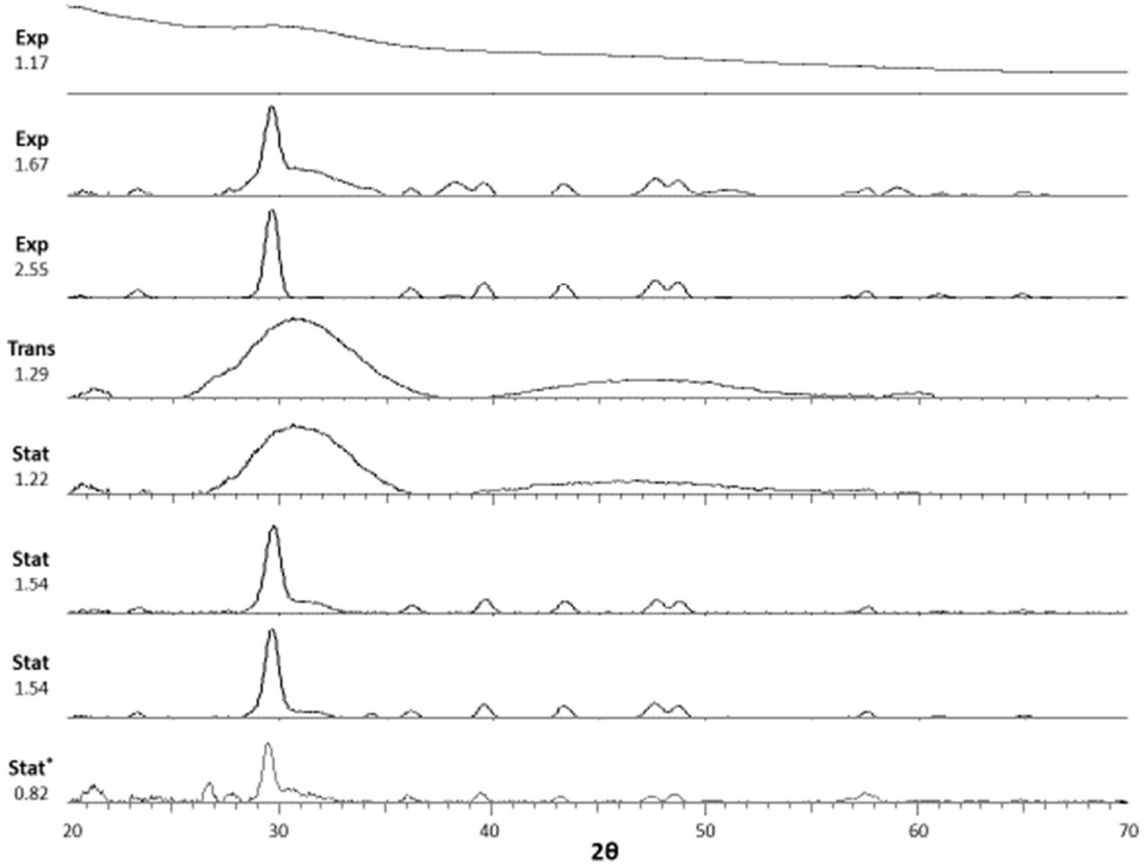

Figure 52: XRD patterns from the N-limited algal solids cultivated in the raceway. The Ca:P molar ratio of the algal solids and their respective growth stage are reported.

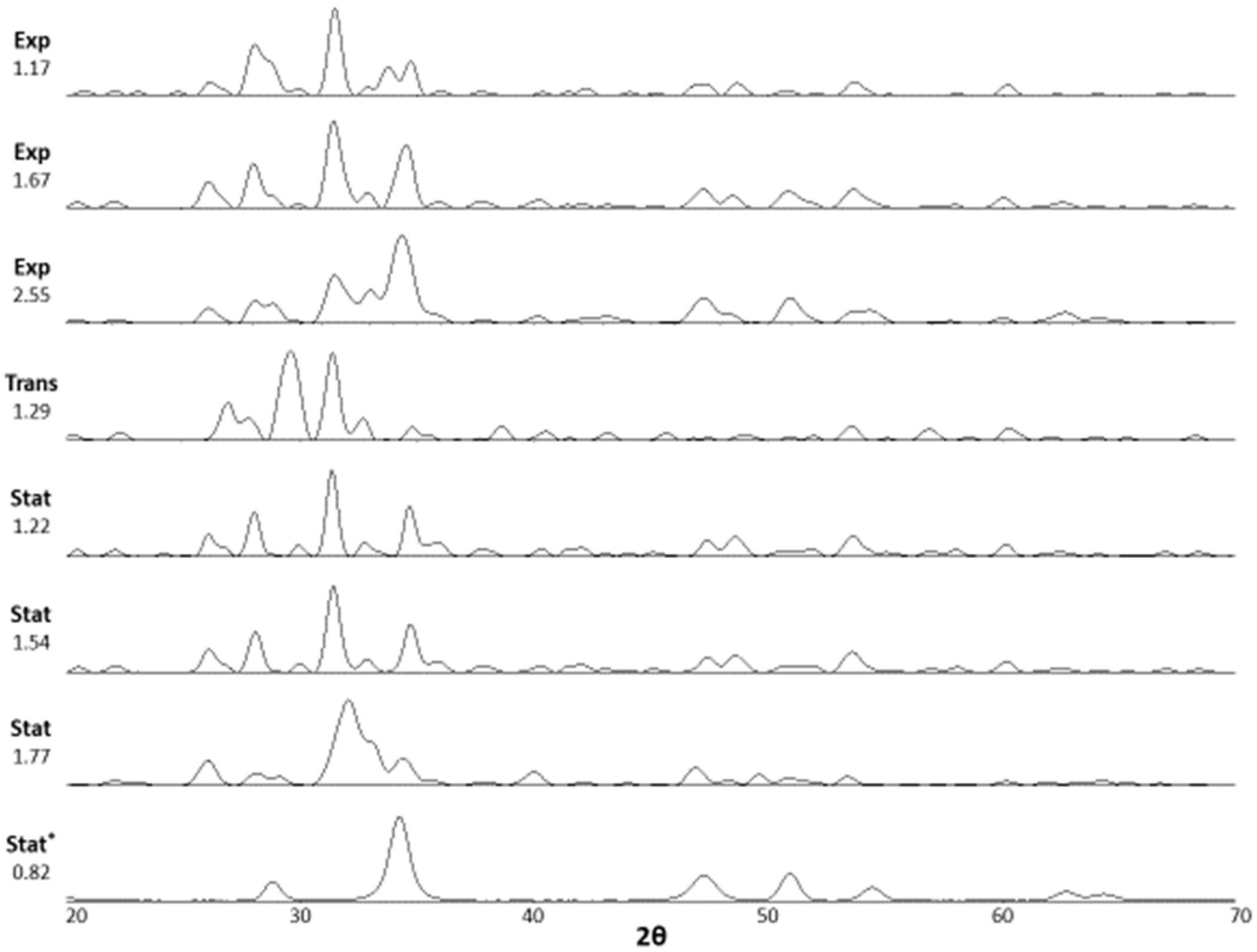

Figure 53: XRD patterns of the algal solid ash from the same respective, N-limited, algal solids and their Ca:P molar ratio referenced in Figure 52.

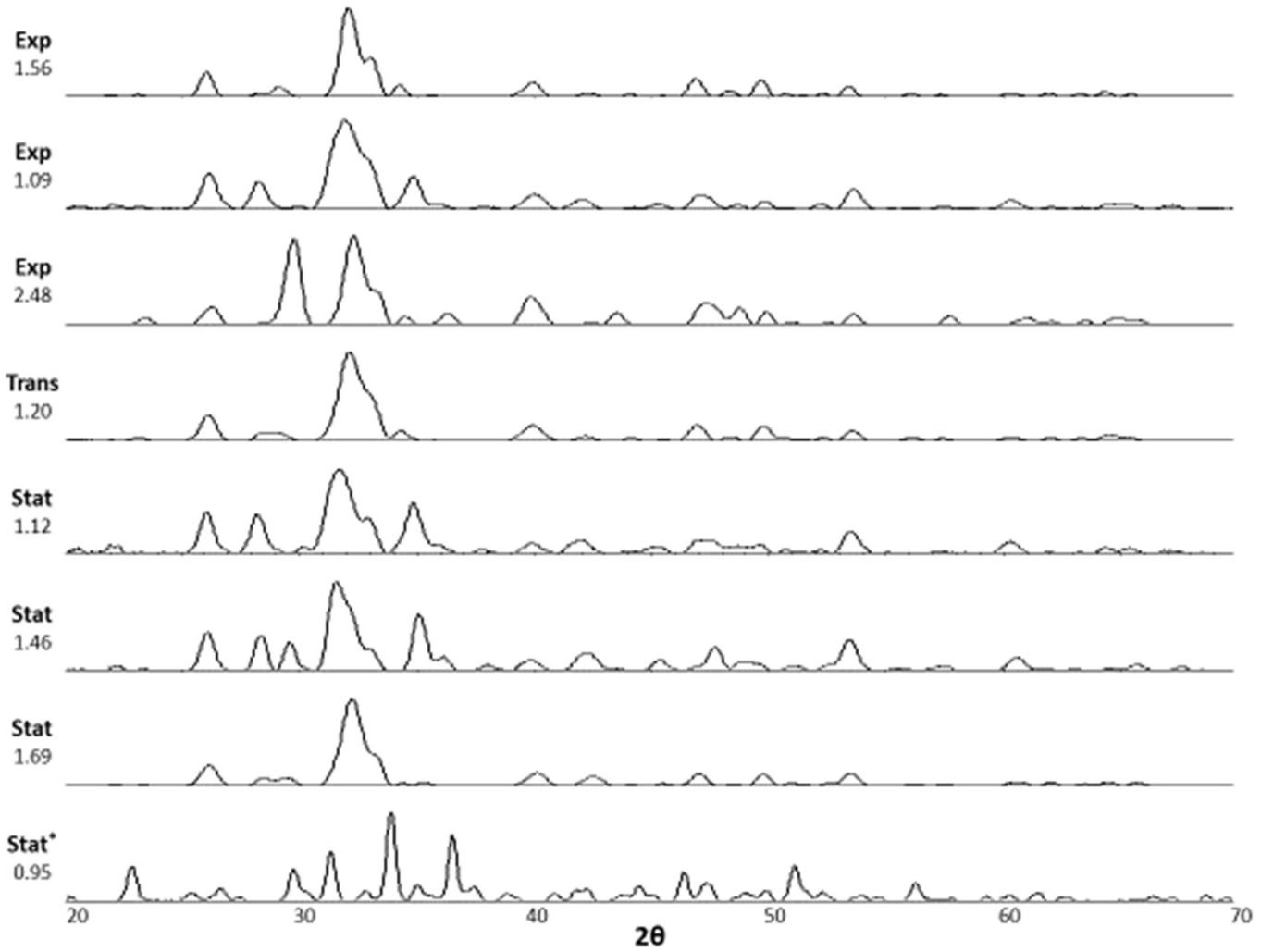

Figure 54: XRD patterns of the HTL solids and their respective Ca:P molar ratio and produced by the same, respective, N-limited algal solids in Figure 52.

8.5 P-Limited Raceway Algal Solid, Algal Ash, and HTL Solids XRD

The following figures are the XRD patterns of algal solids cultivated and harvested from the P-limited raceway pond. Their respective TGA ash and HTL solids XRD patterns are also shown in the respective figures.

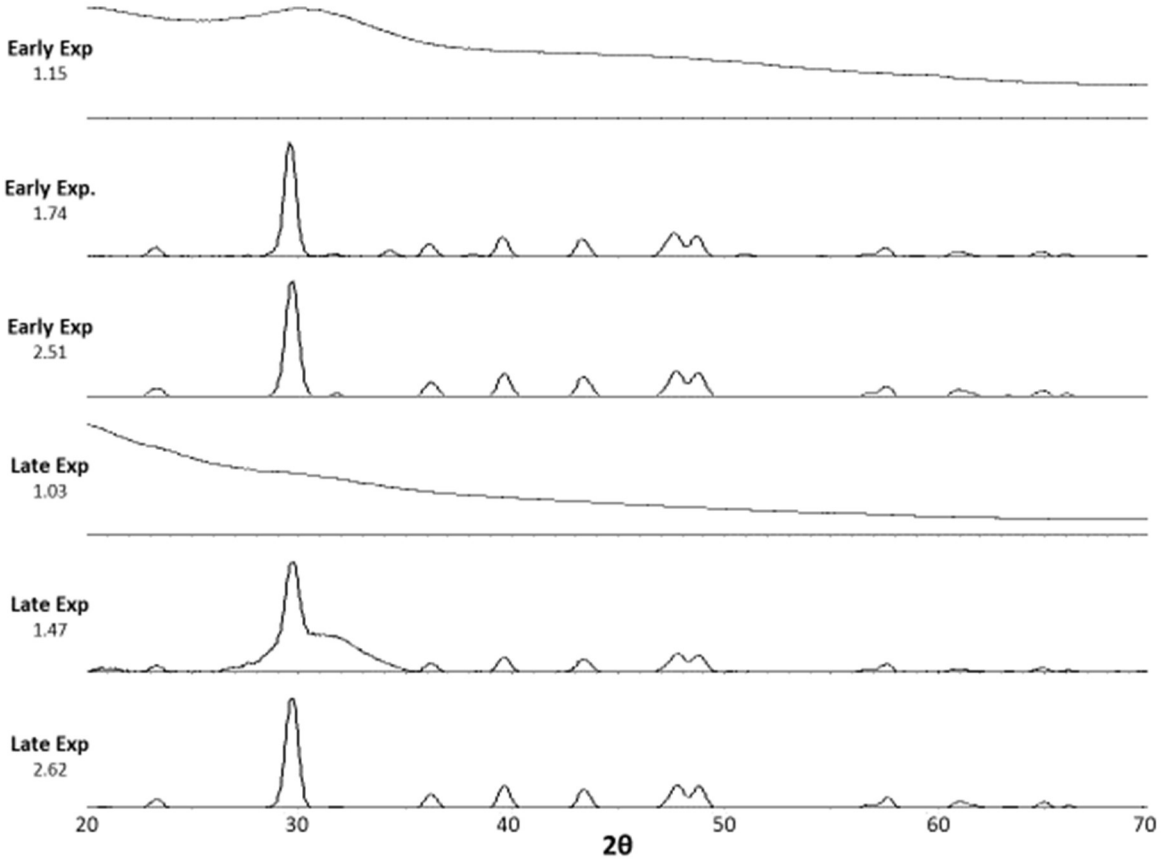

Figure 55: XRD patterns from the early and late exponential growth stages of P-limited algal solids cultivated in the raceway. The Ca:P molar ratio of the algal solids and their repsective growth stage are reported.

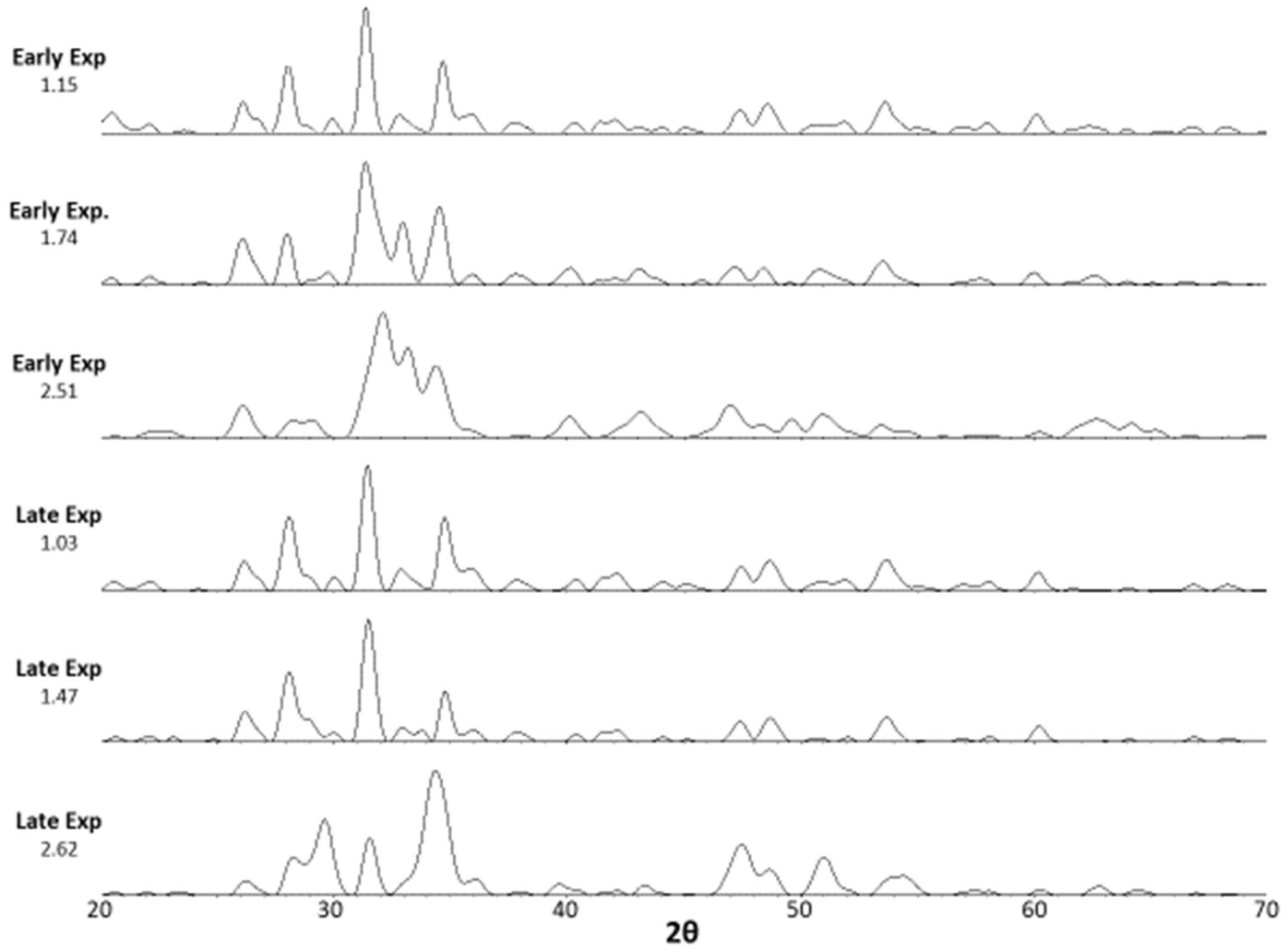

Figure 56: XRD patterns of the algal solid ash from the same respective, P-limited, algal solids and their Ca:P molar ratio referenced in Figure 55.

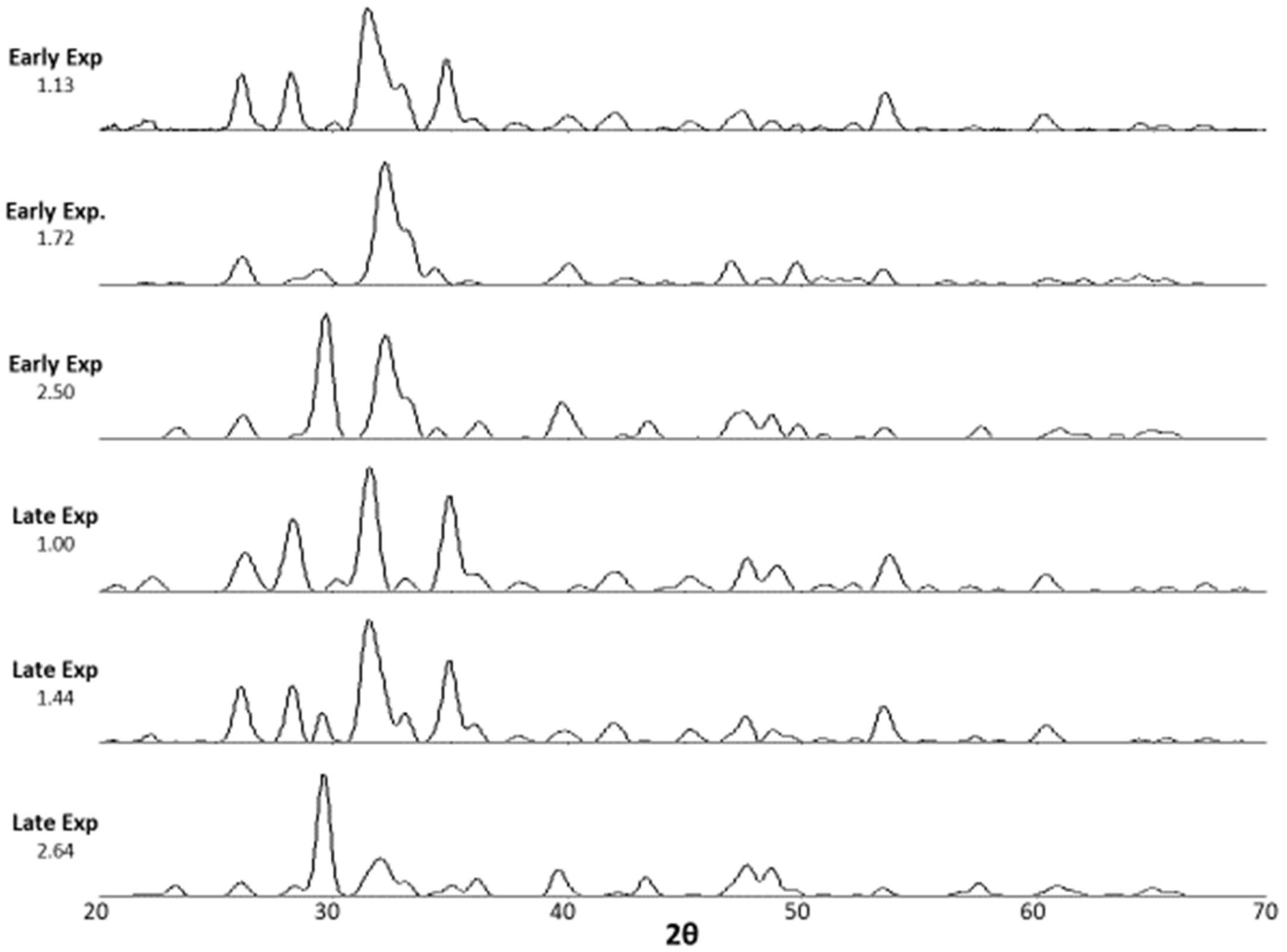

Figure 57: XRD patterns of the HTL solids and their respective Ca:P molar ratio and produced by the same, respective, P-limited algal solids in Figure 55.

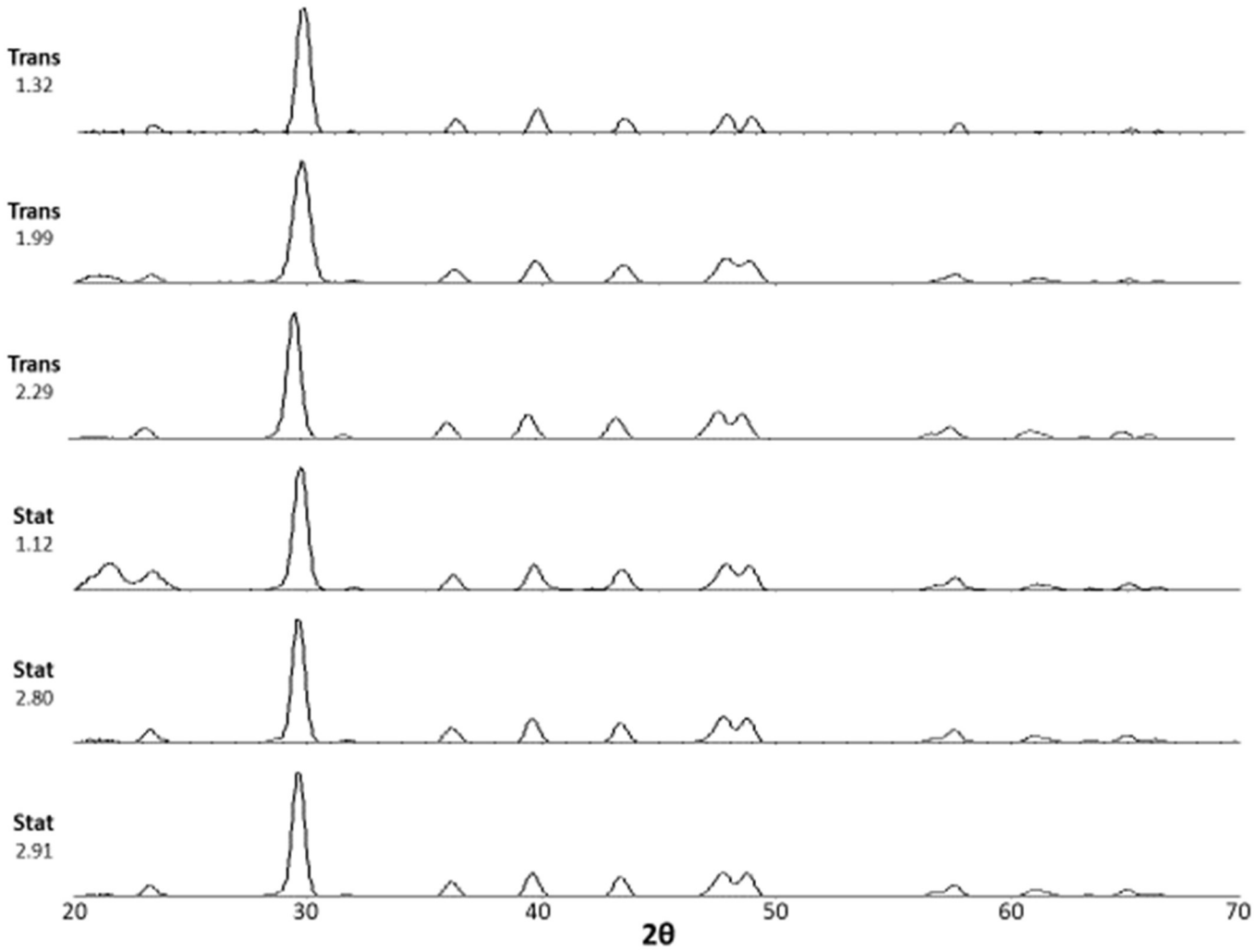

Figure 58: XRD patterns from the transition and stationary growth stages of P-limited algal solids cultivated in the raceway. The Ca:P molar ratio of the algal solids and their respective growth stage are reported.

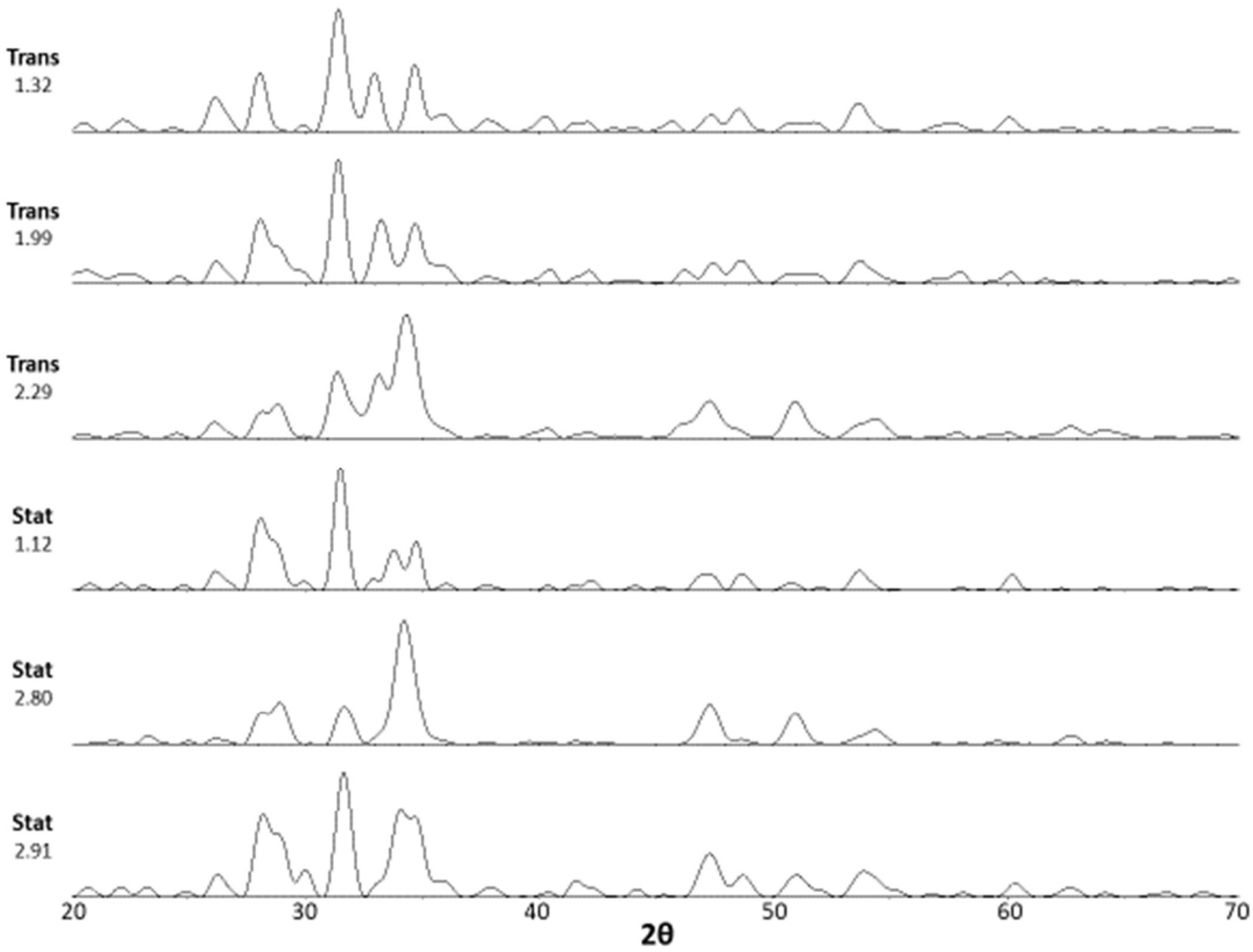

Figure 59: XRD patterns of the algal solid ash from the same respective, P-limited, algal solids and their Ca:P molar ratio referenced in Figure 58.

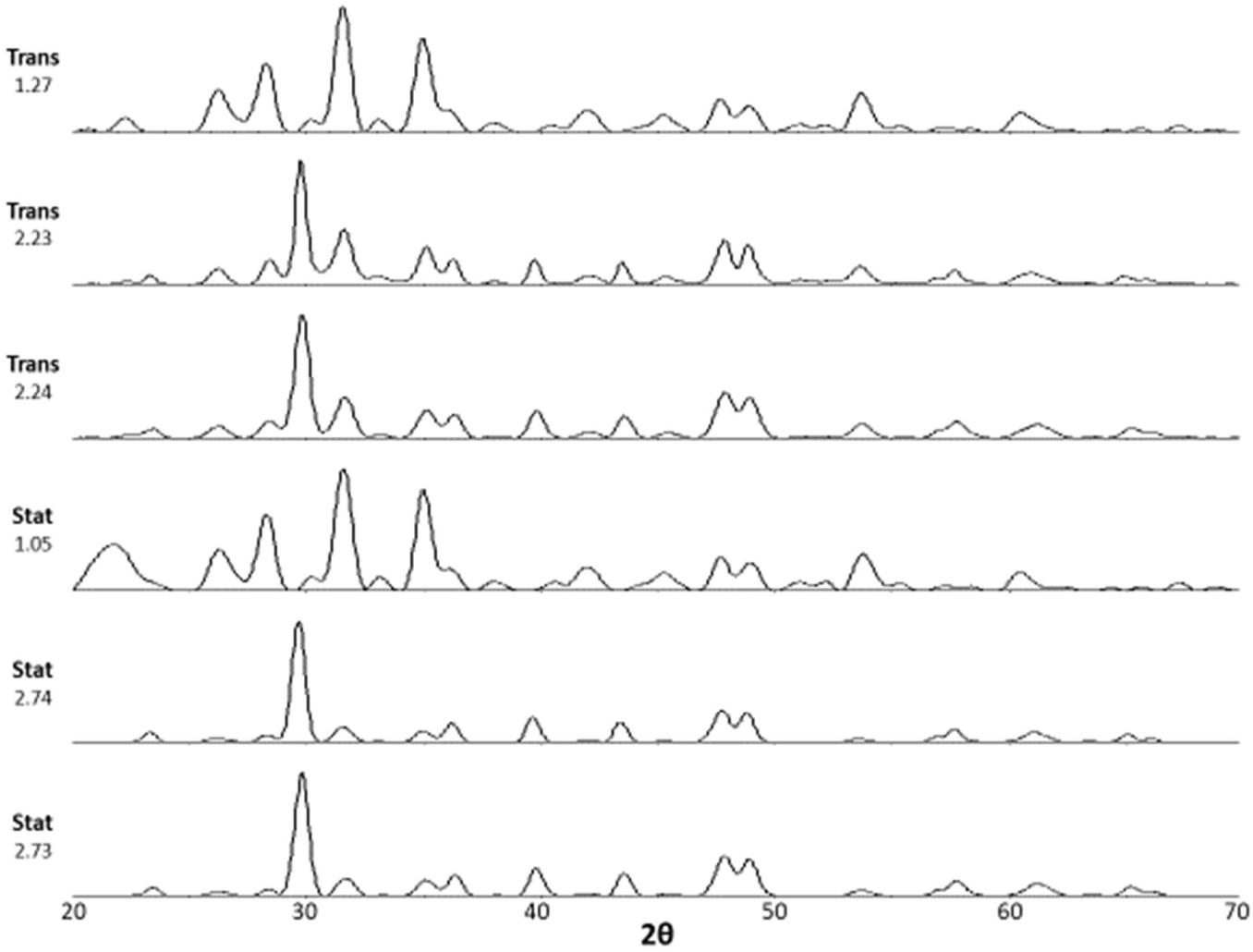

Figure 60: XRD patterns of the HTL solids and their respective Ca:P molar ratio and produced by the same, respective, P-limited algal solids in Figure 58.

8.6 Calcium Carbonate Polymorphs XRD

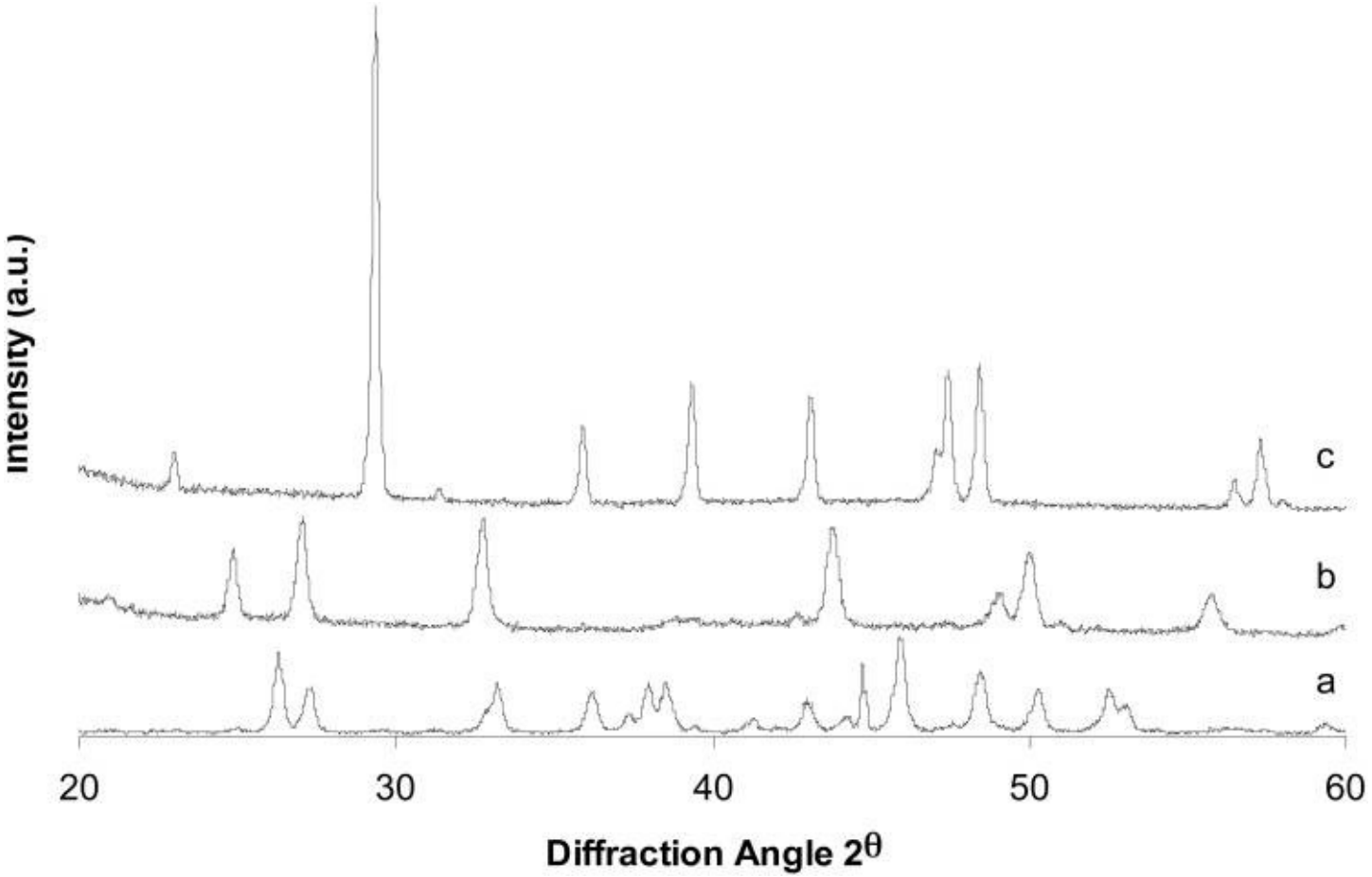

Figure 61: XRD patterns of different $CaCO_3$ structures including a) aragonite b) vaterite and c) calcite. [1]

1. Ni, M.; Ratner, B. D., Differentiation of Calcium Carbonate Polymorphs by Surface Analysis Techniques - An XPS and TOF-SIMS study. *Surf Interface Anal* **2008,** *40* (10), 1356-1361.